

A STUDY OF THE SCATTERING OF ELECTROMAGNETIC WAVES
FROM CERTAIN TYPES OF RANDOM MEDIA

by

RODERIC LLOYD OLSEN

B.A.Sc., The University of British Columbia, 1965

A THESIS SUBMITTED IN PARTIAL FULFILMENT OF
THE REQUIREMENTS FOR THE DEGREE OF

DOCTOR OF PHILOSOPHY

in the Department of Electrical Engineering

We accept this thesis as conforming to the
required standard

Research Supervisor
Members of the Committee
.....
.....
Acting Head of Department

Members of the Department
of Electrical Engineering

THE UNIVERSITY OF BRITISH COLUMBIA

July, 1970

In presenting this thesis in partial fulfilment of the requirements for an advanced degree at the University of British Columbia, I agree that the Library shall make it freely available for reference and study. I further agree that permission for extensive copying of this thesis for scholarly purposes may be granted by the Head of my Department or by his representatives. It is understood that copying or publication of this thesis for financial gain shall not be allowed without my written permission.

Department of ELECTRICAL ENGINEERING

The University of British Columbia
Vancouver 8, Canada

Date July 31, 1970.

ABSTRACT

This work is a study of the scattering of electromagnetic waves from random media of discrete scatterers. The object is primarily the investigation of existing general discrete-scatterer theories and the development of more accurate ones, the technique of Monte Carlo computer simulation being employed to provide "exact" experimental results for comparison with theoretical data.

A one-dimensional model of randomly-positioned planar scatterers is used as a tool in the investigation and as a means of providing insight into the physical and statistical characteristics of discrete-scatterer media. The limitations of the one-dimensional forms of Twersky's theories for the coherent field are illustrated by a presentation of results for a wide range of scattering parameters, and requirements necessary for the approximate validity of these theories are given. Accurate series expressions for several average field functions of interest in the problem of plane-wave scattering from distributions of uniformly-random planar scatterers are presented and verified from simulation results. The asymptotic scattering behavior for a low average density of scatterers is emphasized; a modification to the one-dimensional form of Twersky's free-space theory for the coherent transmitted field to give exact asymptotic behavior is shown to be a considerable improvement for higher average densities also. The relation of the one-dimensional model theory and results to more complex three-dimensional models is discussed where possible.

Simulation methods for the generation of a non-uniform distribution of planar-scatterer configurations weighted towards "periodicity" are presented. Based on the scattering results obtained, criteria for the assumption of a uniform distribution are given. The physical conditions necessary for the approximate validity of the bivariate Gaussian distribution in describing the total field statistics of the one-dimensional model are discussed and

quantitative results based on the third and fourth field moments given.

Also presented is a new physical model of a random medium of discrete spherical scatterers for use in controlled laboratory experiments at millimeter-wave frequencies. The main feature of this model is that the scatterer statistics are directly controlled by an application of the Monte Carlo method. The results of an experimental investigation into the suitability of the model are given.

TABLE OF CONTENTS

	Page
LIST OF ILLUSTRATIONS	viii
LIST OF TABLES	x
LIST OF SYMBOLS	xi
ACKNOWLEDGEMENTS	xvi
1. GENERAL INTRODUCTION	1
2. THEORETICAL CONSIDERATIONS	6
2.1 Introduction	6
2.2 The One-Dimensional Model	8
2.3 Basic Formalism for Scattering from a Fixed Configuration of Arbitrary Scatterers	11
2.4 Explicit Theories for Scattering from a Fixed Array of Planar Scatterers	13
2.4.1 Wave Transmission Matrix Representation	14
2.4.2 Orders-of-Back-Scattering Representation	15
2.5 Scattering from an Ensemble of Scatterer Configurations	19
2.5.1 Average Field Functions of Interest	19
2.5.2 Some Existing Theories for Average Field Functions	23
2.6 Series Approximations for Scattering from an Ensemble of Uniformly-Random Planar-Scatterer Configurations	25
2.6.1 The Coherent Fields	26
2.6.2 The Average Total Intensities	28
2.6.3 The Covariant Fields	31
2.7 Asymptotic Theories for Scattering from Low Average Density Scatterer Distributions	33
2.7.1 Asymptotic Theory for the Coherent Transmitted Field ...	33
2.7.2 Asymptotic Theories for the Average Total Field Intensities	36
2.8 Theoretical Models for the Probability Density of the Total Field	40

2.9	Other Theoretical Considerations	45
2.10	Summary	47
3.	APPLICATION OF MONTE CARLO SIMULATION TO THE STUDY OF SCATTERING FROM RANDOM MEDIA	49
3.1	Introduction	49
3.2	Technique of Simulation Applied to a Random Medium of Discrete Scatterers	50
3.3	Random Number Generation	51
3.4	Accuracy in Monte Carlo Simulation	53
4.	THEORETICAL AND SIMULATION RESULTS FOR A UNIFORM PROBABILITY DENSITY OF PLANAR-SCATTERER CONFIGURATIONS	55
4.1	Introduction	55
4.2	Transmitted Field Moments	57
4.2.1	The Coherent Field	57
4.2.2	The Average Incoherent Intensity	63
4.2.3	The Variances and Covariance	66
4.2.4	Moments of the Amplitude and Phase	66
4.3	Reflected Field Moments	68
4.3.1	The Coherent Field	68
4.3.2	The Average Incoherent Intensity	71
4.3.3	The Variances and Covariance	74
4.4	Distribution of the Total Field	76
4.5	Summary and General Discussion of Results	80
5.	SIMULATION OF A NON-UNIFORM PROBABILITY DENSITY OF PLANAR-SCATTERER CONFIGURATIONS WEIGHTED TOWARDS PERIODICITY	82
5.1	Introduction	82
5.2	Methods of Generating the Distribution	84
5.2.1	Method A	85
5.2.2	Method B	85
5.2.3	Results	86

5.3	Variation of the Distribution between the Limits of Uniform-Randomness and Periodicity for Fixed Scattering Parameters	90
5.4	Comparison of Simulation and Mixed-Space Theory Results for Planar Scatterers of Finite Thickness	99
5.4.1	The Coherent Transmitted Field	99
5.4.2	The Coherent Reflected Field	104
5.5	Summary and General Discussion of Results	107
5.5.1	Summary	107
5.5.2	General Discussion	107
6.	EXPERIMENTAL INVESTIGATION	109
6.1	Introduction	109
6.2	The Physical Model	110
6.2.1	Generation of Uniform Distribution	112
6.2.2	The Support-Medium	114
6.2.3	Comparison with the Sylvania Model	115
6.3	The Scattering Range, Antenna Characteristics, and Scanning Device	118
6.4	Experimental Apparatus, Measurement and Data Processing Methods	121
6.4.1	Experimental Apparatus and Procedures	121
6.4.2	Data Processing Methods	125
6.5	Experimental Results	127
6.5.1	Experiments on the Support-Medium	127
6.5.2	Experiments on Typical Scatterer Distributions	128
6.5.3	Discussion of Overall Results	138
7.	CONCLUSIONS	140
APPENDIX A	SUMMARY OF TWERSKY'S THEORIES FOR RANDOM MEDIA OF DISCRETE SCATTERERS	143
A.1	Twersky's Free-Space Theory for the Coherent Field	143
A.2	Twersky's Mixed-Space Theory for the Coherent Field ...	145

	Page
A.3 Theories for Other Average Field Functions	148
APPENDIX B SCATTERING FROM A SINGLE DIELECTRIC SLAB	150
B.1 Conventional Scattering Amplitudes	150
B.2 Mixed-Space Scattering Amplitudes	153
APPENDIX C VALIDITY OF THE DISCRETE POSITION APPROXIMATION IN SIMULATION STUDIES	155
APPENDIX D DESIGN OF MICROWAVE ANECHOIC CHAMBER AND POSITIONING DEVICE	166
D.1 Design and Testing of Anechoic Chamber	166
D.2 Design of Positioning Device	168
REFERENCES	170

LIST OF ILLUSTRATIONS

Figure		Page
2.1	The One-Dimensional Model	9
2.2	Wave Transmission Matrix Representation	14
2.3	Dominant Multiple-Scattering Processes in O-B-S Representation	16
2.4	Phasor Diagram of the Total Field Resolution	20
4.1.a	Phase of Coherent Transmitted Field as a Function of d_λ	58
4.1.b	Coherent Transmitted Field Intensity as a Function of d_λ	59
4.2	Coherent Transmitted Field as a Function of N (Asymptotic Results)	61
4.3	Coherent Transmitted Field as a Function of w_λ , (Asymptotic Results)	62
4.4	Average Incoherent Intensity of Transmitted Field as a Function of d_λ	64
4.5	Asymptotic Results for the Average Incoherent Intensity of the Transmitted Field	65
4.6	Variances and Covariance of Transmitted Field Components as Functions of d_λ	67
4.7	Standard Deviations of the Transmitted Field Amplitude and Phase as Functions of N (Asymptotic Results)	69
4.8	Coherent Reflected Field as a Function of d_λ	70
4.9	Average Incoherent Intensity of Reflected Field as a Function of d_λ	72
4.10	Asymptotic Results for the Average Incoherent Intensity of the Reflected Field	73
4.11	Variances and Covariance of Reflected Field Components as Functions of d_λ	75
4.12	Skewness and Kurtosis Coefficients as Functions of the Phase Reference	77
4.13	Extreme Values of b and γ as Functions of w_λ ,	78
5.1	One-Scatterer Normalized Probability Density Curves for $N = 4$	87

Figure		Page
5.2	One-Scatterer Normalized Probability Density Curves for $N = 5$	88
5.3	Phase and Intensity of the Transmitted Field as Functions of d_λ for a Periodic Array	92
5.4	Dependence of Average Field Functions on β_0 for Various Values of d_λ	93
5.5	β_0 -Variation Curves for Values of d_λ in the Neighbourhood of Resonance at Periodicity	97
5.6	Coherent Transmitted Field Results for High ρ_λ	101
5.7	Coherent Transmitted Field Results for Low ρ_λ	103
5.8	Comparison of Results for the Coherent Reflected Field	105
6.1	Simplified Diagram of Scattering Geometry	111
6.2	Typical Computer Output for Sphere Coordinates	114
6.3	View of the Physical Model	116
6.4	Plan View of the Geometry of Antennas and Medium	119
6.5	View of the Receiving Antenna and Mixer	120
6.6	View of the Experimental Apparatus	122
6.7	Block Diagram of the Experimental Apparatus	123
6.8	Correlation Coefficient Curves for Amplitude and Phase	134
B.1	Scattering from a Single Dielectric Slab	150
B.2	Scattering Amplitudes as a Function of w_λ , for $\epsilon_r = 2.0$	152
C.1	Dependence of Average Field Functions on β_d for the Non-Uniform Distribution	157
C.2	Dependence of Average Field Functions on β_d for the Uniform Distribution	158
C.3	Single-Scattering Geometry for Three-Dimensional Model	160
D.1	Simplified Plan-View Diagram of the Anechoic Chamber	167
D.2	View of the Positioning Device	169

LIST OF TABLES

Table		Page
6.1	Results for Estimated Average Field Functions	131
6.2	Accuracy Calculations Based on Equivalent Uncorrelated Samples	135
6.3	Accuracy Estimates Based on Twice the Standard Errors of the Means	137

LIST OF SYMBOLS

$\langle F \rangle$	= ensemble average of function F
Re F	= real part of complex function F
Im F	= imaginary part of F
$ F $	= magnitude of F
Arg F	= argument of F
F*	= complex conjugate of F
a_{nm}	= coefficients in asymptotic expression for $\langle T ^2 \rangle$
A_0	= amplitude of constant phasor
A_s, A_i	= amplitudes of random phasors
b_x, b_y	= coefficients of skewness for the distributions of T_x and T_y
b_{nm}	= coefficients in asymptotic expression for $\langle R ^2 \rangle$
B_{nm}	= binomial coefficients
C	= amplitude of coherent field
C^2	= intensity of coherent field
C_x, C_y	= rectangular components of coherent field = $C \cos \alpha, C \sin \alpha$
C_{nm}	= covariant reflected field coefficients
d	= width of slab region containing scatterer centers
d_λ	= width of slab region in free-space wavelengths = d/λ
d_r	= distance of receiving antenna from center of medium
d_t	= distance of transmitting antenna from center of medium
D	= function in free-space and mixed-space theories
e	= distance of closest approach between scatterer centers
e_λ	= e/λ
f	= arbitrary function

\bar{F}	= electric or magnetic field vector
$g(\hat{r}, \hat{k})$	= scattering amplitude for a three-dimensional scatterer
g_+, g_-	= forward- and back-scattering amplitudes for an isolated planar scatterer (normal incidence) = $T_1 - 1, R_1$
g_{+s}, g_{-s}	= g_+, g_- for scatterer s
g'_+, g'_-	= mixed-space planar-scatterer amplitudes associated with mixed-space theory for the coherent field
I	= amplitude of incoherent field
I^2	= intensity of incoherent field
I_x, I_y	= rectangular components of incoherent field = $I \cos\theta, I \sin\theta$
j	= $\sqrt{-1}$
k	= propagation constant in free space = $2\pi/\lambda$
K	= propagation constant in synthetic medium associated with the coherent field
K'	= propagation constant in medium of scatterer
\bar{k}, \bar{K}	= propagation vectors associated with k, K
\bar{k}', \bar{K}'	= propagation vectors \bar{k}, \bar{K} reflected in slab-region face
n	= number of uncorrelated samples
n_R	= resonance index
N	= number of scatterers
$p(\bar{s}_1, \dots, \bar{s}_N)$	= joint probability density function for an ensemble $\{\bar{s}_1, \dots, \bar{s}_N\}$ of scatterer configurations
$p(z_1, \dots, z_N)$	= joint probability density function for the planar-scatterer positions in the one-dimensional model
$p(z'_1, \dots, z'_N)$	= joint probability density function for the "ordered-positions" of the scatterers in the one-dimensional model
$p(T_x, T_y)$	= joint probability density function for the field components T_x and T_y
Q	= function in free-space and mixed-space theories
\bar{r}	= field point position vector

\vec{r}_s	= position vector for scatterer s
R	= overall reflection coefficient for an array of planar scatterers
R_1	= reflection coefficient for an isolated planar scatterer = g_-
R_s	= R_1 for scatterer s
R_I, R_{III}	= contributions to R from first and third orders-of-back-scattering, etc.
s	= covariant field phase
$s, s_1, s_2, \text{ etc.}$	= indices specifying scatterers $s, s_1, s_2, \text{ etc.}$
$\bar{s}_1, \bar{s}_2, \dots, \bar{s}_N$	= random vector variables describing a discrete scatterer configuration
S	= covariant field amplitude
t	= time
t	= index specifying a scatterer t
T	= overall transmission coefficient for an array of planar scatterers
T_1	= transmission coefficient for an isolated planar scatterer = $1 + g_+$
T_s	= T_1 for scatterer s
T_{II}, T_{IV}	= contributions to T from second and fourth orders-of-back-scattering, etc.
u_s	= isolated scatterer function for a scatterer s
U_s	= field scattered by scatterer s
U	= total field scattered by a configuration of scatterers
V	= volume occupied by three-dimensional scatterers
w	= width of dielectric slab scatterer
w_λ	= w/λ
$w_{\lambda'}$	= w/λ'
X	= arbitrary field function
x, y, z	= cartesian coordinates

z_s	= random variable describing position of planar scatterer s
z'_s	= random variable describing "ordered-position" of scatterer s
α	= phase of coherent field
β_0	= fractional volume
β_m	= maximum physically allowable value of β_0
β_d	= occupation ratio
γ_x, γ_y	= coefficients of kurtosis for the distributions of T_x and T_y
Δ'	= single slab scatterer function
ϵ_r	= dielectric constant of scatterer medium
η	= bulk index of refraction of synthetic medium associated with the coherent field
η'	= refractive index of scatterer medium = $\sqrt{\epsilon_r}$
θ_s, θ_i	= phases of random phasors
θ	= angle of incidence for an obliquely incident plane wave
λ	= free-space wavelength
λ'	= wavelength in scatterer medium
μ	= correlation coefficient for T_x and T_y
ν	= phase reference of total field
ξ_i	= space between planar scatterer boundaries
ρ	= average density of scatterers = N/d (one-dimensional model) = N/V (three-dimensional model)
ρ_λ	= $\rho\lambda = N/d_\lambda$
σ	= total scattering cross-section
σ_f	= standard deviation of function f
σ_f^2	= variance of function f
$\sigma_{T_x}^2$	= $\langle I_x^2 \rangle$
$\sigma_{T_y}^2$	= $\langle I_y^2 \rangle$

τ	= phase of normalized total field
T	= amplitude of normalized total field
T_x, T_y	= rectangular components of normalized total field = $T \cos \tau, T \sin \tau$
ϕ	= incident field
ϕ'	= field reflected in slab-region face
ϕ	= phase of incoherent field
ϕ_s	= multiple-scattered field exciting scatterer s
ψ	= total field = $\phi + u$
ω	= angular frequency
∇^2	= Laplacian operator

ACKNOWLEDGEMENTS

I wish to express my sincere gratitude to my research supervisor Dr. M. Kharadly for his initial inspiration and for his continuous encouragement throughout the course of this work.

Grateful acknowledgement is made to the British Columbia Telephone Company for a graduate scholarship in the academic year 1965-1966 and to the National Research Council of Canada for postgraduate scholarships throughout the period 1966-1969 and for support under grants A-6068 and A-3344.

Thanks are due to members of the workshop staff who constructed the apparatus necessary in the project, often making helpful suggestions regarding details of construction; Mr. C. Chubb did the machine work on the positioning device and Mr. C. Sheffield, the wiring. Thanks are due also to Miss S. Haslin who developed the sampling programs for the PDP-9 computer and interface.

I wish to thank Messrs. B. Wilbee and P. O'Kelly for proofreading the final draft. Also, I wish to thank my fellow students for many helpful discussions regarding the work.

Finally, I would like to thank my loving wife, Sally, for her continuous support throughout my work and for typing the initial and final manuscripts.

1. GENERAL INTRODUCTION

The scattering of electromagnetic waves from random media has in recent years become the subject of an increasing amount of research in a variety of disciplines. The subject enters into such areas of investigation as the propagation of radio waves through the atmosphere, radar, radio and optical astronomy, and studies of the microstructure of gases, liquids, and solids. The spectral range of interest correspondingly extends from frequencies below the broadcast bands to those in the X-ray region.

Although the random nature of many media has long been recognized and approximate scattering theories applicable to some media have existed for a number of years, the demands of modern technology have focussed new attention on the development of more accurate theories. Two general models have been used to theoretically describe a random medium: (a) the perturbed continuum model, and (b) the discrete scatterer model.¹ In the perturbed continuum model² the medium is considered to be continuous in character and randomness is accounted for by a statistical description of its permittivity and permeability. Fluctuations in these parameters are assumed to occur about mean values which correspond to the parameters of an idealized homogeneous medium. Different forms of this model have been used in the study of ionospheric and tropospheric scattering of radio waves and in analyzing scintillation of radio and optical celestial sources.

In the discrete scatterer model a homogeneous medium is assumed to be embedded with discrete scattering regions of different permittivity and permeability, with randomness accounted for by a statistical description of these discrete-scatterer characteristics. This model has also been used in the study of radio-wave scattering in the atmosphere where it applies to various forms of precipitation and as a first approximation to small-scale

irregularities in the refractive index.³ It has also been used as a model of the microstructure of gases, liquids, and solids in scattering studies at optical and X-ray frequencies. The present thesis is restricted to an investigation of certain types of discrete scatterer models.

In general a random medium is dependent on both "spatial" variables and time. In a discrete scatterer model the random medium is represented at time t by an ensemble of "spatial" configurations $\{\bar{s}_1, \bar{s}_2, \dots, \bar{s}_N\}$ of N discrete scatterers within an otherwise homogeneous medium. The "spatial" variables $\bar{s}_1, \bar{s}_2, \dots, \bar{s}_N$ are random, each including the significant properties such as position, velocity, size, shape, orientation, and permittivity of one particular scatterer. The ensemble is described by a joint probability density function $p(\bar{s}_1, \dots, \bar{s}_N; t)$ which specifies the probability "weight" associated with a finite range of configurations; $p(\bar{s}_1, \dots, \bar{s}_N; t) d\bar{s}_1 \cdots d\bar{s}_N$ is the probability of finding the scatterers at time t in a configuration in the "volume element" around $\bar{s}_1, \dots, \bar{s}_N$.[†] This function satisfies

$$\int_{-\infty}^{\infty} \cdots \int_{-\infty}^{\infty} p(\bar{s}_1, \dots, \bar{s}_N; t) d\bar{s}_1 \cdots d\bar{s}_N = 1 \quad (1.1)$$

The usual scattering problem associated with random media of discrete scatterers may be stated as follows: An electromagnetic wave $\bar{F}^i(\bar{r})e^{j\omega t}$ is incident on each configuration $\bar{s}_1, \dots, \bar{s}_N$ of the ensemble and gives rise to a resultant field $F(\bar{s}_1, \dots, \bar{s}_N; \bar{r}, t)e^{j\omega t}$ which is specified at a point \bar{r} and time t by

$$\bar{F}(\bar{s}_1, \dots, \bar{s}_N; \bar{r}, t) = \bar{F}^i(\bar{r}) + \bar{F}^s(\bar{s}_1, \dots, \bar{s}_N; \bar{r}, t) \quad (1.2)$$

[†]The common practice of employing a single symbol to represent both a random variable and the values it assumes is followed throughout the thesis. Also used is the convention that p may represent any number of probability density functions, the type being indicated by the random-variable symbols within the parentheses (before the semicolon).

where $\bar{F}^s e^{j\omega t}$ is the scattered field. It is desired to determine the statistics of the field \bar{F} at \bar{r} and t over the ensemble of scatterer configurations, or more specifically, the joint probability density function $p(X, Y; \bar{r}, t)$ of the field components X and Y , where $F = |\bar{F}| = X + jY$ or $F = X e^{jY}$. Usually the scattering process is stationary (see reference 3 for definitions) so that the medium is specified by a single probability density function $p(\bar{s}_1, \dots, \bar{s}_N)$ and the field by $p(X, Y; \bar{r})$.

Since $p(X, Y; \bar{r})$ is a function of various statistical moments of X and Y over the ensemble of configurations, a subsidiary problem is to determine these moments. The m -th moment of a field component X is defined

$$\langle X^m(\bar{r}, t) \rangle \triangleq \int_{-\infty}^{\infty} \dots \int_{-\infty}^{\infty} p(\bar{s}_1, \dots, \bar{s}_N; t) X^m(\bar{s}_1, \dots, \bar{s}_N; \bar{r}, t) d\bar{s}_1 \dots d\bar{s}_N \quad (1.3)$$

and is independent of t for a stationary process. Often the scattering process is ergodic³ as well as stationary so that estimates of $\langle X^m(\bar{r}) \rangle$ can be determined by long-time averages of X^m . Such conditions occur in practice if the time constants of the scatterer motion are much larger than the period of the incident wave (i.e., so that the field is relatively independent of the scatterer velocities) but much shorter than the time interval of measurement.^{4,5}

In this thesis, emphasis is placed on the investigation of existing general discrete-scatterer theories for the field moments of interest and the development of more accurate ones. Such theories are of importance because they explicitly involve the various physical and statistical parameters of the scattering medium (e.g., scattering characteristics of the individual scatterers; parameters of the distributions of scatterer positions, sizes, permittivities, and other "spatial" variables). Thus, for example, in scattering studies of the microstructure of matter they provide a framework for the inversion of field measurements to yield the individual scatterer functions

and distributions of physical interest. Furthermore, when specialized to the naturally-occurring scatterer distributions of the atmosphere and the corresponding communication problem, they provide a basis for the appropriate choice of signal parameters to minimize the effects of the fluctuating medium on coherent propagation. As already stated, the field moments also enter into theoretical models for the complete probability density of the field which are necessary to more completely characterize the scattering process. Some consideration is also given in the thesis to this more general problem area.

As a means of investigating existing general discrete-scatterer theories and providing insight into the physical and statistical characteristics of discrete-scatterer media, much weight is attached in the thesis to the use of a one-dimensional model of randomly-positioned planar scatterers. As a tool in the investigation, the Monte Carlo method is used extensively for a computer simulation of scattering from this model.

The theoretical aspects of the scattering problem are considered in Chapter 2; the two general approaches to the solution of the problem are introduced and some existing theories for the field moments and the complete field distribution are presented. Also in Chapter 2, the theoretical basis for the consideration of the one-dimensional model is outlined in detail and several approximate scattering theories developed for this model in the present work are given.

In Chapter 3 the use of the Monte Carlo simulation in the study of random media of discrete scatterers is discussed and procedures for its application outlined. Results of a comparative study of theoretical and simulation data for scattering from ensembles of configurations of uniformly-random planar scatterers are given in Chapter 4. From these results the approximate theories presented in Chapter 2 are evaluated. In Chapter 5 simulation methods developed for the investigation of non-uniform distributions

of finite-width planar scatterers are presented and scattering results based on these methods given.

Discussed in Chapter 6 is a physical model of a random medium of spherical scatterers which has been developed in this work for use in controlled laboratory experiments at millimeter-wave frequencies. The Monte Carlo method is employed in this model to control the position-statistics of the scatterers. Results of an experimental evaluation of the model are given.

2. THEORETICAL CONSIDERATIONS

2.1 Introduction

Previous theoretical research in the scattering of waves by random media may be divided into three general, related problem areas:

(i) The development of theories for certain average field functions of interest subject to various mathematical models of the random medium.

(ii) The development of theoretical models for the probability density function of the field associated with scattering from a given random medium.

(iii) The development of theories for inverting statistical estimates of average field quantities to determine the physical composition of the random medium.

As stated in Chapter 1, the first two problem areas are considered in this thesis with most of the emphasis being placed on the first.

Two techniques have been used to obtain explicit expressions for the average field functions of interest. Keller⁶ has called these "honest" and "dishonest" methods. In an "honest" method, as applied to random media of discrete scatterers, an explicit expression for the desired field quantity is first determined for a fixed configuration of scatterers. This expression is then directly integrated over the ensemble of configurations using the definition (1.3). In a "dishonest" method, randomness is utilized before an explicit expression for the desired field quantity is obtained. With certain heuristic approximations being made, the defining equation (1.3) is transformed into compact integral or differential equations in the desired average field function. These simpler equations are then solved subject to the boundary conditions of the particular problem at hand.

The "dishonest" technique has been the main theoretical approach for many-scatterer problems in which multiple scattering is considered. It has

advantages over the "honest" technique in that it simplifies the problem to be solved and leads to closed-form expressions for the desired average field functions. Furthermore, the resulting expressions are sometimes sufficiently general to be applicable to distributions of one-, two-, or three-dimensional scatterers. This technique is usually handicapped, however, by the need for employing unproven heuristic approximations.

The "honest" technique, because it requires an explicit field expression for a fixed configuration of scatterers and involves a multiple integration of this expression, is mainly limited to problems involving two or three scatterers or many-scatterer problems in which multiple scattering has either been completely neglected or only partially included. Its application is also limited to a specific scatterer model with the resulting expressions often being less general than expressions obtained by a "dishonest" approach and in series form rather than in closed form. For certain scatterer models, however, the "honest" technique yields more accurate (although more cumbersome) expressions for the various average field functions of interest than does the "dishonest" technique. Also, approximations may be made on a strictly physical basis (usually with respect to the number of multiple-scattering effects included) for the particular scatterer model being considered.

As stated in Chapter 1, throughout the thesis most of the emphasis is placed on the problem of plane-wave scattering from an ensemble of one-dimensionally random configurations of planar scatterers. This model is introduced in section 2.2 and reasons are given for its consideration. For convenience, it is frequently called the "one-dimensional model".

The basic formalism for scattering from a fixed configuration of arbitrary scatterers is presented in section 2.3. In section 2.4 are presented two explicit theories for scattering from a fixed array of planar scatterers,

one of which has been developed in this work to provide a basis for approximate theories for an ensemble of planar-scatterer arrays. Definitions of the average field functions of interest in scattering from an arbitrary ensemble of scatterer configurations are given in section 2.5. The existing general discrete-scatterer theories for average field functions which are studied in detail in this work are also introduced in section 2.5 and a brief mention of some of the previous research in this area is made.

Presented in section 2.6 are approximate series expressions developed in the present work for some of the average field functions of interest in the problem of scattering from an ensemble of uniformly-random planar-scatterer configurations. In section 2.7, asymptotic theories for these average field functions in the limit as the average density of scatterers goes to zero are given. Based on the asymptotic form for the coherent transmitted field in the one-dimensional model, a modification to the one-dimensional form of an existing general discrete-scatterer theory is proposed.

In section 2.8 the more general problem of obtaining a complete statistical representation for the random field in terms of a joint probability density function of its components is discussed. Detailed consideration is given to the one-dimensional model. Generalization of the theories presented in the chapter is discussed in section 2.9 and a summary given in section 2.10.

2.2 The One-Dimensional Model

The model considered in most detail in the thesis is that of an ensemble of configurations of parallel planar scatterers of infinite extent randomly positioned within a slab region of space according to a specified probability density function $p(z_1, \dots, z_N)$ of the scatterer positions z_1, \dots, z_N . A particular configuration from the ensemble is represented in figure 2.1 with "ordered-positions" z'_1, \dots, z'_N satisfying $0 \leq z'_1 < z'_2 < \dots < z'_N \leq d$. A plane

wave incident from the left is scattered by each configuration causing resultant reflected and transmitted waves as indicated. Although they are shown in the diagram as infinitely thin sheets, the one-dimensional scatterers may represent the centers of homogeneous or inhomogeneous dielectric slabs of finite thickness.

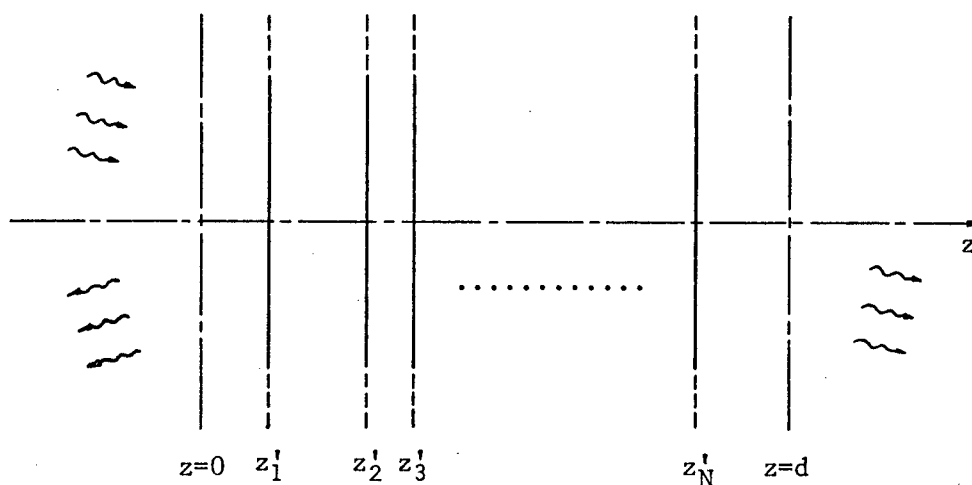


Figure 2.1 The One-Dimensional Model

The main reasons for placing emphasis on this one-dimensional model are as follows:

(i) Certain behavior exhibited by the random field associated with scattering from a one-dimensional random medium of discrete scatterers is also present in more complex random media of discrete scatterers. Thus, a study of the simpler model can to a certain extent contribute to a better understanding of the overall problem.

(ii) The application of Monte Carlo simulation to the problem of scattering from a given ensemble can yield numerical results for the average field quantities which are exact to within a certain statistical error. These "exact" results provide a means of evaluating various approximate theories for the average field quantities. The Monte Carlo technique also allows the complete statistical distribution of the field (e.g., cumulative distribution)

to be sampled as well as the various field moments.

(iii) Certain approximate theories for average field functions which have previously been developed using the "dishonest" technique apply generally to the one-dimensional model and to more complex two- and three-dimensional models of random volume distributions of discrete scatterers. Thus, evaluation of these theories for the one-dimensional model serves to partially evaluate the theories in general, since in principle the approximations involved are independent of any particular model.

(iv) The "honest" technique may be employed for the one-dimensional model to obtain approximate series expressions for the various average field functions. The approximations involved are made on a physical basis in that only lower order multiple-scattering processes are considered. These approximate theories are in general better than existing theories based on the "dishonest" technique and may be used to advantage in improving existing theories.

It should be evident that the choice of this particular one-dimensional model has been based mainly on theoretical considerations. Similar considerations have governed the choice of different one-dimensional models by other workers.⁷ Indeed, many theories developed for models of continuous random media (i.e., perturbed continuum models) have involved randomness in one-dimension only.

Explicit numerical results in the thesis are given only for the special case of normal plane-wave incidence on an ensemble of configurations of N lossless identical planar scatterers. Little is lost by this specialization and it allows different statistical distributions for the scatterer positions to be studied more conveniently. Methods of extending the theory and simulation to the more general cases of oblique incidence, lossy scatterers with random scattering amplitudes, and random N are indicated.

2.3 Basic Formalism for Scattering from a Fixed Configuration of Arbitrary Scatterers

For convenience in this chapter and throughout the thesis a scalar formalism for the field is used. This is a common practice, even for some three-dimensional electromagnetic problems,⁸ and is completely valid for the one-dimensional model. The time factor $e^{j\omega t}$ is also removed from all equations.

For a field $\phi(\bar{r})$ incident on a configuration of N discrete scatterers whose positions and scattering characteristics are specified by $\bar{s}_1, \dots, \bar{s}_N$, the total field at a point \bar{r} outside the scatterers' surfaces is represented by

$$\psi(\bar{s}_1, \dots, \bar{s}_N; \bar{r}) = \phi(\bar{r}) + u(\bar{s}_1, \dots, \bar{s}_N; \bar{r}) \quad (2.1)$$

where u is the total scattered field. The rest of the scattering problem is specified by the conditions at the boundaries of the scatterers, the conditions at infinity, and the scalar Helmholtz equation

$$(\nabla^2 + k^2)\psi = 0, \quad k = 2\pi/\lambda \quad (2.2)$$

Although λ is assumed to be the free-space wavelength, it may equally well be the wavelength of any other medium in which the scatterers are embedded.

The total scattered field may be represented by

$$u(\bar{s}_1, \dots, \bar{s}_N; \bar{r}) = \sum_{s=1}^N U_s(\bar{s}_1, \dots, \bar{s}_N; \bar{r}) \quad (2.3)$$

where U_s is the contribution from scatterer s . Several different representations for U_s and its vector equivalent exist and are useful for three-dimensional problems.^{9,10}

The many-scatterer problem can also be formulated in terms of

isolated scatterer functions.¹¹ The total field is written

$$\psi(\bar{s}_1, \dots, \bar{s}_N; \bar{r}) = \phi(\bar{r}) + \sum_{s=1}^N u_s(\bar{r}-\bar{r}_s) \phi_s(\bar{s}_1, \dots, \bar{s}_N; \bar{r}_s) \quad (2.4)$$

where $u_s(\bar{r})$ is the scattered field due to plane-wave excitation of scatterer s if it were situated alone at the origin. For a three-dimensional scatterer, u_s is of the form of an outgoing spherical wave

$$u_s(\bar{r}) \sim g(\hat{r}, \hat{k}) \frac{e^{-jkr}}{-jkr} \quad (2.5)$$

as $r \rightarrow \infty$. The three-dimensional "scattering amplitude" $g(\hat{r}, \hat{k})$ is a function only of the direction of the incident plane wave and the direction of observation as represented by the unit vectors \hat{k} and \hat{r} .

The quantity ϕ_s is the multiple-scattered "exciting field" for scatterer s and is represented by

$$\phi_s(\bar{s}_1, \dots, \bar{s}_N; \bar{r}_s) = \phi(\bar{r}_s) + \sum_{t=1 \neq s}^N u_t(\bar{r}_s - \bar{r}_t) \phi_t(\bar{s}_1, \dots, \bar{s}_N; \bar{r}_t) \quad (2.6)$$

Essentially, equations (2.4) and (2.6) are operational forms written on the basis of the superposition principle. Since the response of a single scatterer to a plane wave is known, the response to the multiple-scattered exciting field given by (2.6) can in principle be determined by a plane-wave integral expansion of ϕ_s .

The compact forms of (2.4) and (2.6) can be iterated in terms of the isolated scatterer functions u_s and the following expanded form for ψ obtained as an infinite series of "orders-of-scattering":

$$\begin{aligned} \psi(\bar{s}_1, \dots, \bar{s}_N; \bar{r}) = & \phi(\bar{r}) + \sum_s u_s(\bar{r}-\bar{r}_s) \phi(\bar{r}_s) + \sum_s \sum_{t \neq s} u_s(\bar{r}-\bar{r}_s) u_t(\bar{r}_s - \bar{r}_t) \phi(\bar{r}_t) \\ & + \sum_s \sum_{t \neq s} \sum_{m \neq t} u_s(\bar{r}-\bar{r}_s) u_t(\bar{r}_s - \bar{r}_t) u_m(\bar{r}_t - \bar{r}_m) \phi(\bar{r}_m) + \dots \quad (2.7) \end{aligned}$$

A similar form can be obtained for the field intensity $|\psi|^2$.

Because these expansions for ψ and $|\psi|^2$ are quite general and independent of any particular scattering model, they have proved useful in theoretical investigations of the processes of multiple scattering as they effect a configuration of scatterers or an ensemble of configurations.¹¹ Because of the necessity for plane-wave integral expansions of the excitation terms for other than one-dimensional scatterers, however, it is exceedingly difficult for explicit series solutions to be obtained. Furthermore, for particular scattering models they are not always quickly convergent nor necessarily even convergent. A more quickly convergent infinite series expression for the one-dimensional model will be given in the following section.

2.4 Explicit Theories for Scattering from a Fixed Array of Planar Scatterers

Consider now the scattering of a normally incident plane wave $\phi(z) = e^{-jkz}$ from an array of planar scatterers located at z'_1, \dots, z'_N as shown in figure 2.1. For later development of theory for ensembles of arrays it is assumed that the scatterers are located between the planes $z = 0$ and $z = d$ as indicated. The isolated scatterer functions for excitation by $\phi(z)$ are

$$\begin{aligned} u_S(z-z'_S) &= g_{+S} \phi(z-z'_S) & (z > z'_S) \\ u_S(z-z'_S) &= g_{-S} \phi'(z-z'_S) & (z < z'_S) \end{aligned} \tag{2.8}$$

where $\phi'(z) \triangleq e^{jkz}$. The quantities g_{+S} and g_{-S} , termed the forward- and back-scattering amplitudes, are related to the single scatterer transmission and reflection coefficients T_S and R_S by $T_S = 1 + g_{+S}$ and $R_S = g_{-S}$. These quantities are used interchangeably throughout the thesis.

Although the theories to follow are valid for configurations of non-identical scatterers, later numerical results for ensembles of scatterer

configurations are based on configurations of identical scatterers. Numerical values for the scattering amplitudes $g_+ = T_1 - 1$ and $g_- = R_1$ of these identical scatterers are taken to be those for actual dielectric slabs of finite thickness. Explicit expressions for g_+ and g_- are given in Appendix B for a dielectric slab.

In a later development of theory for scattering from an ensemble of uniformly-random planar scatterers, it is assumed that the scatterers are infinitely thin but have finite scattering amplitudes. For the present development, however, the question of finite thickness is immaterial since g_+ and g_- are referred to the scatterer's center.

2.4.1 Wave Transmission Matrix Representation

An exact representation for the total field can be obtained using wave transmission matrices.¹² This theory provides the basis for the "exact" simulation results in the thesis.

Consider the array of planar scatterers shown in figure 2.2.

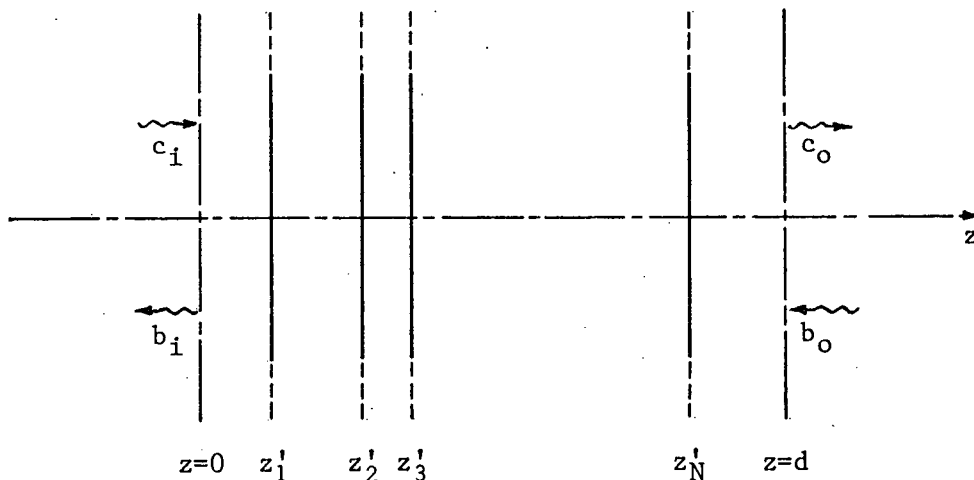


Figure 2.2 Wave Transmission Matrix Representation

The matrix expression relating the complex wave amplitudes c_i, b_i and c_o, b_o at the planes $z = 0$ and $z = d$ is

$$\begin{bmatrix} c_i \\ b_i \end{bmatrix} = \frac{e^{jkd}}{\prod_{s=1}^N T_s} \begin{bmatrix} A_{11} & A_{12} \\ A_{21} & A_{22} \end{bmatrix} \begin{bmatrix} 1 & 0 \\ 0 & e^{-2jk(d-z'_N)} \end{bmatrix} \begin{bmatrix} c_o \\ b_o \end{bmatrix} \quad (2.9)$$

where

$$\begin{bmatrix} A_{11} & A_{12} \\ A_{21} & A_{22} \end{bmatrix} = \prod_{s=1}^N \begin{bmatrix} 1 & 0 \\ 0 & e^{-2jk(z'_s - z'_{s-1})} \end{bmatrix} \begin{bmatrix} 1 & -R_s \\ R_s & T_s^2 - R_s^2 \end{bmatrix} \quad (2.10)$$

(for $s = 1$, $z'_{s-1} \triangleq 0$). Thus, the total field in the forward- and back-scattering regions due to the plane wave incident from the left is

$$\psi(z'_1, \dots, z'_N; z) = T(z'_1, \dots, z'_N) \phi(z) \quad (z > d) \quad (2.11)$$

$$\psi(z'_1, \dots, z'_N; z) = \phi(z) + R(z'_1, \dots, z'_N) \phi'(z) \quad (z < 0) \quad (2.12)$$

where

$$T(z'_1, \dots, z'_N) = e^{jkd} \frac{c_o}{c_i} \Big|_{b_o=0} = \prod_{s=1}^N T_s / A_{11} \quad (2.12)$$

and

$$R(z'_1, \dots, z'_N) = \frac{b_i}{c_i} \Big|_{b_o=0} = \frac{A_{21}}{A_{11}} \quad (2.14)$$

are the overall transmission and reflection coefficients for the array as referred to the plane $z = 0$.

2.4.2 Orders-of-Back-Scattering Representation

Another explicit representation for the total field has been developed in this work. Termed the orders-of-back-scattering (O-B-S) representation, it is useful as a basis for the development of approximate theories for scattering from an ensemble of planar-scatterer configurations.

Consider the scattering diagrams for three scatterers shown in

$$\begin{aligned}
T(z'_1, \dots, z'_N) &= T_0 + T_{II} + T_{IV} + \dots + T_{nth} + \dots \\
R(z'_1, \dots, z'_N) &= R_I + R_{III} + R_V + \dots + R_{nth} + \dots
\end{aligned} \tag{2.15}$$

where

$$\begin{aligned}
T_0 &= \prod_{p=1}^N T_p \\
T_{II} &= \left[\prod_{p=1}^N T_p \right] \sum_{s=2}^N \sum_{t=1}^{s-1} \left[\prod_{q=0}^{s-t-1} T_{t+q}^2 \right] R_s R_t e^{-2jk(z'_s - z'_t)}, \quad T_{t+0} \triangleq 1, \text{ etc.} \\
&\vdots \\
&\vdots \\
T_{nth} &= \left[\prod_{p=1}^N T_p \right] \sum_{s_1=2}^N \sum_{s_2=1}^{s_1-1} \sum_{s_3=s_2+1}^N \dots \sum_{s_n=s_{n-1}+1}^{s_{n-1}-1} \left[\prod_{p_1=0}^{s_1-s_2-1} T_{s_2+p_1}^2 \right] \\
&\quad \left[\prod_{p_2=0}^{s_3-s_4-1} T_{s_4+p_2}^2 \right] \dots \left[\prod_{p_{n/2}=0}^{s_{n-1}-s_n-1} T_{s_{n-1}+p_{n/2}}^2 \right] R_{s_1} R_{s_2} R_{s_3} \dots R_{s_n} \\
&\quad e^{-2jk(z'_{s_1} - z'_{s_2} + z'_{s_3} - \dots - z'_{s_n})} \quad (\text{n even})
\end{aligned} \tag{2.16}$$

and

$$\begin{aligned}
R_I &= \sum_{s=1}^N \left[\prod_{q=0}^{s-1} T_q^2 \right] R_s e^{-2jkz'_s}, \quad T_0 \triangleq 1, \text{ etc.} \\
R_{III} &= \sum_{s=2}^N \sum_{t=1}^{s-1} \sum_{u=t+1}^N \left[\prod_{q=0}^{s-1} T_q^2 \right] \left[\prod_{r=0}^{u-t-1} T_{t+r}^2 \right] R_s R_t R_u e^{-2jk(z'_s - z'_t + z'_u)} \\
&\vdots \\
&\vdots \\
R_{nth} &= \sum_{s_1=2}^N \sum_{s_2=1}^{s_1-1} \sum_{s_3=s_2+1}^N \dots \sum_{s_n=s_{n-1}+1}^{s_{n-1}-1} \left[\prod_{p_1=0}^{s_1-1} T_{p_1}^2 \right] \left[\prod_{p_2=0}^{s_3-s_2-1} T_{s_2+p_2}^2 \right] \dots \\
&\quad \left[\prod_{p_{(n+1)/2}=0}^{s_n-s_{n-1}-1} T_{s_{n-1}+p_{(n+1)/2}}^2 \right] R_{s_1} R_{s_2} R_{s_3} \dots R_{s_n} e^{-2jk(z'_{s_1} - z'_{s_2} + z'_{s_3} - \dots + z'_{s_n})} \\
&\quad (\text{n odd})
\end{aligned} \tag{2.17}$$

These expressions are valid not only for an array of dielectric slabs separated by spaces of the embedded medium, but also for a stack of dielectric slabs with no spaces between their boundaries. Simplification for arrays of identical scatterers is, of course, straightforward.

The O-B-S representation of equations (2.15), (2.16), and (2.17) was obtained by the direct physical approach of successively introducing less dominant multiple-scattering processes contributing to the total field. It may also be obtained (but less easily) by regrouping terms of the orders-of-scattering representation of equation (2.7) on the same physical basis. Thus, the Z-O-B-S contains terms from up to the Nth order-of-scattering, the S-O-B-S contains terms from up to the $(3N - 2)$ th order-of-scattering, and the fourth-order-of-back-scattering (FO-O-B-S) contains terms from up to the $(5N - 4)$ th order-of-scattering, etc. Similarly, terms from up to the $(2N - 1)$, $(4N - 3)$, and $(6N - 5)$ th order-of-scattering contribute to the three dominant O-B-S for the reflected field.

Essentially the same physical approach in terms of ray paths was used by Marcus¹³ to obtain a general series expression for T based also on the reflection and transmission characteristics of the individual "discontinuities" but containing a different grouping of terms. He considered the combinatorial aspects of the problem more thoroughly than has been done in the present work, showing that the series for T could be reduced to the closed-form expression resulting from a matrix approach. In the present work, however, the explicit orders-of-back-scattering forms given for both T and R more readily allow the necessary multiple-scattering approximations to be made in their application to an ensemble of scatterer configurations.

From the numerical results of Chapter 4, convergence of the O-B-S series on an average basis appears to be quick for identical planar scatterers with fairly large back-scattering cross-sections. As shown by Kay and

Silverman,⁷ however, the convergence of the ensemble average of a series expression for a fixed configuration can be faster because of the effects of incoherent scattering in the random case.

Both the wave transmission matrix theory of the previous section and the O-B-S representation can be generalized for plane-wave incidence at an arbitrary angle θ with the normal by the replacement of T_S and R_S with their corresponding values for oblique incidence (see Appendix B) and by the substitution of $k \cos\theta$ for k .

2.5 Scattering from an Ensemble of Scatterer Configurations

2.5.1 Average Field Functions of Interest

The field statistics in the problem of scattering from an ensemble of scatterer configurations are generally related to a normalized field quantity designated $T e^{j\tau}$. For a random medium having the slab-region geometry of figure 2.1 (i.e., bounded by the planes $z = 0$ and $z = d$), this quantity is defined

$$\begin{aligned} T e^{j\tau} &\triangleq \frac{\psi(\bar{s}_1, \dots, \bar{s}_N; \bar{r})}{\phi(\bar{r})} && (z > d) \\ &= T(\bar{s}_1, \dots, \bar{s}_N) \end{aligned} \quad (2.18)$$

in the forward-scattering region and

$$\begin{aligned} T e^{j\tau} &\triangleq \frac{\psi(\bar{s}_1, \dots, \bar{s}_N; \bar{r}) - \phi(\bar{r})}{\phi'(\bar{r})} = \frac{\mathcal{U}(\bar{s}_1, \dots, \bar{s}_N; \bar{r})}{\phi'(\bar{r})} \\ &= R(\bar{s}_1, \dots, \bar{s}_N) && (z < 0) \end{aligned} \quad (2.19)$$

in the back-scattering region. It is commonly called the total field.

Throughout the thesis it will be clear from the context whether use of the term, total field, refers to the actual total field ψ or the normalized total

field as defined in equations (2.18) and (2.19).

The total field is customarily separated into two components^{4,5}

$$T e^{j\tau} = C e^{j\alpha} + I e^{j\phi} \quad (2.20)$$

such that

$$\langle T e^{j\tau} \rangle = C e^{j\alpha}, \quad \langle I e^{j\phi} \rangle = 0 \quad (2.21)$$

The component $C e^{j\alpha}$ is called the "coherent field" and the component $I e^{j\phi}$, the "incoherent" or "variant field". The total, coherent, and incoherent fields are divided into their rectangular components as, for example,

$$\begin{aligned} T e^{j\tau} &= T \cos\tau + jT \sin\tau \\ &= T_x + jT_y \end{aligned} \quad (2.22)$$

such that

$$\begin{aligned} C_x &= \langle T_x \rangle, \quad C_y = \langle T_y \rangle \\ \langle I_x \rangle &= 0, \quad \langle I_y \rangle = 0 \\ \tan\alpha &= C_y / C_x \end{aligned} \quad (2.23)$$

The interrelation of the functions of (2.20) and (2.23) may be represented on a phasor diagram as shown in figure 2.4.

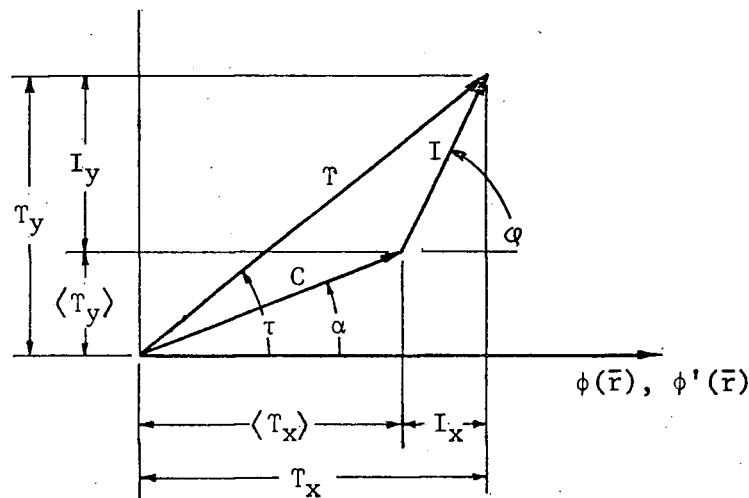


Figure 2.4 Phasor Diagram of the Total Field Resolution

The intensities of the quantities are related by

$$\langle T^2 \rangle = C^2 + \langle I^2 \rangle \quad (2.24)$$

where $\langle T^2 \rangle$ is the "average total intensity", C^2 the "coherent intensity", and $\langle I^2 \rangle$ the "average incoherent intensity". The variances and covariance of the total field components T_x and T_y are given by

$$\begin{aligned} \sigma_{T_x}^2 &= \langle I_x^2 \rangle = \langle T_x^2 \rangle - C_x^2 \\ \sigma_{T_y}^2 &= \langle I_y^2 \rangle = \langle T_y^2 \rangle - C_y^2 \end{aligned} \quad (2.25)$$

$$\mu \sigma_{T_x} \sigma_{T_y} = \langle I_x I_y \rangle = \langle T_x T_y \rangle - C_x C_y$$

where μ is the correlation coefficient between T_x and T_y . These second central moments may also be expressed in terms of the average incoherent intensity $\langle I^2 \rangle$ and a complex function defined^{4,5}

$$\begin{aligned} 2S^2 e^{j2s} &\triangleq \langle I^2 e^{j2\phi} \rangle = \langle (T e^{j\tau} - C e^{j\alpha})^2 \rangle \\ &= \langle T^2 e^{j2\tau} \rangle - C^2 e^{j2\alpha} \end{aligned} \quad (2.26)$$

Thus,

$$\begin{aligned} \langle I_x^2 \rangle &= \frac{1}{2} \langle I^2 \rangle + S^2 \cos 2s \\ \langle I_y^2 \rangle &= \frac{1}{2} \langle I^2 \rangle - S^2 \cos 2s \end{aligned} \quad (2.27)$$

$$\langle I_x I_y \rangle = S^2 \sin 2s$$

and

$$\langle I^2 \rangle = \langle I_x^2 \rangle + \langle I_y^2 \rangle \quad (2.28)$$

$$S^2 \cos 2s = \frac{1}{2} (\langle I_x^2 \rangle - \langle I_y^2 \rangle)$$

Twersky⁵ has termed Se^{js} the "covariant field", S^2 the "covariant intensity", and s the "covariant phase".

Further description of the total field statistics is given by higher central moments of T_x and T_y . In this work the third and fourth central moments $\langle I_x^3 \rangle$, $\langle I_y^3 \rangle$ and $\langle I_x^4 \rangle$, $\langle I_y^4 \rangle$ are used as a measure of the extent to which the joint distribution of T_x and T_y corresponds to a bivariate Gaussian distribution (see section 2.8). Specifically, the "coefficients of skewness"

$$b_x = \frac{\langle I_x^3 \rangle}{\langle I_x^2 \rangle^{3/2}}, \quad b_y = \frac{\langle I_y^3 \rangle}{\langle I_y^2 \rangle^{3/2}} \quad (2.29)$$

and the "coefficients of kurtosis"

$$\gamma_x = \frac{\langle I_x^4 \rangle}{\langle I_x^2 \rangle^2} - 3, \quad \gamma_y = \frac{\langle I_y^4 \rangle}{\langle I_y^2 \rangle^2} - 3 \quad (2.30)$$

are obtained.¹⁴ Expressions for all the higher central moments have been given by Twersky^{4,5} in terms of complex functions $\langle I^n e^{j(n-2m)\phi} \rangle$ [where m ranges from 0 to $n/2$ for the even moments and to $(n-1)/2$ for the odd]. Twersky^{4,5} has also given generalized expressions for the central moments for a change ν in the phase of the reference field [i.e., $\phi(\bar{r})$ and $\phi'(\bar{r})$ in equations (2.18) and (2.19) replaced by $\phi(\bar{r})e^{j\nu}$ and $\phi'(\bar{r})e^{j\nu}$].

Moments of the amplitude T and phase τ of the total field are also of interest. In this work the average field amplitude $\langle T \rangle$ and the average phase $\langle \tau \rangle$ are obtained, as are the variances

$$\begin{aligned} \sigma_T^2 &= \langle T^2 \rangle - \langle T \rangle^2 \\ \sigma_\tau^2 &= \langle \tau^2 \rangle - \langle \tau \rangle^2 \end{aligned} \quad (2.31)$$

Twersky⁴ has obtained the following expansions of these moments to second-order terms in the previously defined moments

$$\langle T \rangle = C + \frac{1}{2C} \left[\frac{1}{2} \langle I^2 \rangle - S^2 \cos 2(s-\alpha) \right] + \dots \quad (2.32)$$

$$\langle \tau \rangle = \alpha - \frac{S^2}{C^2} \sin 2(s-\alpha) + \dots \quad (2.33)$$

$$\sigma_T^2 = \frac{1}{2} \langle I^2 \rangle + S^2 \cos 2(s-\alpha) + \dots \quad (2.34)$$

$$\sigma_T^2 = \frac{1}{C^2} \left[\frac{\langle I^2 \rangle}{2} - S^2 \cos 2(s-\alpha) \right] + \dots \quad (2.35)$$

2.5.2 Some Existing Theories for Average Field Functions

In this section some of the existing contributions to the development of approximate theories for average field functions are briefly mentioned and two coherent field theories for which numerical results are given in the present work are introduced. A more detailed account of previous research is given in the survey papers by Burke¹⁵ and by Twersky.¹⁶

L. Foldy¹⁷ appears to have been the first researcher to apply a "full-wave" treatment to the scattering of waves by random distributions of discrete scatterers. In his 1945 paper, Foldy introduced the concept of obtaining averages of field quantities of interest over an ensemble of scatterer configurations, establishing the basis for nearly all subsequent formulations. Through the use of heuristic approximations for the field ϕ_s exciting a scatterer, he obtained integral expressions for the coherent field, the average total intensity, and the average energy flux for scattering from uniformly-random distributions of isotropic point scatterers. Foldy's treatment of the problem was later generalized by M. Lax^{18,19} to include scattering from distributions of anisotropic point scatterers. Lax introduced further heuristic approximations for the exciting field in order to obtain the necessary integral equations.

More recent theoretical work has been done by Waterman et al.,^{20,21} Mathur and Yeh,²² and Twersky.^{8,11,23-28} Several of Twersky's theories are of particular interest in this thesis because they are sufficiently general to be applicable to random distributions of one-, two-, or three-dimensional scatterers. Much of Twersky's work, furthermore, has been initiated as a

result of experimental research with a physical model of a random medium of discrete scatterers. This type of research is the subject of Chapter 6.

Considered in some detail in the present work are Twersky's "free-space" and "mixed-space" (or "two-space") theories for the coherent field.^{8,24} These theories, which are based on a "dishonest" approach, apply generally to slab-region volume distributions of identical one-, two-, or three-dimensional scatterers. The one-dimensional forms of the theories are summarized in Appendix A and the assumptions and heuristic approximations on which they are based are outlined.

Twersky's free-space theory is most valid for ensembles of scatterer configurations which conform closely to a uniform distribution described by

$$p(\bar{r}_1, \dots, \bar{r}_N) = p(\bar{r}_1) p(\bar{r}_2) \dots p(\bar{r}_N) = (\rho/N)^N \quad (2.36)$$

where ρ is the average density of scatterers in one, two, or three dimensions. A modification to the free-space theory for the coherent transmitted field is proposed in section 2.7 based on the exact asymptotic behavior of $Ce^{j\alpha}$ as $\rho \rightarrow 0$. Numerical results for the one-dimensional form of the theory for the coherent transmitted and reflected fields and the modification to the theory for the coherent transmitted field are compared with "exact" Monte Carlo simulation results for a distribution of uniformly-random planar scatterers in Chapter 4.

As shown by Twersky,²⁴ the mixed-space theory can approximately describe certain dense distributions of finite-size scatterers if the average density ρ is correctly interpreted (see Appendix A). To illustrate the requirements for the approximate validity of the mixed-space theory with ρ interpreted in the correct manner, numerical results for its one-dimensional form are compared with "exact" simulation results for a non-uniform distribution of finite-width planar scatterers in Chapter 5. For completeness and

for later comparison with the results of Chapter 5, results for the mixed-space theory with the actual average density $\rho = N/d$ are also given for uniformly-distributed planar scatterers in Chapter 4.

Other general discrete-scatterer theories for the average incoherent intensity and other average field functions have been developed by Twersky but have not been numerically evaluated for the one-dimensional model in the present work. These are briefly discussed in Appendix A. Theoretical contributions to the study of scattering from non-uniform distributions of scatterers with correlation between the scatterer positions are discussed in Chapter 5.

2.6 Series Approximations for Scattering from an Ensemble of Uniformly-Random Planar-Scatterer Configurations

Considered in this section are certain approximate series expressions developed in the present work for some of the average field functions of interest in the problem of scattering from a distribution of uniformly-random planar scatterers. These series expressions were obtained by the "honest" technique of directly integrating approximate representations for the field functions over the ensemble of scatterer configurations. Although more cumbersome, such series expressions are in general better than closed-form theories developed by means of "dishonest" methods. The primary value of the present theories, however, is considered to be theoretical. They provide a possible means of investigating and eliminating the imperfections of existing closed-form theories based on heuristic approximations, an approach previously illustrated by Twersky.¹¹ Also, they lead naturally to the development of exact asymptotic forms for the average field functions in the limit of $\rho \rightarrow 0$ (see section 2.7).

Direct integration over the ensemble of planar-scatterer

configurations is most easily performed with the use of the joint probability density function for the "ordered-positions" z'_1, \dots, z'_N , i.e.,²⁹

$$p(z'_1, \dots, z'_N) = \frac{N!}{d^N} = N! \left(\frac{\rho}{N}\right)^N \quad (0 \leq z'_1 \leq z'_2 \leq \dots \leq z'_N \leq d) \quad (2.37)$$

The $N!$ multiplier in this function expresses the fact that there are $N!$ permutations of the statistically independent scatterer positions z_1, \dots, z_N in the underlying uniform distribution described by $p(z_1, \dots, z_N) = (\rho/N)^N$. The technique of obtaining approximate series expressions, valid for arbitrary N , is illustrated first for the coherent reflected and transmitted fields.

2.6.1 The Coherent Fields

In order for an explicit series expression for $\langle \psi \rangle$ to be obtained, the reflected field was approximated by the contribution from the F-O-B-S and the transmitted field by the contributions from the Z-O-B-S and the S-O-B-S. Thus, for configurations of identical scatterers,

$$R(z'_1, \dots, z'_N) = R_1 \sum_{s=1}^N T_1^{2(s-1)} e^{-2jkz'_s} \quad (2.38)$$

and

$$T(z'_1, \dots, z'_N) = T_1^N \left[1 + R_1^2 \sum_{s=2}^N \sum_{t=1}^{s-1} T_1^{2(s-t-1)} e^{-2jk(z'_s - z'_t)} \right] \quad (2.39)$$

The integral representations for the ensemble averages of these approximate expressions are then

$$\langle R \rangle = \frac{N! R_1}{d^N} \sum_{s=1}^N T_1^{2(s-1)} \int_0^d \int_0^{z'_N} \dots \int_0^{z'_2} e^{-2jkz'_s} dz'_1 \dots dz'_N \quad (2.40)$$

$$\langle T \rangle = T_1^N \left[1 + \frac{N! R_1^2}{d^N} \sum_{s=2}^N \sum_{t=1}^{s-1} T_1^{2(s-t-1)} \int_0^d \int_0^{z'_N} \dots \int_0^{z'_2} e^{-2jk(z'_s - z'_t)} dz'_1 \dots dz'_N \right] \quad (2.41)$$

The procedure used to obtain general series expressions for $\langle R \rangle$, $\langle T \rangle$, and other average field functions, valid for arbitrary N , was to evaluate the integrals involved for $N = 2$, $N = 3$, $N = 4$, etc., until by induction the general forms could be recognized. Thus, the coherent field expressions determined are

$$\langle R \rangle = R_1 \sum_{n=1}^N \frac{N!}{(N-n)!} \left(\frac{j}{2kd} \right)^n (1 - T_1^2)^{n-1} \left[T_1^{2(N-n)} e^{-2jkd} - 1 \right] \quad (2.42)$$

$$\langle T \rangle = T_1^N \left\{ 1 + R_1^2 \sum_{n=1}^N \frac{N!}{(N-n)!} \left(\frac{j}{2kd} \right)^n (1 - T_1^2)^{n-2} \left[(n-1) T_1^{2(N-n)} e^{-2jkd} + (N-n) T_1^2 - (N-1) \right] \right\} \quad (2.43)$$

Since

$$\frac{N!}{(N-n)!} \left(\frac{j}{2kd} \right)^n \equiv \left(\frac{j}{4\pi} \right)^n \left(\frac{N\lambda}{d} \right)^n \left(1 - \frac{1}{N} \right) \left(1 - \frac{2}{N} \right) \cdots \left(1 - \frac{n-1}{N} \right) \quad (2.44)$$

it is evident that these expressions are finite power series in the average density of scatterers per wavelength $\rho_\lambda = N\lambda/d$. In the limit as $\rho_\lambda \rightarrow 0$, they reduce to

$$\langle R \rangle = \frac{NR_1}{j2kd} \left[1 - T_1^{2(N-1)} e^{-2jkd} \right] \quad (2.45)$$

and

$$\langle T \rangle = T_1^N \quad (2.46)$$

The result of equation (2.46), that the coherent transmitted field in the limit of $\rho_\lambda \rightarrow 0$ is composed only of the term due to in-phase forward scattering (i.e., Z-O-B-S), is exact. The higher O-B-S terms neglected in equation (2.41) all involve exponentials and consequently when integrated over the ensemble would give only terms to first and higher order in ρ_λ . The asymptotic expression of (2.46) is discussed further in section 2.7.

Further examination of the O-B-S representations for R and T reveals that the terms of equations (2.42) and (2.43) for first and higher orders of ρ_λ are the initial terms of infinite series in powers of R_1 corresponding to higher O-B-S. Thus, the expressions obtained for $\langle R \rangle$ and $\langle T \rangle$ can be expected to be good approximations for scatterers with small $|R_1|$. This, of course, is also implied by the initial approximations for R and T. Numerical results given in Chapter 4 confirm this reasoning.

The series expressions of equations (2.42) and (2.43) and those given in the following sections can be generalized for a wave obliquely incident at an arbitrary angle θ with the normal to the slab-region boundaries by a replacement of all occurrences of k with $k\cos\theta$. The oblique-incidence expressions for R_1 and T_1 are given in Appendix B.

2.6.2 The Average Total Intensities

The F-O-B-S approximation was also used to obtain a series expression for the average total intensity of the reflected field. Thus, for configurations of identical scatterers,

$$|R|^2 = |R_1|^2 \sum_{s=1}^N \sum_{t=1}^N T_1^{2(s-1)} T_1^{*2(t-1)} e^{-2jk(z'_s - z'_t)} \quad (2.47)$$

$$= |R_1|^2 \left[\frac{1 - |T_1|^{4N}}{1 - |T_1|^4} \right] + |R_1|^2 \sum_{s=1}^N \sum_{t=1 \neq s}^N T_1^{2(s-1)} T_1^{*2(t-1)} e^{-2jk(z'_s - z'_t)}$$

and

$$\begin{aligned} \langle |R|^2 \rangle = & |R_1|^2 \left[\frac{1 - |T_1|^{4N}}{1 - |T_1|^4} \right] + \frac{N! |R_1|^2}{d^N} \sum_{s=1}^N \sum_{t=1 \neq s}^N T_1^{2(s-1)} T_1^{*2(t-1)} \int_0^d \int_0^{z'_N} \dots \\ & \dots \int_0^{z'_2} e^{-2jk(z'_s - z'_t)} dz'_1 \dots dz'_N \quad (2.48) \end{aligned}$$

Evaluation of the integral of (2.48) gives

$$\langle |R|^2 \rangle = |R_1|^2 \left[\frac{1 - |T_1|^{4N}}{1 - |T_1|^4} \right] + 2|R_1|^2 \sum_{n=1}^N \frac{N!}{(N-n)!} \left(\frac{1}{2kd} \right)^n \left\{ \begin{array}{l} \frac{n+3}{2} \text{Im} \\ \frac{n+2}{2} \text{Re} \end{array} \right. \\ \left. \sum_{m=1}^n (-1)^{m+1} B_{nm} \left(T_1^{2m} \left[\frac{1 - |T_1|^{4(N-m)}}{1 - |T_1|^4} \right] - T_1^{2(N-n+m)} \left[\frac{1 - |T_1|^{4(n-m)}}{1 - |T_1|^4} \right] e^{-2jkd} \right) \right\} \quad (2.49)$$

where the B_{nm} are the well-known binomial coefficients defined by

$$B_{nm} = \binom{n-1}{m-1} = \frac{(n-1)!}{(n-m)!(m-1)!} \quad (2.50)$$

The factors $(-1)^{\frac{n+3}{2}}$ and $(-1)^{\frac{n+2}{2}}$ in equation (2.49) provide the signs for the terms of the summation and are used alternately for odd n and even n .

Similarly, for odd n the imaginary part of the second summation is taken, and for even n the real part is taken.

The first term of equation (2.49) gives the approximate form for $\langle |R|^2 \rangle$ and also $\langle I^2 \rangle = \langle |R|^2 \rangle - \langle |R| \rangle^2$ in the limit of $\rho_\lambda \rightarrow 0$. The exact infinite series form for all O-B-S contributing to the reflected field is given in section 2.7. Results from the numerical evaluation of equation (2.49) are compared with "exact" simulation results in Chapter 4.

The total intensity of the transmitted field for a S-O-B-S approximation applied to configurations of identical planar scatterers can similarly be written

$$|T|^2 = |T_1|^{2N} \left[1 + 2\text{Re}(R_1^2 \zeta_1) + a_{11} |R_1|^4 + \zeta_2 |R_1|^4 \right] \quad (2.51)$$

where

$$a_{11} = \sum_{s=2}^N \sum_{t=1}^{s-1} |T_1|^{4(s-t-1)} = \sum_{i=1}^{N-1} (N-i) |T_1|^{4(i-1)} \quad (2.52)$$

$$\zeta_1 = \sum_{s=2}^N \sum_{t=1}^{s-1} T_1^{2(s-t-1)} e^{-2jk(z'_s - z'_t)} \quad (2.53)$$

$$\zeta_2 = \sum_{s=2}^N \sum_{t=1}^{s-1} \sum_{u=2}^N \sum_{v=1}^{u-1} T_1^{2(s-t-1)} T_1^{*2(u-v-1)} e^{-2jk(z'_s - z'_t - z'_u + z'_v)} \quad (2.54)$$

[The primes on the third and fourth summation of (2.54) indicate that u and v cannot simultaneously equal s and t respectively.] Thus, the average total intensity can be represented by

$$\langle |T|^2 \rangle = |T_1|^{2N} \left[1 + 2\text{Re}(R_1^2 \langle \zeta_1 \rangle) + a_{11} |R_1|^4 + \langle \zeta_2 \rangle |R_1|^4 \right] \quad (2.55)$$

The summation average $\langle \zeta_1 \rangle$ can easily be obtained from the expression for $\langle T \rangle$, i.e.,

$$\langle \zeta_1 \rangle = \sum_{n=1}^N \frac{N!}{(N-n)!} \left(\frac{j}{2kd} \right)^n (1 - T_1^2)^{n-2} \left[(n-1) T_1^{2(N-n)} e^{-2jkd} + (N-n) T_1^2 - (N-1) \right] \quad (2.56)$$

The summation average $\langle \zeta_2 \rangle$, represented by

$$\begin{aligned} \langle \zeta_2 \rangle = \frac{N!}{d^N} \sum_{s=2}^N \sum_{t=1}^{s-1} \sum_{u=2}^N \sum_{v=1}^{u-1} T_1^{2(s-t-1)} T_1^{*2(u-v-1)} \int_0^d \int_0^{z'_N} \dots \\ \dots \int_0^{z'_2} e^{-2jk(z'_s - z'_t - z'_u + z'_v)} dz'_1 \dots dz'_N \end{aligned} \quad (2.57)$$

has not been determined in the present work because of the difficulty involved in recognizing the general expression for arbitrary N by the induction procedure. Instead, results for $\langle |T|^2 \rangle$ have been obtained by an application of Monte Carlo simulation to the S-O-B-S approximation for T .

The third term of equation (2.55) gives the approximate form for $\langle I^2 \rangle = \langle |T|^2 \rangle - |\langle T \rangle|^2$ in the limit of $\rho_\lambda \rightarrow 0$. The exact infinite series form for all O-B-S contributing to the transmitted field is given in section 2.7.

The first two terms of (2.55) contribute to the coherent intensity only. The fourth term contributes both to the coherent and incoherent intensities. Without its evaluation, only the zeroth-order ρ_λ term in the power series for $\langle I^2 \rangle$ [i.e., third term of equation (2.55)] is available.

2.6.3 The Covariant Fields

It is evident from equations (2.27) that an explicit expression for the complex function $2S^2 e^{j2s} = \langle T^2 e^{j2\tau} \rangle - C^2 e^{j2\alpha}$ provides a means of evaluating the second central moments of the total field. Thus, since approximate series have already been given for the coherent fields, only the function $\langle T^2 e^{j2\tau} \rangle$ remains. In the present work, a series expression has been obtained for the reflected field function $\langle T^2 e^{j2\tau} \rangle = \langle R^2 \rangle$ based on the F-O-B-S approximation.

For configurations of identical planar scatterers, the basic equations are

$$\begin{aligned} R^2 &= R_1^2 \sum_{s=1}^N T_1^{4(s-1)} e^{-4jkz'_s} + R_1^2 \sum_{s=1}^N \sum_{t=1 \neq s}^N T_1^{2(s+t-2)} e^{-2jk(z'_s+z'_t)} \\ &= R_1^2 \zeta_3 + R_1^2 \zeta_4 \end{aligned} \quad (2.58)$$

and

$$\langle R^2 \rangle = R_1^2 \langle \zeta_3 \rangle + R_1^2 \langle \zeta_4 \rangle$$

$$\langle \zeta_3 \rangle = \frac{N!}{d^N} \sum_{s=1}^N T_1^{4(s-1)} \int_0^d \int_0^{z'_N} \dots \int_0^{z'_2} e^{-4jkz'_s} dz'_1 \dots dz'_N \quad (2.59)$$

$$\langle \zeta_4 \rangle = \frac{N!}{d^N} \sum_{s=1}^N \sum_{t=1 \neq s}^N T_1^{2(s+t-2)} \int_0^d \int_0^{z'_N} \dots \int_0^{z'_2} e^{-2jk(z'_s+z'_t)} dz'_1 \dots dz'_N$$

The series expression for $\langle \zeta_3 \rangle$ can be obtained by inspection of the expression determined for $\langle R \rangle$. Straightforward integration and induction must be used to

evaluate $\langle \zeta_4 \rangle$ for arbitrary N . Thus,

$$\langle \zeta_3 \rangle = \sum_{n=1}^N \frac{N!}{(N-n)!} \left(\frac{j}{4kd} \right)^n (1 - T_1^4)^{n-1} \left[T_1^{4(N-n)} e^{-4jkd} - 1 \right] \quad (2.60)$$

$$\langle \zeta_4 \rangle = T_1^2 \sum_{n=1}^N \frac{N!}{(N-n)!} \left(\frac{j}{2kd} \right)^n \left(\frac{1 - T_1^2}{2} \right)^{n-2} \left[T_1^{2(N-n)} e^{-2jkd} - 1 \right]$$

$$\sum_{m=1}^{n-1} C_{nm} \left[T_1^{2(N-n+m-1)} e^{-2jkd} - T_1^{2(n-m-1)} \right] \quad (2.61)$$

The constant coefficients C_{nm} are defined in terms of the binomial coefficients B_{nm} by

$$C_{n1} = 1 \quad (n = 2, \dots, N)$$

$$C_{nm} = C_{n(m-1)} + B_{nm} \quad (n = 3, \dots, N; m = 2, \dots, n-1) \quad (2.62)$$

They may also be generated from the recurrence relations

$$C_{n1} = 1 \quad (n = 2, \dots, N)$$

$$C_{nm} = C_{(n-1)(m-1)} + C_{(n-1)m} \quad (n = 3, \dots, N; m = 2, \dots, n-2) \quad (2.63)$$

$$C_{n(n-1)} = 2C_{(n-1)(n-2)} + 1 \quad (n = 3, \dots, N)$$

Approximate series expressions have not been determined for $\langle T^2 e^{j2\tau} \rangle = \langle T^2 \rangle$ in the present work. Instead, results have been obtained for the second central moments of the transmitted field in the S-O-B-S approximation by employment of the simulation technique. The future development of approximate series for both $\langle T^2 e^{j2\tau} \rangle$ and $\langle T^2 \rangle$, however, would allow both the approximate evaluation of the second central moments for T_x and T_y and also, from equations (2.32) to (2.35), the approximate evaluation of the first two moments of the amplitude T and phase τ .

2.7 Asymptotic Theories for Scattering from Low Average Density Scatterer Distributions

A study of scattering from random media of discrete scatterers in the asymptotic region of $\rho \rightarrow 0$ is important for two reasons:

- (i) The constituent scatterers are only sparsely distributed for many naturally-occurring media of interest.
- (ii) The further development of theories for more densely-packed scatterer distributions would be facilitated through the understanding of the scattering behavior of such distributions in the region of low ρ .

In this section, asymptotic theories developed in the present work for the one-dimensional ensemble of planar-scatterer configurations are given and, based on these asymptotic theories, modifications to existing theories applicable to higher density distributions are proposed. Consideration is also given to similarities between the asymptotic coherent transmitted field theory for the one-dimensional distribution and an approximate theory developed by Twersky to describe certain distributions of three-dimensional scatterers.

2.7.1 Asymptotic Theory for the Coherent Transmitted Field

As shown in the previous section, for $\rho_\lambda = N\lambda/d \rightarrow 0$, the coherent transmitted field for the one-dimensional ensemble of uniformly-distributed identical planar scatterers reduces to the simple form

$$\langle T \rangle \phi = (1 + g_+)^N \phi = T_1^N \phi \quad (2.64)$$

the contribution to the total field from the Z-O-B-S. The contributions from the higher O-B-S are therefore entirely incoherent. This is a physically reasonable result since the actual phases of the higher order terms vary over many lengths of the basic phase cycle (0 to 2π), making the equivalent phases on the basic phase cycle effectively uniformly distributed (see section 2.8).

Twersky¹¹ has obtained a similar result for a uniform slab-region

distribution of three-dimensional "forward-type" scatterers such that the scattering amplitude is "tightly peaked" around the forward-scattering direction. In the integral version of the orders-of-scattering series (2.7) for the coherent field, he ignored those terms corresponding to a "back-and-forth" interaction between pairs of scatterers; equivalently, he retained only those successive scattering terms in which all scatterers are different. Using the method of stationary phase for performing the integrations in the coordinates parallel to the slab region, he obtained an explicit series form for $\langle \psi \rangle$ which reduced to the closed-form expression

$$\langle T \rangle \phi = \left[1 + \frac{2\pi\rho dg(\hat{z}, \hat{z})}{k^2 N} \right]^N \phi \equiv \left[1 + \frac{2\pi g(\hat{z}, \hat{z})}{k^2 A} \right]^N \phi \quad (2.65)$$

where $g(\hat{z}, \hat{z})$ is the forward-scattering amplitude for three-dimensional scatterers, $\rho = N/V = N/Ad$ is the average volume density, V is the volume of the finite slab region, and A its area. Twersky also showed this result to be valid for a spherical source wave ϕ .

Twersky has compared the expression in (2.65) to that obtained for planar scatterers whose forward-scattering amplitudes are $g_+ = 2\pi g(\hat{z}, \hat{z})/k^2 A$ and whose back-scattering amplitudes are zero. In view of the present results for planar scatterers, the comparison does not require the restriction to planar scatterers with zero back-scattering amplitudes in the limit of $\rho \rightarrow 0$. This would seem to suggest also that the restriction to "forward-type" scatterers in the three-dimensional medium is also unnecessary for $\rho \rightarrow 0$. Indeed, the physical reasoning used to explain equation (2.64) appears to be equally valid in the three-dimensional case. The multiple-scattering terms neglected by Twersky in the derivation of (2.65) are all higher-order extensions of those included, containing in addition one or more orders of scattering between one or more pairs of scatterers. For an average path length between

scatterers of many wavelengths, these additional terms should be completely incoherent.

As shown by Twersky, as $N \rightarrow \infty$ the result of (2.65) becomes identical to the corresponding result obtained by using the "forward-type" scatterer restriction in the approximate integral equation for $\langle \psi \rangle$, i.e.,

$$\left(1 + \frac{\Delta d}{N}\right)^N \rightarrow e^{\Delta d} \quad \text{as } N \rightarrow \infty \quad (2.66)$$

where $\Delta = 2\pi\rho g(\hat{z}, \hat{z})/k^2$. The form $\langle T \rangle = e^{\Delta d}$ is a special case of Twersky's free-space theory equation with either the "forward-type" scatterer restriction or the restriction $\rho \approx 0$. The result of (2.66) therefore illuminates one of the main limitations of the approximate integral equation and the free-space theory based on it.

The one-dimensional equivalent of the form $\langle T \rangle = e^{\Delta d}$ is $\langle T \rangle = e^{Ng_+}$, the asymptotic form for $\rho_\lambda \rightarrow 0$ given in equation (A.14) of Appendix A. However, for the one-dimensional planar-scatterer distribution, $\langle T \rangle = e^{Ng_+}$ becomes equivalent to the exact result of equation (2.64) only in the trivial case of $\langle T \rangle \rightarrow 0$. Since equation (2.64) is the exact expression for finite N and $\rho_\lambda \rightarrow 0$, it seems plausible to modify the general free-space theory equation

$$\langle T \rangle = D(1 - Q^2) e^{-j(n-1)kd} \quad (2.67)$$

[given also as equation (A.10) in Appendix A; see section A.1 for definition of symbols] to give the correct result in the limit $\rho_\lambda \rightarrow 0$. The modification required is contained in the equation

$$\langle T \rangle = (1 + g_+)^N + \left[D(1 - Q^2) e^{-j(n-1)kd} - e^{Ng_+} \right] \quad (2.68)$$

As shown in Chapter 4, this modification for finite N gives numerical results very close to the actual results (as obtained by Monte Carlo simulation) over

a wide range of ρ_λ . The results, in fact, are better than those obtained from the S-O-B-S approximation for $\langle T \rangle$ as given in equation (2.43). Further theoretical investigation should reveal the reason for the improvement for high ρ_λ as well as low ρ_λ .

Because of the improvement acquired by an asymptotic modification to the free-space theory for the one-dimensional medium with finite N , it is tempting to suggest a similar modification to the free-space theory for a three-dimensional medium based on equation (2.65). However, despite the marked similarities, the coherent field properties of a three-dimensional medium are not identical to those of a one-dimensional medium. In the one-dimensional medium, for example, $\langle T \rangle \rightarrow 0$ as $N \rightarrow \infty$; in the three-dimensional medium $\langle T \rangle$ remains finite for $N \rightarrow \infty$ with $\rho = N/V$ constant. In reference 11 Twersky indicates that corrections for finite N are of interest but states in reference 27 that no practical error results for "forward-type" scatterers and low N in using either equation (2.65) or the free-space theory form $e^{\Delta d}$. The reason for this result is readily apparent, since calculations for the "forward-type" scatterers considered by Twersky give $|\Delta d/N| \ll 1$. Similarly, for planar scatterers with $|g_+| \ll 1$, $e^{Ng_+} \approx (1 + g_+)^N$ even for finite N , as is verified by the numerical results of Chapters 4 and 5. Further investigation is required for three-dimensional distributions, however, to determine which practical combinations of distribution parameters and individual scatterer cross-sections make finite- N corrections necessary and whether the suggested modification to the free-space theory for such distributions is valid.

2.7.2 Asymptotic Theories for the Average Total Field Intensities

The problem of determining the asymptotic expressions for the average total intensities (and correspondingly the average incoherent intensities) is a difficult one because an infinite number of multiple-scattering processes contribute to the incoherent field. Emphasis is therefore again

placed on the one-dimensional model.

The total intensity of the transmitted field for a fixed array of planar scatterers can be written

$$|T|^2 = T_0(T_0^* + T_{II}^* + T_{IV}^* + \dots) + T_{II}(T_0^* + T_{II}^* + T_{IV}^* + \dots) + \dots \quad (2.69)$$

where the components T_0 , T_{II} , etc., are given in equation (2.16). From the results of section 2.6 it is evident that the ensemble averages of the terms in (2.69) are of the infinite series form

$$c_0 + c_1 \left(\frac{N}{kd} \right) + c_2 \left(\frac{N}{kd} \right)^2 + \dots \quad (2.70)$$

where the coefficients c_0 , c_1 , c_2 , etc., are functions of the planar-scatterer parameters. Only the terms of (2.69) involving no exponentials contribute to the c_0 coefficients, and thus it is these terms which contribute to the asymptotic form for $\langle |T|^2 \rangle$. The asymptotic expression may therefore be represented as

$$\begin{aligned} \langle |T|^2 \rangle = & T_0 T_0^* + \text{As} [T_{II} T_{II}^*] + \text{As} [2\text{Re}(T_{IV} T_{II}^*) + T_{IV} T_{IV}^*] \\ & + \text{As} [2\text{Re}(T_{VI} T_{II}^*) + 2\text{Re}(T_{VI} T_{IV}^*) + T_{VI} T_{VI}^*] + \dots \end{aligned} \quad (2.71)$$

where "As" implies that the asymptotic form of the expression in brackets is to be taken.

For an ensemble of identical scatterers, the explicit form of equation (2.71) is

$$\begin{aligned} \langle |T|^2 \rangle = & |T_1|^{2N} \left\{ 1 + a_{11} |R_1|^4 + \left[a_{21} \text{Re}(R_1 T_1^*)^2 |R_1|^4 + a_{22} |R_1|^8 \right] + \dots \right\} \\ = & |T_1|^{2N} \left[1 + \sum_{n=1}^{\infty} \sum_{m=1}^n a_{nm} \text{Re}(R_1 T_1^*)^{2(n-m)} |R_1|^{4m} \right] \end{aligned} \quad (2.72)$$

where the coefficients a_{nm} are real functions of T_1 and N . The first three

coefficients are

$$a_{11} = \sum_{s=2}^N \sum_{t=1}^{s-1} |T_1|^{4(s-t-1)} = \sum_{i=1}^{N-1} (N-i) |T_1|^{4(i-1)} \quad (N = 2, 3, \dots) \quad (2.73)$$

$$a_{21} = \begin{cases} 0 & (N = 2) \\ 2 \sum_{s=2}^{N-1} \sum_{t=1}^{s-1} \sum_{u=s+1}^N |T_1|^{4(u-t-2)} & (N = 3, 4, \dots) \end{cases} \quad (2.74)$$

$$a_{22} = \sum_{s=2}^N \sum_{t=1}^{s-1} \sum_{u=t+1}^N \sum_{v=1}^{u-1} |T_1|^{4(s+u-t-v-2)} \quad (N = 2, 3, \dots) \quad (2.75)$$

As seen from equation (2.72), the asymptotic form cannot be reduced to a sum of contributions from each O-B-S; there are also "cross terms" (i.e., $m \neq n$) contributed by sets of two O-B-S.

From equations (2.64) and (2.72), the asymptotic expression for the average incoherent intensity in the S-O-B-S approximation is

$$\langle I^2 \rangle \approx |T_1|^{2N} a_{11} |R_1|^4 \quad (2.76)$$

As shown in Chapter 4, this approximation gives results in close agreement with "exact" results for a wide range of the parameters $|R_1|$ and N .

The infinite-series asymptotic form for the average total intensity of the reflected field is obtained in a similar manner to that for the transmitted field. The explicit expression for an ensemble of identical planar scatterers is

$$\langle |R|^2 \rangle = \sum_{n=1}^{\infty} \sum_{m=1}^n b_{nm} \operatorname{Re}(R_1 T_1^*)^{2(n-m)} |R_1|^{2(2m-1)} \quad (2.77)$$

where $b_{n1} = 0$ for $n \geq 2$ (i.e., all cross terms between the F-O-B-S and higher O-B-S are zero) and the other coefficients b_{nm} are real functions of $|T_1|$ and N .

The first two coefficients are

$$b_{11} = \sum_{s=1}^N |T_1|^{4(s-1)} = \frac{1 - |T_1|^{4N}}{1 - |T_1|^4} \quad (2.78)$$

$$b_{22} = \sum_{s=2}^N \sum_{t=1}^{s-1} \sum_{u=t+1}^N |T_1|^{4(s+u-t-2)} \quad (2.79)$$

Since $|\langle R \rangle|^2 \rightarrow 0$ as $\rho_\lambda \rightarrow 0$, the asymptotic series for $\langle I^2 \rangle$ is also given by equation (2.77).

As shown in Chapter 4, the F-O-B-S term of (2.77),

$$\langle I^2 \rangle \approx b_{11} |R_1|^2 \quad (2.80)$$

gives results in close agreement with "exact" results for a wide range of $|R_1|$ and N . Better agreement is obtained with the addition of the T-O-B-S term, i.e.,

$$\langle I^2 \rangle \approx b_{11} |R_1|^2 + b_{22} |R_1|^6 \quad (2.81)$$

The F-O-B-S approximation for $\langle |R|^2 \rangle$ of equation (2.49) can be improved for a wide range of ρ_λ with the use of more accurate asymptotic terms, such as that of (2.81). The result of this asymptotic modification to the F-O-B-S theory is shown in Chapter 4.

An examination of equations (2.76) and (2.80) reveals that to first order, $\langle I^2 \rangle \propto |R_1|^4 = |g_-|^4$ for the transmitted field and $\langle I^2 \rangle \propto |R_1|^2 = |g_-|^2$ for the reflected field. This result is in marked contrast to that given by equations (A.22) and (A.23) of Appendix A for Twersky's approximation based on the conservation of energy principle. As shown by these equations for the one-dimensional ensemble, the incoherent power is divided approximately equally between the transmitted and reflected fields, with $\langle I^2 \rangle$ for the transmitted field also approximately proportional to $|g_-|^2$. Since the O-B-S approximations

for the average intensities do not satisfy the energy principle, but give very accurate results as shown in Chapter 4, it is evident that little importance should be attached to complete adherence to this principle except under special conditions. For the "forward-type" scatterers considered by Twersky¹¹ this principle must be satisfied for the accuracy of the theories for $|\langle T \rangle|^2$ and $\langle |T|^2 \rangle$ to be equivalent.

2.8 Theoretical Models for the Probability Density of the Total Field

The statistics of the total field associated with scattering from a random medium cannot completely be defined until the joint probability density function, $p(T_x, T_y)$ or $p(T, \tau)$, of the field components has been obtained. Because the problem of completely specifying $p(T_x, T_y)$ is a particularly difficult one, especially for the one-dimensional model where multiple scattering is important, more emphasis has been placed in the thesis on the problem of determining the field moments. A partial investigation has been carried out for an ensemble of uniformly-random planar scatterers, however, to determine the extent to which T_x and T_y conform to a bivariate Gaussian distribution for certain ranges of parameters. The results are given in Chapter 4.

The commonly used approach in the development of theoretical models for the field statistics has been to investigate the properties of random phasor sums of the form

$$T e^{j\tau} = A_0 e^{j\theta_0} + \sum_{s=1}^N A_s e^{j\theta_s} \quad (2.82)$$

on the basis of known statistical properties of the A_s and θ_s . In this expression $A_0 e^{j\theta_0}$ is usually a constant phasor and the phasors $A_s e^{j\theta_s}$ are random and in general statistically dependent. Many workers have investigated this problem area, including Beckmann,^{3,30-32} Bremmer,³³ Hoyt,³⁴ Nakagami,³⁵

Norton et al.,³⁶ and Rice.³⁷

The general method used in the solution of the problem has been to begin with a study of the statistical properties of the components

$$T_x = T \cos \tau = A_0 \cos \theta_0 + \sum_{s=1}^N A_s \cos \theta_s \quad (2.83)$$

$$T_y = T \sin \tau = A_0 \sin \theta_0 + \sum_{s=1}^N A_s \sin \theta_s$$

If the terms of the sums in these expressions are statistically independent, if N is large, and if the total variances of T_x and T_y are much larger than the variances of the individual terms (i.e., the conditions of the Central Limit Theorem), then T_x and T_y are jointly Gaussian with probability density function³

$$p(T_x, T_y) = \frac{1}{2\pi \sqrt{\langle I_x^2 \rangle \langle I_y^2 \rangle (1-\mu^2)}} \exp \left\{ -\frac{1}{2(1-\mu^2)} \left[\frac{(T_x - C_x)^2}{\langle I_x^2 \rangle} - 2\mu \frac{(T_x - C_x)(T_y - C_y)}{\sqrt{\langle I_x^2 \rangle \langle I_y^2 \rangle}} + \frac{(T_y - C_y)^2}{\langle I_y^2 \rangle} \right] \right\} \quad (2.84)$$

For T_x and T_y conforming to this distribution, a variety of amplitude distributions $p(T)$ and phase distributions $p(\tau)$ are possible. These are obtained by transforming to polar coordinates from

$$p(T, \tau) = T p(T_x, T_y) \quad (2.85)$$

and using the relations

$$p(T) = \int_0^{2\pi} p(T, \tau) d\tau \quad (0 \leq \tau \leq 2\pi) \quad (2.86)$$

$$p(\tau) = \int_0^{\infty} p(T, \tau) dT \quad (0 \leq T)$$

The most general expression for $p(T)$ under the given conditions has been obtained by Nakagami.³⁵ Less general relations for specific distributions $p(A_s, \theta_s)$ of the components of the random phasor sum have been obtained or studied by the other researchers mentioned.

Of specific interest in this work is the distribution

$$p(T, \tau) = \frac{T}{2\pi\tilde{\sigma}^2} e^{-T^2/2\tilde{\sigma}^2} \quad (0 \leq T, 0 \leq \tau \leq 2\pi) \quad (2.87)$$

$$\langle I_x^2 \rangle = \langle I_y^2 \rangle = \frac{1}{2} \sum_{s=1}^N \langle A_s^2 \rangle \triangleq \tilde{\sigma}^2, \quad \mu = 0$$

which occurs when (a) the constant phasor of equation (2.82) is zero, (b) the phases θ_s are uniformly distributed over the basic phase cycle, i.e.,

$$p(\theta_s) = \frac{1}{2\pi} \quad (0 \leq \theta_s \leq 2\pi) \quad (2.88)$$

and (c) the A_s and θ_s are mutually uncorrelated. Under these conditions the phase τ is uniformly distributed over the basic phase cycle and the amplitude T follows the well-known Rayleigh distribution

$$p(T) = \frac{T}{\tilde{\sigma}^2} e^{-T^2/2\tilde{\sigma}^2} \quad (2.89)$$

Also of interest is the Nakagami-Rice distribution for the amplitude^{35,37}

$$p(T) = \frac{T}{\tilde{\sigma}^2} e^{-(T^2+A_0^2)/2\tilde{\sigma}^2} I_0\left(\frac{TA_0}{\tilde{\sigma}^2}\right) \quad (2.90)$$

where I_0 is the modified Bessel function of order zero. This distribution arises when the constant phasor in equation (2.82) is not equal to zero. The corresponding distribution for the phase is³³

$$p(\tau) = \frac{1}{2\pi} e^{-A_0^2/2\tilde{\sigma}^2} \left[1 + G\sqrt{\pi}e^{G^2}(1 + \operatorname{erf}G) \right], \quad G = \frac{A_0 \cos(\tau - \theta_0)}{\sqrt{2}\tilde{\sigma}} \quad (2.91)$$

The statistical behavior of the total field for the one-dimensional model can to a certain extent be predicted by observation of the first and second O-B-S approximations for the reflected and transmitted fields. For identical scatterers these are respectively

$$T e^{j\tau} = R_1 \sum_{s=1}^N T_1^{2(s-1)} e^{-2jkz'_s} \quad (2.92)$$

and

$$T e^{j\tau} = T_1^N + T_1^N R_1^2 \sum_{s=2}^N \sum_{t=1}^{s-1} T_1^{2(s-t-1)} e^{-2jk(z'_s - z'_t)} \quad (2.93)$$

The resulting amplitude and phase components for the reflected field corresponding to the A_s and θ_s of equation (2.82) are therefore

$$\begin{aligned} A_0 &= 0 \\ A_s &= |R_1| |T_1|^{2(s-1)} \quad (s = 1, \dots, N) \\ \theta_s &= \text{Arg}R_1 + 2(s-1) \text{Arg}T_1 - 2kz'_s \quad (s = 1, \dots, N) \end{aligned} \quad (2.94)$$

The components for the transmitted field can be obtained by rewriting (2.93) as

$$T e^{j\tau} = T_1^N + T_1^N R_1^2 \sum_{i=1}^{N(N-1)/2} T_1^{2(q_i-1)} e^{-2jkz'_i} \quad (2.95)$$

where $z'_i = z'_s - z'_t$ and $q_i = s - t$. Thus,

$$\begin{aligned} A_0 e^{j\theta_0} &= T_1^N \\ A_i &= |R_1|^2 |T_1|^{N+2(q_i-1)} \quad [i = 1, \dots, N(N-1)/2] \\ \theta_i &= 2 \text{Arg}R_1 + [N + 2(q_i-1)] \text{Arg}T_1 - 2kz'_i \quad [i = 1, \dots, N(N-1)/2] \end{aligned} \quad (2.96)$$

Since the ordered-positions z'_1, \dots, z'_N in equation (2.92) are

statistically dependent, the problem of predicting the statistical behavior of the reflected field is seen to be a difficult one in general. For specific ensembles of planar scatterers in which the θ_s assume values over many lengths of the basic phase cycle, however, it is felt that this dependence can to a certain extent be ignored. Under this condition, which occurs for low average densities of scatterers (i.e., $\rho_\lambda \ll 1$), it is useful to write the individual phase distributions over the basic phase cycle in the form³

$$p(\theta_s) = \frac{1}{2\pi} + \epsilon_s(\theta_s) \quad (0 \leq \theta_s \leq 2\pi; s = 1, \dots, N) \quad (2.97)$$

Since $|\epsilon_s| \ll 1/2\pi$ for $\rho_\lambda \ll 1$, the equivalent θ_s are effectively uniformly distributed over the basic phase cycle. They should also be less correlated than the actual θ_s . As $|T_1| \rightarrow 1$, T_x and T_y will be uncorrelated and normally distributed for large N , and τ will correspondingly be Rayleigh distributed. As $|T_1| \rightarrow 0$, however, the $s = 1$ term in (2.92) contributed by the first scatterer will predominate over the others, eventually breaking the "variance condition" of the Central Limit Theorem and making the resulting reflected field distribution more complex.

The problem of predicting the transmitted field distribution is even more difficult. The terms in equation (2.95) corresponding to $q_i = 1$ have equal amplitudes $A_i = |T_1|^N |R_1|^2$ and will predominate over the other terms for $|T_1| \rightarrow 0$. Under this condition it can be expected that the distributions of T_x and T_y will be approximately Gaussian for large N . However, the equivalent phases θ_i over the basic phase cycle are highly correlated, irrespective of the number of cycles over which the actual phases vary, since the θ_i for the $q_i = 1$ terms add to give the θ_i for the less dominant terms. As $|T_1| \rightarrow 1$ these other terms will therefore become more important, making the distribution more complex.

2.9 Other Theoretical Considerations

Generalization of the theories presented in this chapter to the cases of oblique incidence and lossy scatterers is straightforward and the changes have been indicated where applicable. Two other extensions not yet discussed involve the cases of random N and random g_{+s} and g_{-s} .

The case of a random number of scatterers N within the incident beam is an important consideration in such problems as scattering from inhomogeneities in the atmosphere and meteor trails. A more immediate example of this situation is illustrated with the physical model of a random discrete-scatterer medium discussed in Chapter 6. Here the number of spheres illuminated by a narrow-beam transmitting antenna varies randomly as the medium is "scanned".

In the development of most approximate theories for the average field functions based on the "dishonest" approach, the random- N consideration is not important. The fixed- N requirement inherent in the definition (1.3) is bypassed in the transformation of the problem to one involving the solution of integral equations. In the resulting equations, only the average density ρ appears explicitly.

In random media problems involving a finite number of scatterers, however, the random- N consideration cannot be ignored. Furthermore, in theories based on the "honest" approach, N appears explicitly in the equations. The extension of the theories developed in the present work for a fixed number of planar scatterers (and, indeed, for any distribution of a fixed number of scatterers) to the case of random N is made possible by the theorem of total probability.³ For $p(z_1, \dots, z_N | N)$ the joint conditional probability density function of an ensemble of fixed- N configurations [i.e., the function $p(z_1, \dots, z_N)$ previously used in the chapter] and $p(z_1, \dots, z_N, N)$ the

corresponding joint probability density function for the ensemble of random- N configurations in which the fixed- N ensemble is contained, this theorem gives the result

$$p(z_1, \dots, z_N, N) = \sum_{N=0}^{\infty} P(N) p(z_1, \dots, z_N | N) \quad (2.98)$$

where $P(N)$ is the probability distribution of N . The average of a field function F over the ensemble of random- N configurations is therefore given by

$$\begin{aligned} \langle F \rangle &= \sum_{N=0}^{\infty} P(N) \int_0^d \cdots \int_0^d F(z_1, \dots, z_N) p(z_1, \dots, z_N | N) dz_1 \cdots dz_N \\ &= \sum_{N=0}^{\infty} P(N) \langle F \rangle_N \end{aligned} \quad (2.99)$$

where $\langle F \rangle_N$ are the averages for fixed N . Thus, the theories for fixed N are the basis of more general theories for random N , the additional function necessary being the probability distribution for N .

The distribution function for N of most immediate interest is the Poisson distribution given by

$$P(N) = \frac{\langle N \rangle^N}{N!} e^{-\langle N \rangle} \quad (2.100)$$

This distribution, for example, describes the probability of finding a given number of scatterers N within the scattering volume when those of the entire medium are uniformly distributed throughout a much larger volume. It is applicable, therefore, to the physical model discussed in Chapter 6.

The effect of random N on the distribution of the field components T_x and T_y is also of interest. Beckmann^{3,32} has developed a criterion for T_x and T_y to be considered normally distributed for random N given that they are normally distributed for fixed N sufficiently large. This criterion, which can be expressed as

$$\frac{\sigma_N}{\langle N \rangle} = \sqrt{\frac{\langle N^2 \rangle}{\langle N \rangle^2} - 1} \rightarrow 0 \quad (2.101)$$

effectively states that the distribution $P(N)$ must assume significant values only in an interval about $\langle N \rangle$ small compared to the size of $\langle N \rangle$. Since $\sigma_N^2 = \langle N \rangle$ for a Poisson distribution, this criterion is satisfied for $\langle N \rangle \gg 1$.

Generalization of the one-dimensional model theories for the case of random individual scatterer amplitudes is difficult and a study of the problem is beyond the scope of this work. Even in the simplest case of identically distributed and statistically independent amplitudes, it is evident that R_1 and T_1 in the given equations cannot simply be replaced by $\langle R_1 \rangle$ and $\langle T_1 \rangle$, etc. In the F-O-B-S approximation for $\langle R \rangle$, for example, while R_1 can be replaced by $\langle R_1 \rangle$, $\langle T_1^2 \rangle$ (not $\langle T_1 \rangle^2$) must be substituted for T_1^2 . Generalization of the S-O-B-S approximation for $\langle T \rangle$ further involves the individual scatterer averages $\langle R_1 T_1 \rangle$, $\langle T_1 \rangle$, and $\langle T_1^3 \rangle$. The Z-O-B-S term T_1^N of this approximation, however, can be replaced by $\langle T_1 \rangle^N$, making $|\langle T_1 \rangle|^{2N}$ the dominant term of the coherent intensity. Since the dominant term of $\langle |T|^2 \rangle$ would then be $\langle |T_1|^2 \rangle^N$ (not in general equal to $|\langle T_1 \rangle|^{2N}$), it is evident that the incoherent transmitted field would contain a Z-O-B-S component. Although the theoretical complexity makes insight into the problem difficult to attain, "experimental" studies involving Monte Carlo simulation provide an alternative future approach.

2.10 Summary

The new theoretical developments considered in this chapter may be summarized as follows:

(i) An explicit series representation in orders-of-back-scattering has been given for the total field in plane-wave scattering from a fixed array of non-identical planar scatterers.

(ii) Approximate series expressions based on the O-B-S representation have been obtained for several average field functions of interest in the problem of scattering from an ensemble of configurations of uniformly-random identical planar scatterers. These expressions have been shown to be useful in predicting the exact or approximate asymptotic behavior of the average field functions in the limit $\rho \rightarrow 0$ and it is believed that they may also prove useful in further theoretical research directed towards the improvement of general discrete-scatterer theories.

(iii) The exact asymptotic forms for $\rho \rightarrow 0$ in the planar-scatterer model have been obtained for the coherent transmitted field and the average total and incoherent intensities of both the transmitted and reflected fields. In particular, the exact asymptotic form $(1 + g_+)^N$ for the coherent transmitted field has been used to modify the one-dimensional form of Twersky's free-space theory and the possibility of a similar finite-N correction to the three-dimensional form of Twersky's theory has been suggested.

(iv) Based on the O-B-S approximation for the transmitted and reflected fields and the existing theory of random phasor sums, physical conditions necessary for the approximate validity of the bivariate Gaussian distribution in describing the total field statistics of the one-dimensional model have been discussed. Conditions necessary for the occurrence of a Rayleigh-distributed incoherent field amplitude with uniformly-distributed phase have also been considered.

3. APPLICATION OF MONTE CARLO SIMULATION TO THE STUDY OF SCATTERING FROM RANDOM MEDIA

3.1 Introduction

The method of Monte Carlo simulation is an important tool in the present investigation. Although Monte Carlo methods have been used extensively in the fields of nuclear physics and operations research, they have only been used sporadically in other fields.³⁸ Hochstim and Martens^{39,40} have recently applied a Monte Carlo method to the study of radar scattering from a one-dimensionally random slab region with discrete permittivity variations. Their work has largely been directed, however, towards the investigation of scattering theories for continuous random media (i.e., the perturbed continuum model). The present work, while also involving random media with discrete permittivity variations, is mainly directed towards the investigation of theories based on a discrete-scatterer formalism.

The Monte Carlo method is essentially an "experiment" with random numbers. Problems handled by the method are either probabilistic, as in this thesis, or deterministic in nature.³⁸ For either type of problem the application of the method is greatly facilitated by the use of a digital computer with a means of generating a large quantity of suitably-random numbers.

Two distinct types of Monte Carlo simulation are considered in this work. For both types of simulation, the random numbers generated represent the random positions of discrete scatterers in a discrete-scatterer model. The difference in the two types of simulation is in the amount of computer involvement. In the first type, as illustrated in Chapters 4 and 5 with the planar-scatterer model, a computer is used for all phases of the simulation with an exact or approximate theory being required for the field in scattering from a fixed configuration of scatterers. In the second type, as discussed in

Chapter 6, a computer is used only to generate scatterer configurations from the desired distribution and to statistically analyze the scattering results; the total fields due to scattering from the generated configurations are obtained by experimental measurements on a physical model of the random medium.

Several applications of Monte Carlo simulation to the study of scattering from random media are illustrated in this thesis. As in the work of Hochstim and Martens, "exact" simulation results for average field functions (i.e., those based on an exact theory for scattering from a fixed configuration of scatterers) are used to determine the validity of various approximate theories for these field functions over a wide range of scattering parameters. In the present work, however, "exact" simulation results are also used to determine the extent to which certain theoretical models for the probability density function of the field components describe actual behavior. In a further application, "approximate" simulation results based on approximate theories for scattering from a fixed configuration of scatterers are employed to validate the corresponding theories for the ensemble.

A possible future application of Monte Carlo simulation lies in its use to check inversion techniques for determining the physical and statistical composition of a random medium from sampled estimates of the field moments. Twersky²⁸ has developed techniques based on approximate scattering theory which require measurement of first and second field moments.

3.2 Technique of Simulation Applied to a Random Medium of Discrete Scatterers

The object in Monte Carlo simulation, as applied to scattering from a random medium of discrete scatterers, is to approximate the exact integral expression

$$\langle X(\bar{r}) \rangle = \int_{-\infty}^{\infty} \cdots \int_{-\infty}^{\infty} p(\bar{s}_1, \dots, \bar{s}_N) X(\bar{s}_1, \dots, \bar{s}_N; \bar{r}) d\bar{s}_1 \cdots d\bar{s}_N \quad (3.1)$$

by

$$\langle X(\bar{r}) \rangle = \frac{1}{n} \sum_{i=1}^n X_i(\bar{s}_1, \dots, \bar{s}_N; \bar{r}) \quad (3.2)$$

where X_i are the individual samples of the field function X for n different scatterer configurations from the ensemble. By the "law of large numbers",³ the approximation (3.2) will converge to the theoretical value represented by (3.1) in the limit as $n \rightarrow \infty$. The accuracy of the estimation after a finite number of samples is discussed in section 3.4.

Each random sample of a field function requires the generation of a sequence of random numbers from the desired statistical distribution $p(\bar{s}_1, \dots, \bar{s}_N)$. If, for example, each scatterer is described by an ℓ -component random vector $\bar{s}_i = (s_{i1}, s_{i2}, \dots, s_{i\ell})$ whose elements are the position coordinates and other scatterer parameters (e.g., size, permittivity, etc.), a sequence of $N\ell$ random numbers must be generated for the configuration of N scatterers associated with each field sample. For the one-dimensional and three-dimensional models of identical scatterers considered in the present work, the necessary sequences are of length N and $3N$ respectively, since only position coordinates are random.

3.3 Random Number Generation

The random numbers used in the Monte Carlo simulation of this work are not truly random, but "pseudo-random", since they are generated by an arithmetic method but manage to pass certain statistical tests for randomness. The generators employed produce uniformly-distributed numbers on the unit interval $(0, 1)$, as is most common.^{41,42} Such generators often form the basis for the generation of numbers from more complex distributions, since it is sometimes possible by a transformation to derive other distributions from a uniform distribution.⁴² For the simulation results of Chapter 4, the uniformly-

distributed numbers could of course be used directly.

The simulation was performed on an IBM 7044 computer during the earlier part of the work and on an IBM 360/67 during the later part. The random number program RAND as supplied for each computer by the University of British Columbia Computing Centre was used. The generator for the IBM 7044 was of the multiplicative congruential type^{41,42} with multiplier constant $2^7 + 1$ and additive constant 1111_8 . The algorithm for the IBM 360/67 generator is given in reference 43.

Various detailed tests have been used in determining the "randomness" of sequences generated by a variety of random number generators,^{41,42} although such tests for the sequences themselves do not guarantee that a random number generator will be suitable for a particular application. Results obtained during the course of this work, however, have verified the suitability of the generators used. Much evidence is provided by the fact that, for a low average density of scatterers, "exact" simulation results for several average field functions agree with the corresponding numerical data for the asymptotic theories (see Chapter 4). The agreement between "approximate" simulation results and theoretical results based on the same approximation over a wide range of scattering parameters provides further evidence.

Another method used to check the suitability of the generator RAND for the IBM 7044 computer was to compare the simulation results with results obtained using a second generator. No deviations larger than the statistical accuracy of estimation were noticed between the corresponding results. The second generator used was a modification of the generator RAND as follows: The generator RAND was used initially to fill a large array (ten times larger than the length of a sequence of numbers describing a single configuration of scatterers) with pseudo-random numbers; whenever a number was needed, two more were generated by RAND, one determining the element of the array to be used and

the other replacing it. This technique has been applied by Gebhardt⁴⁴ to a very poor basic generator and shown to yield good results. The basis of the method is that it effectively eliminates any correlation which may exist between closely adjacent numbers in a sequence by shuffling the sequence. A similar technique was originally proposed by MacLaren and Marsaglia⁴⁵ whereby two separate generators are used, one for filling the array and the other for specifying the sequence order.

3.4 Accuracy in Monte Carlo Simulation

The accuracy of the estimated mean $\langle X \rangle = \sum_{i=1}^n X_i/n$ can be readily obtained since its sampling distribution is Gaussian for large n with the standard error $\sigma_{\langle X \rangle}$ related to σ_X by³⁸

$$\sigma_{\langle X \rangle} = \frac{\sigma_X}{\sqrt{n}} \quad (3.3)$$

Thus, for example, at the 95% level of confidence, the error of the Monte Carlo estimate with respect to the true mean given by equation (3.1) is less than twice the standard error $2\sigma_{\langle X \rangle}$.

The factor \sqrt{n} in the denominator of (3.3) implies that in order to double the statistical accuracy of the estimated mean, four times as many samples must be obtained, etc. Because of the effect of this factor on the computation time in a complete computer simulation, the number of samples n must be limited. Most of the simulation results obtained in the present work were based on 1,000 samples, although some results were based on 4,000 samples to improve the estimates of certain functions of very small magnitude.

Because of the large number of samples taken, biased estimates of the second, third, and fourth central moments of the field components were used with only a very small error introduced. Biased estimates of the variances, for example, differ from unbiased estimates by a multiplication factor of $(n-1)/n$.

Errors due to the use of biased estimate formulas are similarly small for the third and fourth central moments and the corresponding coefficients of skewness and kurtosis when n is large.⁴⁶

In the computer simulation with the one-dimensional model (Chapters 4 and 5), accuracy estimates were obtained for all the first and second field moments based on twice the estimated standard errors of the means. For estimated field quantities such as C and α whose sampling variances could not be obtained directly, "worst-case" accuracy estimates based on approximate relations with the directly obtained variances of the basic components were determined. For example, from a Taylor series expansion to first-order terms¹⁴

$$\sigma_C^2 \approx \frac{C_x^2 \sigma_{T_x}^2 + C_y^2 \sigma_{T_y}^2 + 2C_x C_y \mu \sigma_{T_x} \sigma_{T_y}}{nC^2} \leq \frac{[|C_x| \sigma_{T_x} + |C_y| \sigma_{T_y}]^2}{nC^2} \quad (3.4)$$

and

$$\sigma_\alpha^2 \approx \frac{C_y^2 \sigma_{T_x}^2 + C_x^2 \sigma_{T_y}^2 + 2C_x C_y \mu \sigma_{T_x} \sigma_{T_y}}{nC^4} \leq \frac{[|C_y| \sigma_{T_x} + |C_x| \sigma_{T_y}]^2}{nC^4} \quad (3.5)$$

with the upper bounds of these expressions giving "worst-case" estimates (i.e., $C_x C_y \mu = |C_x C_y|$) of the sampling variances. Because of the large number of data points obtained in the complete computer simulation (and the inaccuracy of certain of the "worst-case" estimates), accuracy estimate results are not given in the thesis. A good indication of the accuracy is given by the "statistical scatter" of the data points (resulting from the generation of a different pseudo-random number sequence for each set of data) on many of the graphs in Chapters 4 and 5.

In the simulation with the three-dimensional physical model discussed in Chapter 6, certain of the sampling variances for complete sets of data were estimated from the variances of the means for sections of the data.

4. THEORETICAL AND SIMULATION RESULTS FOR A UNIFORM PROBABILITY DENSITY OF PLANAR-SCATTERER CONFIGURATIONS

4.1 Introduction

The uniform probability density of scatterer positions has been the basis of most approximate scattering theories so far developed, being the easiest to apply and adequately describing situations where a sparse distribution of finite-size scatterers exists (i.e., where the volume occupied by the scattering material is much less than the volume of the containing region). Studies of distributions of uniformly-random scatterers have furthermore provided a starting point for studies of more complex denser distributions of scatterers. In this chapter, simulation and approximate theoretical results are given for the scattering of a normally incident plane wave from an ensemble of configurations of uniformly-random identical planar scatterers. The requirements for the approximate validity of the uniform probability density for distributions of finite-width planar scatterers are discussed in detail in Chapter 5.

The scattering parameters for the one-dimensional model introduced in Chapter 2 are N , d_λ , g_+ , and g_- . Since g_+ and g_- for the infinitely-thin scatterers are taken to be those for lossless dielectric slabs of finite thickness, the scattering parameters are equivalently N , d_λ , w_λ , and ϵ_r . In order for an evaluation of the approximate theories to be most easily made and the physical behavior of the random medium illustrated, results are given for the variation of one of these parameters at a time.

The complexity of the physical behavior of the medium is largely dependent on the average number of scatterers per wavelength $\rho_\lambda = N/d_\lambda$, and increases as ρ_λ increases. The effect of ρ_λ variation over a wide range of values on the various first and second field moments of interest is best

illustrated by the variation of d_λ rather than N , since effects resulting from N variation overshadow those resulting from d_λ variation. The effects of variation of the parameters N , g_+ , and g_- on the physical behavior of the medium and on the accuracy of the approximate theories is adequately displayed by results for a few of the average field functions in the limit of $\rho_\lambda \rightarrow 0$.

The fixed parameters for the d_λ -variable results have the values $N = 10$, $\epsilon_r = 2.0$, and $w_\lambda = 0.1/\sqrt{2}$ (or $w_{\lambda'} = 0.1$, where λ' is the wavelength in the dielectric material of the equivalent slab scatterers). The resulting values for the scattering amplitudes, $g_+ = 0.2107 \underline{-101.7^\circ}$ and $g_- = 0.2035 \underline{-102.2^\circ}$, indicate that the individual scatterers considered are almost one-dimensional monopoles. In fact, the "thin-slab" approximation for the scattering amplitudes gives $g_+ \approx g_- \approx 0.2276 \underline{-102.5^\circ}$ (see Appendix B). These values have been chosen because the effects of higher orders of multiple scattering are sufficiently large to display fine differences in the various simulation and theoretical results. They are used also for the N -variable results. For the g_+, g_- -variable results given, $N = 10$.

The simulation results for d_λ variation are based on 4,000 sample configurations and those for variation of the other parameters on 1,000 samples. The execution time on the IBM 360/67 computer for generation and statistical analysis of 1,000 sample configurations is about 0.24 minutes. Throughout the chapter, simulation results for the various O-B-S approximations considered in Chapter 2 are given where necessary to validate the theories based on the same approximations.

Results for the various average transmitted field functions of interest are given in section 4.2 and results for the reflected field functions in section 4.3. Emphasis is placed on the complete statistical distribution of total field in section 4.4 and quantitative results based on the third and fourth field moments are presented. A general discussion and summary of the

results is given in section 4.5.

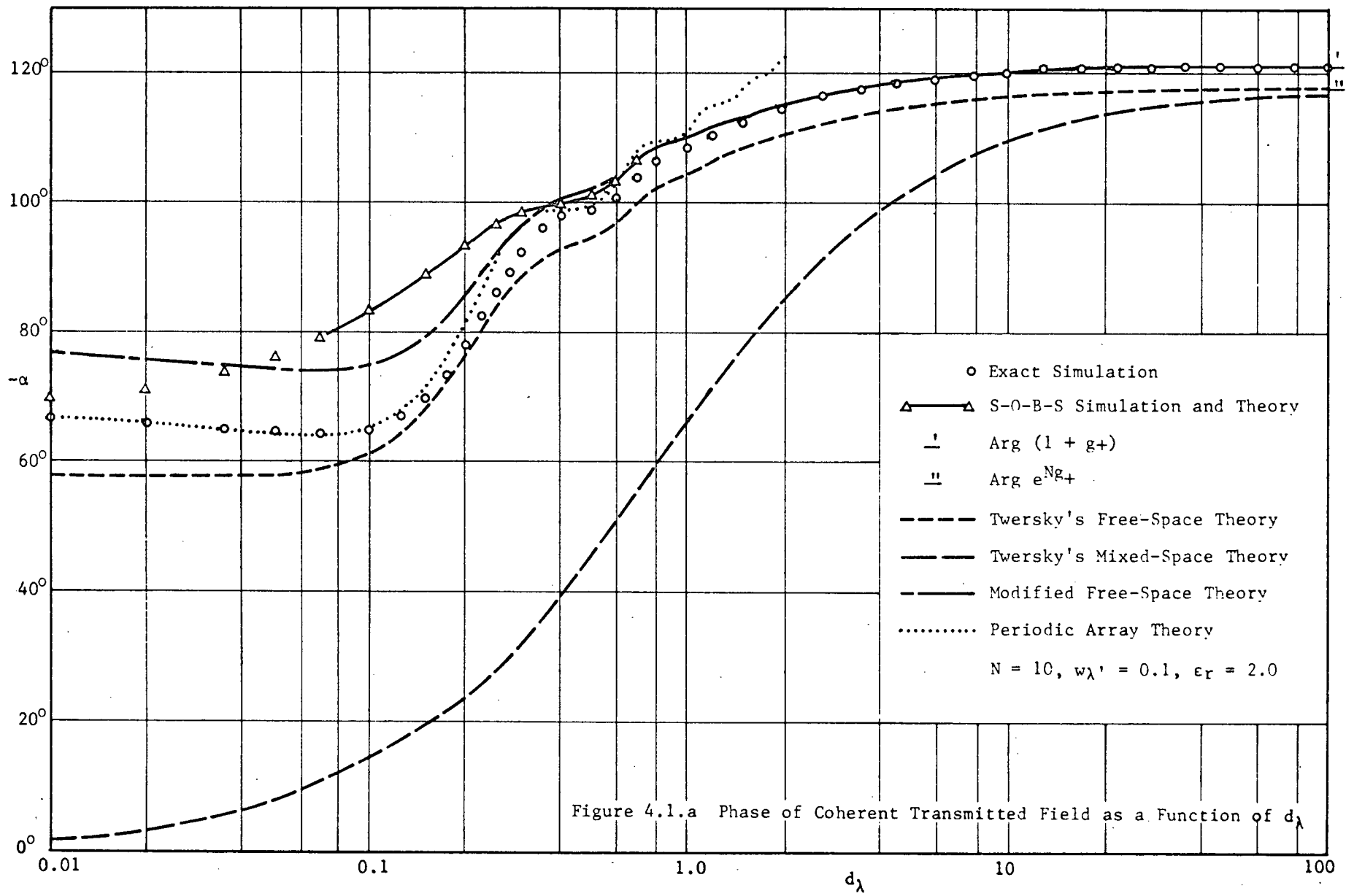
4.2 Transmitted Field Moments

4.2.1 The Coherent Field - $Ce^{j\alpha}$

Results for the phase and intensity of the coherent transmitted field are given in figures 4.1a and 4.1b for a variation of d_λ . From the "exact" simulation results, $Ce^{j\alpha} \rightarrow (1 + g_+)^N$ for $\rho_\lambda \rightarrow 0$ (or $d_\lambda \rightarrow \infty$) as was shown analytically in Chapter 2. In the other limit of $\rho_\lambda \rightarrow \infty$ (or $d_\lambda \rightarrow 0$), $Ce^{j\alpha}$ tends asymptotically to the value of the transmitted field for a periodic array of scatterers. The behavior of the transmitted field for a periodic array is both oscillatory and periodic in d_λ , with a resonance condition occurring when the spacing between the scatterers is approximately a multiple of $\lambda/2$ (see Chapter 5). As seen from figures 4.1a and 4.1b, approximately the same oscillatory behavior remains in $Ce^{j\alpha}$ for high ρ_λ although because of incoherent scattering it becomes increasingly damped out as ρ_λ increases.

As discussed in Chapter 2, the asymptotic limit of $Ce^{j\alpha}$ as $\rho_\lambda \rightarrow 0$ for Twersky's free-space and mixed-space theories is e^{Ng_+} . For the present fixed parameters, this form gives a result appreciably different from the exact result of $(1 + g_+)^N$, particularly in the coherent intensity C^2 . Because of this discrepancy in the asymptotic limit, the free-space theory does not accurately describe the actual results for high ρ_λ either. On the other hand, the modified free-space theory presented in section 2.7.1, containing the correct asymptotic limit, shows very good agreement with exact results over the entire range of d_λ .

As seen from figures 4.1a and 4.1b, Twersky's mixed-space theory does not accurately describe the actual characteristics of $Ce^{j\alpha}$ for uniformly-random planar scatterers. The limiting behavior of $C^2 \rightarrow 1$ as $\rho \rightarrow \infty$, however, is in approximate agreement with the physical behavior of certain dense distributions



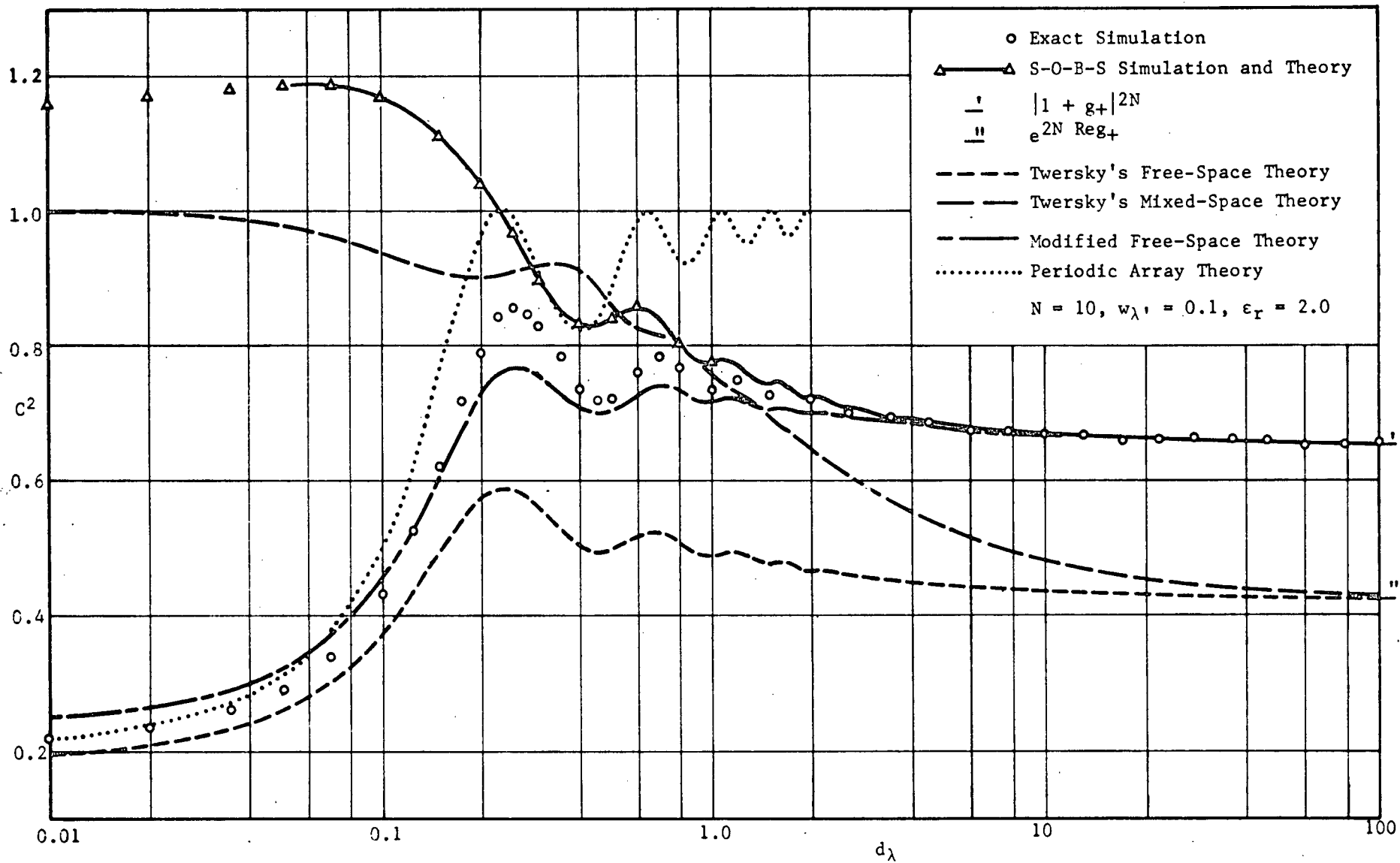


Figure 4.1.b Coherent Transmitted Field Intensity as a Function of d_λ

of finite-size scatterers. The application of the mixed-space theory to such distributions is considered in Chapter 5.

The S-O-B-S approximation for $Ce^{j\alpha}$ developed in the present work is also shown in figures 4.1a and 4.1b. The portion of the theory curves for small d_λ could not be computed because the higher-order terms of the series expression obtained "blow up", resulting in insufficient accuracy of computation. The approximate simulation results, however, give the remaining portion of the curves and verify the correctness of the approximate theory. As seen from the curves, the S-O-B-S theory gives good agreement with exact results for a wide range of d_λ . Over most of the range of d_λ , the agreement is approximately the same as that for the modified free-space theory. For very large ρ_λ , however, the S-O-B-S theory gives results which differ markedly from the exact results for C^2 . In fact, the trend of behavior in C^2 as $\rho_\lambda \rightarrow \infty$ is similar to that for the mixed-space theory. It is interesting that the free-space and modified free-space theories give reasonably good agreement with exact results for $\rho_\lambda \rightarrow \infty$ while the S-O-B-S theory does not. The reason for this is not immediately apparent and further theoretical investigation of these theories is thus required.

Figure 4.2 shows the effect on $Ce^{j\alpha}$ of a variation in N and illustrates the effect of this parameter on the accuracy of the asymptotic form e^{Ng_+} . The loss of coherent transmitted field energy for increasing N corresponds to an increase in the energy of the incoherent transmitted and reflected fields, as is illustrated by results of following sections. As discussed in Chapter 2, $e^{Ng_+} \rightarrow (1 + g_+)^N$ as $N \rightarrow \infty$. For the one-dimensional model, however, this is an unsatisfactory result, making necessary the correction for finite N contained in the modified free-space theory.

The effect of a variation of the total scattering cross-section $\sigma = -2 \text{Re}g_+$ on the accuracy of the form e^{Ng_+} is shown in figure 4.3. The

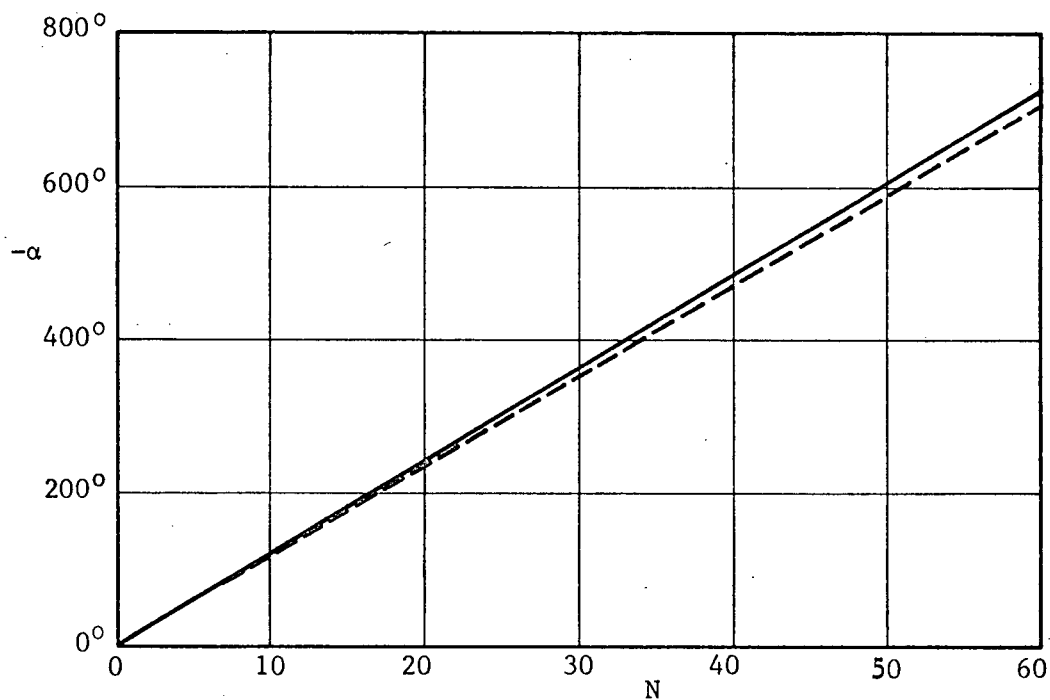
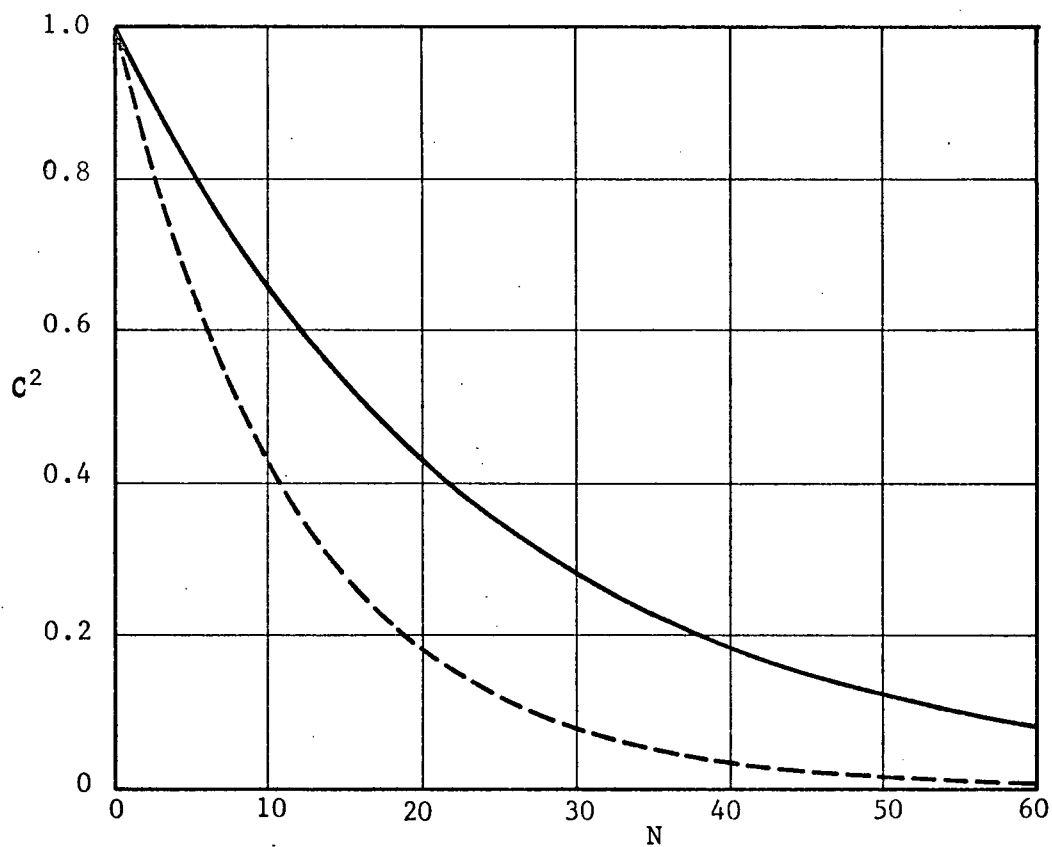
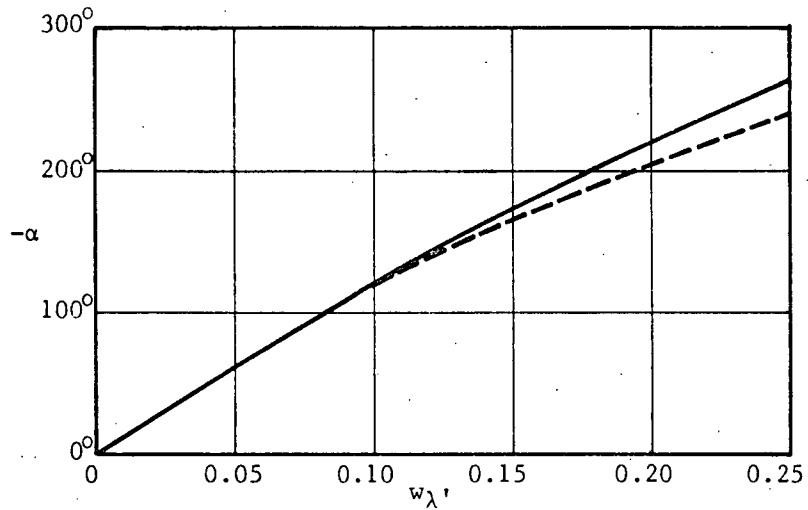
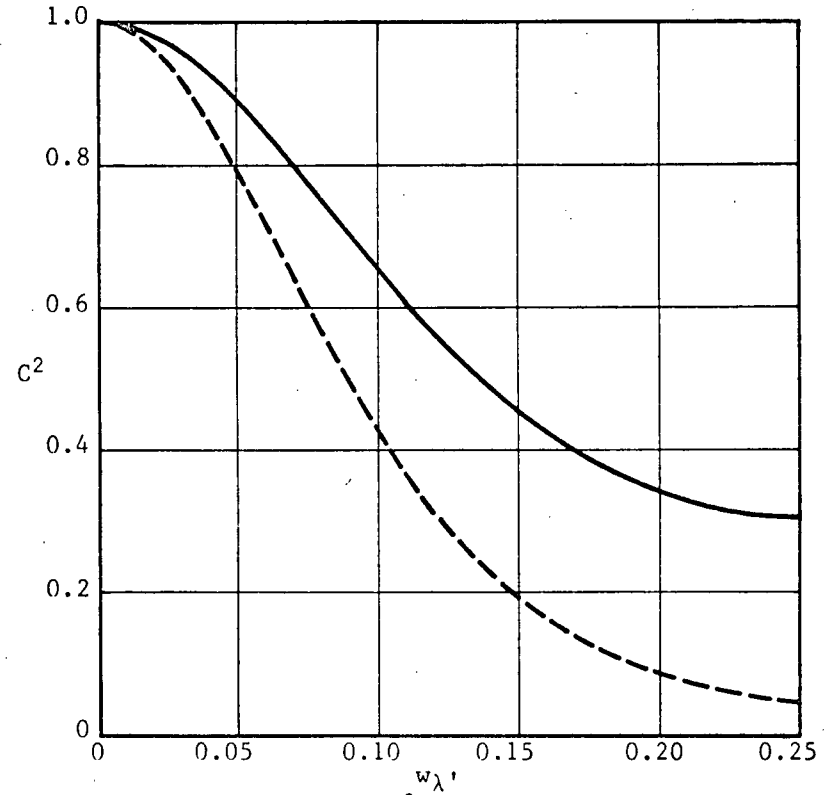
(a) $-\alpha$ versus N (b) C^2 versus N

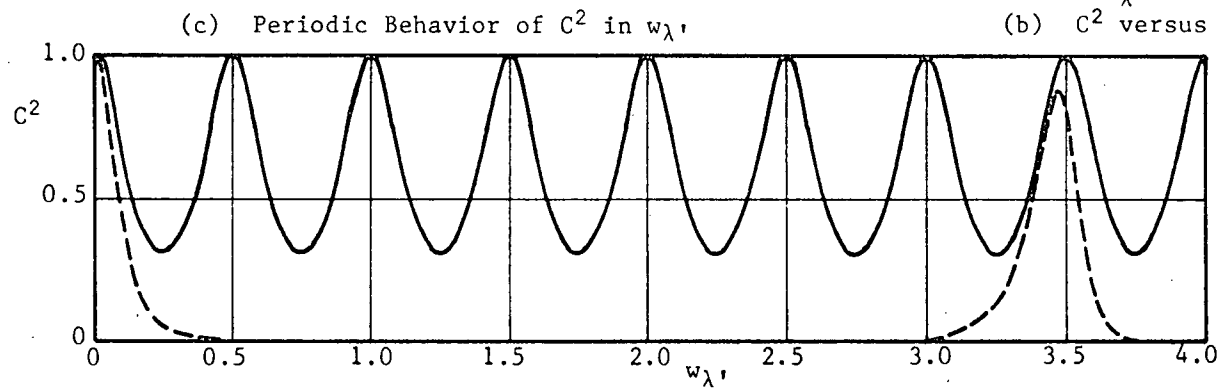
Figure 4.2 Coherent Transmitted Field as a Function of N (Asymptotic Results)
 $w_\lambda = 0.1$, $\epsilon_r = 2.0$; ——— $Ce^{j\alpha} = (1+g)^N$, - - - $Ce^{j\alpha} = e^{Ng}$



(a) $-\alpha$ versus $w_{\lambda'}$



(b) C^2 versus $w_{\lambda'}$



(c) Periodic Behavior of C^2 in $w_{\lambda'}$

Figure 4.3 Coherent Transmitted Field as a Function of $w_{\lambda'}$, (Asymptotic Results). $N = 10$, $\epsilon_r = 2.0$;
 — $Ce^{j\alpha} = (1 + g_+)^N$, --- $Ce^{j\alpha} = e^{Ng_+}$

cross-section is changed by variation of $w_{\lambda'}$, rather than ϵ_r , which is fixed at a value of 2.0. The aim is only to determine the effect of increased σ and this can be done by either a variation of ϵ_r or $w_{\lambda'}$. The curves of figures 4.3a and 4.3b are shown only up to $w_{\lambda'} = 0.25$, or a half period in $|1 + g_+|$. Figure 4.3c gives results for C^2 up to $w_{\lambda'} = 4$.

Curves for the rectangular components of g_+ in the range $w_{\lambda'} = 0$ to 0.5 are given in Appendix B. Results for higher $w_{\lambda'}$ with $\epsilon_r = 2.0$ show that σ (and $|g_+|$) varies periodically in w approximately every $3.4\lambda'$, reaching its first maximum at about $w_{\lambda'} = 1.7$. The free-space theory form $e^{2N\text{Re}g_+}$ for C^2 correspondingly has the same periodic behavior as seen from figure 4.3c, but with its maxima occurring at the minima of σ . It is thus required that σ be small in order that $e^{Ng_+} \approx (1 + g_+)^N$ for finite N . For dielectric slab scatterers this occurs for very thin slabs (i.e., $w_{\lambda'} \ll 0.25$) and at periodic values in w for thick slabs (e.g., $w = 3.4\lambda'$, $6.8\lambda'$, for $\epsilon_r = 2.0$). This result is discussed further in Chapter 5.

4.2.2 The Average Incoherent Intensity - $\langle I^2 \rangle$

Simulation results for $\langle I^2 \rangle$ as a function of d_λ are given in figure 4.4. The approximate results from the S-O-B-S are in good agreement with the exact results although the oscillatory effects for high ρ_λ are not contained in the approximate results. Maximum $\langle I^2 \rangle$ occurs for $\rho_\lambda \rightarrow 0$ since only the Z-O-B-S component $|1 + g_+|^{2N}$ is contributing to the coherent field, all higher O-B-S contributions being diverted to the incoherent field.

Figure 4.5 shows the effect of N variation and $w_{\lambda'}$ variation on $\langle I^2 \rangle$ in the limit of $\rho_\lambda \rightarrow 0$ and displays the accuracy of the asymptotic S-O-B-S theory presented in section 2.7.2. The simulation results were obtained for $d_\lambda = 10^5$. As seen by these curves, the level of $\langle I^2 \rangle$ is quite small, being approximately proportional to $|g_-|^4$.

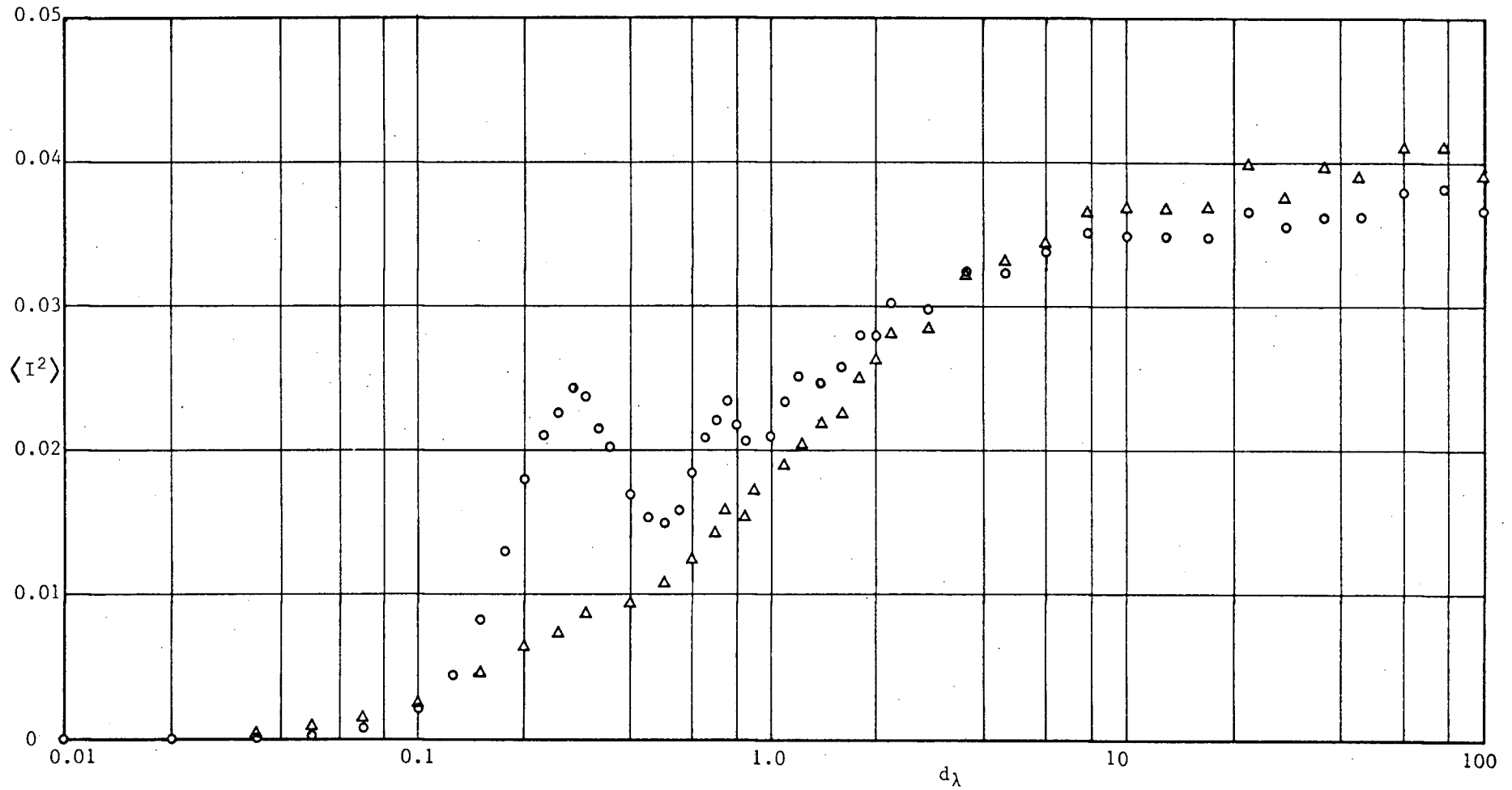
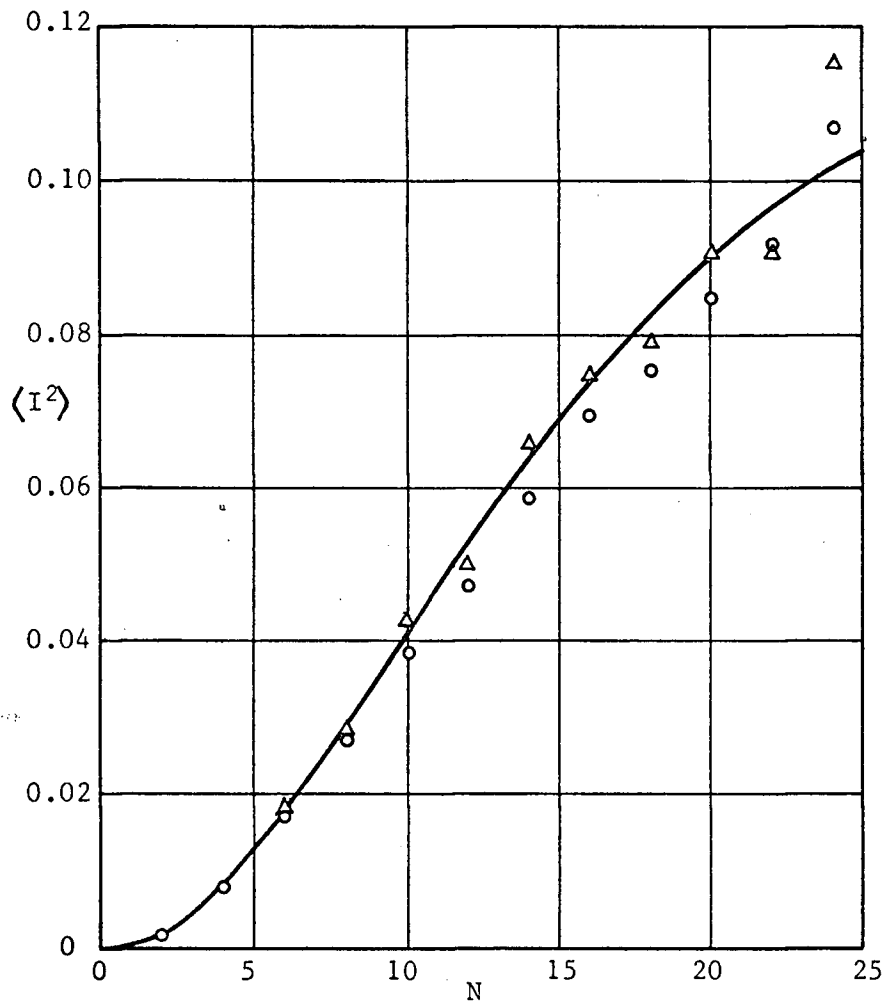
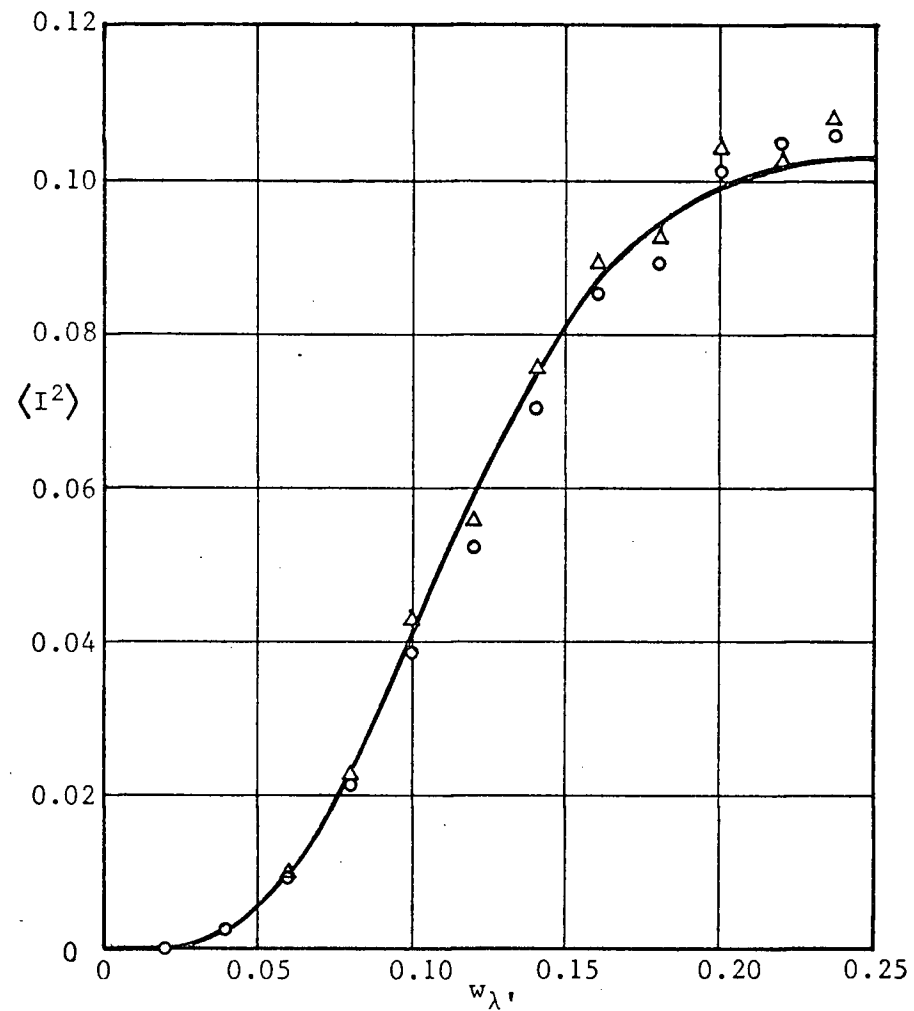


Figure 4.4 Average Incoherent Intensity of Transmitted Field as a Function of d_λ
 $N = 10, w_\lambda = 0.1, \epsilon_r = 2.0$; \circ Exact Simulation, Δ S-O-B-S Simulation



(a) $\langle I^2 \rangle$ versus N for $w_{\lambda'} = 0.1$, $\epsilon_r = 2.0$



(b) $\langle I^2 \rangle$ versus $w_{\lambda'}$, for $N = 10$, $\epsilon_r = 2.0$

Figure 4.5 Asymptotic Results for the Average Incoherent Intensity of the Transmitted Field

○ Exact Simulation with $d_{\lambda} = 10^5$, △ S-O-B-S Simulation with $d_{\lambda} = 10^5$,

— Asymptotic S-O-B-S Theory

4.2.3 The Variances and Covariance - $\langle I_x^2 \rangle$, $\langle I_y^2 \rangle$, $\langle I_x I_y \rangle$

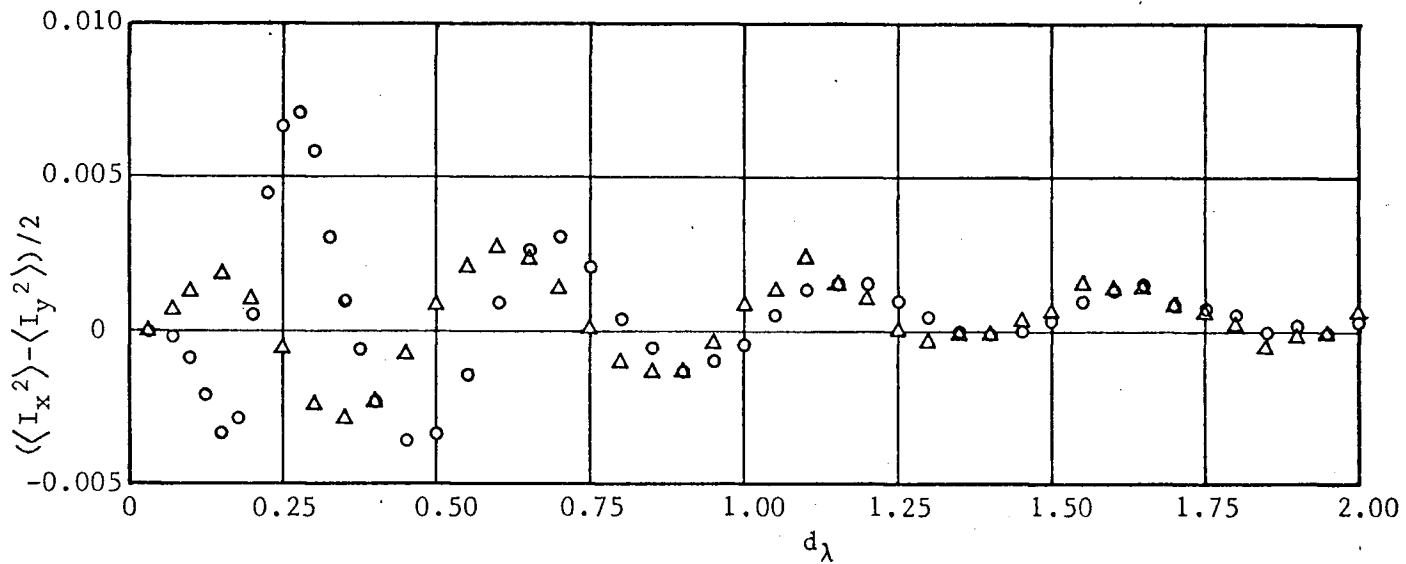
Simulation results for the rectangular components $(\langle I_x^2 \rangle - \langle I_y^2 \rangle)/2$ and $\langle I_x I_y \rangle$ of the complex function $2S^2 e^{j2s}$ defined in section 2.5.1 are shown in figure 4.6. In agreement with the elementary theory of that section, $\langle I_x^2 \rangle = \langle I_y^2 \rangle$ when $|\langle I_x I_y \rangle|$ is maximum and the difference between $\langle I_x^2 \rangle$ and $\langle I_y^2 \rangle$ is greatest when $\langle I_x I_y \rangle = 0$. The exact results and those for the S-O-B-S approximation differ most for high ρ_λ although both show that $\langle I_x^2 \rangle \rightarrow \langle I_y^2 \rangle$ and $\langle I_x I_y \rangle \rightarrow 0$ as $\rho_\lambda \rightarrow 0$.

These functions are important because they give the parameters of a bivariate Gaussian distribution for the total field components T_x and T_y (see section 2.8) when the scattering behavior of the medium is such that this distribution is valid. The asymptotic behavior for $\rho_\lambda \rightarrow 0$ as shown in figure 4.6 is particularly important because, under the condition of jointly Gaussian T_x and T_y , the total field amplitude is described by the well-known Nakagami-Rice distribution (or equivalently the incoherent field amplitude is Rayleigh distributed). The applicability of these distributions to the scattering behavior of the one-dimensional model is discussed in section 4.4.

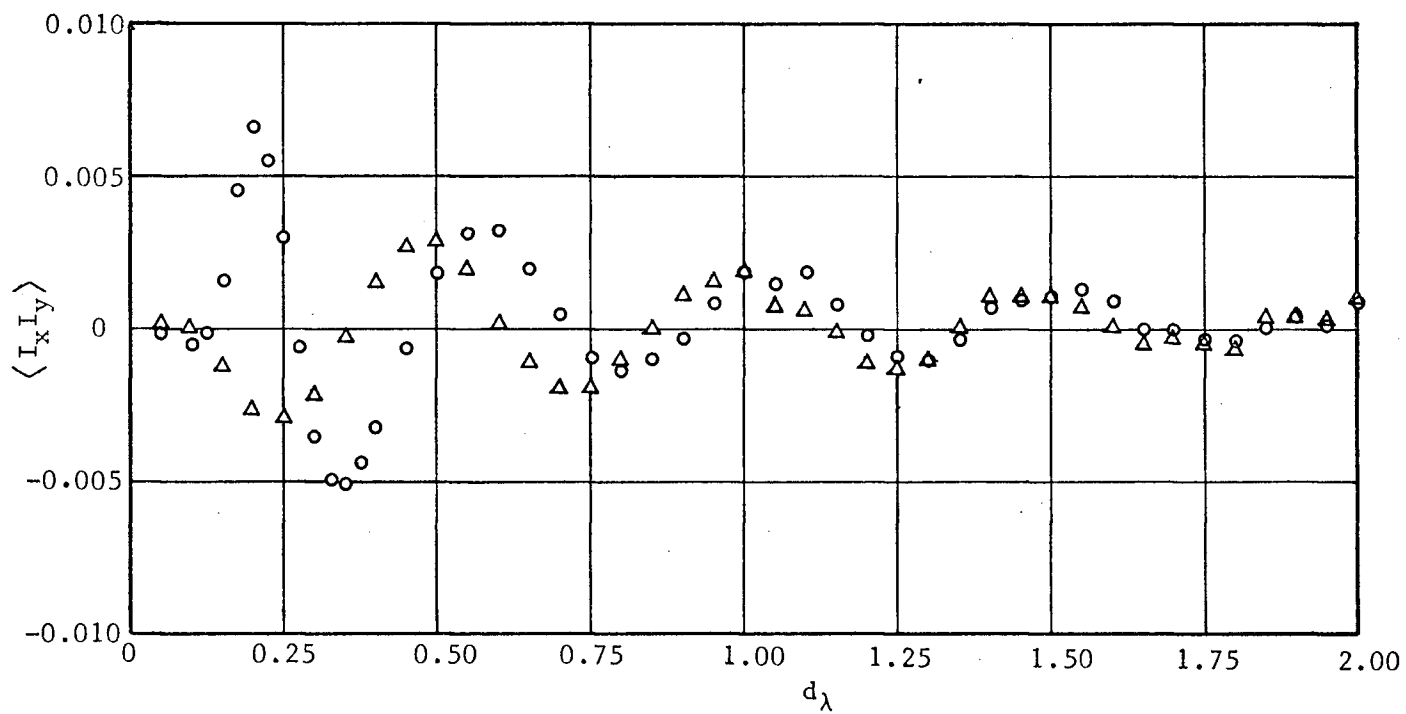
4.2.4 Moments of the Amplitude and Phase - $\langle T \rangle$, σ_T , $\langle \tau \rangle$, σ_τ

Simulation results were also obtained for the first and second moments of the transmitted field amplitude and phase for a variation of d_λ . These results showed the amplitude and phase moments to also be oscillatory in behavior for high ρ_λ , with σ_T and σ_τ reaching their maximum values as $\rho_\lambda \rightarrow 0$. The agreement between the "exact" simulation results and those based on the S-O-B-S approximation was comparable with that already shown for the first and second moments of T_x and T_y .

The accuracy of the approximate relations for $\langle T \rangle$, $\langle \tau \rangle$, σ_T^2 , and σ_τ^2 based on equations (2.32) to (2.35) to second-order terms was also investigated by a comparison of the direct simulation results for these functions with those



(a) $(\langle I_x^2 \rangle - \langle I_y^2 \rangle)/2$ versus d_λ



(b) $\langle I_x I_y \rangle$ versus d_λ

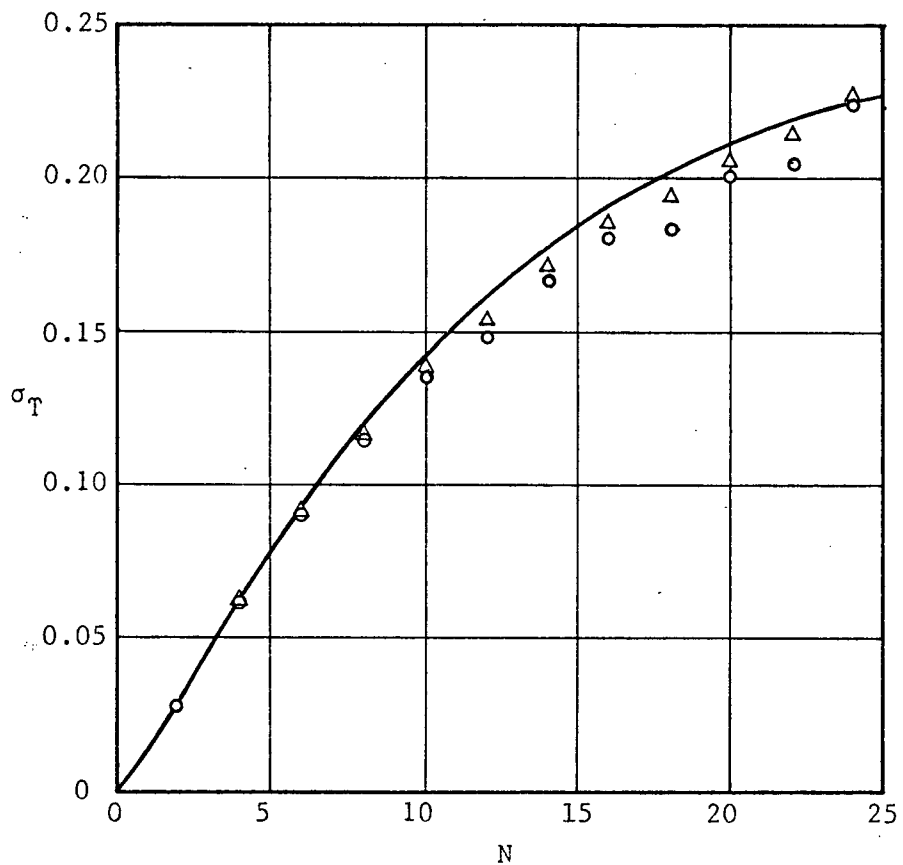
Figure 4.6 Variances and Covariance of Transmitted Field Components as Functions of d_λ . $N = 10$, $w_\lambda = 0.1$, $\epsilon_r = 2.0$;
 ○ Exact Simulation, ▲ S-O-B-S Simulation

indirectly obtained from the values of the first and second moments of T_x and T_y using these relations. The accuracy of the relations for $\langle T \rangle$ and $\langle \tau \rangle$ was good over the entire range of ρ_λ , statistically significant, but negligible differences occurring only for high ρ_λ where the covariant intensity S^2 is greatest. Differences between the directly and indirectly obtained results for σ_T and σ_τ were larger but still quite small. Since differences were greatest for $\rho_\lambda \rightarrow 0$, the accuracy of the approximate relations for σ_T and σ_τ is best indicated by the asymptotic results for a variation of N and w_λ . Shown in figure 4.7 are the results for a variation of N , the indirect results based on the approximate relations labelled as the "second moment approximation". Shown also are the asymptotic theory curves based on both the S-O-B-S approximation and the second moment approximation. As seen from figure 4.7b, these two approximations partially cancel one another for σ_τ . Results for a variation of w_λ were similar, the greatest deviation between the direct and indirect results occurring for the largest values of $|g_-|$.

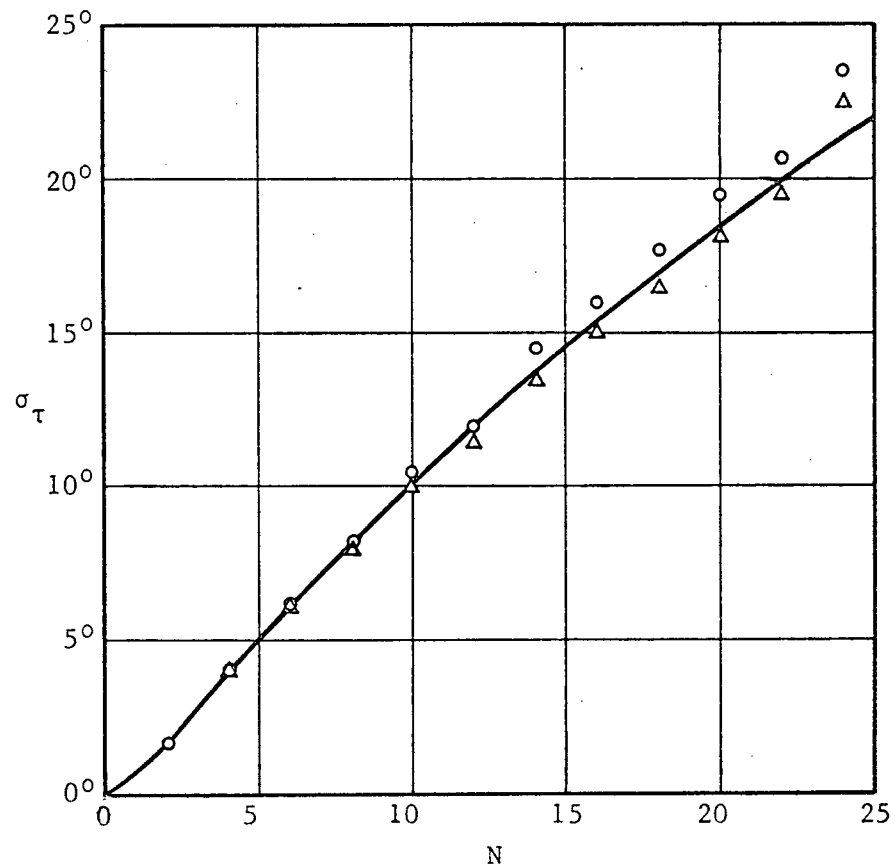
4.3 Reflected Field Moments

4.3.1 The Coherent Field - $Ce^{j\alpha}$

Results for the phase and intensity of the coherent reflected field are given in figure 4.8 for the first three wavelengths in d . The coherent intensity is plotted in decibels below the level of the incident field intensity. As seen from figure 4.8, $Ce^{j\alpha}$ is a damped oscillatory function, its amplitude decreasing to zero for $\rho_\lambda \rightarrow 0$ as predicted by theory (simulation results consequently become increasingly inaccurate as ρ_λ decreases). Minima in C^2 occur when the phase cancellation of the multiple-scattering contributions from the individual scatterers is greatest; maxima occur when it is least. The rapidly decreasing amplitude as $\rho_\lambda \rightarrow 0$ (i.e., $C \propto 1/d$) is due to the fact that, as the phases of the multiple-scattering contributions from the individual



(a) σ_T versus N



(b) σ_τ versus N

Figure 4.7 Standard Deviations of the Transmitted Field Amplitude and Phase as Functions of N (Asymptotic Results). $w_{\lambda_1} = 0.1$, $\epsilon_r = 2.0$; \circ Exact Simulation with $d_\lambda = 10^5$,
 Δ Exact Simulation ($d_\lambda = 10^5$) with Second Moment Approximation,
 — S-O-B-S Theory with Second Moment Approximation

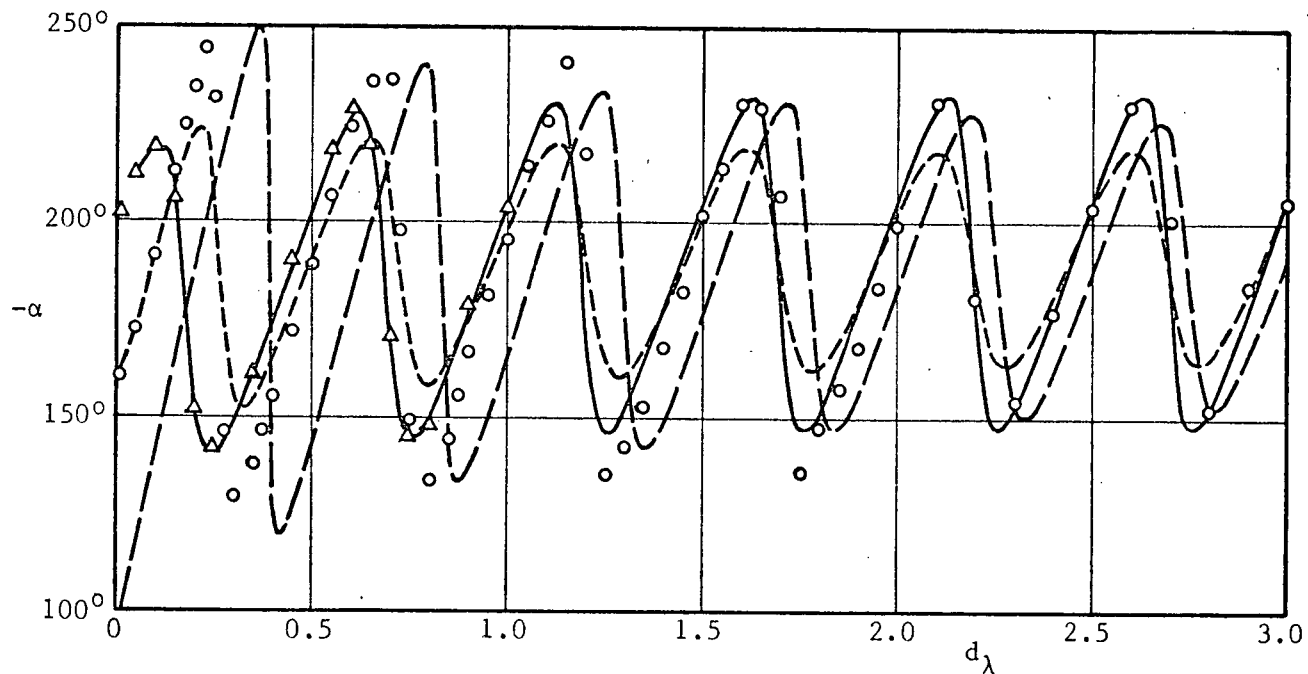
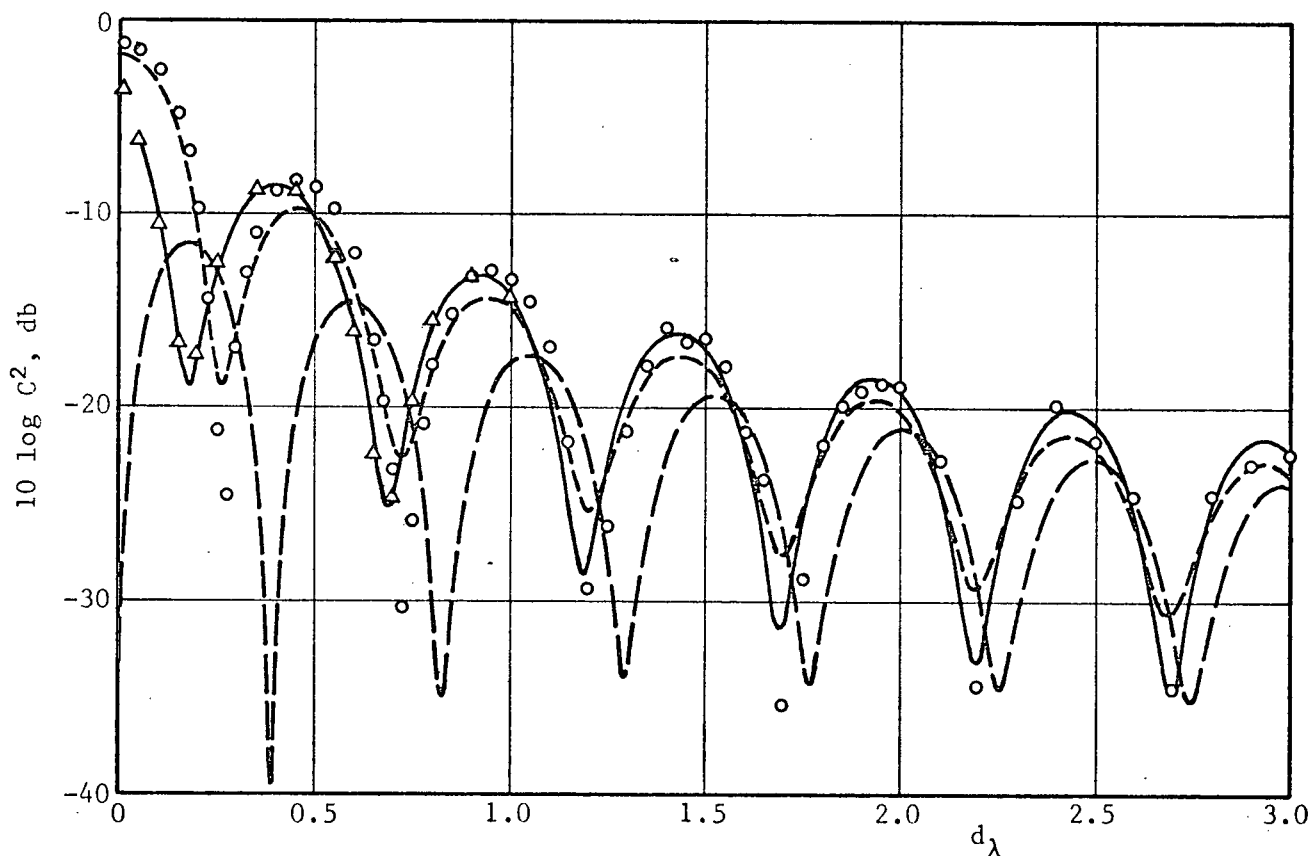
(a) $-\alpha$ versus d_λ (b) $10 \log C^2$ versus d_λ

Figure 4.8 Coherent Reflected Field as a Function of d_λ . $N = 10$, $w_\lambda = 0.1$, $\epsilon_r = 2.0$; \circ Exact Simulation, \triangle — \triangle F-O-B-S Simulation and Theory, --- Twersky's Free-Space Theory, ——— Twersky's Mixed-Space Theory

scatterers become more uniformly distributed, coherent energy is diverted to the incoherent field (see section 2.8). Although not shown in figure 4.8, the behavior of $Ce^{j\alpha}$ tends to that of the reflected field for a periodic array of scatterers as $\rho_\lambda \rightarrow \infty$.

It is evident from figure 4.8 that Twersky's free-space theory gives very good agreement with "exact" results in the location of the maxima and minima of C^2 and α . Like the theory for the coherent transmitted field, it also accurately describes the behavior for $\rho_\lambda \rightarrow \infty$. The F-O-B-S theory (note agreement between F-O-B-S theory and simulation results) gives better agreement in the magnitudes of the maxima and minima but less accurately describes their locations for high ρ_λ . The mixed-space theory for the coherent reflected field, as for the coherent transmitted field, does not describe the physical behavior of the uniformly-random ensemble of configurations as $\rho_\lambda \rightarrow \infty$. Its significance is that it can approximately describe the behavior of certain distributions of finite-size scatterers if the average density ρ is correctly interpreted. This is shown in Chapter 5, section 5.4.

4.3.2 The Average Incoherent Intensity - $\langle I^2 \rangle$

Results for $\langle I^2 \rangle$ as a function of d_λ are given in figure 4.9. The F-O-B-S theory gives relatively good agreement with exact results over a wide range of ρ_λ although for large ρ_λ it does not describe the oscillatory behavior evident in the exact results. (The theory curve is shown to a point where the computational accuracy breaks down.) The modified F-O-B-S theory based on including the effect of the T-O-B-S in the asymptotic term of the F-O-B-S series gives better agreement with exact results except for $\rho_\lambda \rightarrow \infty$ (not shown). This again illustrates the effect that an "asymptotic correction" can have on the accuracy of certain theories applicable to low and mid-range values of ρ_λ .

Figure 4.10 gives results for N variation and w_λ variation in the limit of $\rho_\lambda \rightarrow 0$, displaying the relative accuracies of the asymptotic F-O-B-S

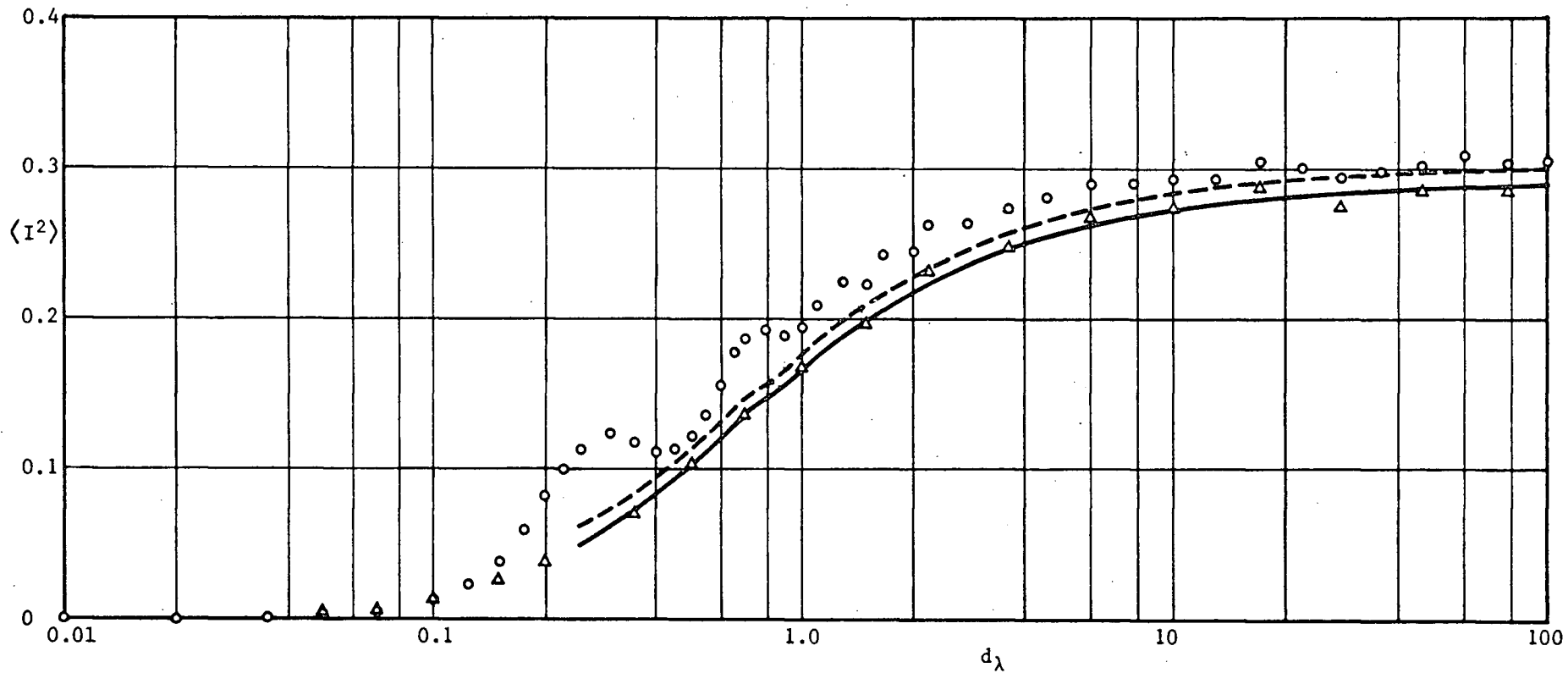
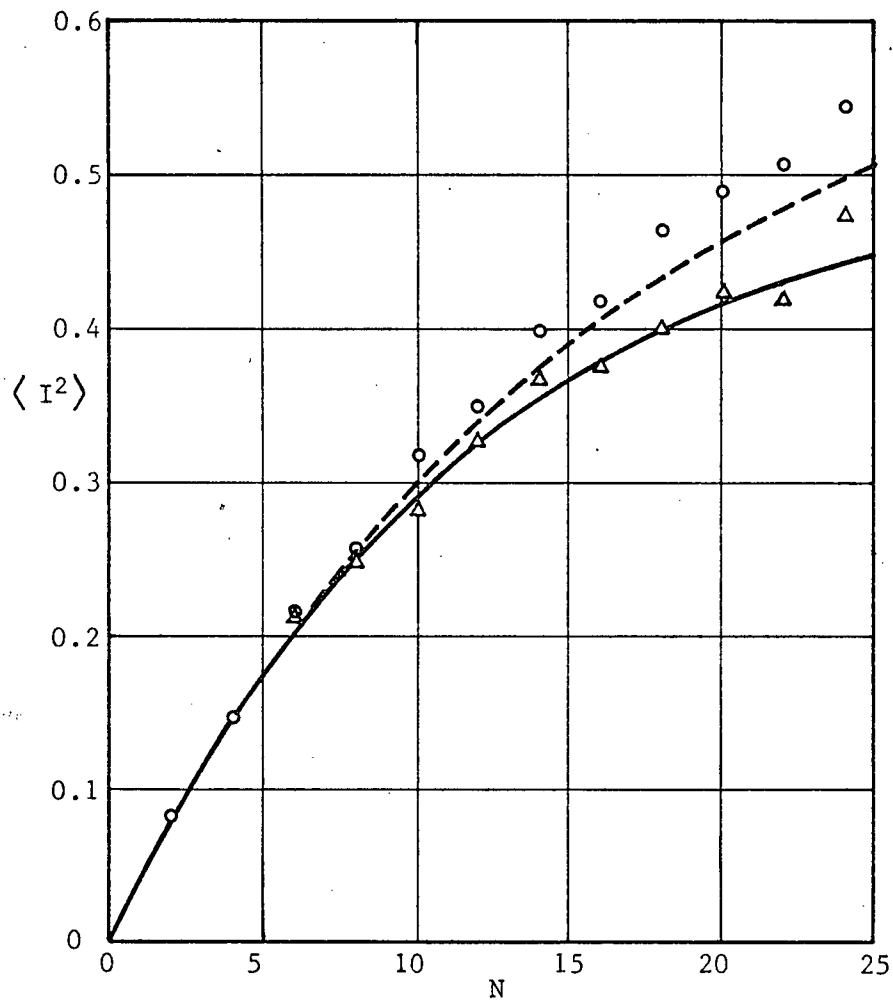
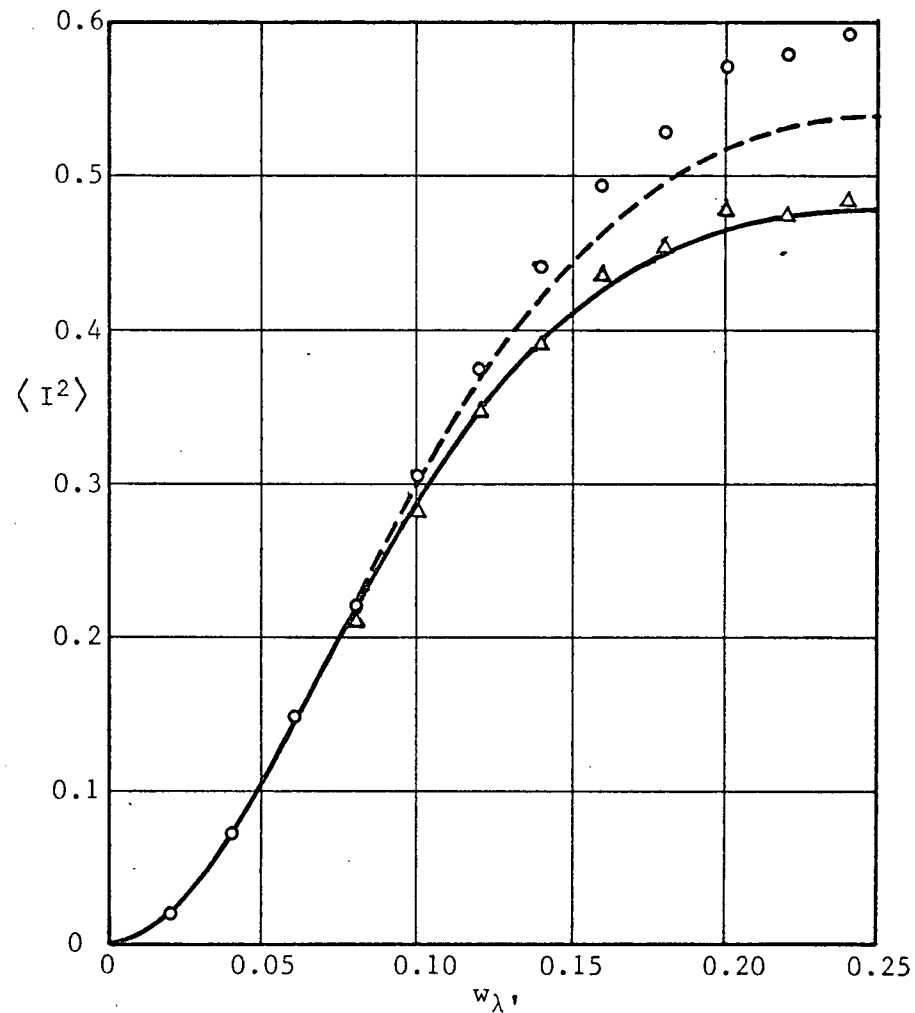


Figure 4.9 Average Incoherent Intensity of Reflected Field as a Function of d_λ
 $N = 10, w_\lambda = 0.1, \epsilon_r = 2.0$; o Exact Simulation, Δ F-O-B-S
 Simulation and Theory, --- Modified F-O-B-S Theory



(a) $\langle I^2 \rangle$ versus N for $w_\lambda = 0.1$, $\epsilon_r = 2.0$



(b) $\langle I^2 \rangle$ versus w_λ , for $N = 10$, $\epsilon_r = 2.0$

Figure 4.10 Asymptotic Results for the Average Incoherent Intensity of the Reflected Field

- Exact Simulation with $d_\lambda = 10^5$, Δ F-O-B-S Simulation with $d_\lambda = 10^5$,
- Asymptotic F-O-B-S Theory, - - - Asymptotic T-O-B-S Theory

and T-O-B-S theories. Maximum deviation between approximate theoretical and "exact" simulation results occurs for the largest N and largest $|g_-|$ (i.e., largest w_λ) employed. As is evident by a comparison of these results with those of figure 4.5 on page 65, the average incoherent intensity of the reflected field is much greater than that of the transmitted field, being approximately proportional to $|g_-|^2$ rather than to $|g_-|^4$. For the d_λ -variation parameters in the limit of $\rho_\lambda \rightarrow 0$, the "signal-to-noise ratio" $C^2/\langle I^2 \rangle$ of the transmitted field is approximately 17.9 whereas for the entire medium (i.e., $\langle I^2 \rangle$ for both transmitted and reflected fields included as noise) it is approximately 1.92.

4.3.3 The Variances and Covariance - $\langle I_x^2 \rangle$, $\langle I_y^2 \rangle$, $\langle I_x I_y \rangle$

Results for the complex function $2S^2 e^{j2s}$ of the variances and covariance of T_x and T_y are shown in figure 4.11. The behavior of the rectangular components of this function for varying d_λ is seen to be similar to that for the corresponding transmitted field functions. The asymptotic behavior as $d_\lambda \rightarrow \infty$ is not reached as quickly, however, and the period of oscillation is smaller.

The computational accuracy of the F-O-B-S theory curves based on equations (2.59) to (2.61) for $\langle T^2 e^{j2\tau} \rangle = \langle R^2 \rangle$ and the already validated equation (2.42) for $Ce^{j\alpha} = \langle R \rangle$ appears to break down in the vicinity of $d_\lambda = 0.75$. The poorer computational accuracy for lower values of d_λ occurs for the $\langle R^2 \rangle$ equations because of the larger denominator constants in the terms of the series. However, even for $d_\lambda > 0.75$, the theory curves appear to deviate significantly from the F-O-B-S simulation results, although they correctly describe the oscillatory behavior. Thus, although the series expression for $\langle R^2 \rangle$ has been carefully checked, its validity has not yet been established.

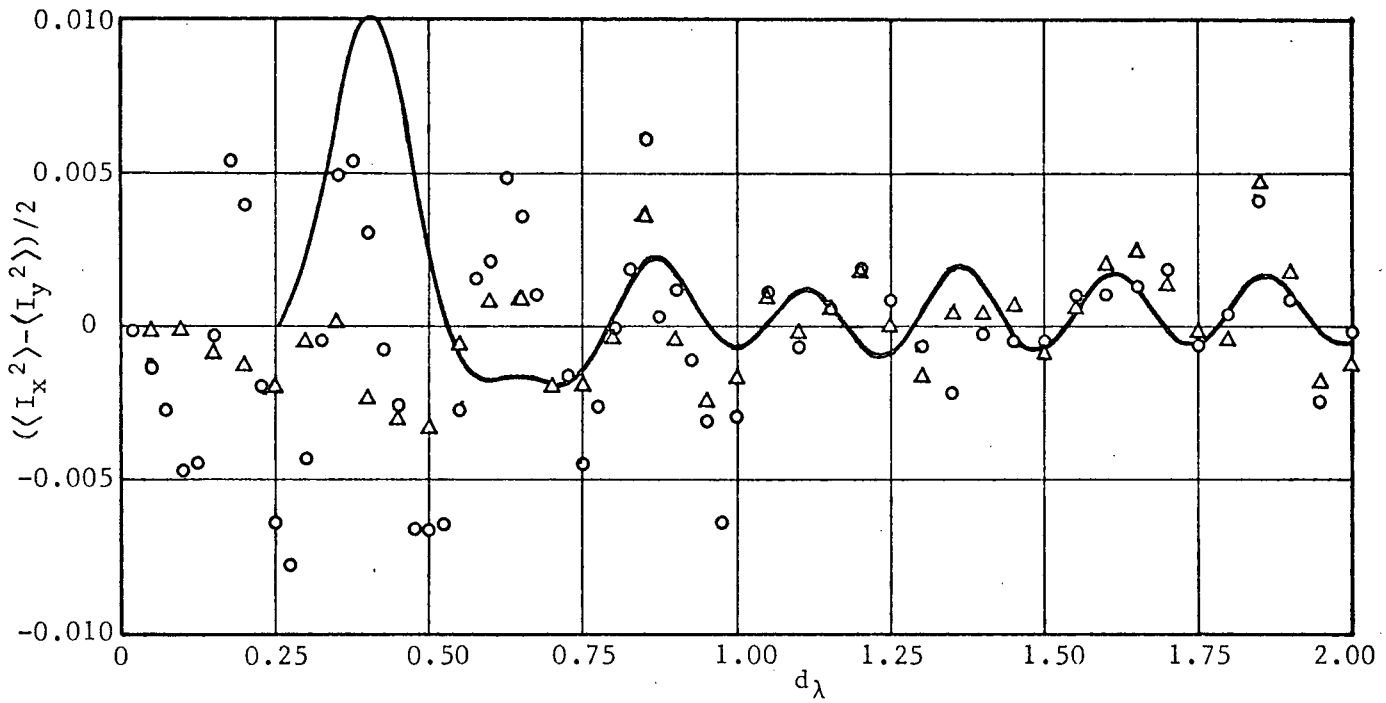
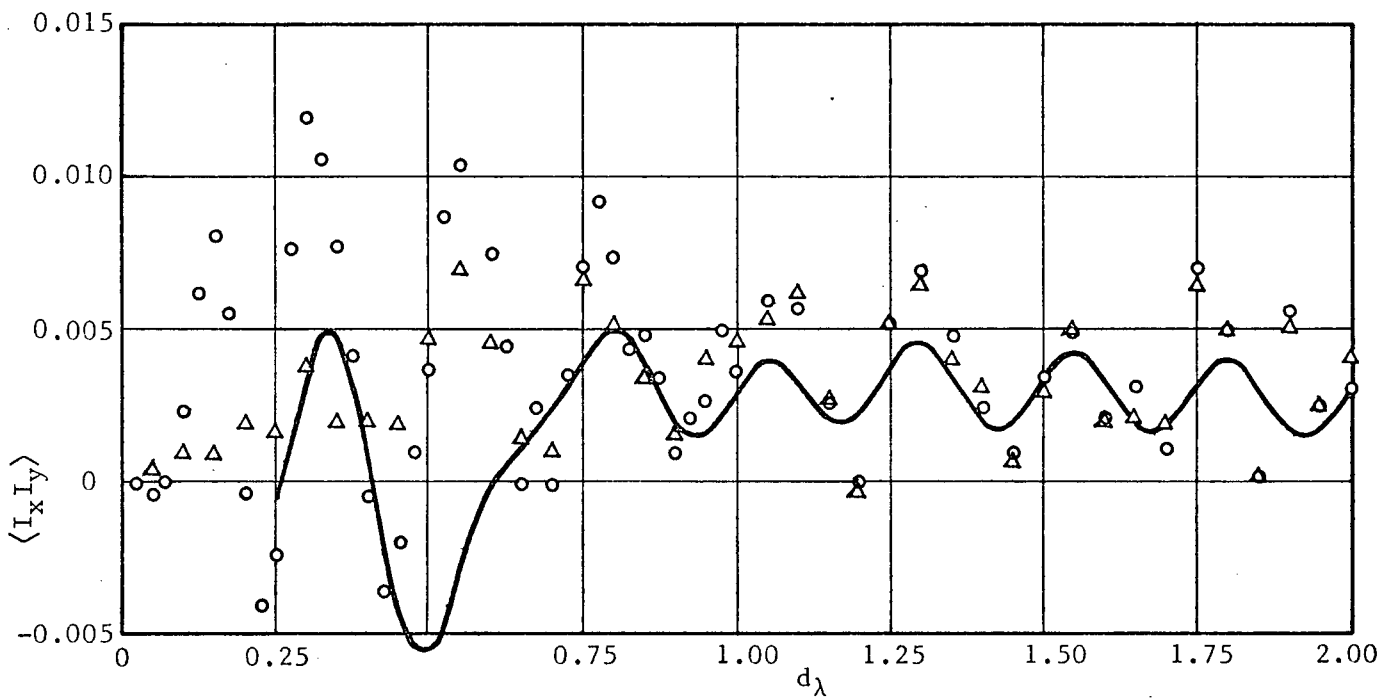
(a) $(\langle I_x^2 \rangle - \langle I_y^2 \rangle)/2$ versus d_λ (b) $\langle I_x I_y \rangle$ versus d_λ

Figure 4.11 Variances and Covariance of Reflected Field Components as Functions of d_λ . $N = 10$, $w_\lambda = 0.1$, $\epsilon_r = 2.0$;

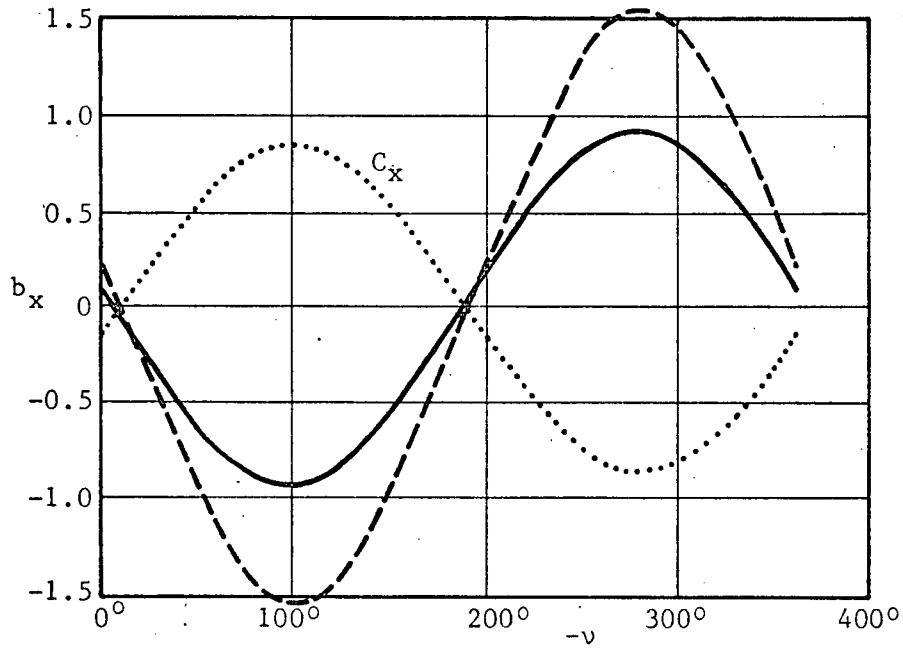
○ Exact Simulation, △ F-0-B-S Simulation, — F-0-B-S Theory

4.4 Distribution of the Total Field

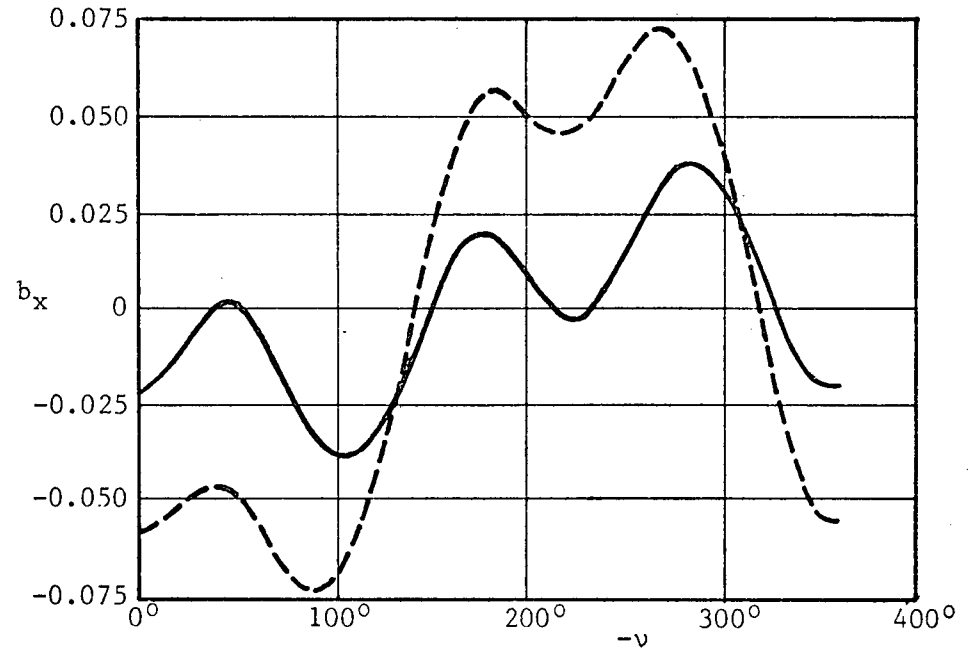
The object of this section is to determine the extent to which the transmitted and reflected field components T_x and T_y deviate from Gaussian behavior in the region of low ρ_λ for a range of the parameters w_λ , and N . Quantitative results are given by means of the coefficients of skewness (b_x , b_y) and kurtosis (γ_x , γ_y), obtained from the third and fourth field moments respectively (see section 2.5.1). All results are based on 1,000 field samples.

Typical plots of b_x and γ_x for a variation of the phase reference v are given in figures 4.12a and 4.12b for the transmitted field. The plot for b_y is identical to that for b_x but displaced by 90° . Similarly the plot for γ_y is displaced 90° from that for γ_x . Shown on the same graph as b_x in figure 4.12a is the in-phase component C_x of the coherent field. A comparison of this curve with that for b_x shows that the distribution of T_x is symmetrical for $C_x = 0$ and most highly skewed for maximum C_x . The shortest tail of the distribution is that closest to the physical truncation limits of +1 or -1 for T_x . Plots of the equivalent quantities for the reflected field are given in figures 4.12c and 4.12d. The periodic behavior of the third and fourth field moments with v as shown by these curves has been theoretically predicted by Twersky⁴ and similarly checked by means of experiments on a physical model of a distribution of spherical scatterers.⁵

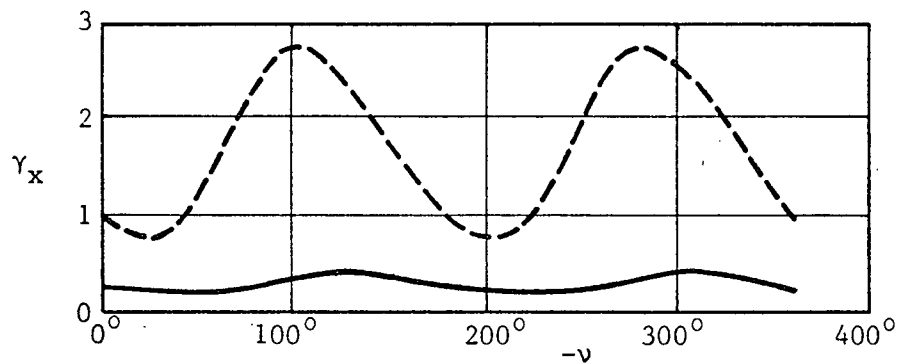
Plots of the maximum value of $|b|$ reached over a full period of v variation as a function of w_λ , are given in figure 4.13a for the transmitted field. The scattering parameters are $N = 10$, $\epsilon_r = 2.0$, and $d_\lambda = 100$. The limit within which 95% of the sampled values of b_x and b_y would be expected to be found for Gaussian behavior of the field components is shown on this graph.¹⁴ Plots of the maximum and minimum values of γ obtained with the corresponding 95% limits for Gaussian behavior are given in figure 4.13b.



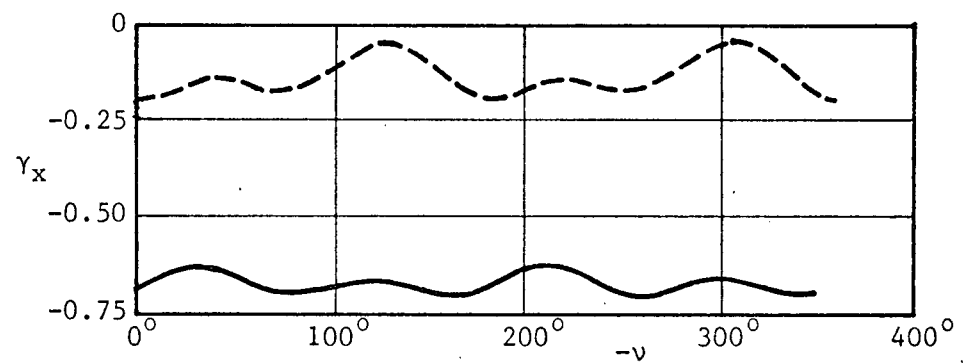
(a) b_x, C_x versus $-v$ - Transmitted Field



(c) b_x versus $-v$ - Reflected Field

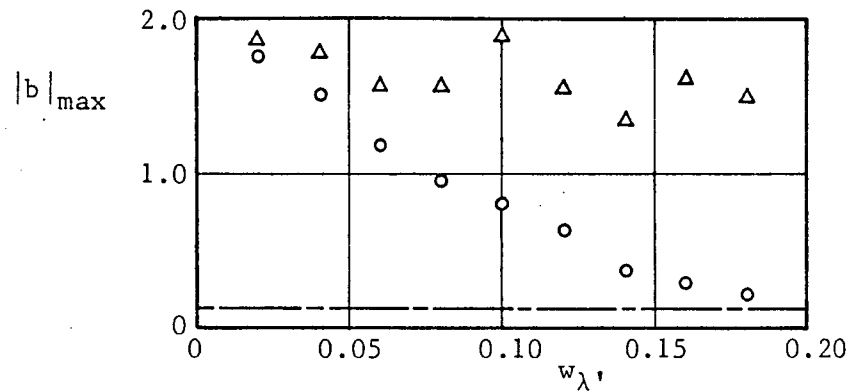


(b) γ_x versus $-v$ - Transmitted Field

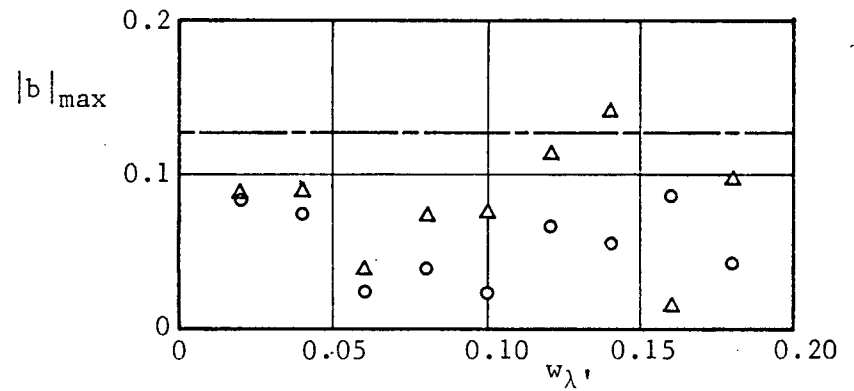


(d) γ_x versus $-v$ - Reflected Field

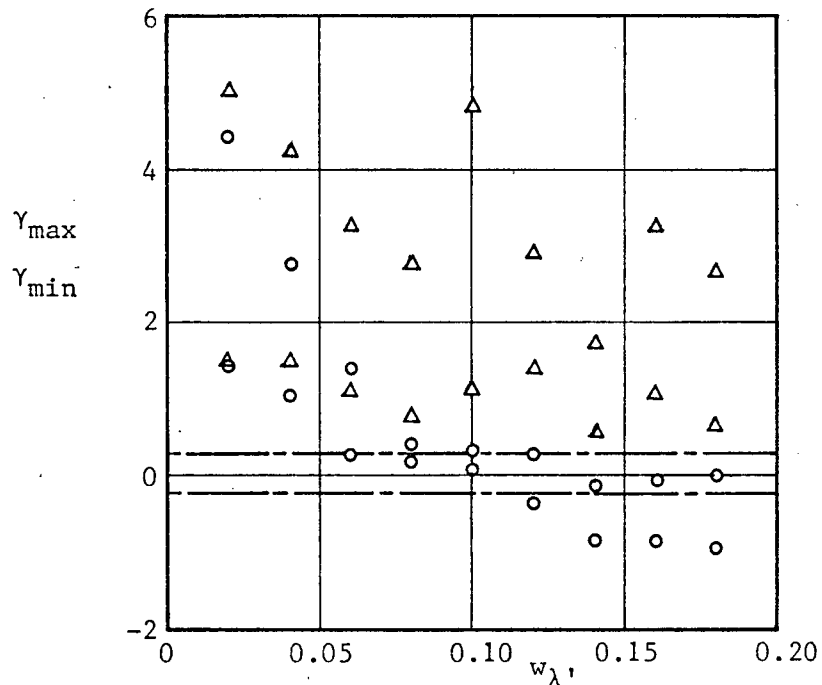
Figure 4.12 Skewness and Kurtosis Coefficients as Functions of the Phase Reference. $N = 10$, $d_\lambda = 100$, $w_{\lambda'} = 0.08$, $\epsilon_r = 2.0$; — Exact Simulation, - - - Approximate Simulation



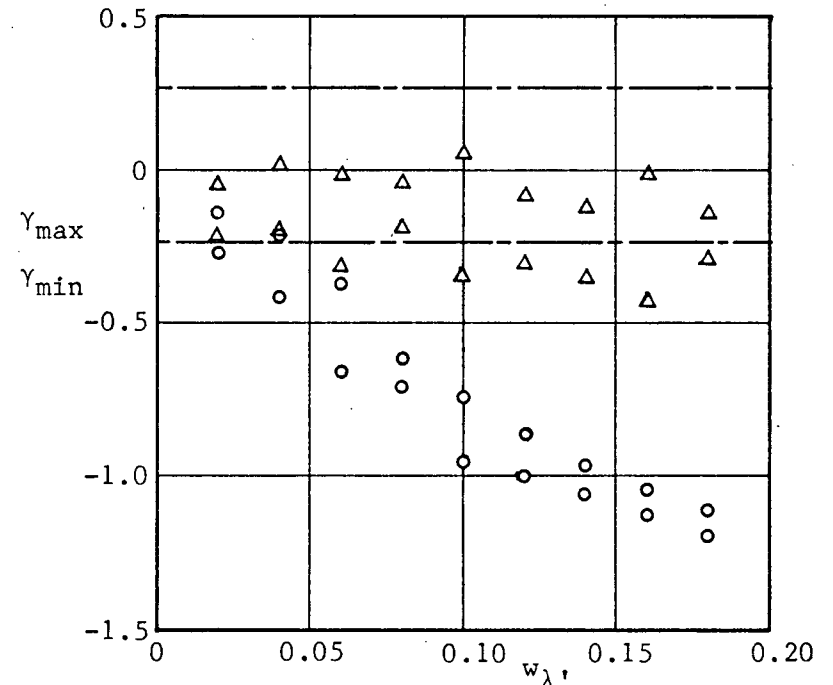
(a) $|b|_{\max}$ versus w_λ , - Transmitted Field



(c) $|b|_{\max}$ versus w_λ , - Reflected Field



(b) $\gamma_{\max}, \gamma_{\min}$ versus w_λ , - Transmitted Field



(d) $\gamma_{\max}, \gamma_{\min}$ versus w_λ , - Reflected Field

Figure 4.13 Extreme Values of b and γ as Functions of w_λ . $N = 10$, $\epsilon_r = 2.0$, $d_\lambda = 100$; \circ Exact Simulation, \triangle Approximate Simulation, ——— 95% Confidence Limits for Gaussian Behavior

As seen by these figures and as discussed in section 2.8, the distribution of the field components is more nearly Gaussian for large values of $|g_-|$. The results show, however, that the distribution of the actual field is less highly skewed and less sharply peaked than that of the field as approximated by the S-O-B-S.

The corresponding results for the reflected field are given in figures 4.13c and 4.13d. As seen by these results and as discussed in section 2.8, the distributions of T_x and T_y are more nearly Gaussian for low values of $|g_-|$. The distributions of the actual field components, however, are somewhat flatter than those of the approximate field components for the F-O-B-S, as shown by the plots for γ . Furthermore, deviation of the actual field from Gaussian behavior occurs more quickly for an increase of $|g_-|$ than does that of the approximate field. From the statistical scatter of the data points in figure 4.13, it appears that the variances of the b and γ statistics are greater for the approximate field than for the actual field.

Curves are not given for the effect of N variation on the skewness and kurtosis coefficients. As expected, the results obtained showed a transmitted field approaching Gaussian behavior for large N . The rate of approach, however, was quite slow. With scattering parameters of $w_\lambda = 0.06$, $\epsilon_T = 2.0$, and $d_\lambda = 100$, maxima in the $|b|_{\max}$ and $\gamma_{\max}, \gamma_{\min}$ plots occurred at approximately $N = 12$. For these same parameters, however, the distributions of the reflected field components appeared to change little beyond about $N = 6$, being somewhat flatter than Gaussian for lower N . This result is of course physically reasonable since contributions to the reflected field from scatterers further removed from the origin become increasingly smaller.

As seen from the results of sections 4.2.3 and 4.3.3, T_x and T_y become uncorrelated for low ρ_λ . Thus, it can be assumed that as the distributions of T_x and T_y approach the Gaussian distribution, the distributions

of the incoherent transmitted and reflected field amplitudes will approach a Rayleigh distribution. Likewise, the distribution of the total transmitted field amplitude will approach the Nakagami-Rice distribution. Further investigation is required, however, to determine the extent to which deviations of T_x and T_y from Gaussian behavior cause a similar deviation of the incoherent field amplitude I from Rayleigh behavior.

Plots of the cumulative distributions of T_x and T_y in standard normal deviates¹⁴ were also obtained as an additional check for deviation from Gaussian behavior. Such plots, however, are less sensitive to deviations than are the b and γ coefficients. Straight-line plots for the exact reflected field cumulative distribution were obtained up to $w_{\lambda'} = 0.08$, for example; the values for γ of figure 4.13d indicate a somewhat flattened distribution at this point.

4.5 Summary and General Discussion of Results

The main developments of this chapter may be summarized as follows:

(i) Results have been given demonstrating the accuracy of the various O-B-S theories developed in the present work. This opens the way for future theoretical work directed toward a comparison of these theories with the one-dimensional forms of more general discrete-scatterer theories.

(ii) The importance of the low average density asymptotic behavior of the medium on the evaluation and improvement of existing theories applicable to more dense scatterer distributions has been quantitatively illustrated.

(iii) Results have been given for the one-dimensional forms of Twersky's theories for the coherent field for a wide variation of parameters, showing the limitations of these theories in a manner not as easily allowed by experiments on physical models of discrete-scatterer distributions. Since the uniform-randomness of the scatterers has not been an approximation as it must be for

physical distributions of finite-size scatterers, the effect of the heuristic approximations contained in these theories has been separated from the effect of a uniform-distribution approximation. Results have also been given which demonstrate the improvement contained in the modified free-space theory for the coherent transmitted field presented in Chapter 2.

(iv) A quantitative analysis of the total field distribution based on the third and fourth field moments has been made and some effects of multiple scattering on this distribution illustrated. Physical conditions necessary for the approximate validity of the bivariate Gaussian distribution as discussed in Chapter 2 have been verified.

(v) Monte Carlo simulation has been demonstrated to be a useful tool in the study of random media of discrete scatterers and associated scattering theory.

The "exact" simulation results presented in this chapter provide a basis for future evaluation of the one-dimensional forms of other general theories developed by means of the "dishonest" technique discussed in Chapter 2. Further results for oblique angles of incidence, lossy scatterers, and Poisson-distributed random N would complement those already obtained. The exponential distribution for the spaces ξ_i between the scatterer centers,

$$p(\xi_i) = \rho e^{-\rho \xi_i}, \quad \rho = \langle N \rangle / d \quad (i = 1, 2, \dots, N + 1) \quad (4.1)$$

required to give Poisson-distributed N is easily generated from⁴⁷

$$\xi_i = -\frac{1}{\rho} \log_e(z_i) \quad (4.2)$$

where the z_i are uniformly-random numbers from the unit interval.

5. SIMULATION OF A NON-UNIFORM PROBABILITY DENSITY OF PLANAR-
SCATTERER CONFIGURATIONS WEIGHTED TOWARDS PERIODICITY

5.1 Introduction

The uniform probability density function and scattering theory based on it are most valid for "gas-like" scatterer distributions of low average density. For distributions of higher average densities the uniform probability density function is inappropriate and more accurate functions must be considered. Ideally, a probability density function is required which is applicable over the entire range of scatterer concentrations from a "rare gas", through a "liquid", to the other limit of a "crystal-like solid".

One theoretical approach to the problem has been to limit consideration to the two-scatterer probability density function²⁶

$$p(\bar{r}_s, \bar{r}_t) = p(\bar{r}_s) p(\bar{r}_t | \bar{r}_s) \quad (5.1)$$

Specifically, a two-scatterer conditional probability density function of the form

$$p(\bar{r}_t | \bar{r}_s) = h(|\bar{r}_s - \bar{r}_t|) \quad (5.2)$$

(i.e., a function of the separation of two scatterers) has been pursued such that h reduces to the case of a "rare gas" and a "crystal" in the appropriate limits. This approach is suited to the usual scattering theories based on a "dishonest" method in which only a two-scatterer probability density function is required. For the case of a "one-dimensional liquid", a suitable h exists and has been applied to scattering by one-dimensionally random distributions of cylinders.⁴⁸ This function, however, seems limited to the case of an infinite number of scatterers in the development of approximate scattering theory. For three-dimensional scatterer distributions, there exist no explicit

forms of h that cover the full range from "rare gas" to any one of the appropriate "crystals".

Another theoretical approach to the problem has been to consider a "two-phase" system whose population of scatterers is divided between a "gas-like" phase and a "crystal-like" phase.²⁵ The scatterers in both phases contribute to the coherent field, but only those in the gas phase contribute to the incoherent field. A third more heuristic approach has been to assume uniform-randomness for more dense scatterer distributions and use an average density ρ based on the volume available to the scatterers (i.e., volume of the containing region less the volume occupied by the finite-size scatterers). This approach, discussed in Appendix A (section A.2), has been used by Twersky²⁴ for his mixed-space theory for the coherent field.

In the present work, the theoretical problem requiring a suitable probability density function for more dense scatterer distributions has been bypassed. In order that the scattering characteristics of dense distributions of finite-size planar scatterers might be investigated, a computer simulation technique has been used to generate an appropriate one-dimensional distribution ranging between the limits of uniform-randomness and "periodicity" (i.e., periodically-positioned scatterers). Such an approach is not limited to the one-dimensional model; similar techniques could be used in Monte Carlo simulation studies with more complex mathematical models or with physical models of the type discussed in Chapter 6.

Two similar methods have been developed in this work for generating a suitable one-dimensional distribution of scatterers ranging between the limits of uniform-randomness and periodicity. These methods are essentially "rejection" techniques;⁴⁷ however, random numbers are generated to conform to a physical requirement rather than a theoretical distribution. The requirement is that no scatterers be allowed to approach one another more

closely than a distance e between their centers. This parameter may be the physical width of the scatterer or some hypothetical "distance of closest approach".

The methods of generating the distribution are discussed in section 5.2 and results given which illustrate the type of distribution generated. In section 5.3 results are given for a variation of the distribution parameter e between the limits of uniform-randomness and periodicity with the scattering parameters remaining fixed. Criteria for the validity of assuming the planar scatterers to be uniformly distributed are presented, based on the average density per wavelength ρ_λ and the fractional "volume" $\beta_0 = Ne/(d + e)$ occupied. In section 5.4 a comparison is made between numerical results obtained from Twersky's mixed-space theory and simulation results for distributions of finite-width planar scatterers. A general discussion and summary of results is given in section 5.5.

5.2 Methods of Generating the Distribution

The uniform random number generator provided the basis for the two methods used to generate a non-uniform distribution with the desired limits of uniform-randomness and periodicity. The initial steps of the procedure were:

(i) N uniformly-random numbers were generated on the unit interval corresponding to the normalized positions of the scatterers (i.e., $z_1/d, z_2/d, \dots, z_N/d$). These numbers were placed in an "array" of computer memory in the sequence of generation; i.e., for an array $A(I)$ with $I = 1, 2, \dots, N$, the first number occupied position 1, the second, position 2, etc.

(ii) The N random numbers were then sorted within memory so that they occupied the array $A(I)$ in order of size; i.e., in the sequence of the ordered-positions z'_1, z'_2, \dots, z'_N .

Once these initial steps had been completed the physical requirement that no

adjacent pair of numbers be closer than e/d , the normalized distance of closest approach, was applied. The two methods developed differ in the manner in which numbers which did not satisfy this requirement were rejected and new ones generated.

5.2.1 Method A

In this method a new random number was generated after each rejection. The steps of the procedure were as follows:

(i) The array $A(I)$ was scanned beginning at position 1 until an adjacent pair of numbers were found to be closer than e/d . Depending on the value of the previous random number generated, either the larger or the smaller of the pair was rejected. If the previous number generated was less than 0.5, the smaller number of the pair was rejected; if it was 0.5 or greater, then the larger was rejected. Thus, both numbers were rejected with equal probability.

(ii) For each random number rejected a new one was generated to take its place in the array. This new number was then merged with the remaining $N - 1$ by an interchange procedure to place it in the correct order of size.

(iii) Steps (i) and (ii) were then repeated with a change in the scanning direction of step (i), scanning beginning at element N of the array rather than at element 1. This process of rejecting and generating one number at a time, with scanning of the array beginning alternately with elements 1 and N , was repeated until a suitable configuration of N numbers was obtained, with no adjacent pair closer than e/d .

5.2.2 Method B

In this method the entire array was scanned with one of each pair of numbers breaking the required condition being simultaneously rejected and replaced by a new one. The steps of this second procedure were as follows:

(i) The array $A(I)$ was scanned beginning with element 1 and all pairs of numbers not satisfying the distance-of-closest-approach criterion were recorded.

(ii) New random numbers were generated corresponding to the number of unacceptable pairs. These were stored in another array $B(J)$, with $J = 1, \dots, L$ (L being the number of unacceptable pairs).

(iii) Depending upon the value of the new random number in the storage location J of $B(J)$, either the smaller or the larger of the J -th pair of unacceptable numbers in $A(I)$ was rejected. The equal-probability rejection rule of method A was again used. In the event that two unacceptable number-pairs were adjacent to one another (i.e., a sequence of three numbers) and the one rejected from each pair was common (i.e., the center number of the sequence), one less number from the array $B(J)$ was required.

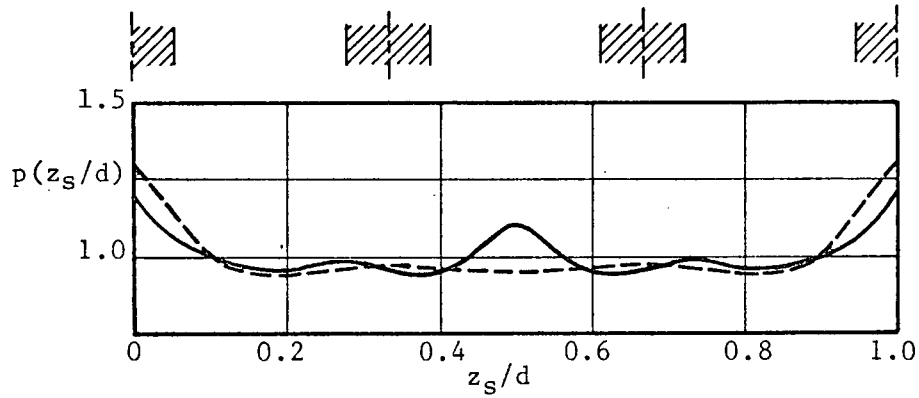
(iv) The required numbers from the array $B(J)$ were then sorted in order of size and merged with those not rejected from $A(I)$.

(v) The preceding steps were repeated until a suitable configuration of N numbers was obtained.

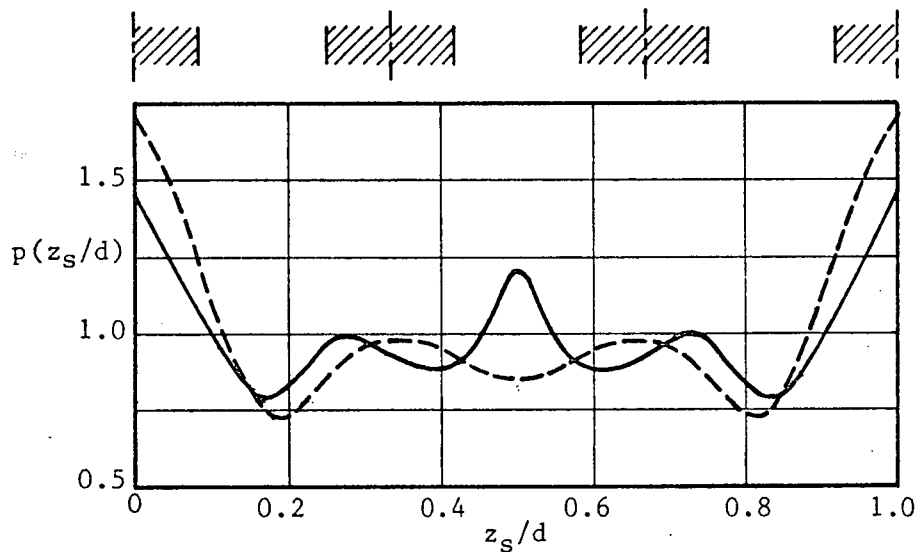
5.2.3 Results

The one-scatterer normalized probability density function $p(z_s/d) = \rho(z_s/d)d/N$ was determined for both methods A and B, for several values of N and distances of closest approach e/d . Plots of this function for three values of e/d are given in figures 5.1 and 5.2 for $N = 4$ and $N = 5$ respectively. The periodic position of each scatterer and the "excluded region" surrounding it are shown at the top of each graph for comparison with the probability density curves determined. The graphs were obtained by drawing smooth curves through the experimental points resulting from 20,000 sample configurations and fifty histogram intervals.

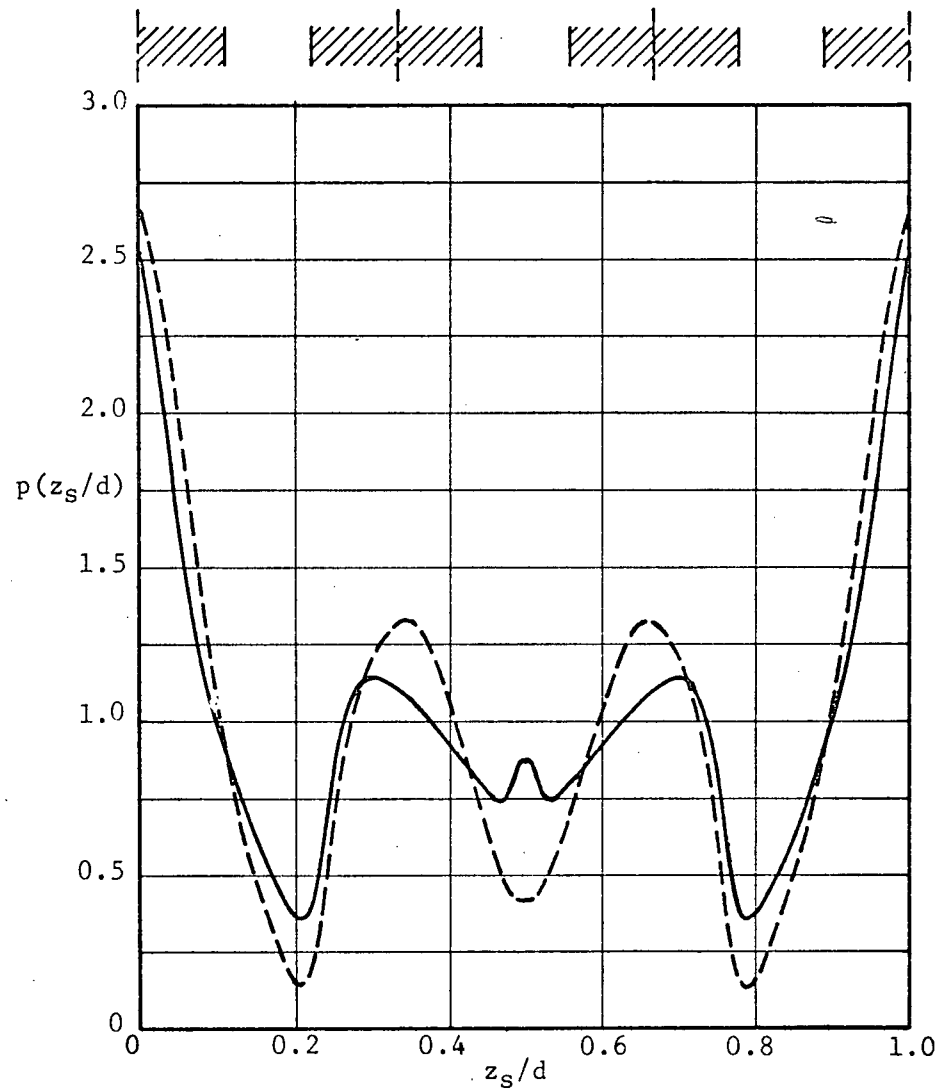
As seen from figures 5.1 and 5.2, as e/d is increased the probability density curves become more highly peaked. For $N = 5$ the peaks of the curves for both methods correspond closely to the periodic positions, but for $N = 4$, only for method B. For $N = 4$ and low values of e/d the curves for method A



(a) $e/d = 1/9$ ($\beta_0 = 0.4$)

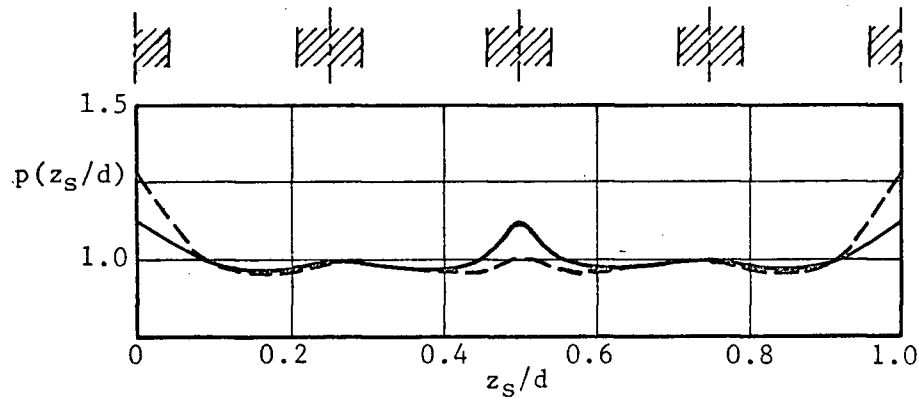


(b) $e/d = 1/6$ ($\beta_0 = 0.572$)

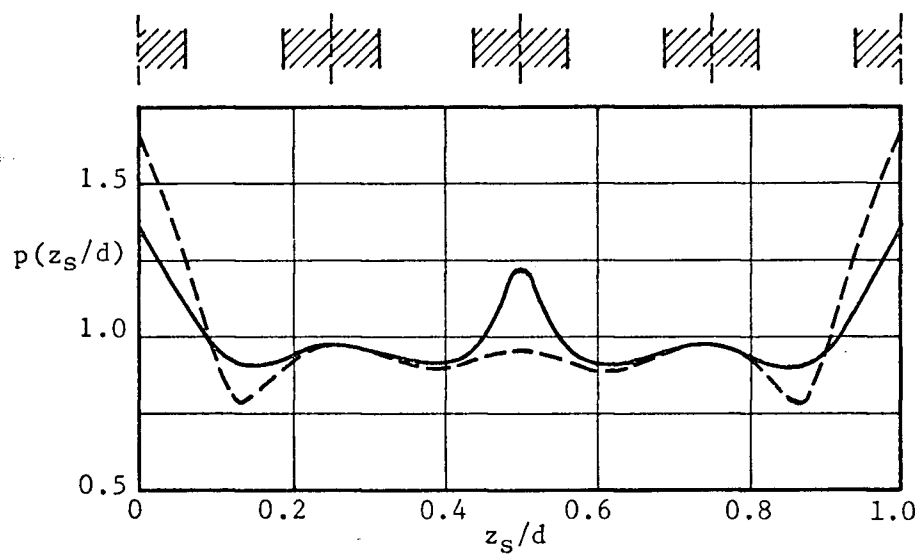


(c) $e/d = 2/9$ ($\beta_0 = 0.728$)

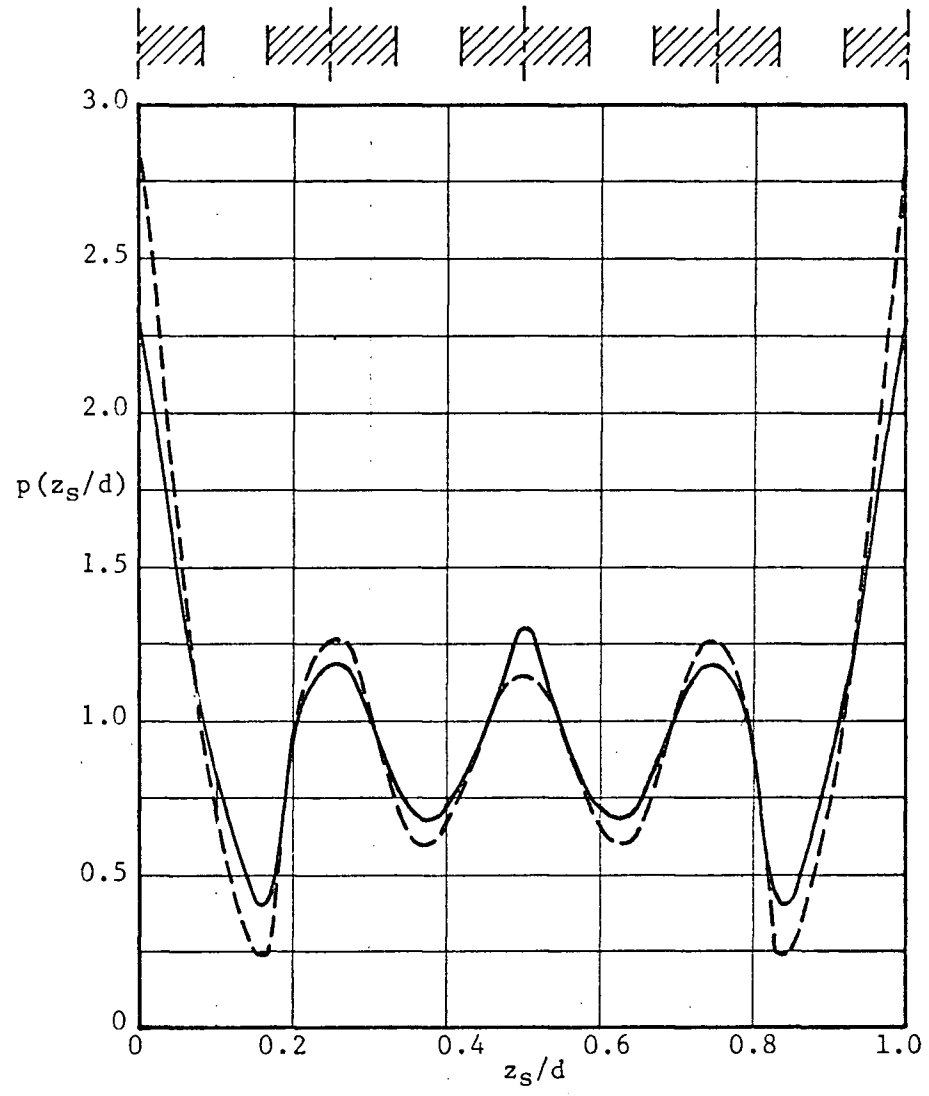
Figure 5.1 One-Scatterer Normalized Probability Density Curves for $N = 4$
 — Method A, - - - Method B



(a) $e/d = 1/12$ ($\beta_0 = 0.385$)



(b) $e/d = 1/8$ ($\beta_0 = 0.556$)



(c) $e/d = 1/6$ ($\beta_0 = 0.715$)

Figure 5.2 One-Scatterer Normalized Probability Density Curves for $N = 5$
 ——— Method A, - - - Method B

contain an extra peak at the center of the distribution. This center peak, however, gradually disappears as e/d is increased, leaving the remaining peaks to correspond closely to the periodic positions. Both methods give a distribution symmetrical about the center of the slab region containing the scatterers. This was achieved in method A by the procedure of alternately scanning the array in opposite directions to detect unsatisfactory pairs of numbers. (An initial test of the method with scanning in only one direction showed the distribution to become increasingly non-symmetric for increasing e/d .) Similar results were obtained for higher values of N .

Other differences in the one-scatterer probability density curves for the two methods are apparent. The peaks corresponding to the outermost scatterers are higher for method B than method A, and the heights of the peaks for method B gradually diminish towards the center of the distribution. Such differences are to be expected, however, because of the different manner in which the distributions are generated. In method A the random number rejection process proceeds gradually from the outer ends of the array towards the center, whereas in method B it is applied "uniformly" over the entire array.

Although some differences in the one-scatterer probability densities generated by the two methods are evident for mid-range values of e , these differences of course disappear for $e \rightarrow 0$ and in principle must disappear for $e \rightarrow d/(N - 1)$. Towards the periodic limit, the peaks of the one-scatterer distributions generated by both methods must separate entirely for $d - Ne < 0$ or equivalently $\beta_0 = Ne/(d + e) > N/(N + 1)$, providing certain regions in which no scatterer can be located. In the periodic limit, the one-scatterer probability density functions must be of the form

$$p(z_s) = \frac{1}{N} \sum_{i=1}^N \delta\left(z_s - \frac{i-1}{N-1} d\right) \quad (s = 1, \dots, N) \quad (5.3)$$

where δ is the Dirac delta function.

Although both methods can in principle generate a distribution approaching the periodic limit, in practice they are suitable only if the fractional "volume" β_0 is below a certain value. For $N = 10$, the computer time involved increased sharply for $\beta_0 > 0.65$ because of the great number of rejections required. There appeared, furthermore, to be a limit beyond which no suitable configuration could be obtained with the available generator. This is considered possible because the generator has a finite population of numbers.^{41,42} For $N = 10$ this limit appeared to be about $\beta_0 = 0.8$ for the IBM 7044 computer generator RAND. The limit appeared furthermore to decrease with increasing N . Method A usually required the rejection of more random numbers than method B before a suitable configuration could be obtained, although method A, being a somewhat simpler procedure, was always faster. Such differences, however, were not large and in the factors discussed in this section the two methods are considered to be approximately equivalent.

Test runs of the two methods for the type of results of the following sections furthermore showed them to differ very little for the average field functions investigated. The results given are therefore based on method A. The disadvantage that explicit results cannot be obtained for $0.8 < \beta_0 < 1.0$ is not serious because the behavior in this interval can be inferred from the results for mid-range values of β_0 and the result for the periodic limit itself (i.e., $\beta_0 = 1$). Methods of eliminating this disadvantage and generating a suitable distribution on a more theoretical basis are discussed in section 5.5.

5.3 Variation of the Distribution Between the Limits of Uniform-Randomness and Periodicity for Fixed Scattering Parameters

In this section "exact" simulation results are given which show the effect of a variation of the distribution between the limits of uniform-

randomness and periodicity on the coherent field and average incoherent intensity. Based on these results, criteria are developed for the assumption of uniformly-distributed "finite-width" planar scatterers (i.e., $e \neq 0$) to be valid. For convenient comparison with the results of Chapter 4, the fixed scattering parameters $N = 10$, $\epsilon_r = 2.0$, and $w_{\lambda'} = 0.1$ are again used. All simulation results are for 1,000 sample configurations.

Shown in figure 5.3 are the phase and intensity d_λ -variation curves of the transmitted field for a periodic array of the scatterers. These curves are of importance in the following discussion of results for the "periodicity-weighted" random distribution whose scattering behavior becomes "periodic" as $e \rightarrow d/(N - 1)$ or equivalently $\beta_0 = Ne/(d + e) \rightarrow 1$. The well-known resonance behavior which occurs at periodic intervals in d_λ is specified on the x-axis of the graphs by the index n_R which takes the values $n_R = 0, 1, 2, \dots$. For the present parameters the resonance interval in d_λ is 4.5. This gives a separation between scatterers at resonance of approximately $n_R \lambda / 2$, a slight deviation from this value occurring because of the different wavelength λ' in the scatterer material.

The first set of results illustrate the effect of e variation on the average field functions for a number of widely-spaced slab-region widths d_λ . Curves for the coherent phase and intensity of the transmitted field are given in figures 5.4a and 5.4b; curves for the average incoherent intensity of the reflected field are given in figure 5.4c. The five values of d_λ chosen to display the results are all approximately mid-way between adjacent resonance values and give identical periodic limits for $Ce^{j\alpha}$. Smooth curves have been drawn through all "experimental" points except those for $d_\lambda = 97$ where the actual curves are too oscillatory in nature to display accurately from the present results. The points are included for $d_\lambda = 2.5$ and $d_\lambda = 7$. Curves for $\langle I^2 \rangle$ of the transmitted field are not shown because they are similar in form

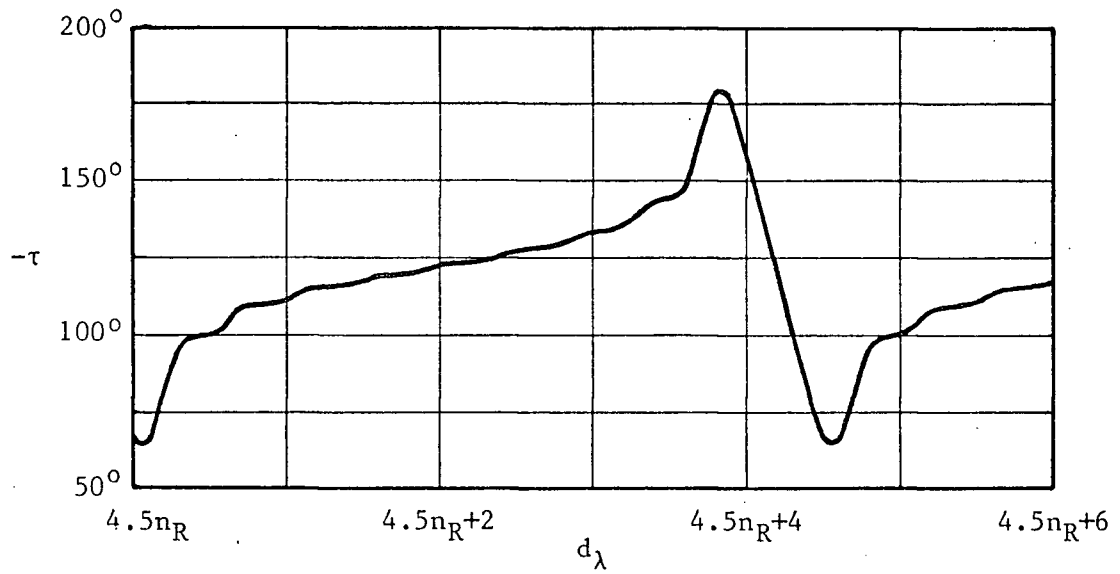
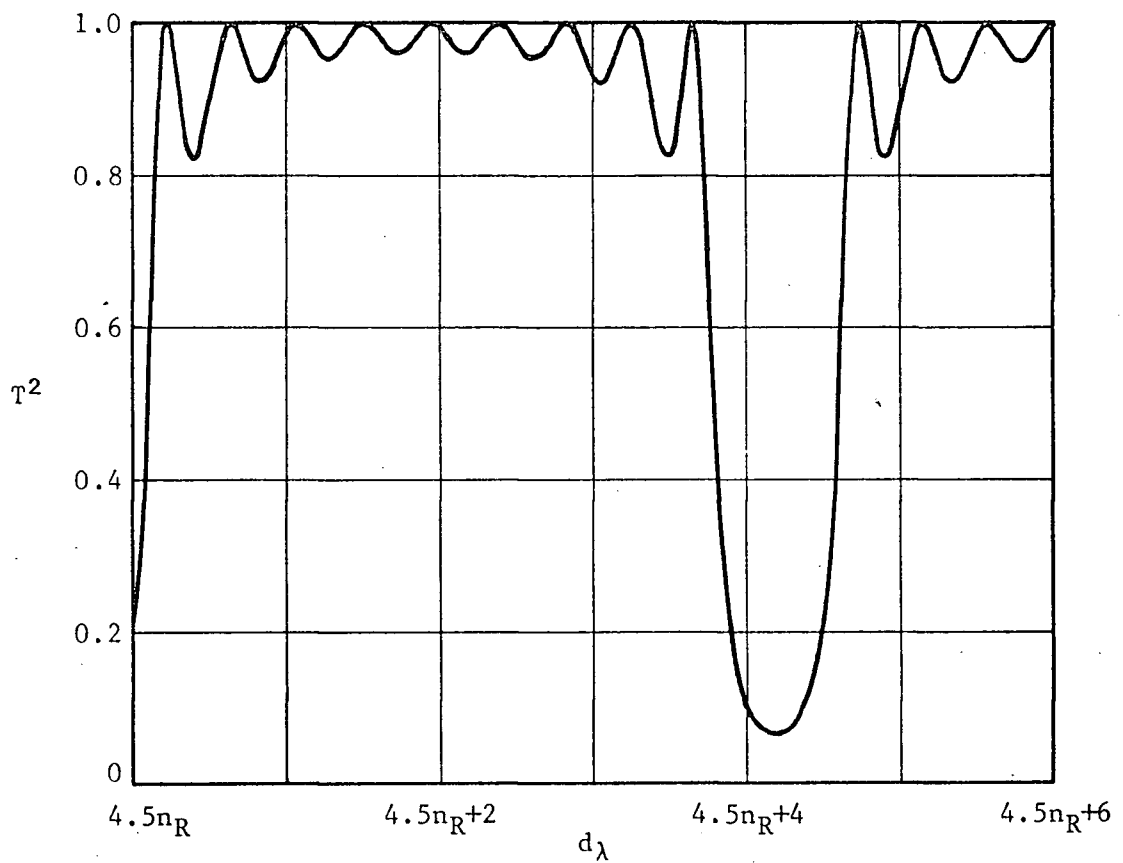
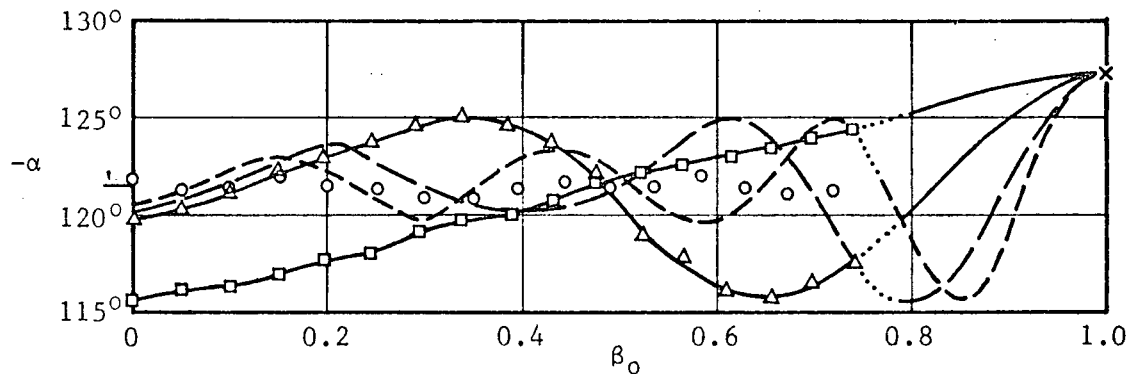
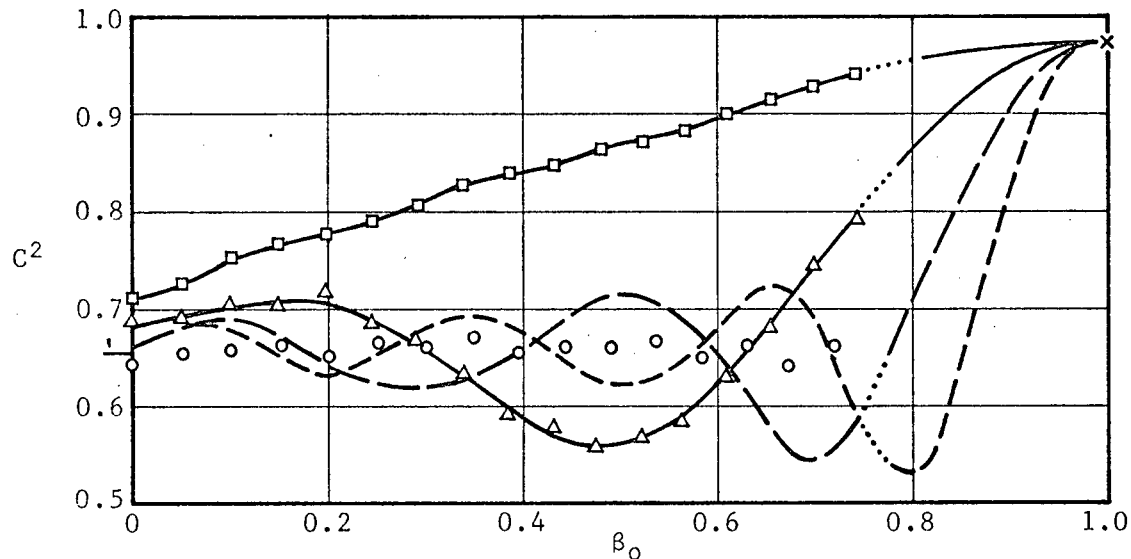
(a) $-\tau$ versus d_λ (b) T^2 versus d_λ

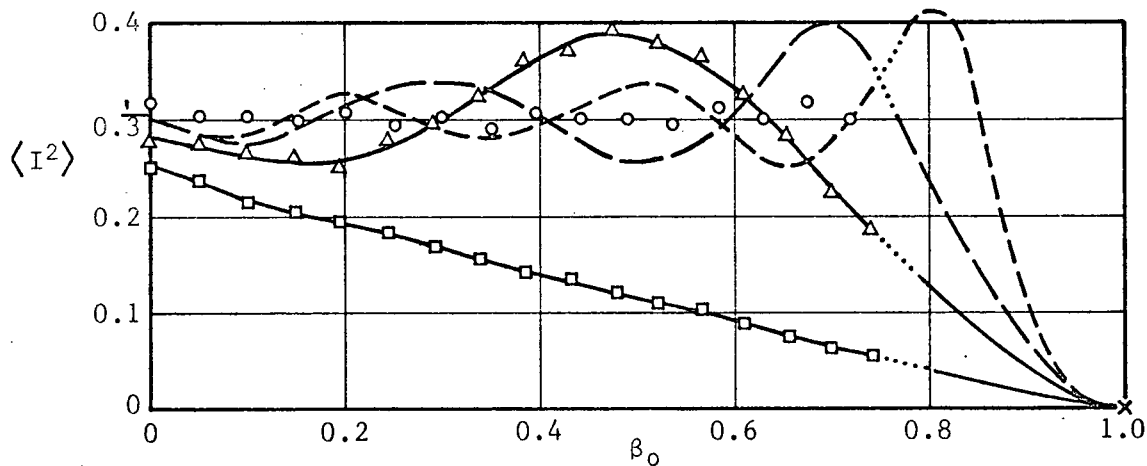
Figure 5.3 Phase and Intensity of the Transmitted Field as Functions of d_λ for a Periodic Array. $N = 10$, $w_\lambda = 0.1$, $\epsilon_r = 2.0$



(a) $-\alpha$ versus β_0 - Transmitted Field



(b) C^2 versus β_0 - Transmitted Field



(c) $\langle I^2 \rangle$ versus β_0 - Reflected Field

Figure 5.4 Dependence of Average Field Functions on β_0 for Various Values of d_λ . $N = 10$, $w_\lambda = 0.1$, $\epsilon_r = 2.0$; \square — \square $d_\lambda = 2.5$, \triangle — \triangle $d_\lambda = 7$, ——— $d_\lambda = 11.5$, - - - - $d_\lambda = 16$, \circ $d_\lambda = 97$, — Asymptotic Values for $\rho_\lambda \rightarrow 0$, \times Periodicity Values

to those for the reflected field. The section of each curve for $\beta_0 \rightarrow 1$ has been interpolated from the available results, the beginning of the section being indicated by a "dotted" break in the curve. The asymptotic behavior of the interpolated sections in the periodic limit has been assumed on the basis of the occurrence of the same behavior for $d_\lambda \rightarrow 0$.

As seen from figure 5.4, the given curves are very oscillatory in character. The number of primary oscillations over the interval $0 \leq \beta_0 \leq 1$ increases for increasing d_λ (or decreasing ρ_λ) but the oscillations decrease in magnitude for increasing d_λ . For the periodic spacing between scatterers in the interval

$$\frac{n_R}{2} < \frac{d_\lambda}{N-1} < \frac{n_R + 1}{2} \quad (5.4)$$

the number of apparent relative maxima or minima in the curves (not including the periodic value) is given by the "resonance index" n_R . The results for $d_\lambda = 2.5$ indicate the possible presence of secondary oscillations in the curves, although more accurate results are necessary for this to be established. Such behavior in the periodicity-weighted distribution would seem possible because of the secondary oscillations in the curves of figure 5.3 for a periodic array.

The results of figure 5.4 show that as n_R increases the distribution does not begin to exhibit "periodic" behavior until increasingly higher values of β_0 . For $d_\lambda < (N-1)/2$ the curves proceed directly to the periodic limits as β_0 increases; for $d_\lambda \gg (N-1)/2$ (e.g., $d_\lambda = 97$) the distribution behaves as though the scatterers were uniformly distributed up to a very high value of β_0 .

The reasons for the observed behavior can be explained in terms of the theory of random phasor sums discussed in section 2.8. It is useful to write the transmitted field as

$$T_e j^\tau = A_0 e^{j\theta_0} + \sum_{s=1}^N A_s e^{j\theta_s} = A_0 e^{j\theta_0} + T' e^{j\tau'} \quad (5.5)$$

where the constant phasor $A_0 e^{j\theta_0} = (1 + g_+)^N$ is the Z-0-B-S contribution to $T_e j^\tau$ and the random phasor $A_s e^{j\theta_s}$ is the multiple-scattering contribution from scatterer s composed of all other even 0-B-S. (The values of θ_0 and A_0^2 for the present parameters and that for $\langle I^2 \rangle$ as $\rho_\lambda \rightarrow 0$ are shown on the scales of the graphs in figure 5.4.) Then,

$$C e^{j\alpha} = \langle T_e j^\tau \rangle = A_0 e^{j\theta_0} + C' e^{j\alpha'} \quad (5.6)$$

where

$$C' e^{j\alpha'} = \langle T' e^{j\tau'} \rangle = \sum_{s=1}^N \langle A_s e^{j\theta_s} \rangle \quad (5.7)$$

Thus, maxima in the curves for C^2 occur when $C' e^{j\alpha'}$ is in phase with $A_0 e^{j\theta_0}$ (i.e., $\alpha = \alpha' = \theta_0$); minima occur when $C' e^{j\alpha'}$ is 180° out of phase (i.e., $\alpha = \alpha' - \pi = \theta_0$). The energy lost from the coherent transmitted field when C^2 is minimum reappears in the incoherent fields.

The theory of section 2.8 showed that the random components of the θ_s represent approximately double the "electrical lengths" between adjacent scatterers. Physical reasoning then requires that for $e = 0$,

$$\sigma_{\tau'} \approx \sigma_{\theta_s} \approx 4\pi d_\lambda / (N - 1) \quad (5.8)$$

Similarly, for $e \neq 0$,

$$\sigma_{\tau'} \approx 4\pi \left(\frac{d_\lambda}{N - 1} - e_\lambda \right) \approx 4\pi(1 - \beta_0) \frac{d_\lambda}{N - 1} \quad (5.9)$$

Thus, for a periodic spacing between scatterers in the interval given by (5.4),

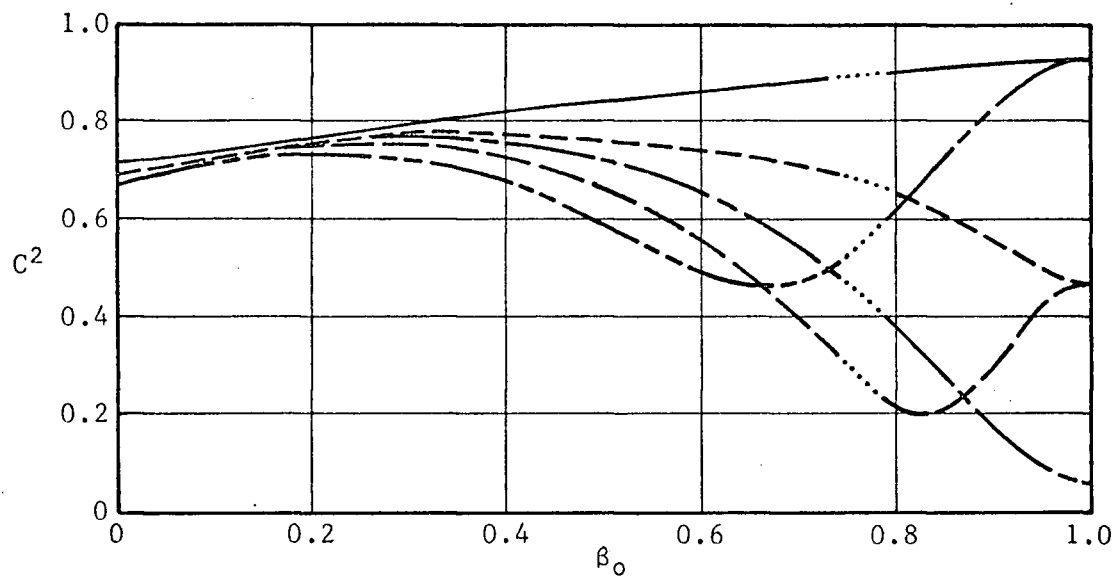
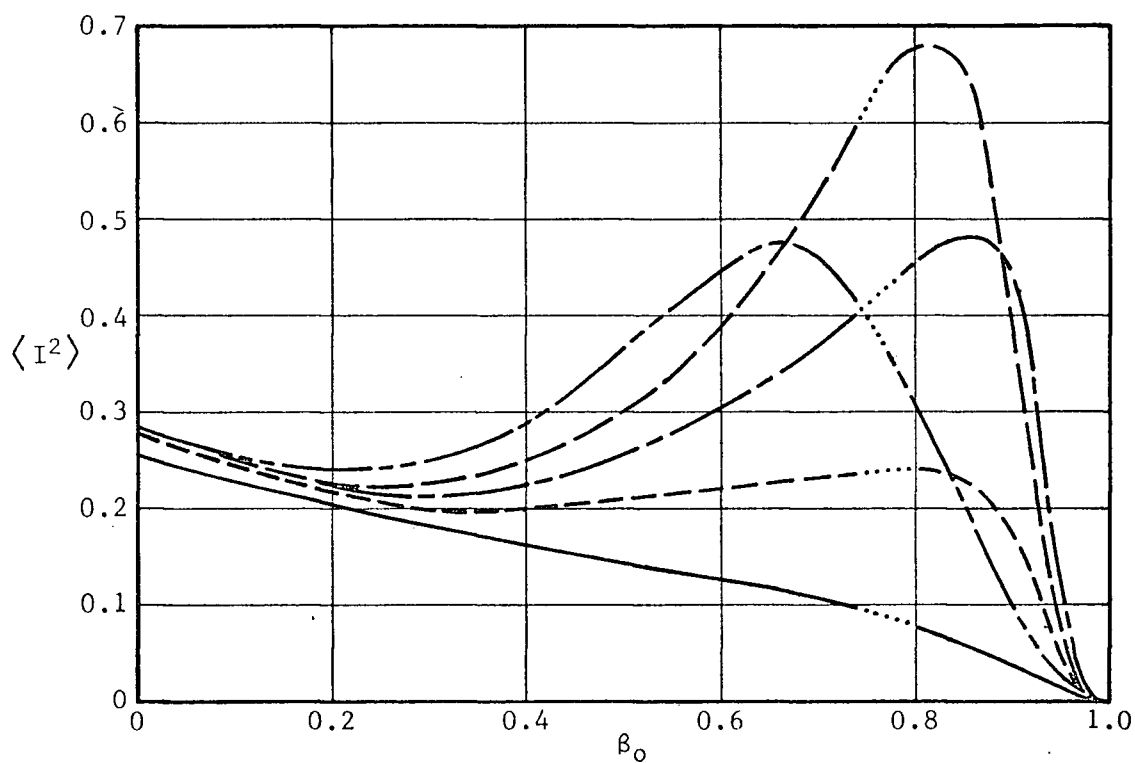
$$2\pi n_R(1 - \beta_0) \lesssim \sigma_{\tau'} \lesssim 2\pi(n_R + 1)(1 - \beta_0) \quad (5.10)$$

If $\sigma_{\tau'} \gg 2\pi$, the basic phase cycle equivalent of τ' is effectively uniformly

distributed, the random component $\tau' e^{j\tau'}$ of the total field then completely incoherent (i.e., $C' e^{j\alpha'} = 0$), and therefore $C e^{j\alpha} = (1 + g_+)^N$. The fact that this situation occurs for large $n_R(1 - \beta_0)$ agrees with the results of figure 5.4. The oscillatory behavior of the curves develops because, as β_0 varies between zero and one, the weighting of the equivalent distribution of τ' towards different sections of the basic phase cycle varies in a periodic manner causing the phasor $C' e^{j\alpha'}$ to periodically rotate. For larger n_R , $\sigma_{\tau'}$ varies over a larger number of basic phase cycles as β_0 varies between zero and one and the curves therefore contain more oscillations as shown. Furthermore, as $n_R(1 - \beta_0)$ is decreased (either by a decrease in n_R or an increase in β_0), the deviation of τ' from a uniform distribution on the basic phase cycle must increase, causing the magnitude of the oscillations to become larger. This is also apparent from the curves of figure 5.4.

Similar reasoning can be used to explain an oscillatory behavior in the coherent reflected field for a variation of β_0 in the interval $0 \leq \beta_0 \leq 1$. Curves are not given because of the inaccuracy of simulation results for the small magnitudes involved and because the equivalent behavior for a variation of d_λ was illustrated in Chapter 4.

For periodic spacing of the scatterers in the neighbourhood of a resonance condition, the scattering behavior of the distribution for $\beta_0 \rightarrow 1$ is highly variable for slight changes in d_λ . Figure 5.5 illustrates the effect in a series of curves for C^2 of the transmitted field and $\langle I^2 \rangle$ of the reflected field in the neighbourhood of the second resonance (i.e., $n_R = 1$). Actual resonance occurs at about $d_\lambda = 4.2$. These curves also illustrate the beginning of the large-amplitude oscillatory behavior after the second resonance. The observed diversion of a large fraction of energy to the incoherent reflected field just above resonance (e.g., at $d_\lambda = 4.6$) is of interest although a reason for this behavior is not immediately evident. A similar

(a) C^2 versus β_0 - Transmitted Field(b) $\langle I^2 \rangle$ versus β_0 - Reflected FieldFigure 5.5 β_0 -Variation Curves for Values of d_λ in the Neighbourhood ofResonance at Periodicity. $N = 10$, $w_\lambda = 0.1$, $\epsilon_r = 2.0$;— $d_\lambda = 3$, - - - $d_\lambda = 3.8$, - - - $d_\lambda = 4.2$,— $d_\lambda = 4.6$, - - - $d_\lambda = 5.4$

effect occurs for the incoherent transmitted field.

The results of this section clearly indicate when it is valid to assume that a distribution of planar scatterers of finite width is uniform. For high ρ_λ the average spacing between the scatterers must be much greater than the minimum spacing. Since the average spacing is approximately equal to the spacing $d_\lambda/(N - 1)$ at periodicity, this condition can be written

$$\frac{d_\lambda}{N - 1} > \frac{d_\lambda}{N} = \frac{1}{\rho_\lambda} \gg e_\lambda \quad (5.11)$$

or

$$\beta_0 \ll 1 \quad (5.12)$$

Typically, as indicated by the results of figure 5.4, for $0.4 < \rho_\lambda < 4$, it is required that $\beta_0 \gtrsim 0.1$ for the assumption of uniform-randomness to be reasonably valid for the given scatterers. For $\rho_\lambda > 100$, as seen by the results of Chapter 4, it makes little difference whether the scatterer positions are uniformly-random or periodic and thus the value of β_0 is not important.

For distributions of low ρ_λ the requirement of (5.12) for uniform-randomness is too stringent, as is indicated by the results of figure 5.4 for $d_\lambda = 97$. A less stringent condition is that the standard phase deviation σ_τ of the random component of the transmitted field be much greater than 2π radians, or equivalently from equation (5.9),

$$(1 - \beta_0)/\rho_\lambda \gg 1 \quad (5.13)$$

Thus, for even a large fraction of the containing slab region filled by the excluded regions of the scatterers, uniform-randomness may be assumed as long as ρ_λ is small.

For distributions of three-dimensional scatterers a criterion similar to that of (5.12) has often been used (i.e., $\beta_0 \ll \beta_m$, where β_m is the maximum

β_0 physically achievable). In view of the validity of the less stringent criterion (5.13) for low- ρ_λ distributions of planar scatterers, the question of the possible validity of a similar criterion for distributions of three-dimensional scatterers arises (i.e., where ρ_λ is the average density per cubic wavelength). The validity of such a criterion would seem possible for the multiple-scattering contributions to the random component of the field in a three-dimensional distribution since even for large β_0 a low average density of scatterers per cubic wavelength would give a large σ_{θ_S} for each contribution and a resulting uniform distribution for the equivalent θ_S on the basic phase cycle. As shown in Appendix C, however, the σ_{θ_S} for the dominant single-scattering contributions to the forward-scattered field in a three-dimensional distribution can be quite small, even for a low ρ per cubic wavelength. Thus, the more stringent criterion appears to be necessary.

5.4 Comparison of Simulation and Mixed-Space Theory Results for Planar Scatterers of Finite Thickness

In this section a comparison is made between numerical results for the coherent field obtained from Twersky's mixed-space theory and "exact" results based on the simulation of a non-uniform distribution of planar scatterers of finite width. For the simulation, the width e of the scatterer excluded region is set equal to the physical width w of the dielectric slab scatterers employed. As discussed in Appendix A (section A.2), the modified form $\rho = N/(d + w - Nw)$ of the average density is used in the mixed-space theory and the slab-region width d containing the scatterer centers is replaced by $d + w$, that containing the scatterer boundaries. Results are also given for the mixed-space coherent reflected field theory with only the modified ρ .

5.4.1 The Coherent Transmitted Field

Results for the coherent transmitted field are based on a "compression

process" similar to that used for a physical-model distribution of a slab region of spherical scatterers.⁴⁹ The width of the planar scatterers and the width of the slab region containing them are fixed so that as an increasing number are placed within the region the distribution is gradually compressed, the scatterers eventually filling the region. The parameters have been chosen so that the slab region is filled for $N = 25$.

The first set of curves of figure 5.6 give results for a high ρ_λ occurring in the limit of $\beta_0 = Nw/(d + w) \rightarrow 1$. The single scatterer parameters for these curves are again $\epsilon_r = 2.0$ and $w_\lambda = 0.1$. The w_λ value and the $N = 25$ limit for $\beta_0 = 1$ were chosen to give the limiting result $C^2 = 1$ (i.e., since $d_\lambda + w_\lambda = 2.5$), although this was not necessary for the mixed-space theory to give exact results in the $\beta_0 = 1$ limit. Shown also for comparison in figure 5.6 are simulation results for uniformly-distributed infinitely-thin scatterers having the same scattering amplitudes. Both sets of simulation results are based on 1,000 samples.

As seen from figure 5.6, the general trend of the coherent field behavior for increasing N is approximately predicted by the mixed-space theory. The coherent intensity at first decreases (as for a uniform distribution), reaches a minimum, and then increases as the distribution becomes more "ordered" and energy is diverted from the incoherent fields. Approximately the same behavior has been measured on the model distribution of spherical scatterers, although the experimental results obtained agree more closely with the mixed-space theory results for mid-range values of β_0 .⁴⁹ The discrepancy in the present results for the one-dimensional model is due to the fact that the total scattering cross-section $\sigma = -2 \text{Re}g_+$ is sufficiently large that the asymptotic form $\langle T \rangle = e^{Ng_+}$ for the mixed-space theory is not accurate. This was shown in figure 4.3 on page 62. As pointed out in Chapter 4, only certain parameters give sufficiently small σ that adequate agreement in the asymptotic

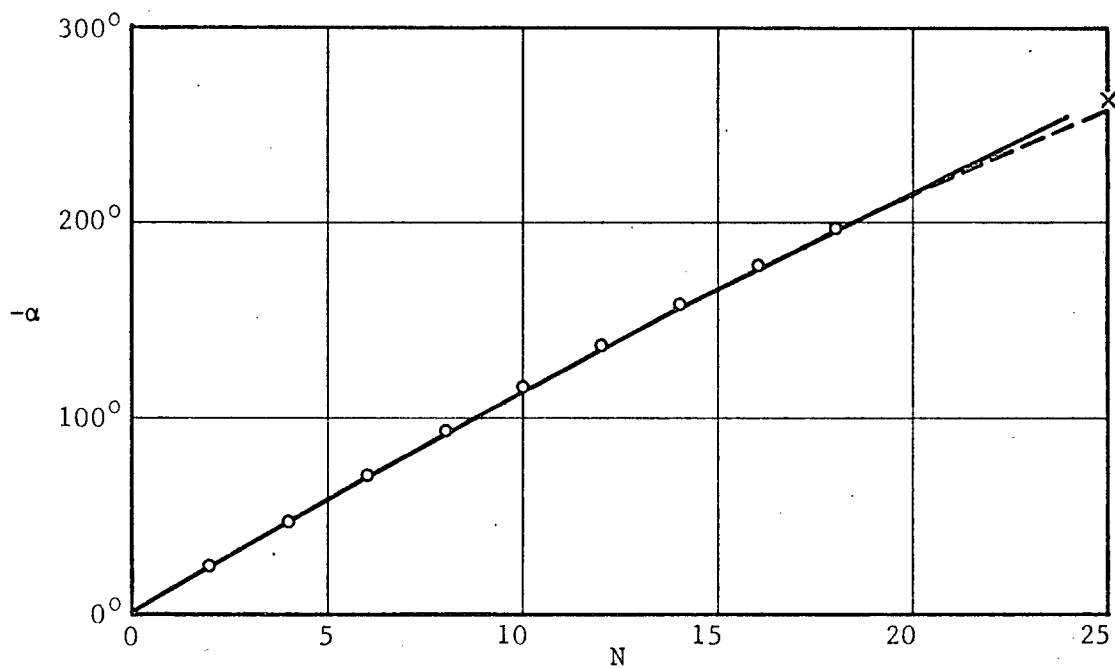
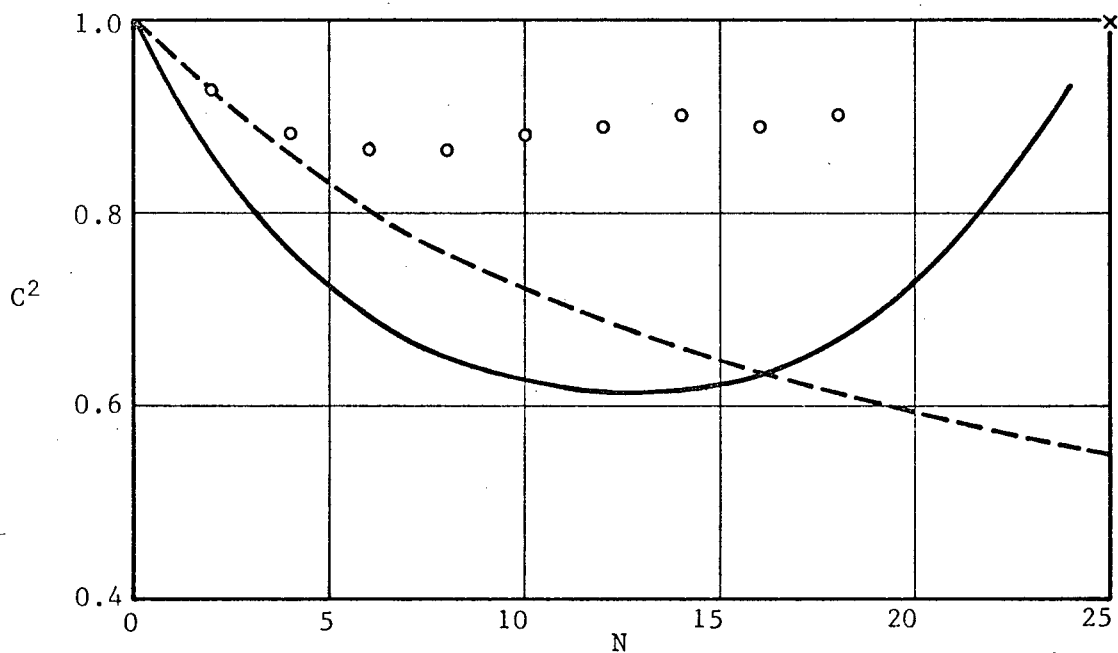
(a) $-\alpha$ versus N (b) C^2 versus N

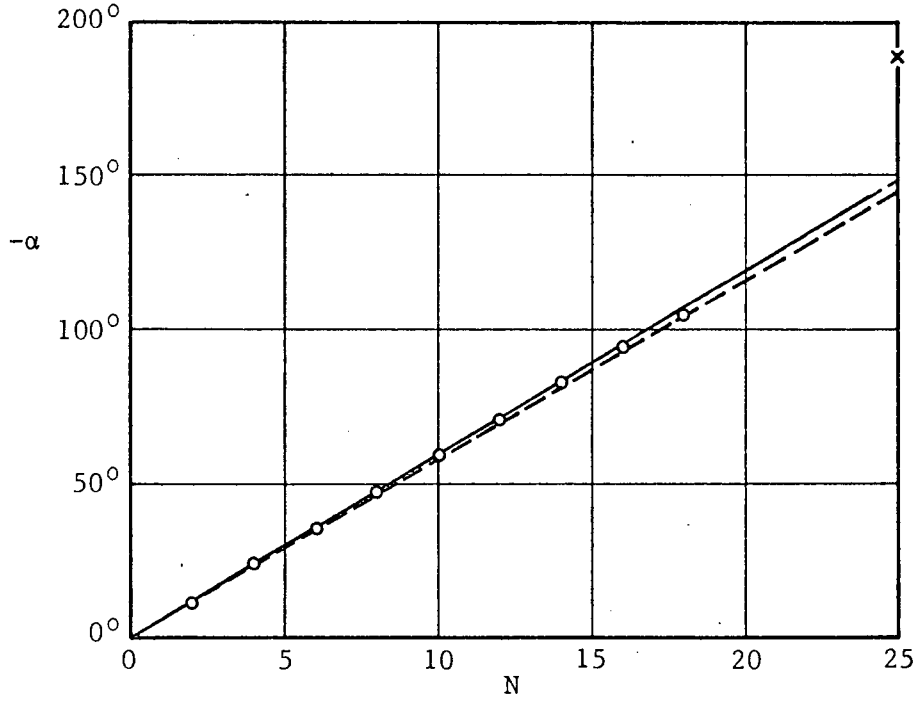
Figure 5.6 Coherent Transmitted Field Results for High ρ_λ . $w_\lambda = 0.1$, $\epsilon_r = 2.0$, $d_\lambda = 1.697$; \circ Non-Uniform Distribution Simulation, $---$ Uniform Distribution Simulation, $---$ Twersky's Mixed-Space Theory, \times Periodicity Values

forms can be obtained for finite N (e.g., for $w_{\lambda} \ll 0.25$ or at periodic values in w_{λ} , for thick slabs). The situation may not be as critical for three-dimensional scatterers.

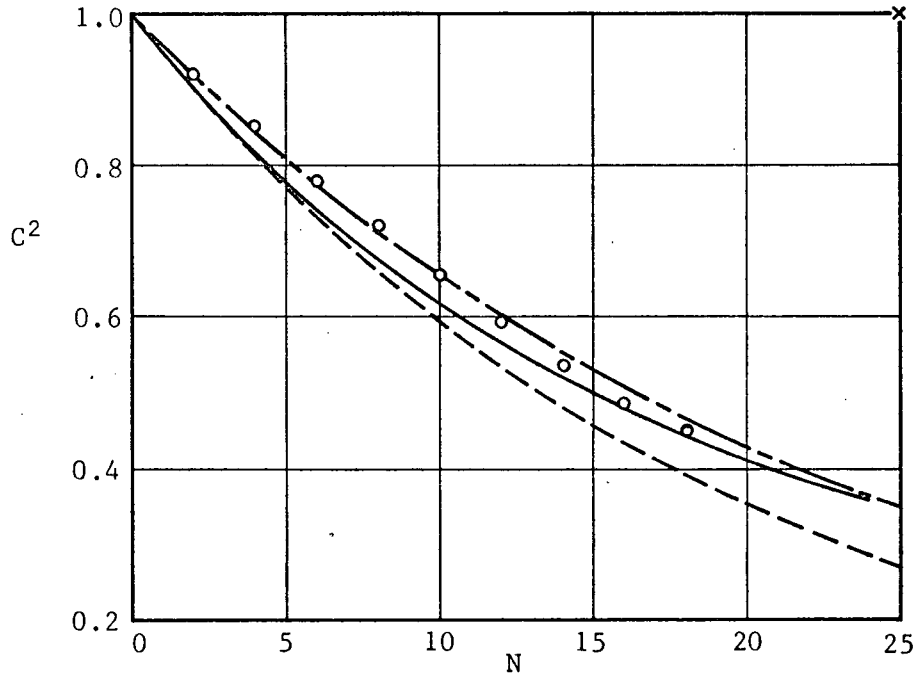
In figure 5.6 the apparently correct limiting behavior predicted by the mixed-space theory for $\beta_0 \rightarrow 1$ is achieved because the scatterers completely fill the containing region and are sufficiently "thin" that $g_-'/g_+ \rightarrow 1$ and $\eta \rightarrow \eta'$ (see Appendix A, section A.2, and Appendix B, section B.2). If the excluded-region width e is chosen to be larger than w (i.e., spaces existing between the scatterer boundaries for $\beta_0 = 1$), the mixed-space theory does not give exact results in the "periodic" limit. This situation is somewhat equivalent to that occurring for distributions of spheres discussed by Beard et al.,⁴⁹ where the slab region cannot be completely filled with scattering material.

Exact results in the "periodic" limit are also not achieved if the limits $g_-'/g_+ \rightarrow 1$ and $\eta \rightarrow \eta'$ for $\beta_0 \rightarrow 1$ do not hold. This is illustrated by the results of figure 5.7 for low ρ_{λ} . For these results the scatterer width of $w_{\lambda} = 6.9$ has been chosen to give sufficiently small σ that $e^{Ng_+} \approx (1 + g_+)^N$, as shown in figure 5.7. The resulting scattering amplitudes are now $g_+ = 0.1044$ $/-104.5^\circ$ and $g_- = 0.2035$ $/84.07^\circ$, but the value of $|1 + g_+|^{2N}$ remains the same as that for $w_{\lambda} = 0.1$. Again the "periodic" limit for C^2 is unity for the chosen parameters.

The simulation results of figure 5.7 follow closely the asymptotic curves as obtained from $(1 + g_+)^N$, even for relatively high values of β_0 . This, of course, is in agreement with the results of section 5.3. Because the present methods of generating the distribution do not allow higher values of β_0 to be reached, the exact point at which the distribution begins to exhibit marked "periodic" behavior is not known, although it is estimated to be in the neighbourhood of $N = 23$. As seen from figure 5.7, the mixed-space theory does



(a) -α versus N



(b) C² versus N

Figure 5.7 Coherent Transmitted Field Results for Low ρ_λ . $w_{\lambda'} = 6.9$
 $\epsilon_r = 2.0$, $d_\lambda = 117.1$; \circ Non-Uniform Distribution Simulation,
 — Twersky's Mixed-Space Theory, — $Ce^{j\alpha} = (1 + g_+)^N$,
 - - - $Ce^{j\alpha} = e^{Ng_+}$, \times Periodicity Values

not give the correct "periodic" limit although it gives good agreement with simulation results for most of the range of β_0 . Several other sets of numerical results obtained for the mixed-space theory appear to indicate that approximately the correct limiting behavior occurs only for "thin" slabs.

In summary, it has been shown that the requirement for the "one-dimensional" mixed-space theory to give adequate agreement with typical simulation results for finite N and low or mid-range values of β_0 is that $|g_+| \ll 1$ (or $\sigma \ll 1$ for the scatterers used). For exact results in the limit of "periodicity", the scattering material must completely fill the slab region available and the requirements $g_-'/g_+' \rightarrow 1$ and $\eta \rightarrow \eta'$ as $\beta_0 \rightarrow 1$ must be fulfilled. If these "periodicity" conditions are not satisfied, however, the mixed-space theory can still adequately describe the distribution behavior for low and mid-range values of β_0 if the forward amplitude condition is satisfied.

The required conditions for the approximate validity of the mixed-space theory for finite- N distributions of three-dimensional scatterers are believed to be identical to those given for distributions of one-dimensional scatterers, except that the forward amplitude condition must be replaced by $|2\pi\rho dg(\hat{z}, \hat{z})/k^2N| \ll 1$ (see section 2.7.1). This forward amplitude condition has previously been implied by Twersky,²⁷ and Beard et al.⁴⁹ have shown that the "periodicity" conditions need not be satisfied for the theory to be approximately valid for low and mid-range values of β_0 .

5.4.2 The Coherent Reflected Field

Results for the coherent reflected field can best be shown by a "compression process" in which the width of the slab region containing a fixed number of planar scatterers is gradually decreased. Curves are given in figure 5.8 for variable d_λ with scattering parameters $N = 10$, $\epsilon_r = 2.0$, and $w_{\lambda'} = 0.1$. For these parameters, "periodicity" occurs when $d_{\lambda'} + w_{\lambda'} = 1$ or, to four figures of accuracy, $d_\lambda = 0.6364$. The simulation results are

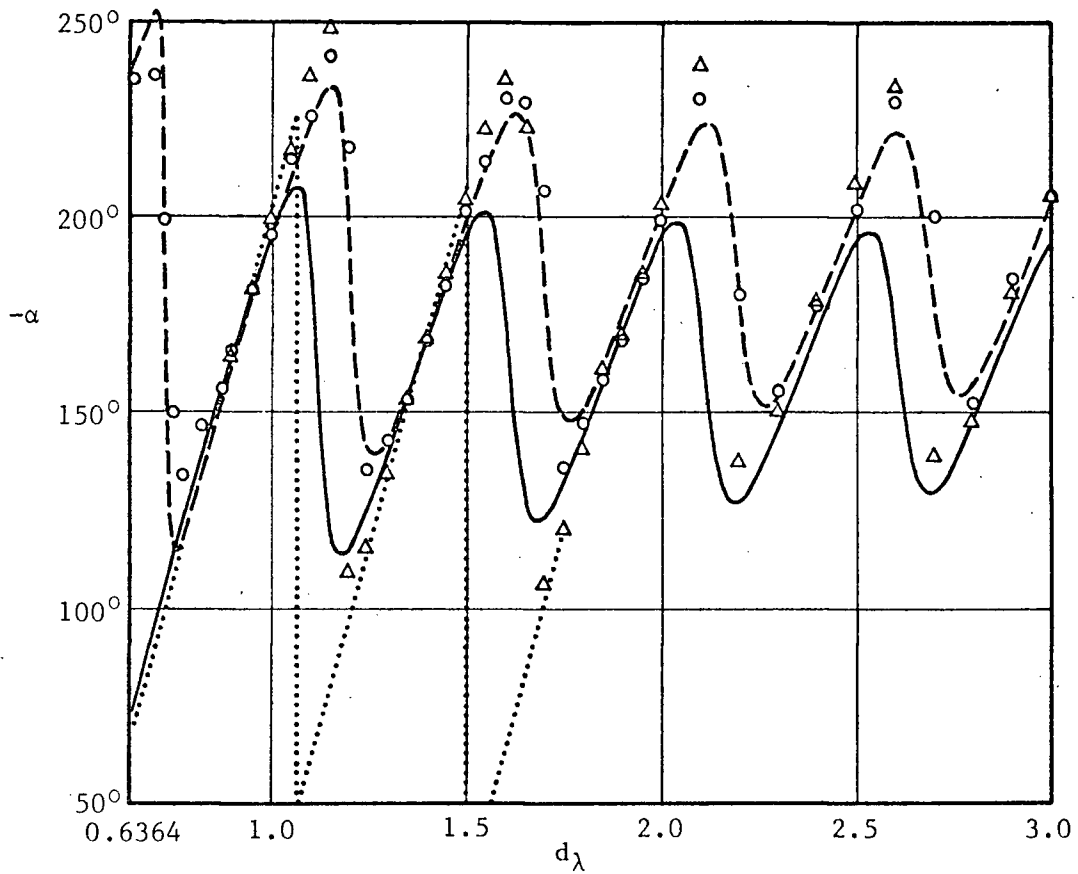
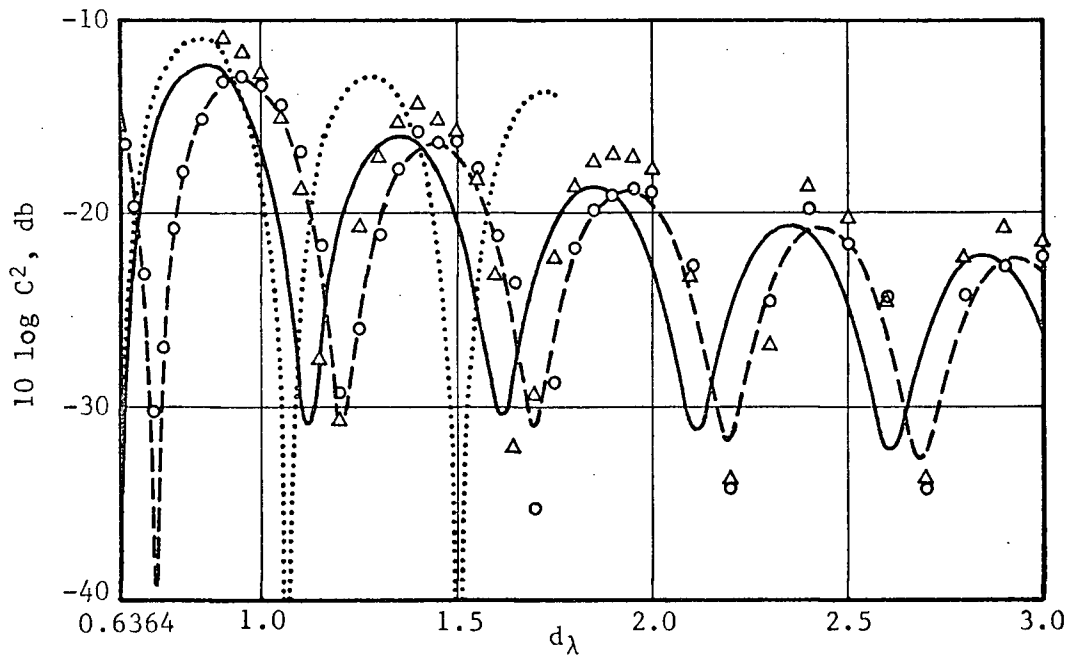
(a) $-\alpha$ versus d_λ (b) $10 \log C^2$ versus d_λ

Figure 5.8 Comparison of Results for the Coherent Reflected Field. $N = 10$, $w_{\lambda'} = 0.1$, $\epsilon_r = 2.0$; Δ Non-Uniform Distribution Simulation, \circ Uniform Distribution Simulation, — Twersky's Mixed-Space Theory with Modified ρ and d , --- Mixed-Space Theory with Modified ρ , Periodic Array Theory

based on 4,000 sample configurations.

Curves are given for Twersky's mixed-space theory with and without d being replaced by $d + w$. Since a replacement of d with $d + w$ in the mixed-space equation for $\langle R \rangle$ (termed "modified d " in figure 5.8) changes the phase reference with respect to that used for the simulation, an additional multiplier e^{-jkw} has been inserted in the equation to allow comparison of results for the coherent phase α .

As seen by a comparison of results for the modified- d form of the mixed-space theory with results for the theory for a periodic array, the mixed-space theory appears to have the correct limiting behavior as $\beta_0 \rightarrow 1$ (i.e., $d_\lambda \rightarrow 0.6364$). (Results for the mixed-space theory were obtained down to $d_\lambda = 0.644$, beyond which the iteration method employed to solve the mixed-space theory equations did not converge.) The mixed-space theory with unmodified d does not, of course, have the correct limiting behavior for $\beta_0 \rightarrow 1$ but reduces to the form displayed in Chapter 4 (figure 4.8, page 70) for $\beta_0 \rightarrow 0$ since $\rho = N/(d + w - Nw) \rightarrow N/d$ as $d_\lambda \rightarrow \infty$. Although both forms of the theory displayed in figure 5.8 give $Ce^{j\alpha} \rightarrow 0$ as $d_\lambda \rightarrow \infty$, a displacement in the curves for both α and C^2 must remain even for large d_λ .

As expected, the simulation results given in figure 5.8 for the periodicity-weighted distribution differ increasingly from those for the uniform distribution for decreasing d_λ , approaching the results for a periodic array as $\beta_0 \rightarrow 1$. Each form of the mixed-space theory gives results approaching the simulation results in one of the two limits. It is interesting that the form of the theory with only modified ρ gives almost exact agreement with the simulation results for the uniform distribution; a reason for this is not immediately evident.

The present work is believed to be the first comparison of Twersky's mixed-space theory for $\langle R \rangle$ with "experimental" results. Further experimental

and theoretical research with this theory and that for the coherent transmitted field applied to other scatterer distributions (particularly three-dimensional distributions) is required.

5.5 Summary and General Discussion of Results

5.5.1 Summary

The main contributions of this chapter may be summarized as follows:

(i) Two simulation methods of generating non-uniform one-dimensional scatterer distributions weighted towards periodicity have been developed.

(ii) A study has been made of the variation of a planar scatterer distribution between the limits of uniform-randomness and periodicity. Criteria based on the average density of scatterers per wavelength and the fractional "volume" occupied have been given for the validity of assuming planar scatterers of finite width to be uniformly-random.

(iii) The one-dimensional form of Twersky's mixed-space theory for the coherent field has been investigated and the requirements for its approximate validity clearly outlined. The requirements necessary for the validity of the three-dimensional form of the theory have been considered.

5.5.2 General Discussion

The rejection methods developed for generating a suitable non-uniform distribution of N random variables suffer the same practical disadvantage of most rejection methods for single random variables in that they are wasteful of computation time. In addition, they do not generate the scatterer position variables from known theoretical distributions and cannot give results for a fractional "volume" approaching unity. These last two disadvantages (at least) could be overcome by allowing a random number of scatterers N within the containing slab region and generating the spaces between their boundaries rather than their positions. A suitable probability density function for the

spaces ξ_i between the scatterer boundaries is the exponential function

$$p(\xi_i) = \rho e^{-\rho \xi_i}, \quad \rho = \frac{\langle N \rangle}{d - \langle N \rangle e} \quad (i = 1, 2, \dots, N + 1) \quad (5.14)$$

where ρ is essentially the modified average density used in this chapter for fixed N , e is the minimum spacing between scatterers, and d is the width of the slab region containing the boundaries of the random number of scatterers (i.e., d is equivalent to the $d + e$ used in this chapter). The exponential function (5.14) is the "adjacent-scatterer" form of the more general two-scatterer conditional probability density function used by Twersky.⁴⁸ For $e \rightarrow 0$ it reduces to the form of equation (4.1) for infinitely-thin scatterers and N becomes Poisson distributed. For $e \rightarrow d/\langle N \rangle$, the scatterers become periodically positioned and N is no longer random. The spaces ξ_i between the scatterer boundaries can be generated using the transformation of equation (4.2).

The generation of a random- N distribution in this manner should give results differing little from those presented in this chapter. The theoretical problem of determining a suitable two-scatterer probability density function of fixed- N scatterer configurations for the basis of an approximate scattering theory, however, still remains. Theoretical work directed to obtaining such a function and applying it to the O-B-S approximations for the field developed in the present work would be of interest.

6. EXPERIMENTAL INVESTIGATION

6.1 Introduction

In this chapter a physical model of a random medium of discrete scatterers for possible use in detailed scattering studies is proposed and the results of initial experiments to determine the suitability of this model are given. The model consists of three-dimensional scatterers randomly positioned within a slab region according to statistics generated by computer from a desired distribution. A narrow microwave beam scans this slab region and the resulting fluctuating field is measured at a point outside the region and statistically analyzed. Initial measurements of the forward-scattered field from a "uniformly-random" configuration of one-half inch diameter polyethylene spheres have been made at 0.86 centimeter wavelength.

A series of experiments on a similar physical model have previously been carried out by a group of researchers at Sylvania Electronic Defence Laboratories.^{5,49-54} As illustrated by the Sylvania group, experiments on a controlled-distribution model, unlike experiments on uncontrolled naturally-occurring scatterer distributions, provide the physical and statistical characteristics of the distribution in addition to the scattering data of interest. These known physical and statistical characteristics can be used in various approximate scattering theories and the theoretical predictions compared with scattering measurements on the same distribution to determine their validity. Thus, the advantages of experiments on a physical model constructed and controlled to conform to a mathematical model are similar to those gained by Monte Carlo computer simulation with a mathematical model. Such experiments have the additional advantages, however, that more complex models can be studied, real-life antenna beams used, and new measurement techniques investigated.

The main feature of the physical model presented in this chapter is that the statistics of the scatterer positions are directly controlled as in a complete Monte Carlo computer simulation. Thus, the scatterer statistics are known from the beginning, unlike those of the Sylvania model where they are controlled indirectly by a physical process[†] and monitored by means of movie films or a method requiring initial knowledge of the scattering medium.^{5,49,50} The primary advantage of such direct control, however, is that it presents the possibility of experimental studies on other than "uniform" distributions.

The construction details of the present physical model are outlined in section 6.2 and a more thorough analysis of its advantages and disadvantages is given. The scattering range, antenna characteristics, and scanning device are described in section 6.3. The experimental apparatus, measurement techniques, and data processing methods are discussed in section 6.4. The results of the initial experiments to investigate certain aspects of the model suitability are presented and discussed in section 6.5.

6.2 The Physical Model

The present physical model consists of spherical scatterers (e.g., polyethylene balls) positioned at "uniformly-random" discrete locations within a slab region of a relatively transparent support-medium constructed of layers of polystyrene foam. A narrow millimeter-wave beam illuminates a small volume region of the fixed configuration of scatterers and the resultant

[†]The Sylvania model consists of a slab-region Styrofoam container whose bottom and top are grids which allow for the passage of turbulent air streams. For low average densities of light-weight scatterers (usually Styrofoam spheres), a relatively uniform distribution is developed by a system of blowers, turbulence-creating wedges, and collision processes. The ergodicity of the process allows a direct comparison between the time averages of field quantities measured and approximate theoretical estimates of the corresponding ensemble averages.

scattering process produces a random field in the space both inside and outside the slab region containing the scatterers. A procedure of moving the slab region in front of a transmitting antenna in a direction perpendicular to that of the incident beam therefore causes a random fluctuating field at the location of a receiving antenna. The desired components of the random field produced by this "scanning" process are measured and sampled at discrete distance intervals. A processing of these sampled signals by standard digital averaging methods results in estimates of the ensemble averages of the desired field quantities.

A simplified diagram of the scattering geometry used for the experiments described in this chapter is given in figure 6.1 (see section 6.3 for distances of antennas from the scattering region). Although measurements

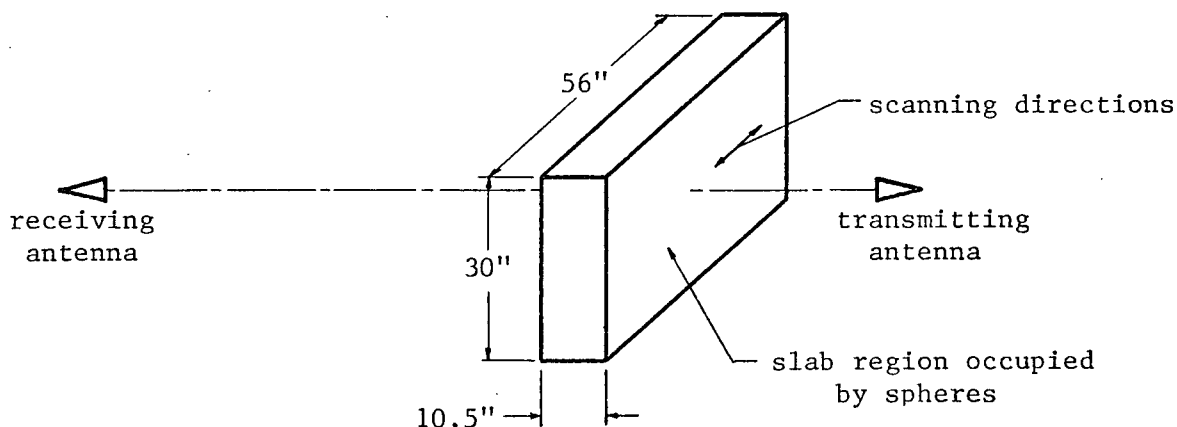


Figure 6.1 Simplified Diagram of Scattering Geometry

were made of the forward-diffracted field on the axis of the transmitting antenna, similar measurements may be obtained for the forward field in various directions off the axis and for the back-scattered field. The transverse dimensions of the distribution (56" \times 30") were decided on the basis of the width of the anechoic chamber available and on the vertical movement of the

device for scanning the region (see section 6.3). The 10.5 inch dimension parallel to the beam axis is approximately the same as that of the Sylvania model.[†]

In order for the spheres to be placed in position within the slab region, the support-medium was divided into twenty-one vertical layers of one-half inch width. This therefore made necessary a discrete distribution in at least the direction parallel to that of the incident beam, each layer containing a plane of randomly-positioned spheres. The layer width was chosen as a matter of convenience for the initial experiments described in section 6.5 and to maximize the number of layers possible for the sphere diameter of one-half inch. As a further convenience in placing the spheres in position, the transverse coordinates of each layer were also truncated at one-half inch intervals. The validity of such a "discrete position approximation" is discussed in Appendix C with results from similar approximations applied to the one-dimensional model of planar scatterers being used to provide insight into the problem.

6.2.1 Generation of Uniform Distribution

A "uniformly-random" array of discrete sphere positions throughout the slab region was generated as follows: Each layer of the support-medium was divided into six equal-area sections of 28" x 10", making a total of 126 sections in all. A sequence of uniformly-random numbers from the unit interval, equal in number to the desired number of spheres within the slab region, was generated. Each number was then multiplied by 126 and truncated to designate one of the sections for a sphere to be placed.

[†]The aim in the original Sylvania experiments was that measurements be comparable with the plane-wave theory existing at the time.⁵⁰ One requirement was that the inverse distance variation of the illuminating field be small over the depth of the distribution for a given distance from the transmitting antenna to the distribution center.

Corresponding to the number of spheres to be placed in each section, pairs of discrete uniformly-random "x and y" coordinates were generated. Because of the physical requirement that no more than one sphere occupy any one position, each successive position was chosen uniformly from those remaining. Thus, the overall distribution was not truly uniform, although it was effectively uniform for a low average number of available locations occupied.†

Immediately after the sphere coordinates were generated for each section, they were obtained in a pictorial form as shown in figure 6.2 for two of the sections ("stars" correspond to sphere positions). This picture of sphere positions for each section, and a rectangular metal grid with holes at one-half inch intervals placed over the desired section of one of the support-medium layers, provided a means of quickly marking the positions.

The uniformly-random numbers were obtained by means of the modified generator discussed in section 3.3, the basic generator RAND being used to generate a different initial array of 1,000 numbers for each section and then to randomly choose the desired number of coordinates from these. The generator was designed so that it could be "initialized" by one number and so that the initial array of random numbers for each section would be the same regardless of the number of coordinates required. Thus, if a set of experiments were being carried out in which the number of spheres within the slab region progressively increased, each new experiment would only require that additional spheres be added to those for the previous experiment. A second

†The size of the equal-area sections is arbitrary and was chosen to keep the amount of computer memory required by the program within a reasonable limit, since this is approximately proportional to the number of discrete positions in a single section. In this method of generation the section designation is essentially the "z" coordinate; for sections equal in area to the support-medium layers it would correspond to the "z" coordinate in the distribution.

PADD - N = 4000 NX = 126 NY = 60 NZ = 20 IRR = 0.489999												
ARRAY OF SPHERE POSITIONS FOR SECTION 115												
NUMBER OF SPHERES = 34												
	1	5	10	15	20	25	30	35	40	45	50	60
1	C	C	C	C	C	C	C	C	C	C	C	C
2	*	C	C	C	C	C	C	C	C	C	C	C
3	C	C	C	C	C	C	C	C	C	C	C	C
4	C	C	C	C	C	C	C	C	C	C	C	C
5	C	C	C	C	C	C	C	C	C	C	C	C
6	C	C	C	C	C	C	C	C	C	C	C	C
7	C	C	C	C	C	C	C	C	C	C	C	C
8	C	C	C	C	C	C	C	C	C	C	C	C
9	C	C	C	C	C	C	C	C	C	C	C	C
10	C	C	C	C	C	C	C	C	C	C	C	C
11	C	C	C	C	C	C	C	C	C	C	C	C
12	C	C	C	C	C	C	C	C	C	C	C	C
13	C	C	C	C	C	C	C	C	C	C	C	C
14	C	C	C	C	C	C	C	C	C	C	C	C
15	C	C	C	C	C	C	C	C	C	C	C	C
16	C	C	C	C	C	C	C	C	C	C	C	C
17	C	C	C	C	C	C	C	C	C	C	C	C
18	C	C	C	C	C	C	C	C	C	C	C	C
19	C	C	C	C	C	C	C	C	C	C	C	C
20	C	C	C	C	C	C	C	C	C	C	C	C
1	5	10	15	20	25	30	35	40	45	50	55	60
ARRAY OF SPHERE POSITIONS FOR SECTION 116												
NUMBER OF SPHERES = 28												
	1	5	10	15	20	25	30	35	40	45	50	60
1	C	C	C	C	C	C	C	C	C	C	C	C
2	C	C	C	C	C	C	C	C	C	C	C	C
3	*	C	C	C	C	C	C	C	C	C	C	C
4	C	C	C	C	C	C	C	C	C	C	C	C
5	C	C	C	C	C	C	C	C	C	C	C	C
6	C	C	C	C	C	C	C	C	C	C	C	C
7	C	C	C	C	C	C	C	C	C	C	C	C
8	C	C	C	C	C	C	C	C	C	C	C	C
9	C	C	C	C	C	C	C	C	C	C	C	C
10	C	C	C	C	C	C	C	C	C	C	C	C
11	C	C	C	C	C	C	C	C	C	C	C	C
12	C	C	C	C	C	C	C	C	C	C	C	C
13	C	C	C	C	C	C	C	C	C	C	C	C
14	C	C	C	C	C	C	C	C	C	C	C	C
15	C	C	C	C	C	C	C	C	C	C	C	C
16	C	C	C	C	C	C	C	C	C	C	C	C
17	C	C	C	C	C	C	C	C	C	C	C	C
18	C	C	C	C	C	C	C	C	C	C	C	C
19	C	C	C	C	C	C	C	C	C	C	C	C
20	C	C	C	C	C	C	C	C	C	C	C	C
1	5	10	15	20	25	30	35	40	45	50	55	60

Figure 6.2 Typical Computer Output for Sphere Coordinates

program was developed to distinguish between "old" and "new" spheres by means of different characters to minimize the labour required to insert additional spheres for each experiment.

6.2.2 The Support-Medium

The scatterer-supporting material used for the initial experiments described in section 6.5.2 was a locally obtained "beaded" variety of polystyrene foam sheet of one-half inch width and density of 1.0 lb/ft³. The experimental investigation which led to the choice of this material is discussed in section 6.5.1.

For the one-half inch diameter spheres used in the initial experiments, holes of slightly smaller diameter were first drilled in the support-medium layers at the computer-generated positions. This allowed the spheres to stay

easily in place with a minimum compression of the surrounding material.

A box of the same material with two-inch thick sides was used to hold the sphere-loaded layers in place. One of the wide faces was left unfastened so that the layers could be easily inserted or removed. It was fastened into place with small spikes inserted from the sides of the box. The sides of the box were glued together at only a few locations to minimize unwanted diffraction. Figure 6.3 shows the medium in place with the side removed and one of the layers with spheres inserted open to view.

6.2.3 Comparison with the Sylvania Model

The main advantages of the present model over the Sylvania model are the following:

(i) Unlike the Sylvania model, the present model lends itself fairly well to the experimental study of other complex, but still theoretically predictable, scatterer distributions besides the uniform distribution. Generalization of the technique used for generating a uniform distribution to one which would allow the average density of scatterers to vary non-uniformly in the direction parallel to that of the incident beam, according to either a mathematically or empirically specified probability density, is straightforward. The including of scatterer size, shape, orientation, and dielectric properties as random variables in the distribution function is also possible, although it would increase the labour involved in placing the scatterers in position. A more difficult type of distribution for possible investigation is one in which the scatterer positions are correlated in some manner (e.g., a distribution in which the scatterer positions are weighted towards certain "periodic positions" of higher probability as in the one-dimensional distribution investigated in Chapter 5). The type of correlation which could be used, however, and the manner in which the desired distribution could be generated are problems which would require much future research.

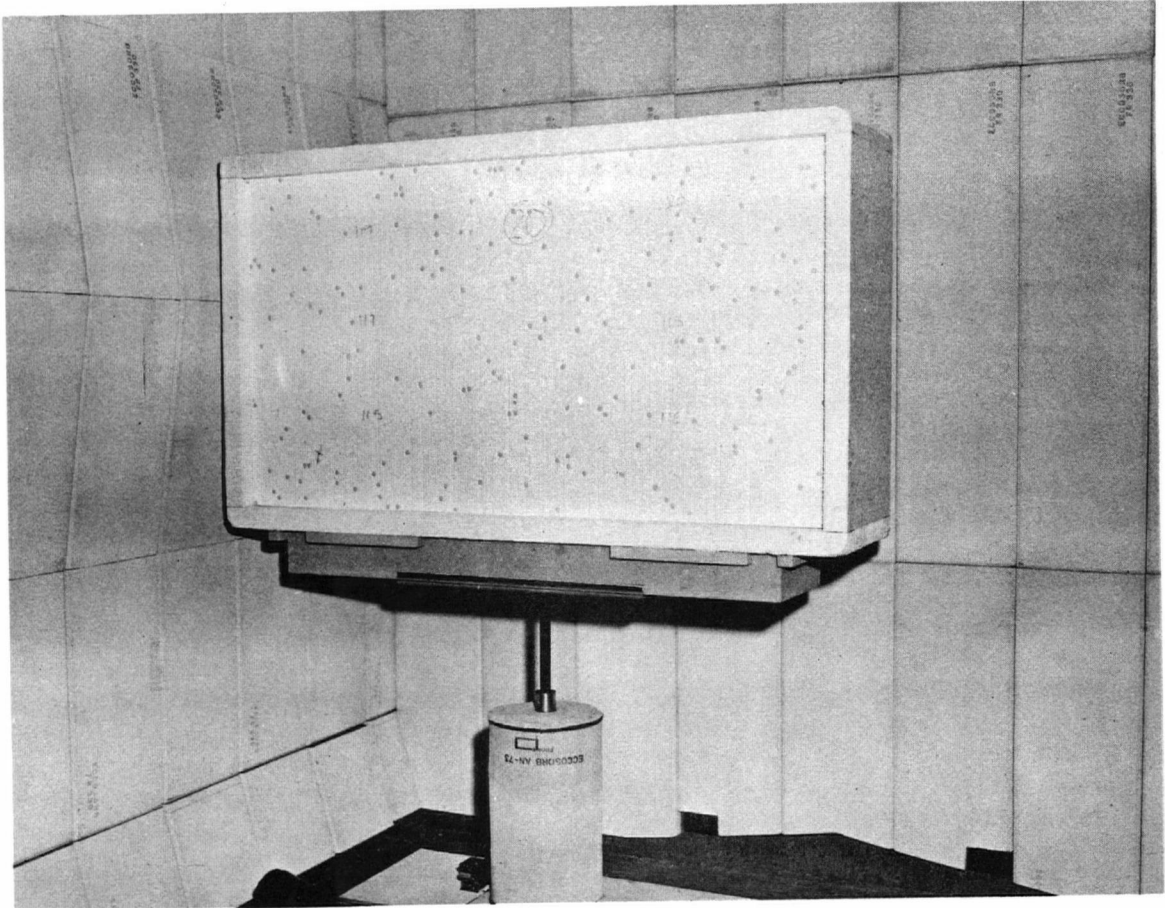


Figure 6.3 View of the Physical Model

(ii) Heavier scatterers, usually having higher permittivity, may be used in the present model since they are embedded in a rigid supporting material and need not satisfy a "buoyancy" requirement as in the Sylvania model.

(iii) Because the statistical distribution of the scatterers in the present model is directly controlled by a known pseudo-random process, it need not be monitored as in the Sylvania model.

(iv) An experiment on the present model can be repeated using the same scatterer configurations (as in a complete Monte Carlo simulation), making it relatively easy to determine measurement errors introduced by equipment alone.

The main drawbacks of the present model in comparison with the Sylvania model, with possible methods of minimizing them, are as follows:

(i) The accuracy of the estimated ensemble averages obtainable with the

present model is governed largely by its transverse dimensions since this determines the number of uncorrelated samples. In the Sylvania model, only the unimportant time factor governs the accuracy. Because of practical considerations such as the size of room and scanning device available, the size and ease of handling of the plastic foam sheets available, and the labour involved in setting up the medium, the transverse dimensions of the model must be limited. One of the main objects of the experiments described in section 6.5.2 was to determine, for typical scatterer distributions, the statistical accuracy obtainable from a model of a given size.

Without completely changing the sphere positions, it is possible to improve the accuracy of the results for a uniform distribution. The method proposed involves randomly shuffling, sliding, or changing the orientation (all four edges reversed) of the sphere-loaded layers with respect to one another to obtain new configurations, or a combination of these operations. With the exception of the sliding, which would require a larger container, this method was used to improve the accuracy of the results in section 6.5.2.

(ii) The necessity for a discrete position approximation appears to limit the present model to relatively low average density distributions of scatterers. The details of this disadvantage are discussed in Appendix C.

(iii) The necessity for a support-medium places heavy importance on the "uniformity-of-propagation" characteristics of the material used. The results and recommendations from an experimental investigation of this problem are given in section 6.5.1. This support-medium factor also means that scatterers having a low relative dielectric constant cannot be used with the same guarantee of accuracy as in the Sylvania model.

(iv) The long term stability of the signal source during experiments on the present model is a more important factor than for the Sylvania model, since the time required to record the data is much longer. Fortunately, this

problem can be minimized with existing equipment. The effects of phase instability are quantitatively analyzed in section 6.5.2.

(v) The time and labour involved in setting up the distribution in the present model is much greater than in the Sylvania model, because of the necessity of physically positioning each scatterer to a mathematically specified position. It is felt, however, that this is a minor disadvantage as the time involved is still only a fraction of that required to analyze the experimental results.

6.3 The Scattering Range, Antenna Characteristics, and Scanning Device

A general purpose microwave anechoic chamber was designed and constructed for the experiments, for preliminary antenna pattern measurements, and for future scattering and propagation studies. Details of the design and testing of this chamber are given in Appendix D.

The millimeter-wave region of the spectrum was considered the most suitable for experiments with the present model. This spectral region provides a fairly large range of sphere-diameter-to-wavelength ratios (for easily handled spheres from one-eighth inch to one-half inch in diameter) and allows narrow beams to be easily acquired for maintaining the transverse dimensions of the model within reasonable limits. Because of available equipment considerations, the band 26.5-40.0 GHz was chosen as being most suitable for the initial experiments. The results of section 6.5 were obtained at a frequency of approximately 35 GHz.

The geometry of antennas and medium is given in figure 6.4. In figure 6.3 on page 116, which shows the scattering medium at one side of its horizontal travel, the transmitting antenna protruding from the front wall of the chamber is hidden behind the right hand edge of the medium. Shown in

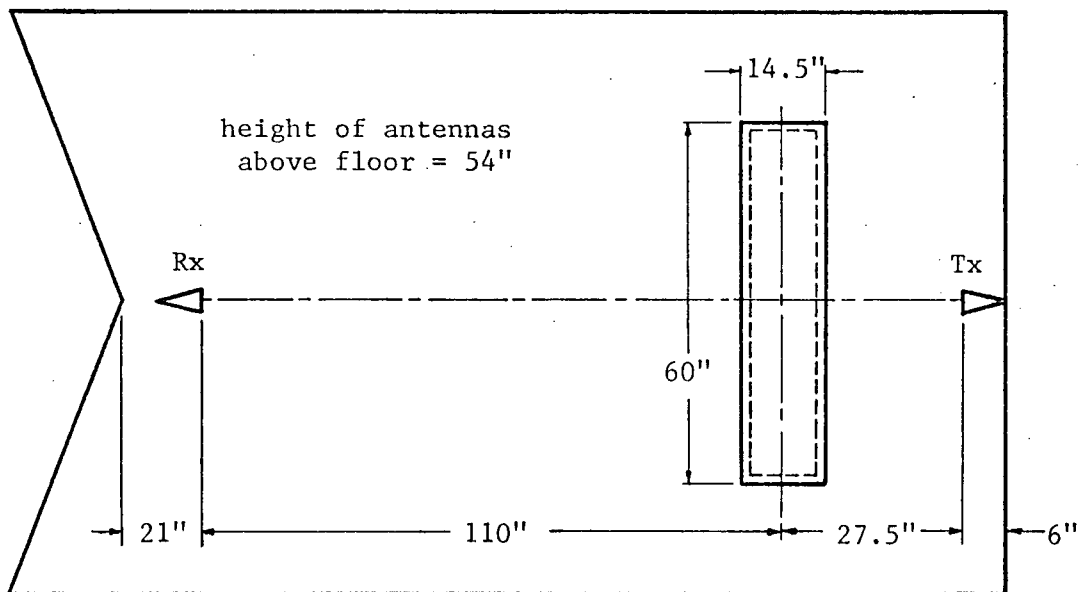


Figure 6.4 Plan View of the Geometry of Antennas and Medium

figure 6.5 is a view of the receiving antenna and mixer mounted on a pedestal in front of the back wall.

Available horn-lens combinations designed for 35 GHz were considered to have suitably narrow beamwidths for use as both transmitting and receiving antennas in the initial experiments. The measured antenna parameters at this frequency were

aperture dimensions: 2.97" × 2.38"

half-power beamwidth: H-plane - 7.4°, E-plane - 7.3°

beamwidth to first null: H-plane - 18.3°, E-plane - 16.0°

level of first side-lobe: H-plane - 22db down, E-plane - 16db down

The diameter of the approximately circular area of the medium center illuminated by the half-power beam of the transmitting antenna is 3.6 inches. The fact that the diameter $D_F \approx 2 \sqrt{\lambda d_t} = 6.1$ inches of the first Fresnel zone of the transmitter on the medium center is greater than the diameter of the "3db circle" previously assumed to be the necessary limit for the approximate validity of plane-wave theory⁵⁰ is unimportant for the experimental

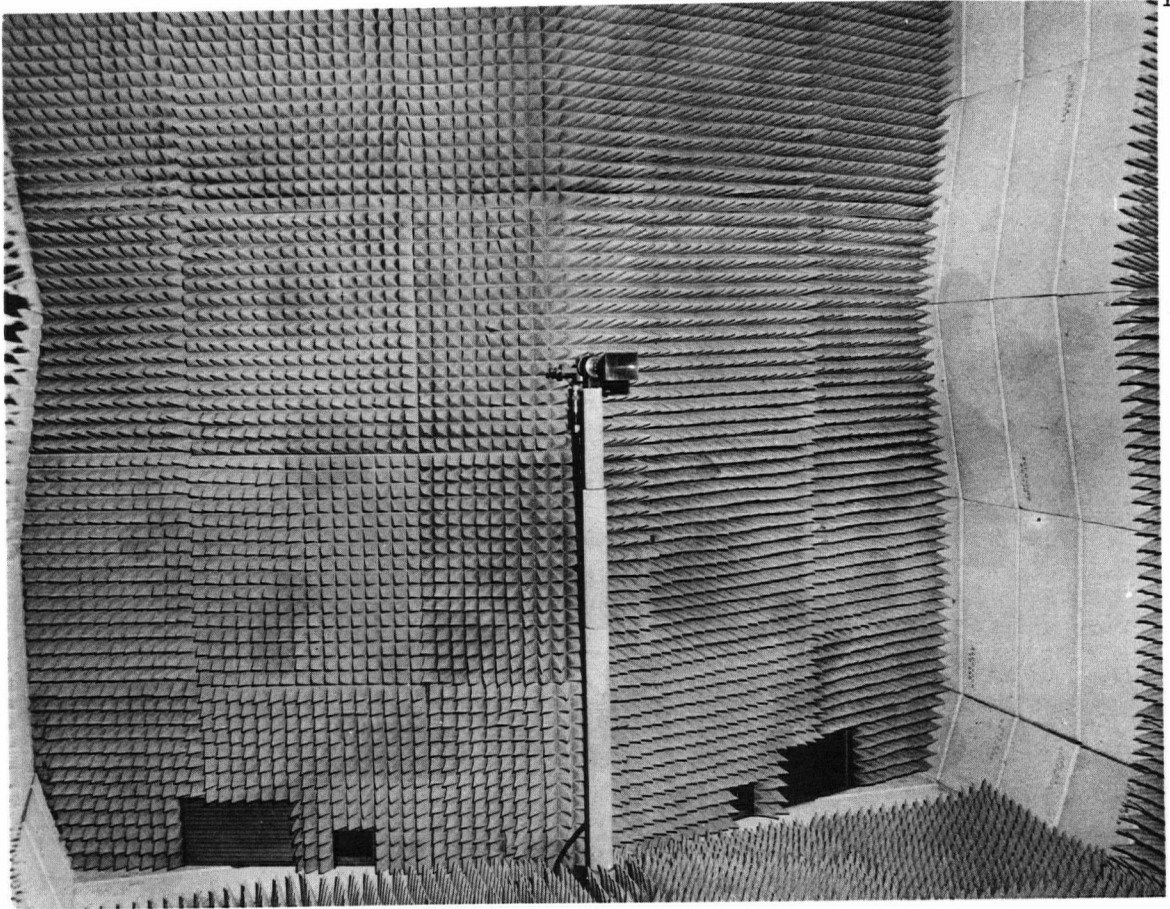


Figure 6.5 View of the Receiving Antenna and Mixer

investigation described in section 6.5.2. The consideration of a spherical incident wave in more recent theoretical work^{5,27} would also seem to eliminate the necessity of satisfying any plane-wave requirement in possible future studies with the present model.

The distance of $d_t = 27.5$ inches from the transmitting antenna to the center of the medium was set on the basis of the commonly-used far-field criterion $d_t \geq D^2/\lambda$,⁵⁵ where D is the largest dimension of the horn aperture. The receiving antenna distance of $d_r = 110$ inches corresponds to that obtained by satisfying the far-field criterion $d_r \geq D_F^2/\lambda = 4d_t$, with the first Fresnel zone regarded as a radiating aperture. Originally this criterion was considered to be necessarily satisfied for the observation of the far-field form of the average incoherent intensity;⁵⁰ more recent measurements, however, have shown

$\langle I^2 \rangle$ to be relatively constant for a wide variation in d_t and d_r .⁵¹ Approximate theory accounting for finite d_t and d_r now allows the variation of these parameters in studies comparing theoretical and experimental results.^{5,27}

A general purpose positioning device was designed and constructed to serve as a scanning platform for the model and as an antenna positioner for tests on the anechoic chamber and for pattern measurements. Design details for this device, which can be remotely controlled from outside the anechoic chamber, are given in Appendix D.

The dimensions of the area of the slab region scanned were 40.8" × 12.0". The 40.8 inch dimension was set by the width of the anechoic chamber and the extra width of the slab region considered necessary to minimize diffraction at the edges. The twelve inch dimension was set by the vertical movement of the scanning device. The transverse dimensions of the slab region (56" × 30") were designed so that the width of the edges not illuminated by the first Fresnel zone at the limits of the scanning area were approximately equal to the diameter of this zone. The intensity of illumination at the edges is below -20db, minimizing edge diffraction (see section 6.5.1).

6.4 Experimental Apparatus, Measurement and Data Processing Methods

6.4.1 Experimental Apparatus and Procedures

All the signal generation and measurement apparatus is located outside the anechoic chamber as shown in figure 6.6. A block diagram of the millimeter-wave equipment with superheterodyne receiver is given in figure 6.7a and a block diagram of the signal processing and recording equipment in figure 6.7b.

The equipment and measurement techniques are similar to those used already by the Sylvania group.^{5,49,51,53} The main change is the introduction of commercial receiving and signal processing equipment, including the

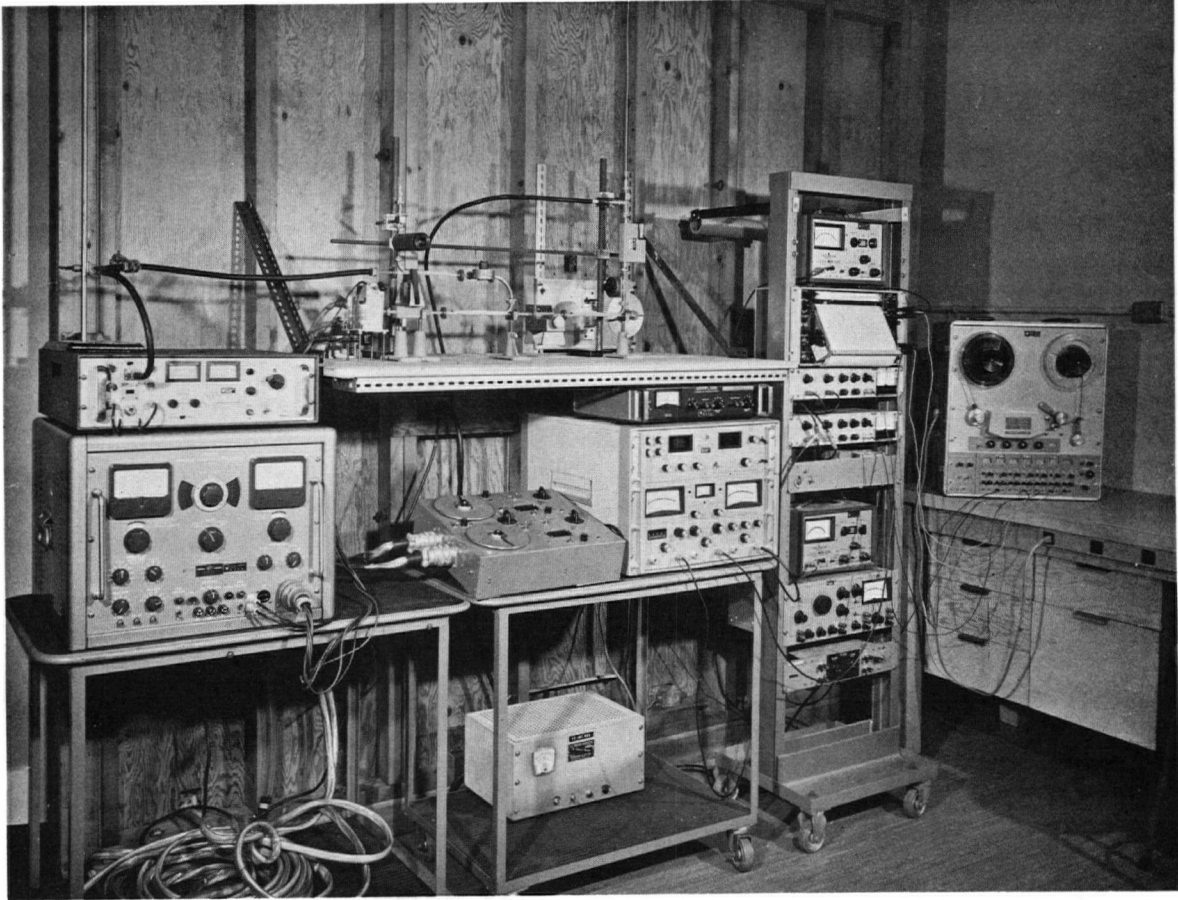
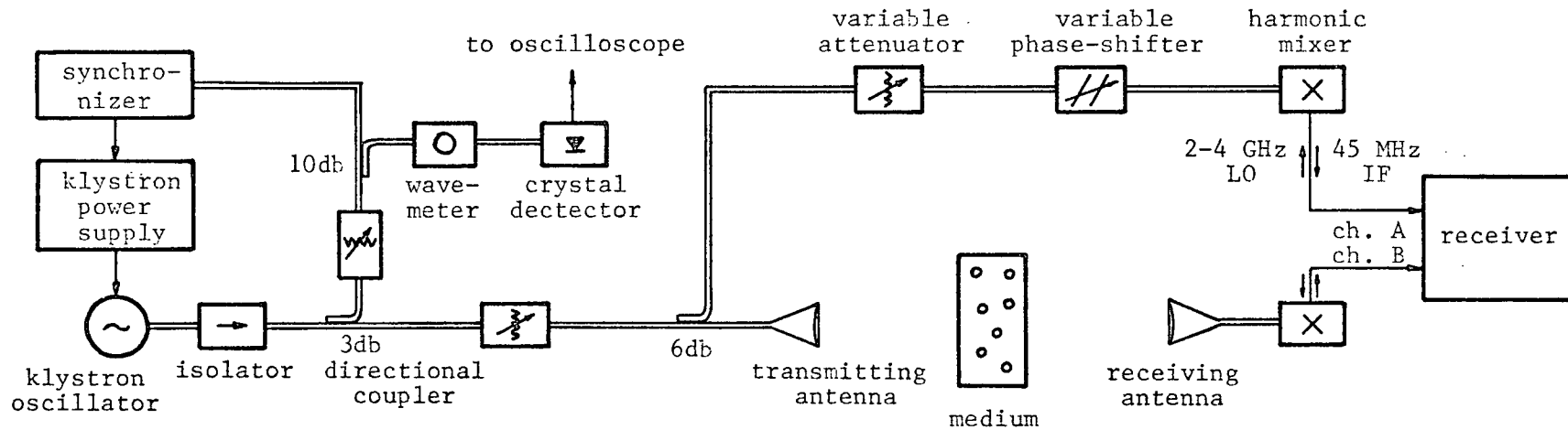


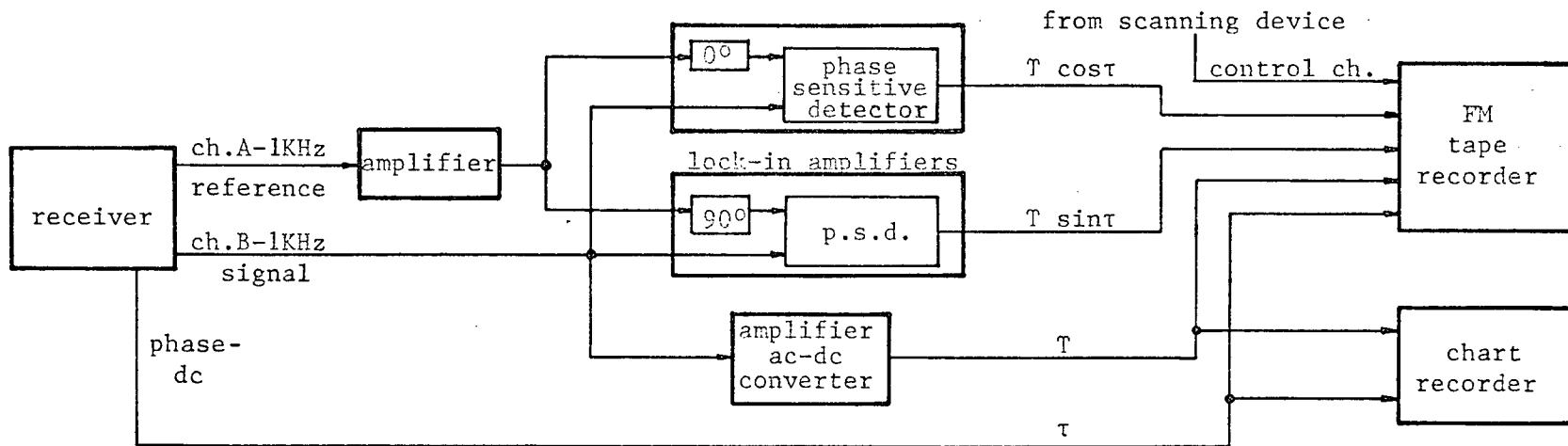
Figure 6.6 View of the Experimental Apparatus

Scientific-Atlanta wide-range phase/amplitude receiver (model 1751) and the two PAR lock-in amplifiers (model 120). The receiver is a two-channel device containing two intermediate-frequency (IF) stages and employing automatic phase control circuits. For operation in the millimeter-wave spectral region, external harmonic mixers are used to derive the first IF of 45 MHz. The phase and amplitude measurements are both made at 1 KHz, the second IF in the double-conversion chain. Recorder outputs are provided for both the amplitude channels (1 KHz) and the phase channel (0 to -3.6 vdc for ranges $\pm 180^\circ$, $\pm 45^\circ$, or $\pm 18^\circ$).

As shown in figure 6.7a, the RF signal from the klystron is split into two main paths, one path (direct path) passing through the scattering medium and the other (reference path) passing through a variable attenuator



(a) Millimeter-Wave Apparatus



(b) Signal Processing Apparatus

Figure 6.7 Block Diagram of the Experimental Apparatus

and phase-shifter. The reference path provides a phase reference signal for use in measuring the phase shift τ of the wave passing through the scatterer distribution and for deriving the phase quadrature components $T_x = T \cos \tau$ and $T_y = T \sin \tau$ (see section 2.5.1).

The phase of the reference channel is adjusted as follows: For a wave passing through free space only, the variable phase-shifter in the reference path and a 0.1° -increment digital control on the receiver are set so that the phase-shift indicated on the receiver phase-meter is zero. At the same time the phase controls on the lock-in amplifiers are adjusted so that the level from the in-phase detector is maximum and that from the in-quadrature detector is zero. A positive phase-shift is then introduced in the reference path to offset that introduced from the unloaded support-medium by readjusting the variable phase-shifter to the desired value (see section 6.5.2) using the receiver phase indicators. Thus, when the medium loaded with spheres is introduced, the changes in the field components T_x , T_y , T , and τ are due to the spheres alone.

As shown in figure 6.7b, the signals representing the four field components were recorded on an FM tape recorder. The machine used for the present experiments was a seven channel Ampex SP-300. The amplitude and phase were also recorded on chart paper for an instantaneous visual check of the results during the experiments and for later comparison with the signals recorded on magnetic tape.

The phase-lock feedback loop containing the klystron synchronizer shown in figure 6.7a was intended to be used for stabilizing the output frequency of the klystron and hence the phase variation between the signals in the reference and direct paths. The synchronizer, an FEL model 136-AK, proved however to be unsatisfactory for a number of klystrons at different frequencies. It was only capable of providing a short-term phase-lock (approximately five

minutes), not long enough for the desired measurements.

Although it is felt that a suitable synchronizer should be used for future more-precise measurements, the frequency stability obtainable without the synchronizer was considered sufficient for the initial experiments. The problem was minimized through the use of a water cooling-system, consisting of a coil of copper tubing immersed in a jacket of the low melting point metal Cerrobend (Wood's metal) surrounding the klystron. Initial stability measurements showed a maximum amplitude variation of 2% and a maximum phase variation of less than 3° over an hour period with the EMI R9521 klystron. At the time of the experiments described in section 6.5.2, however, a phase stability of only 6° over a one-half hour period could be achieved. The quantitative effect on the results is estimated in that section.

6.4.2 Data Processing Methods

The recorded four-channel analog data was sampled and processed on a DEC PDP-9 computer having a remote interface which contains multiplexing and analog/digital (A/D) conversion equipment.

During an experiment, a two-level control voltage was recorded on a fifth channel (see figure 6.7, page 123) to designate those sections of the four analog signals (corresponding to scanning of the medium) to be sampled. The "sampling level" was switched on and off with the power to the horizontal drive motor in the scanning device. The sampling program was designed so that sampling of the four signal channels and the control channel would be a continuous process once begun, with the presence of the sampling level on the control channel specifying which signal samples to be retained. The multiplexer in the interface provided very quick switching between channels so that effectively all five channels were sampled instantaneously by the A/D converter. The desired time interval between each set of samples was specified in the sampling program. Samples were initially stored in memory during the sampling

process and then copied on to magnetic tape (DEC tape) after each block of analog data had been sampled. The digital data corresponding to each scan of the medium was contained in separate files on DEC tape. In the present procedure the sampling process stops after each block of data has been obtained and the operator must restart the process for the next block of data and specify the desired file.

Once the digital data had been obtained on DEC tape it was normalized according to predetermined reference levels and processed by means of other computer programs to determine the means, variances, autocorrelation functions, and other average field functions of the field components recorded. The reference levels corresponded to the values of the field components obtained with only the unloaded support-medium in place. These levels were recorded on the FM recorder before the beginning of a set of data scans and were sampled in the same manner as the actual data to determine suitable values for use in scaling (see section 6.5.2).

The available A/D converter has a twelve-bit resolution capability (4096 levels of quantization) and, with accuracy of only one bit less, is suitable for sampling the data obtained from the present type of experiment. Quantization noise was less than that generated by the FM tape recorder, as observed by a comparison of sampled values with the corresponding analog records reproduced on chart paper from the tape recorder. The amount of noise generated by the tape recorder was not considered sufficiently high to require the use of low-pass filtering before the interface.

Because of the capability of sampling all four signal channels simultaneously, two of these channels were redundant. Thus, a comparison of the directly sampled data against the corresponding computed data for both sets of channels provided one method of checking for measurement or data processing errors (see section 6.5.2).

6.5 Experimental Results

6.5.1 Experiments on the Support-Medium

The main problem associated with the support-medium was to obtain a suitable material and a suitable orientation of the constituent layers to present a minimum of discontinuity to the millimeter-wave beam as it passed through. Initial measurements of the transmitted wave amplitude and phase for horizontally-stacked layers of Dow Styrofoam FR (1.9 lb/ft³) showed wide variations of these quantities in the scanning direction perpendicular to the layers. Further measurements on blocks of the same material having a single joint parallel to the direction of propagation showed a marked diffraction pattern as the beam crossed the joint for both parallel and perpendicular polarization. This effect, apparently caused by a large reflection at the joint due to almost grazing incidence, precludes the use of any joints parallel to the beam except close to the edges of the medium where the beam intensity is low.

The best arrangement of the support-medium layers was therefore found to be a stacked array perpendicular to the direction of the incident beam. Vertical layers of Styrofoam resulted in very uniform transmission characteristics, although the necessity for joints parallel to the beam in the narrow widths of board obtainable (twenty-four inches maximum) made this material unsuitable.

The "beaded" variety of polystyrene foam (1.0 lb/ft³) supplied a reasonably satisfactory solution to the problem. Sheets of this material can be obtained in a variety of lengths, widths, and thicknesses suitable to the requirements. Because of the bead-bead interfaces in this material, however, it is not as uniform in transmission properties as Styrofoam. A set of seven horizontal scans (separated by two inches) of the unloaded support-medium,

consisting of the two inch thick sides of the container and the twenty-one one-half inch thick layers, showed a maximum variation in the reference level amplitude of 4% and in the phase of 5° . This variation was considered to be low enough for the experiments described in the next section where the sphere distributions presented a fairly large scattering cross-section to the beam.

Experiments were also performed to measure the dielectric constant of the "beaded" polystyrene foam and to determine how close the transmitting antenna could approach the edge of the support-medium before the onset of a noticeable diffraction pattern. A dielectric constant of 1.018 at 35.1 GHz was obtained by measuring the phase shift of the transmitted wave through a two-inch thick slab of the material. In the other experiment, a noticeable diffraction pattern was obtained with the beam center less than about nine inches from the edge of the medium, consistent with the initial design of the model.

For future more precise experiments, the use of a support-medium material having smaller and more well-packed beads than the present material (average bead diameter in the one-eighth to three-sixteenth inch range) should result in more uniform transmission characteristics. The problem might also be alleviated somewhat with the sanding of the material surfaces (surfaces produced by a hot-wire cutter are not as smooth) to allow the layers to be pressed more firmly together. The use of a non-beaded material such as polyurethane foam or poly-vinyl-chloride (PVC) foam could also provide a more satisfactory solution. Both these materials, and particularly PVC foam, are considerably more expensive than polystyrene foam, however, and the dielectric properties at millimeter-wavelengths do not appear to be tabulated.

6.5.2 Experiments on Typical Scatterer Distributions

Experiments were performed on two different average density distributions of one-half inch diameter polyethylene spheres at a frequency of

35.1 GHz. These two average densities of 183 and 366 spheres per cubic foot (scf) are typical values from a range of distribution densities which could be studied in a more detailed experiment such as one carried out by the Sylvania group.⁴⁹ They correspond to totals of 2,000 and 4,000 spheres in a slab region four inches longer than that used, the two-inch edge being replaced by the sides of the foam container. The one-half inch sphere diameter gives a typical ka-factor (4.66 at 35.1 GHz) from a range of values of interest and is convenient for use in the present model.

As indicated in section 6.2.3, data was obtained for more than one configuration of spheres to increase the statistical accuracy of the average field functions estimated in the experiment. This was done by a combination of shuffling the support-medium layers according to a random computer-generated permutation⁵⁶ and at the same time randomly adjusting the orientation of the layers to give an equal probability for two possible orientations: right side up or all four edges reversed. Horizontal scans of 40.8 inch length were taken at two-inch vertical intervals with vertical E-field polarization on both sides of three different layer-configurations, giving a total of forty-two scans (seven scans per medium side) in all. The analog signal recordings of the four field components of interest were sampled at the rate of 304 samples per scan (sampling interval of 0.134 inch) to produce accuracy close to that obtainable from an analog averaging method.

The phase of the reference path signal was shifted 147° with respect to the direct-path signal through free space to offset that introduced by the unloaded support-medium. Because this value was obtained by visually averaging the phase shift of the transmitted wave through the unloaded support-medium, it cannot be considered to provide an accurate absolute reference with respect to this medium. Such a reference, however, was not considered necessary for the present experiments.

Results for estimated average field functions. The average field functions estimated in the experiment are given in Table 6.1. Section (a) of this table lists those functions least susceptible to phase-drift errors (due to frequency drift of klystron) and errors in the phase reference setting between the two sets of channels; section (b) lists the functions most susceptible to these errors. In processing mode 1, the components T_x and T_y were computed from the sampled values of T and τ , while in mode 2, T and τ were computed from T_x and T_y .

As seen from Table 6.1a, a greater deviation between the mode 1 and mode 2 results occurs for the 183 scf density (maximum of 7.7% for $C^2/\langle I^2 \rangle$) than for the 366 scf density (maximum of 1.5% for C^2). The improved agreement between the corresponding results for the 366 scf density resulted from a more careful scaling procedure (i.e., the first set of scale factors were obtained by sampling each of two sets of reference levels 500 times to average out the effects of tape recorder noise; the second set were obtained by sampling each of three sets of reference levels - recorded after every 14 scans - 1,500 times). The discrepancy between the mode 1 and mode 2 results in Table 6.1b is due mainly to an initial error in phase setting between the τ channel and the T_x , T_y channels (except for σ_τ where the small discrepancy is due to the inaccuracy in scaling). The functions $\langle I_x^2 \rangle$, $\langle I_y^2 \rangle$, $\langle I_x I_y \rangle$, and μ are affected by this discrepancy because of their periodic behavior with the variation of the phase reference.^{5,51} A thorough calibration of the lock-in amplifiers with the receiver phase detector and a more careful initial adjustment should minimize this discrepancy in future work.

As seen by the values for the average total intensity $\langle T^2 \rangle$ in Table 6.1a, the fraction of total average power transmitted in the axial direction with the medium in place is considerably less than that without the medium. This indicates a high degree of scattering by the present spheres in

TABLE 6.1

RESULTS FOR ESTIMATED AVERAGE FIELD FUNCTIONS

(a) Functions Least Susceptible to Phase Errors

Average Density	Mode*	C	$\langle T \rangle$	$\langle T^2 \rangle$	C^2	$\langle I^2 \rangle$	$C^2/\langle I^2 \rangle$	σ_T
183 † scf	1	0.657	0.666	0.455	0.431	0.0237	18.2	0.106
	2	0.645	0.656	0.441	0.417	0.0247	16.9	0.107
366 † scf	1	0.447	0.464	0.227	0.200	0.0265	7.55	0.107
	2	0.444	0.460	0.224	0.197	0.0265	7.45	0.109

(b) Functions Most Susceptible to Phase Errors

Average Density	Mode*	α	$\langle \tau \rangle$	$\langle I_x^2 \rangle$	$\langle I_y^2 \rangle$	$\langle I_x I_y \rangle$	μ	σ_T
183 † scf	1	-0.26°	-0.67°	0.0115	0.0122	0.0029	0.24	9.9°
	2	1.35°	0.95°	0.0117	0.0130	0.0027	0.22	10.3°
366 † scf	1	2.28°	1.42°	0.0119	0.0146	0.0027	0.20	16.0°
	2	5.00°	5.94°	0.0132	0.0133	-0.0032	-0.24	15.9°

†results for 183 scf density based on 35 data scans;
 results for 366 scf density based on 39 data scans

*mode 1: T_x and T_y computed from T and τ ;
 mode 2: T and τ computed from T_x and T_y

the off-forward and backward directions, in contrast to the results for similar average densities of large Styrofoam spheres obtained by the Sylvania group.⁴⁹ This difference is of course to be expected and highlights the necessity for future experiments with a wide range of constituent scatterer parameters.

Results of accuracy estimates. As indicated previously, the primary purpose of the present experiments was to determine the suitability of the physical model with respect to the statistical accuracy obtainable. This was accomplished by means of two different methods used to compute the sampling variances of the four estimated mean values: $\langle T_x \rangle$, $\langle T_y \rangle$, $\langle T \rangle$ and $\langle \tau \rangle$.

The first method was based on computation of the spatial autocorrelation and autocovariance functions for T_x , T_y , T and τ . The autocovariance for a function f is defined

$$\begin{aligned} K_f(X) &\triangleq \langle f(0)f(X) \rangle - \langle f \rangle^2 \\ &= R_f(X) - \langle f \rangle^2 \end{aligned} \quad (6.1)$$

where $R_f(X)$ is the autocorrelation function and X is the separation distance. The autocorrelation functions were first computed for each data scan using the formula⁵⁷

$$R_f(m\Delta X) = \frac{1}{n_s - m} \sum_{i=1}^{n_s - m} f(i\Delta X) f(i\Delta X + m\Delta X) \quad (6.2)$$

where ΔX is the distance between adjacent samples, m is the separation distance in terms of samples, and n_s is the number of samples per scan. The overall estimates for the R_f were then obtained by averaging the results over all scans, and the overall estimates for the K_f were obtained from the definition (6.1). The correlation coefficients, or normalized autocovariance functions,

$$K_f'(m\Delta X) \triangleq \frac{K_f(m\Delta X)}{K_f(0)} \quad (6.3)$$

for the amplitude T and phase τ are given in figure 6.8. The curves for T_x and T_y are not given because they are almost identical to those for T and τ respectively.

The autocovariance curves obtained are only accurate for separation distances m up to about 5% or 10% of the number of samples per data scan (i.e., $n_s = 304$).⁵⁷ The sections of the curves in figure 6.8 computed for separation distances beyond those given showed very erroneous behavior due to the inherent unequal weighting of certain sections of samples with the use of formula (6.2), and the loss of accuracy from fewer samples. It can be assumed, however, that the true correlation beyond a separation distance of about thirty samples is very close to zero because of the fact that the half-power beam of the transmitting antenna illuminates a circular area of only 3.6 inches diameter at the center of the medium. The combining of all data scans as a single data segment to obtain greater accuracy of the autocovariance function tails could be easily accomplished on a computer with a larger memory capacity than the present PDP-9.

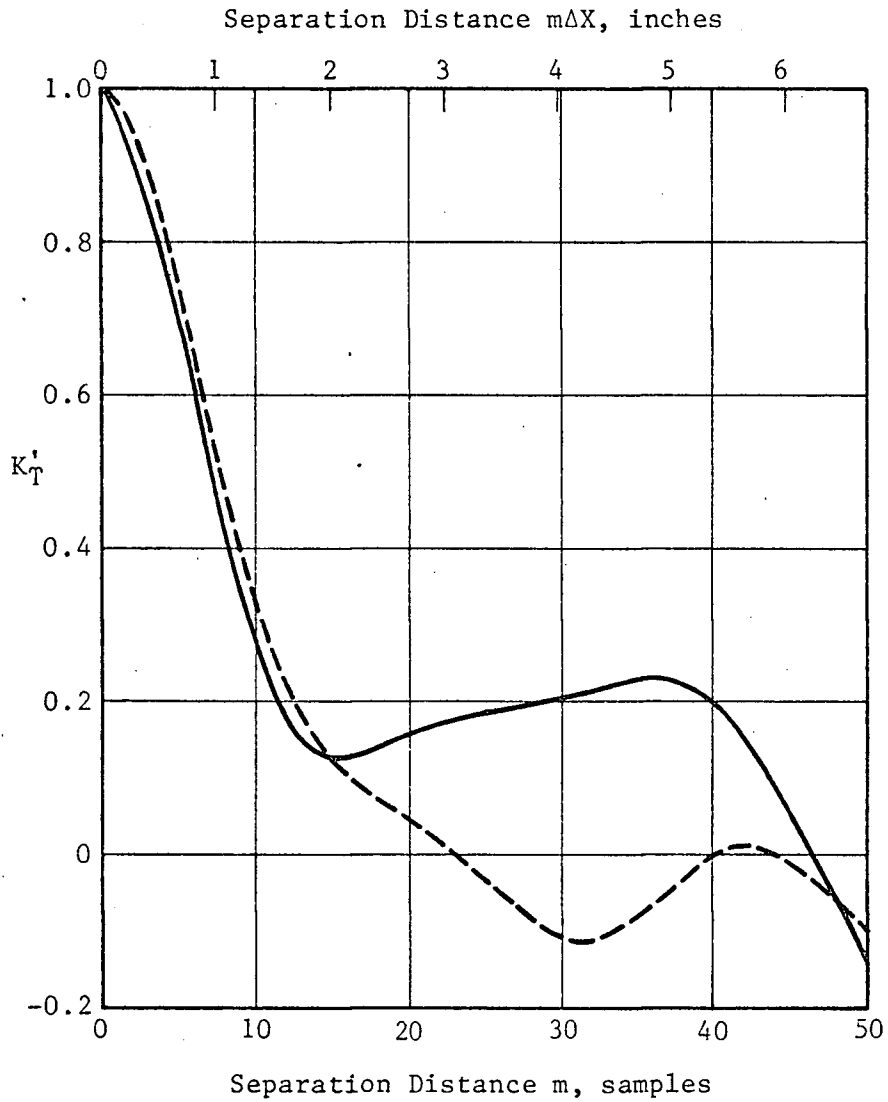
Estimates of the sampling distribution variances for $\langle T_x \rangle$, $\langle T_y \rangle$, $\langle T \rangle$ and $\langle \tau \rangle$, based on the correlation data, were obtained from the formula⁵⁸

$$\sigma_{\langle f \rangle}^2 = \frac{1}{n_c} \left[\sigma_f^2 + 2 \sum_{i=1}^{n_c-1} \left(1 - \frac{i}{n_c} \right) K_f(i\Delta X) \right] \quad (6.4)$$

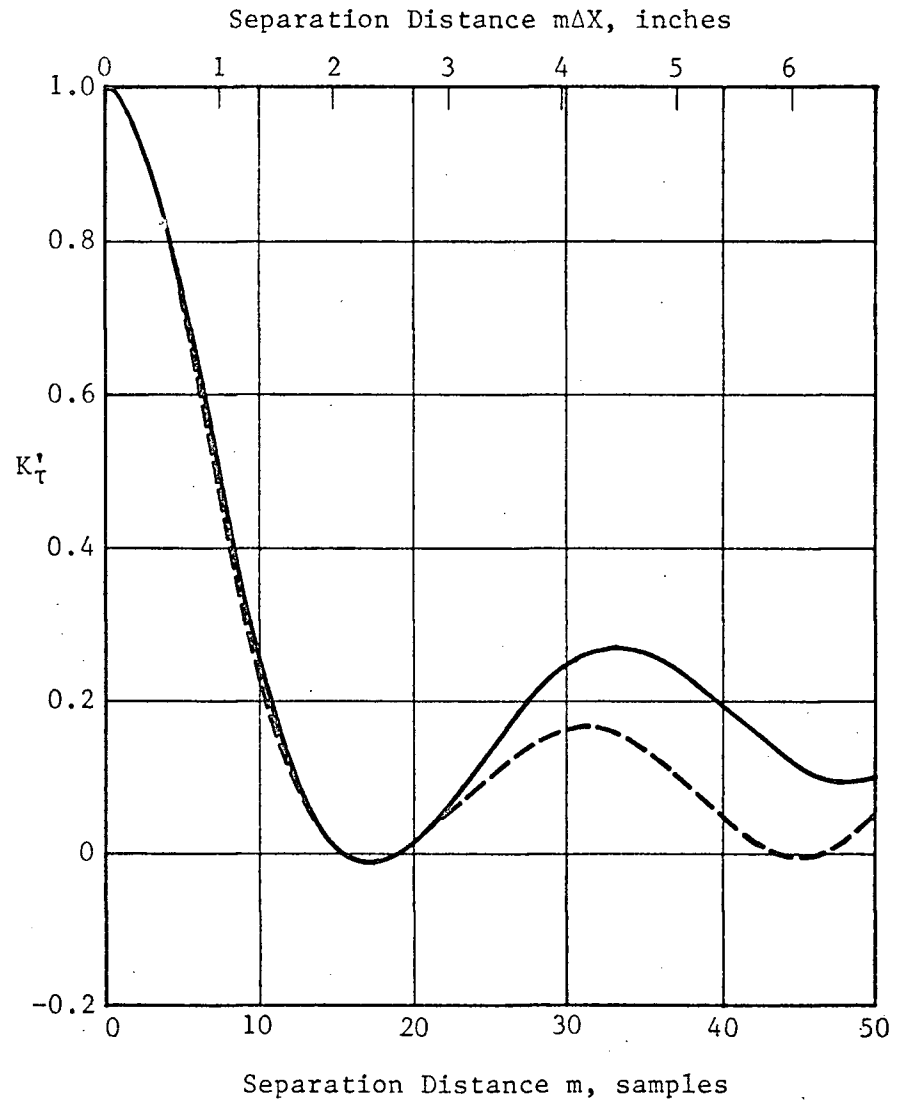
where n_c is the total number of correlated samples. The equivalent number of uncorrelated samples n for each field component was then obtained from

$$\sigma_{\langle f \rangle}^2 = \frac{\sigma_f^2}{n} \quad (6.5)$$

Table 6.2 (method 1) gives the computed results using this approach in the form of the equivalent number of uncorrelated samples per scan and the corresponding distance between these samples for each of the four field



(a) Amplitude



(b) Phase

Figure 6.8 Correlation Coefficient Curves for Amplitude and Phase
 — 183 scf, - - - 366 scf

TABLE 6.2

ACCURACY CALCULATIONS BASED ON EQUIVALENT
UNCORRELATED SAMPLES

- (a) Equivalent Number of Uncorrelated Samples per Scan of T_x , T_y , T , and τ .

Average Density	Method [†]	T_x	T_y	T	τ
183 scf	1	14	16	15	17
	2	20	5	22	5
366 scf	1	18	19	18	19
	2	25	10	24	9

- (b) Distance in Inches between Equivalent Uncorrelated Samples of T_x , T_y , T , and τ .

Average Density	Method [†]	T_x	T_y	T	τ
183 scf	1	2.8	2.6	2.7	2.3
	2	2.0	9.2	1.8	7.6
366 scf	1	2.3	2.1	2.3	2.2
	2	1.6	4.2	1.7	4.6

- [†]Method 1 - using covariance calculations and equation (6.4)
Method 2 - using variance calculations of means over individual scans

components. The results are based on approximating the summation in (6.4) by the sum of positive terms only, up to and including $i = 30$.

The accuracy obtainable from an analog average of the data scans can be estimated by dropping the σ_f^2 term in the calculation of $\sigma_{\langle f \rangle}^2$ in equation (6.4). The approximately one more uncorrelated sample per scan which would be added from such a scheme indicates that a faster sampling rate for the digital technique would be unwarranted.

The second method used in determining the accuracy was to estimate the variances of the mean values over the individual data scans, dividing by the number of scans to obtain estimates of the variances over all scans. The results obtained by this approach, given also in Table 6.2 (method 2), are in good agreement with the corresponding results for method 1, except for the components T_y and τ . The reason for the discrepancy is that the first method, with the dropping of terms from the tails of K_{T_y} and K_τ in the computations based on (6.4), is much less sensitive to phase drift than the second method. The second set of results can therefore be considered to be more accurate under the actual conditions of considerable phase drift (see section 6.4.1). This result strongly points to the need for improved phase stability in future experiments.

The values for some of the field functions and their accuracy estimates obtained by the second method are given in Table 6.3. These figures are based in the normal manner on twice the standard errors of the means (see section 3.4). Two sets of accuracy values are given, one assuming all data scans contribute to the accuracy and the other assuming half the data scans contribute to the accuracy. The reason for this is that the first set of estimates are based on the assumption that all data scans are mutually uncorrelated. Since half the scans were obtained by scanning the back sides of the three layer-configurations, however, the mean field component values for

TABLE 6.3

ACCURACY ESTIMATES BASED ON TWICE THE STANDARD ERRORS OF THE MEANS

(a) Results for 183 scf Average Density (35 data scans)

	C_x	C_y	$\langle T \rangle$	$\langle \tau \rangle$	$\langle I_x^2 \rangle$	$\langle I_y^2 \rangle$	σ_T^2	σ_τ^2
Function Estimate	0.645	0.0153	0.666	-0.67°	0.0117	0.0130	0.0112	97.2
Accuracy Estimate 1	0.008	0.018	0.008	1.4°	0.0010	0.0008	0.0011	6.4
Accuracy [†] Estimate 2	0.012	0.026	0.011	2.0°	0.0014	0.0012	0.0016	9.0

(b) Results for 366 scf Average Density (39 data scans)

	C_x	C_y	$\langle T \rangle$	$\langle \tau \rangle$	$\langle I_x^2 \rangle$	$\langle I_y^2 \rangle$	σ_T^2	σ_τ^2
Function Estimate	0.442	0.0387	0.464	1.42°	0.0132	0.0133	0.0114	257
Accuracy Estimate 1	0.007	0.012	0.007	1.7°	0.0009	0.0008	0.0009	16
Accuracy [†] Estimate 2	0.010	0.017	0.010	2.4°	0.0013	0.0012	0.0012	23

[†]accuracy estimates with maximum correlation between front-side scans and back-side scans assumed

the corresponding scans were probably highly correlated. The second set of estimates can therefore be assumed to be "worst-case" estimates under the condition of maximum correlation between front-side data scans and back-side scans.

The accuracy of estimation could be increased still further by taking data scans of more layer-configurations. It should be emphasized, however, that calculations of overall accuracy are only accurate if the data scans are taken in a manner so as to be relatively uncorrelated. One anomaly in the present technique for obtaining new sphere-configurations is that the density of spheres in the center region of the medium remains the same after the support-medium layers have been shuffled and oriented randomly. The effect of the higher weight placed on this particular density has been visually observed by obtaining averages of the field-component signals over all data scans. Although this anomaly probably effects the accuracy estimates of this section very little because of the size of the medium, it could be eliminated by further introducing a random sliding between layers as suggested in section 6.2.3.

6.5.3 Discussion of Overall Results

The tests on the support-medium indicate that the problem of obtaining uniform transmission characteristics of the incident beam is solvable. Two other possible problems associated with the support-medium which could not be investigated because of the difficulty involved are: (a) the effect of the joints between the layers on the scattered fields of the constituent scatterers, and (b) the effect on the scattered fields of the unavoidable inhomogeneity of the region surrounding the inserted scatterers. In general, because of the presence of the support-medium, the validity of any comparison between experimental and theoretical results is a problem which requires further research.

The experimental results on typical scatterer distributions indicate that the proposed physical model is reasonably suitable from the point of view

of statistical accuracy obtainable. Under conditions of negligible phase reference instability and measurement errors, the accuracy should only be dependent on the size of the medium and the degree of correlation between samples. The results show that considerable overlap between the circular regions of half-power beamwidth illumination is possible before the corresponding field samples become highly correlated.

The statistical accuracy appears to be sufficient that trends in the results for the first two field moments (for a variation in the average density of scatterers, for example) could be established from a set of data scans from one side of a model having transverse dimensions comparable with those of the present one. More accurate results can be obtained for uniform distributions by changing the layer-configuration of the support-medium. For other distributions which do not allow this procedure (e.g., distributions in which the scatterer positions in other than a single layer are correlated), a slab region of larger transverse dimensions would be necessary. The maximum dimensions practicable are probably about $8' \times 4'$.

From the two sets of results obtained, the accuracy of estimation seems little affected by the average density of the distribution. The parameter most affecting such accuracy is probably the transmitting antenna beamwidth, although further experiments with different beamwidths are required to determine the exact behavior. The present experimental results give only an indication of the accuracy obtainable for particular distribution and incident beam parameters. Any future experiments performed using the present model must always include some means of estimating statistical accuracy.

7. CONCLUSIONS

The main developments of this thesis which are considered to be contributions to the subject of scattering from random media of discrete scatterers may be summarized as follows:

I. The One-Dimensional Model

Extensive use has been made of the one-dimensional model of randomly-positioned planar scatterers as a tool in the investigation of general discrete-scatterer theories and as a basis for providing further knowledge of the physical and statistical characteristics of discrete-scatterer media:

A. Theoretical Developments

(i) An explicit series representation in orders-of-back-scattering has been developed for the total field in plane-wave scattering from a fixed array of non-identical planar scatterers.

(ii) Approximate series expressions based on the O-B-S representation have been obtained for several average field functions of interest in the problem of scattering from an ensemble of configurations of uniformly-random identical planar scatterers. These expressions have been shown to be useful in predicting the exact or approximate asymptotic behavior of the average field functions in the limit as $\rho \rightarrow 0$ and it is believed that they may also prove useful in further theoretical research directed towards the improvement of general discrete-scatterer theories.

(iii) The exact asymptotic forms for $\rho \rightarrow 0$ in the planar-scatterer model have been obtained for the coherent transmitted field and the average total and incoherent intensities of both the transmitted and reflected fields. The importance of the asymptotic forms in the improvement of theories applicable to higher ρ has been illustrated. In particular, the exact asymptotic form $(1 + g_+)^N$ for the coherent transmitted field $\langle T \rangle$ has been used to modify the

one-dimensional form of Twersky's free-space theory; the possibility of a similar finite-N correction to the three-dimensional form of Twersky's theory has been suggested.

(iv) Based on the O-B-S approximations for the transmitted and reflected fields and the existing theory of random phasor sums, physical conditions necessary for the approximate validity of the bivariate Gaussian distribution in describing the total field statistics of the one-dimensional model have been given. Conditions necessary for the occurrence of a Rayleigh-distributed incoherent field amplitude with uniformly-distributed phase have also been outlined.

B. Monte Carlo Simulation

(i) "Exact" simulation results for use in the evaluation of approximate theories for the one-dimensional model have been obtained.

(ii) Monte Carlo simulation applied to the approximate O-B-S representations for the field has been used to validate the approximate series expressions for the average field functions obtained; the expression derived for $\langle R^2 \rangle$ remains to be verified. A comparison of "exact" simulation results and theoretical data has shown certain of these theories to be in the main better than the one-dimensional forms of existing general discrete-scatterer theories.

(iii) The limitations of the one-dimensional form of Twersky's free-space theory for the coherent field and conditions necessary for its approximate validity have been illustrated by a presentation of results for a wide range of scattering parameters. The improvement contained in the "asymptotic correction" to the free-space theory for $\langle T \rangle$ has been verified. The comparison of theoretical data for the free-space theory for $\langle R \rangle$ with "experimental" results is believed to be the first.

(iv) A quantitative analysis of the total field distribution based on the third and fourth field moments has been made and certain effects of multiple scattering illustrated. The stated physical conditions necessary for the

approximate validity of the bivariate Gaussian distribution have been verified.

(v) Simulation methods for the generation of a non-uniform distribution of planar-scatterer configurations weighted towards periodicity have been developed. Based on the scattering results obtained, criteria for the assumption of uniform-randomness have been determined. The limitations of the one-dimensional form of Twersky's mixed-space theory for the coherent field have been illustrated and conditions necessary for its approximate validity given.

II. The Three-Dimensional Physical Model

(i) A new three-dimensional physical model of spherical scatterers in which the Monte Carlo method is employed to control the scatterer statistics has been developed for use in laboratory experiments at millimeter-wave frequencies. It is believed that this model may be of value in theoretical-experimental investigations of the type performed previously on the Sylvania physical model and in this work on the one-dimensional model.

(ii) An initial experimental investigation into the suitability of the proposed model has been carried out. Experiments have been performed on the support-medium and measurements of the forward-diffracted field in scattering from typical distributions have been obtained and analyzed to determine the importance of disadvantages associated with the model. From the results obtained, the disadvantages investigated appear to be minimal.

(iii) An initial investigation into the validity of the discrete position approximation used in the three-dimensional model has been carried out employing the results for similar approximations applied to the one-dimensional model. A basis for a partial comparative-evaluation of the approximation in the two models has been found and factors important in the future development of more firm criteria outlined. Approximate theory necessary in the comparison has been developed.

APPENDIX A SUMMARY OF TWERSKY'S THEORIES FOR SCATTERING FROM
RANDOM MEDIA OF DISCRETE SCATTERERS

A.1 Twersky's Free-Space Theory for the Coherent Field⁸

This theory is applicable to the problem of a plane wave $\phi(\vec{r}) = e^{-j\vec{k}\cdot\vec{r}}$ obliquely incident at an arbitrary angle θ on a slab-region distribution (i.e., bounded by the planes $z = 0$ and $z = d$) of one-, two-, or three-dimensional scatterers random in one, two, or three dimensions respectively. It contains the following assumptions:

- (i) The scatterers are identical and similarly aligned.
- (ii) The one-scatterer probability density function, defined

$$p(\vec{r}_1) \triangleq \int \dots \int p(\vec{r}_1, \dots, \vec{r}_N) d\vec{r}_2 d\vec{r}_3 \dots d\vec{r}_N \quad (\text{A.1})$$

is of the form

$$p(\vec{r}_1) = \rho(\vec{r}_1)/N \quad (\text{A.2})$$

and is the same for all scatterers [$\rho(\vec{r}_1)$ is the average density of scatterers at \vec{r}_1].

(iii) The two-scatterer probability density function is the product of one-scatterer forms, i.e.,

$$p(\vec{r}_1, \vec{r}_2) \triangleq \int \dots \int p(\vec{r}_1, \dots, \vec{r}_N) d\vec{r}_3 d\vec{r}_4 \dots d\vec{r}_N = \left[\frac{\rho(\vec{r}_1)}{N} \right] \left[\frac{\rho(\vec{r}_2)}{N} \right] \quad (\text{A.3})$$

or equivalently, the two-scatterer conditional probability density function defined

$$p(\vec{r}_2 | \vec{r}_1) \triangleq \int p(\vec{r}_1, \vec{r}_2) d\vec{r}_2 \quad (\text{A.4})$$

is equal to $p(\vec{r}_1)$.

The free-space theory equations are also based on the approximate relation

$$\sum_{s=1 \neq t}^N p(\bar{r}_t | \bar{r}_s) = (N-1) \left[\frac{\rho(\bar{r}_s)}{N} \right] \approx \rho(\bar{r}_s) \quad (\text{A.5})$$

valid for large N , and the heuristic approximation

$$\langle \psi \rangle_{st} \approx \langle \psi \rangle_s \quad (\text{A.6})$$

where $\langle \psi \rangle_s$ is the average total field with the position vector \bar{r}_s held fixed, etc. These two approximations can be combined to give the single approximate equation

$$\langle \psi \rangle_s \approx \langle \psi \rangle + \langle U \rangle_s \quad (\text{A.7})$$

where $\langle U \rangle_s$ is the average scattered field from a scatterer with its position vector \bar{r}_s held fixed.

Recognizing that equation (A.7) is the form of the solution for a single object excited by a set of plane waves and scattering into free space, and using the following two additional assumptions, Twersky solved the resulting integral equations to obtain explicit expressions for the coherent field:

(iv) The coherent field internal to the medium is of the form

$$\langle \psi \rangle = A(z)e^{-j\bar{k} \cdot \bar{r}} + B(z)e^{-j\bar{k}' \cdot \bar{r}} \quad (0 \leq z \leq d) \quad (\text{A.8})$$

where A and B are unknown functions of position within the medium (\bar{k}' has the magnitude k and the direction of the incident field reflected in the slab-region face).

(v) The average density ρ of scatterers within the slab region is constant.

Altogether, because of the assumptions and approximations required for mathematical manageability, the expressions obtained by Twersky are most valid for uniformly-distributed anisotropic point scatterers (line scatterers in two dimensions, plane scatterers in one dimension), i.e.,

$$p(\bar{r}_1, \dots, \bar{r}_N) = (\rho/N)^N \quad (\text{A.9})$$

For the problem of a plane wave normally incident on a slab-region distribution of identical planar scatterers, the free-space theory gives the following equations for the coherent transmitted and reflected fields:

$$\langle T \rangle = D(1 - Q^2) e^{-j(\eta-1)kd} \quad (z \geq d) \quad (\text{A.10})$$

$$\langle R \rangle = -QD(1 - e^{-2jnk d}) \quad (z \leq 0) \quad (\text{A.11})$$

where

$$Q = \frac{\rho g_-}{\rho g_+ - jk(\eta + 1)}, \quad D = \frac{1}{1 - Q^2 e^{-2jnk d}}, \quad \rho = \frac{N}{d} \quad (\text{A.12})$$

$$\eta^2 = \left[1 - \rho(g_+ + g_-)/jk \right] \left[1 - \rho(g_+ - g_-)/jk \right] \quad (\text{A.13})$$

As discussed by Twersky,⁸ these approximate expressions are identical to those pertaining to the field produced when a normally incident plane wave scatters from a homogeneous dielectric slab of width d and refractive index η .

The asymptotic forms of these equations in the limit as $\rho \rightarrow 0$ are

$$\langle T \rangle \sim e^{Ng_+} \quad (\text{A.14})$$

$$\langle R \rangle \sim \rho g_- (1 - e^{2Ng_+ - 2jkd})/2jk \quad (\text{A.15})$$

$$Q \sim j\rho g_-/k(\eta + 1) \quad (\text{A.16})$$

$$\eta \sim 1 + j\rho g_+/k \quad (\text{A.17})$$

Other details of the free-space theory are discussed in reference 8.

A.2 Twersky's Mixed-Space Theory for the Coherent Field²⁴

This theory is also applicable to the problem of a plane wave incident on a slab-region distribution of scatterers but is based on "two-space"

or "mixed-space" isolated scatterer amplitudes rather than the conventional amplitudes. In a mixed-space isolated scatterer problem the incident wave travels in one medium (propagation constant K) and scatters from a single scatterer into another medium (e.g., free space with propagation constant k).²³

The mixed-space theory includes all the assumptions and approximations of the free-space theory except assumption (iv), the form of the coherent field internal to the medium. In the mixed-space theory $\langle \psi \rangle$ is assumed to be of the form

$$\langle \psi \rangle = Ae^{-j\bar{K}\cdot\bar{r}} + Be^{-j\bar{K}'\cdot\bar{r}} \quad (0 \leq z \leq d) \quad (\text{A.18})$$

where A and B are now constants, independent of position z , and K is the "bulk propagation constant" of the medium. For a coherent field of this form, equation (A.7) represents a mixed-space isolated scatterer problem.

For the one-dimensional ensemble of planar scatterers, the mixed-space formalism results in the free-space theory equations (A.10) and (A.11) for $\langle T \rangle$ and $\langle R \rangle$. However, for the mixed-space theory

$$Q = \frac{(\eta - 1)g'_-}{(\eta + 1)g'_+} \quad (\text{A.19})$$

and the bulk refractive index $\eta = K/k$ satisfies the functional equation

$$F(\eta) = \eta^2 + \frac{\rho}{jk} (g'_+ - g'_-)\eta + \frac{\rho}{jk} (g'_+ + g'_-) - 1 = 0 \quad (\text{A.20})$$

In these equations g'_+ and g'_- are the mixed-space forward- and back-scattering amplitudes for a wave normally incident in "K-space" on an isolated planar scatterer which scatters into "k-space". Explicit expressions for g'_+ and g'_- for a dielectric slab of finite width are given in Appendix B. The asymptotic free-space theory equations (A.14) to (A.17) apply also to the mixed-space theory since $g'_+ \rightarrow g_+$, $g'_- \rightarrow g_-$, and $\eta \rightarrow 1$ as $\rho \rightarrow 0$.

The solution of the mixed-space equations involving η and the

mixed-space scattering amplitudes is straightforward for certain types of scatterers. Twersky²⁴ has obtained explicit approximate solutions for the separate cases of small spherical scatterers and large tenuous scatterers. In Appendix B an approximate solution is given for "thin" dielectric slab scatterers and it is shown for these scatterers (as shown by Twersky for small spheres) that $g'_+ = g'_- \rightarrow 0$ and $\eta \rightarrow \eta'$ as $\rho \rightarrow \infty$ (where η' is the refractive index of the slab material). More generally, the exact solution of the mixed-space theory equations is difficult and a numerical method must be used. A numerical solution of equation (A.20) and those of g'_+ and g'_- for dielectric slab scatterers of finite width was performed in the present work and is discussed in Appendix B, section B.2.

The difference between the mixed-space and free-space theories arises for high ρ . As shown by Twersky,²⁴ the mixed-space theory can approximately describe certain dense distributions of finite-size scatterers if ρ is interpreted as $\rho = N/(V - NV_s)$, where V is the volume of the containing region and V_s the volume occupied by a single scatterer. For slab-region distributions of small spheres he has shown that the bulk parameter equations of the mixed-space theory reduce to existing forms and that the limiting behavior of such distributions and distributions of large tenuous scatterers as $\rho \rightarrow \infty$ is approximately correct. Experimental measurements on a model distribution of large tenuous scatterers have furthermore confirmed the approximate validity of the mixed-space theory for that particular case.⁴⁹

For a distribution of "thin" dielectric slabs such that the approximate expressions in Appendix B for g'_+ , g'_- , and η are valid, the mixed-space theory gives almost exact results in the limit as $\rho \rightarrow \infty$ if $\rho = N/(d+w-Nw)$ and if d in the equations for $\langle T \rangle$, $\langle R \rangle$, and D is replaced by $d+w$, the width of the slab region occupied by the scatterers including their boundaries. This is easily seen from equations (A.10), (A.11), and (A.19), since $g'_-/g'_+ \approx 1$ for

"thin" slabs and $-Q$ is the Fresnel reflection coefficient for the boundary between the medium of the incident field and the slab region filled with scatterers of refractive index $\eta = \eta'$. It is confirmed from the numerical results in Chapter 5, section 5.4.

A.3 Theories for Other Average Field Functions

General discrete-scatterer theories for other average field functions have also been of interest in the present work but have not been numerically evaluated for the one-dimensional model. One theory for $\langle I^2 \rangle$ developed by Twersky^{8,11} is based on the conservation of energy principle. The general relation obtained by Twersky for a slab region of uniformly-distributed identical scatterers

$$\langle I^2 \rangle \approx \rho \int |u_s|^2 d\bar{r}_s \quad (\text{A.21})$$

(u_s is the isolated scatterer function defined in section 2.3) can be readily evaluated for the one-dimensional model. The $\langle I^2 \rangle$ expressions obtained for the transmitted and reflected fields involve the free-space theory functions Q , D , and η . In the limit of $\rho \rightarrow 0$, these expressions reduce to

$$\langle I^2 \rangle \sim - \frac{|g_+|^2}{2 \text{Reg}_+} (1 - e^{2N\text{Reg}_+}) \quad (z \geq d) \quad (\text{A.22})$$

$$\langle I^2 \rangle \sim - \frac{|g_-|^2}{2 \text{Reg}_+} (1 - e^{2N\text{Reg}_+}) \quad (z \leq 0) \quad (\text{A.23})$$

Thus, from the forward amplitude theorem for lossless planar scatterers (see equation B.4 of Appendix B) and from the asymptotic forms for the coherent intensities as obtained from equations (A.14) and (A.15), it is readily observed that energy is conserved. This fact does not result in an accurate theory for the one-dimensional model, however, as shown by the theoretical results of section 2.7.

Another theory for $\langle |\psi|^2 \rangle$ developed by Twersky¹¹ which also

satisfies the energy principle is the $\langle \psi \rangle$ -consistent approximation. This theory was obtained by the introduction of similar approximations into the series representation for $\langle |\psi|^2 \rangle$ as were shown to exist in the expanded form of the compact representation for $\langle \psi \rangle$. Numerical results for this theory as applied to a distribution of large tenuous scatterers have been shown to compare well with experimental results from a physical model of the distribution.⁴⁹ Similar results for the application of this theory to the one-dimensional model could also be of value.

APPENDIX B SCATTERING FROM A SINGLE DIELECTRIC SLAB

B.1 Conventional Scattering Amplitudes

For a plane wave normally incident in free space on a lossless dielectric slab of width $w = 2a$ and refractive index $\eta' = \sqrt{\epsilon_r}$ as shown in figure B.1, the forward- and back-scattering amplitudes g_+ and g_- are given respectively by

$$1 + g_+ = T_1 = \frac{4\eta' e^{2jka}}{\Delta'} \quad (\text{B.1})$$

and

$$g_- = R_1 = \frac{(\eta'^2 - 1)(e^{-2jn'ka} - e^{2jn'ka})e^{2jka}}{\Delta'} \quad (\text{B.2})$$

where

$$\Delta' = (\eta' + 1)^2 e^{2jn'ka} - (\eta' - 1)^2 e^{-2jn'ka} \quad (\text{B.3})$$

The single slab transmission and reflection coefficients T_1 and R_1 are referred to the slab center as are the scattering amplitudes. The forward amplitude theorem⁸ for the slab scatterer, relating the total scattering cross-section $\sigma = |g_+|^2 + |g_-|^2$ to the forward-scattering amplitude g_+ is

$$\sigma = |g_+|^2 + |g_-|^2 = -2 \text{Reg}_+ \quad (\text{B.4})$$

Expansion of the exponentials in the expressions for g_+ and g_- yields

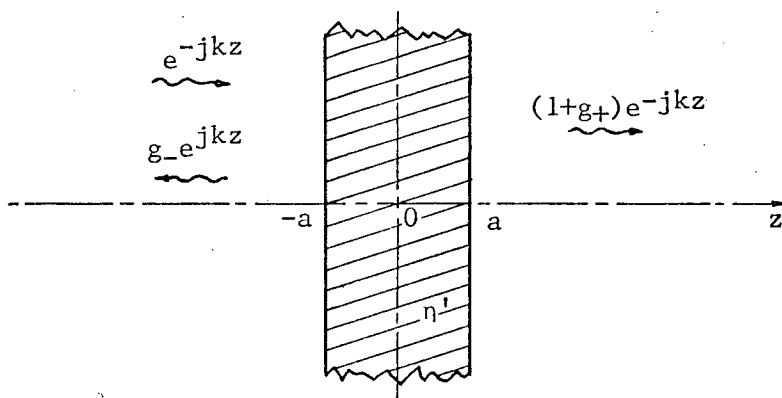


Figure B.1 Scattering from a Single Dielectric Slab

the approximate expression for "thin" slabs (i.e., $\eta'ka \ll 1$)

$$g_+ \approx g_- \approx -(\eta'^2 - 1)ka \left[(\eta'^2 - 1)ka + j \right] \triangleq g_m \quad (\text{B.5})$$

Thus, for a "thin" slab, the back-scattering cross-section $2|g_-|^2$ and the forward-scattering cross-section $2|g_+|^2$ are approximately equal. For a slab of dielectric constant $\epsilon_r = 2.0$ (i.e., the value used for the numerical results in the thesis), the rectangular components of g_+ , g_- and g_m are plotted as functions of the slab width w_λ (i.e., width in wavelengths λ' within the slab material) in figure B.2.

For a plane wave obliquely incident on the slab at an angle θ with the interface normal, the scattering amplitudes are more generally given by

$$1 + g_+ = \frac{4Z'e^{2jkac\cos\theta}}{(1 + Z')^2 e^{2jn'kac\cos\theta_r} - (1 - Z')^2 e^{-2jn'kac\cos\theta_r}} \quad (\text{B.6})$$

$$g_- = \frac{(1 - Z'^2)(e^{-2jn'kac\cos\theta_r} - e^{2jn'kac\cos\theta_r})e^{2jkac\cos\theta}}{(1 + Z')^2 e^{2jn'kac\cos\theta_r} - (1 - Z')^2 e^{-2jn'kac\cos\theta_r}} \quad (\text{B.7})$$

where

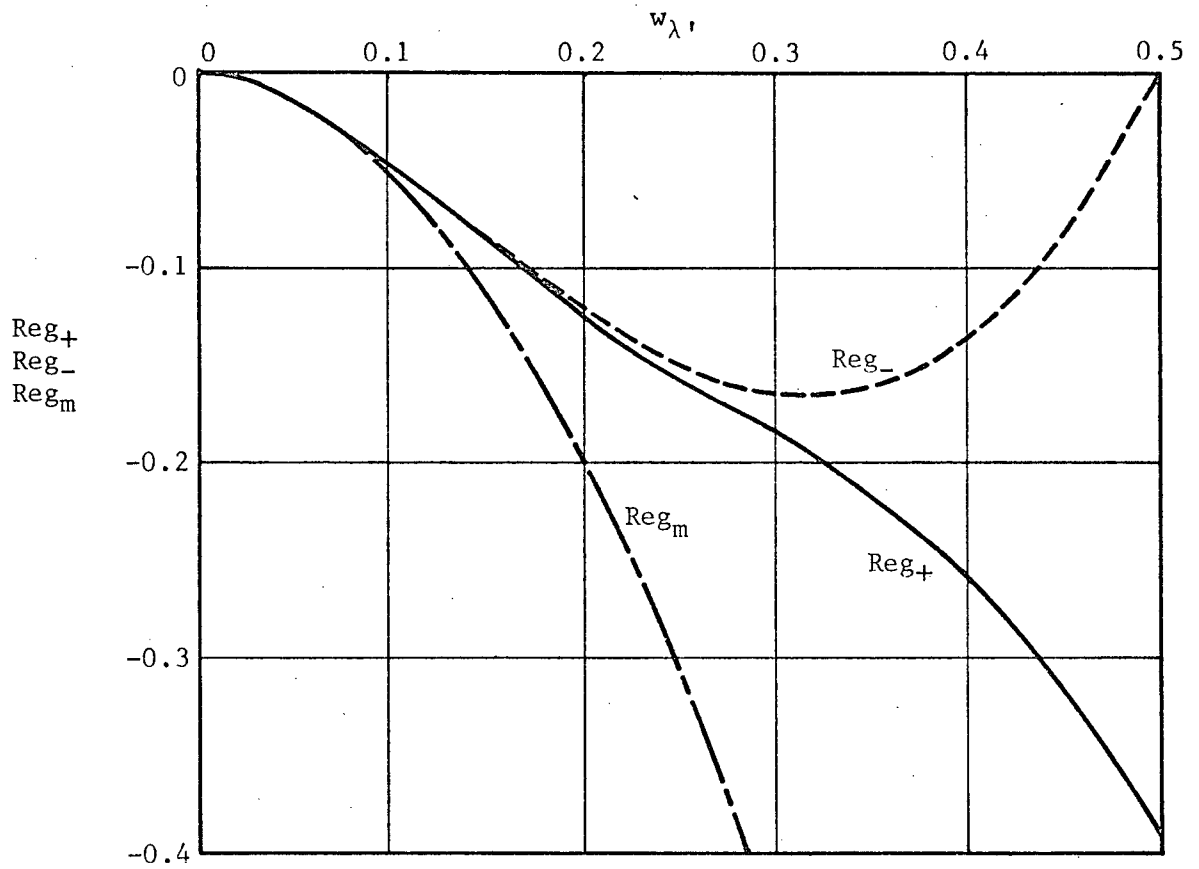
$$\cos\theta_r = \frac{1}{\eta'} \sqrt{\eta'^2 - \sin^2\theta} \quad (\text{B.8})$$

For a wave of perpendicular polarization (i.e., electric field vector perpendicular to the plane containing the interface normal and the propagation vector),

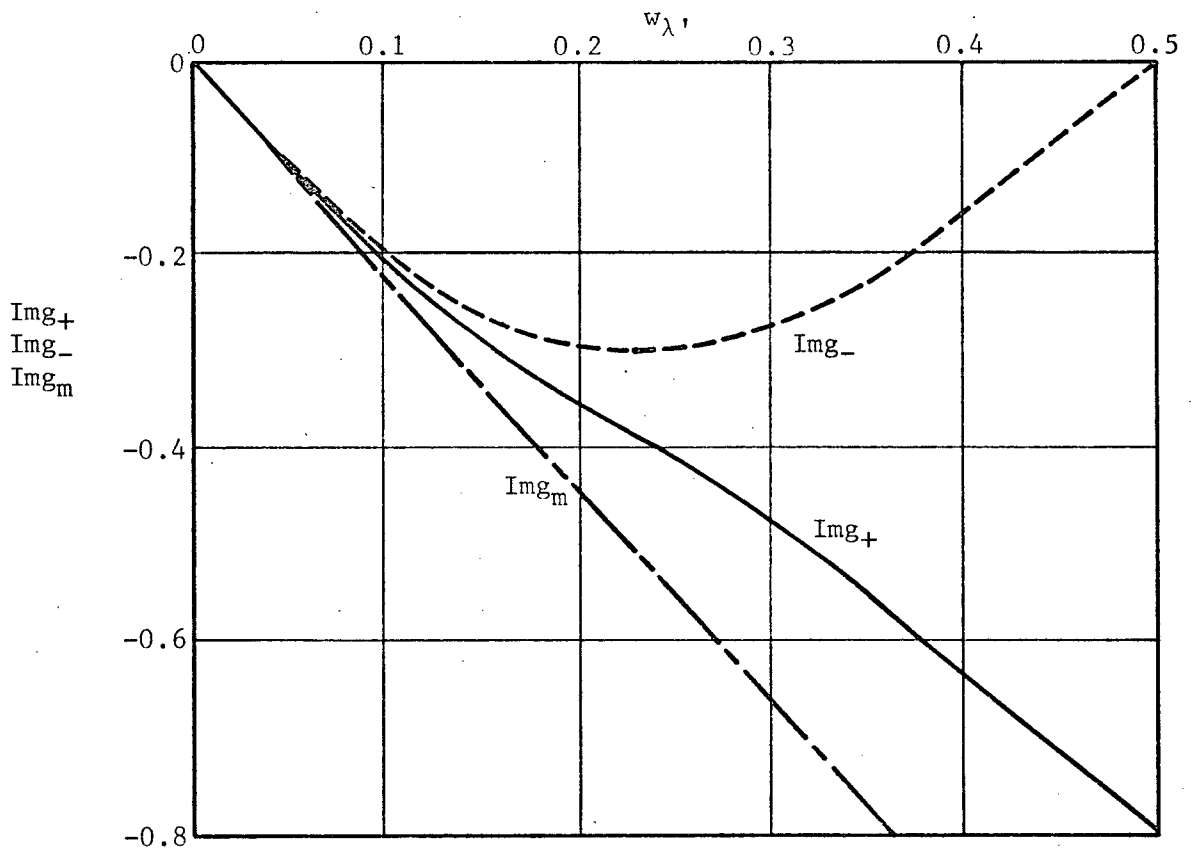
$$Z' = \frac{\cos\theta}{\sqrt{\eta'^2 - \sin^2\theta}} \quad (\text{B.9})$$

For a wave of parallel polarization,

$$Z' = \frac{\sqrt{\eta'^2 - \sin^2\theta}}{\eta'^2 \cos\theta} \quad (\text{B.10})$$



(a) Reg_+ , Reg_- , and Reg_m versus $w_{\lambda'}$,



(b) Img_+ , Img_- , and Img_m versus $w_{\lambda'}$,

Figure B.2 Scattering Amplitudes as a Function of $w_{\lambda'}$, for $\epsilon_r = 2.0$

All the given equations can be generalized to include losses in the slab by replacement of ϵ_r with the complex quantity $\epsilon_r(1 - j \tan\delta)$, where $\tan\delta$ is the loss tangent of the slab material.

B.2 Mixed-Space Scattering Amplitudes

For a plane wave $\phi(z) = e^{-j\eta kz}$ normally incident on the slab within a medium of refractive index η , and with the scattered waves again travelling in free space, the more general scattering amplitudes are given by²³

$$g_+^1 = \frac{e^{jka}}{\Delta'} \left[2\eta'(1 + \eta)e^{jnka} + (\eta' - 1)(\eta' - \eta)e^{-j(\eta+2\eta')ka} - (\eta' + 1)(\eta' + \eta)e^{-j(\eta-2\eta')ka} \right] \quad (\text{B.11})$$

$$g_-^1 = \frac{e^{jka}}{\Delta'} \left[2\eta'(1 - \eta)e^{-jnka} - (\eta' + 1)(\eta' - \eta)e^{j(\eta+2\eta')ka} + (\eta' - 1)(\eta' + \eta)e^{j(\eta-2\eta')ka} \right] \quad (\text{B.12})$$

For a "thin" slab, these mixed-space scattering amplitudes are given by the approximate expression

$$g_+^1 \approx g_-^1 \approx -(\eta'^2 - \eta^2)ka \left[(\eta'^2 - 1)ka + j \right] \triangleq g_m^1 \quad (\text{B.13})$$

corresponding to the result of equation (B.5) for the conventional amplitudes.

For $\eta \rightarrow 1$, these equations all reduce to the conventional forms.

In Twersky's mixed-space theory for the coherent field, η is identified with the bulk refractive index of the random medium, given by equation (A.20) of Appendix A. Substitution of the "thin" slab equation (B.13) into equation (A.20) yields

$$\eta^2 = \frac{1 + 2ap \left[1 - j(\eta'^2 - 1)ka \right] \eta'^2}{1 + 2ap \left[1 - j(\eta'^2 - 1)ka \right]} \quad (\text{B.14})$$

Thus, as seen by this expression and that of equation (B.13), $\eta \rightarrow \eta'$ and $g_+^i \approx g_-^i \approx g_m^i \rightarrow 0$ as $\rho \rightarrow \infty$. For ρ interpreted as $\rho = N/(d + w - Nw)$ in the manner discussed in Appendix A (where $w = 2a$ is the scatterer width), equation (B.14) can be rewritten in terms of the fractional "volume" $\beta_0 = Nw/(d + w)$ as

$$\eta^2 = 1 + \frac{\beta_0(\eta'^2 - 1) [1 - j(\eta'^2 - 1)ka]}{1 - j\beta_0(\eta'^2 - 1)ka} \quad (\text{B.15})$$

$$\approx 1 + \beta_0(\eta'^2 - 1) [1 - j(1 - \beta_0)(\eta'^2 - 1)ka]$$

Exact solution of the mixed-space theory equations (B.11), (B.12), and (A.20) is possible only by means of a numerical technique. For comparison of mixed-space theory results with "exact" simulation results in Chapters 4 and 5, the Newton-Raphson method⁵⁹ was employed. This well-known iterative technique makes use of the equation

$$\eta_i = \eta_{i-1} - \frac{F(\eta_{i-1})}{F'(\eta_{i-1})} \quad (\text{B.16})$$

where η_i is the value for η after i iterations and $F'(\eta)$ is the derivative of $F(\eta)$ with respect to η . The initial value η_0 used in the iteration was the free-space theory value given by equation (A.13). For the specific scattering parameters chosen for study, this initial value was sufficiently close to the actual mixed-space value for quick convergence of equation (B.16).

APPENDIX C VALIDITY OF THE DISCRETE POSITION APPROXIMATION
IN SIMULATION STUDIES

The validity of a discrete probability density approximation to a continuous probability density of scatterer positions is of interest in this work mainly as it pertains to the construction of the three-dimensional physical model discussed in Chapter 6. However, the application of such an approximation in computer simulation studies of mathematical models may also allow the use of simplified efficient techniques for processing the random numbers involved (e.g., in the sorting or rejection procedures used) and its validity is therefore of more general interest. In order that insight into the problem might be obtained, the discrete position approximation (DPA) has been applied to the one-dimensional model considered in previous chapters. The results of the study are given in this section and related where possible to the three-dimensional model.

Results are given for two types of discrete probability densities of scatterer positions. In the first type (labelled "discrete non-uniform"), the one-dimensional equivalent of that used for the three-dimensional model, the scatterer positions are chosen uniformly at random from those available under the condition that at most one scatterer occupy any one position (i.e., Fermi-Dirac "statistics" in statistical mechanics). In the second type (labelled "discrete uniform"), the positions are chosen uniformly at random from all those available with no restriction on the number of the N scatterers per position (i.e., Bose-Einstein "statistics" in statistical mechanics). The average field functions shown for both types of discrete distribution are plotted against the "occupancy ratio" $\beta_d = N/n_d$, where n_d is the number of equally-spaced positions available. To most clearly display the effect of the DPA, n_d is varied rather than N , which is fixed at $N = 10$. The planar scatterer amplitudes employed, $g_+ = 0.2107 \angle -101.7^\circ$ and $g_- = 0.2035 \angle -102.2^\circ$,

are the same as those used earlier. The results are based on the exact wave matrix theory for a fixed configuration with 1,000 sample configurations.

Results for the discrete non-uniform distribution are given in figure C.1. Shown are curves of the phase and intensity of the coherent transmitted field and the average incoherent intensity of the reflected field for a series of d_λ values. The entire curves for $d_\lambda = 2, 7, \text{ and } 12$ are shown for completeness although it is the first monotonically-varying portions which are of present interest. Smooth curves have been drawn through all "experimental" points (included for $d_\lambda = 7$) except those for small values of n_d where straight-line segments are used to indicate the discrete nature of the results. Curves for $\langle I^2 \rangle$ of the transmitted field are not given because they are similar in form to those for the reflected field.

The results of figure C.1 show the combined effect of the DPA and the single-scatterer-per-position requirement. They may be likened to those of section 5.3 for the continuous non-uniform distribution and essentially the same arguments may be applied to explain the oscillatory behavior displayed in the curves. The main difference in the present results is that resonance phenomena occur for certain mid-range values of β_d where the discrete-position interval d/n_d is approximately equal to an integral multiple of $\lambda/2$. For later comparison with the discrete non-uniform results for $\rho_\lambda = 5$ (i.e., $d_\lambda = 2$), results for a continuous non-uniform distribution are also given in figure C.1. To provide a valid comparison, these results have been obtained using method A of Chapter 5 with the additional requirement that the distance of closest approach of z_1' and z_N' with the slab region boundaries be $e/2$, where $e = d/n_d$. The fractional "volume" $\beta_0 = Ne/d$ for the continuous distribution is then equivalent to the occupation ratio $\beta_d = N/n_d$ for the discrete distribution.

The effect of the DPA alone is displayed by the discrete uniform distribution results of figure C.2. Although resonance phenomena occur also

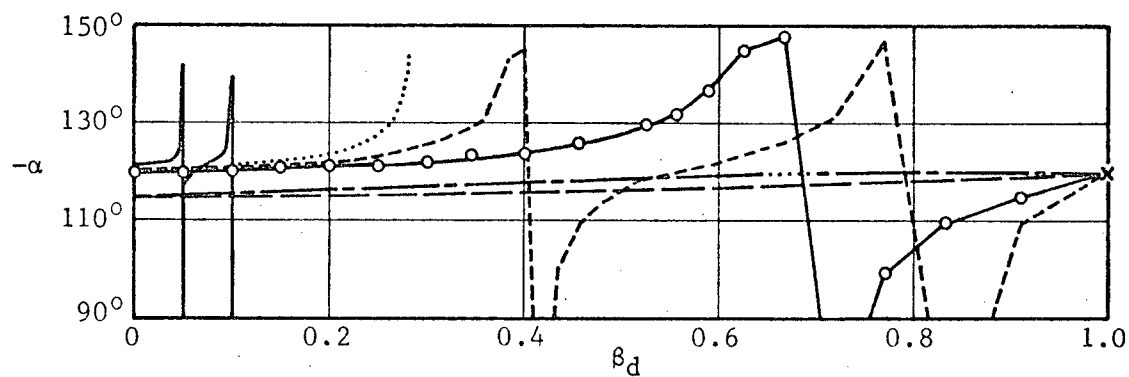
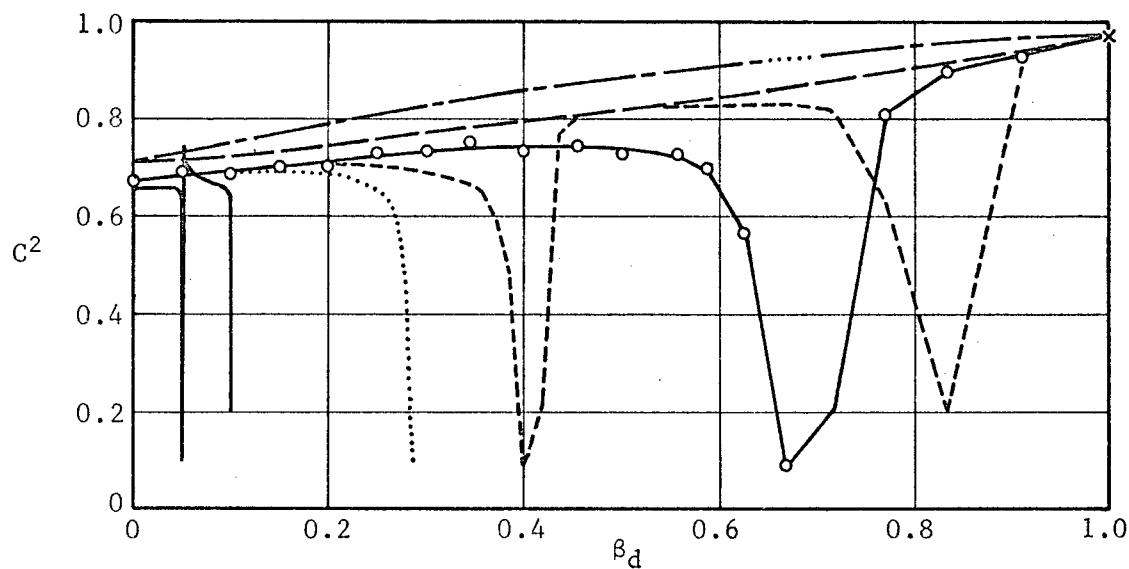
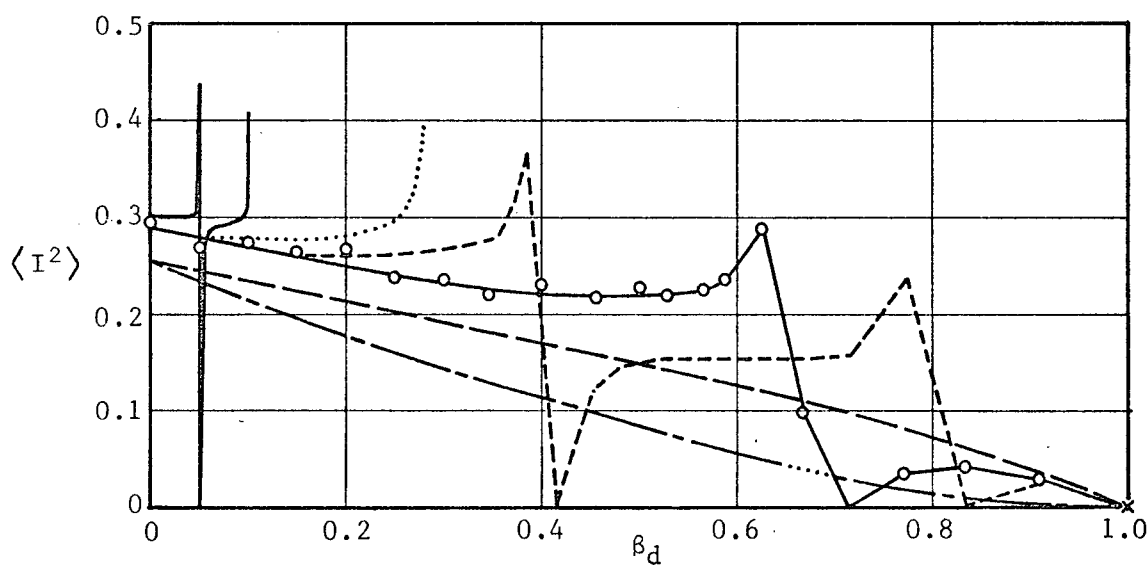
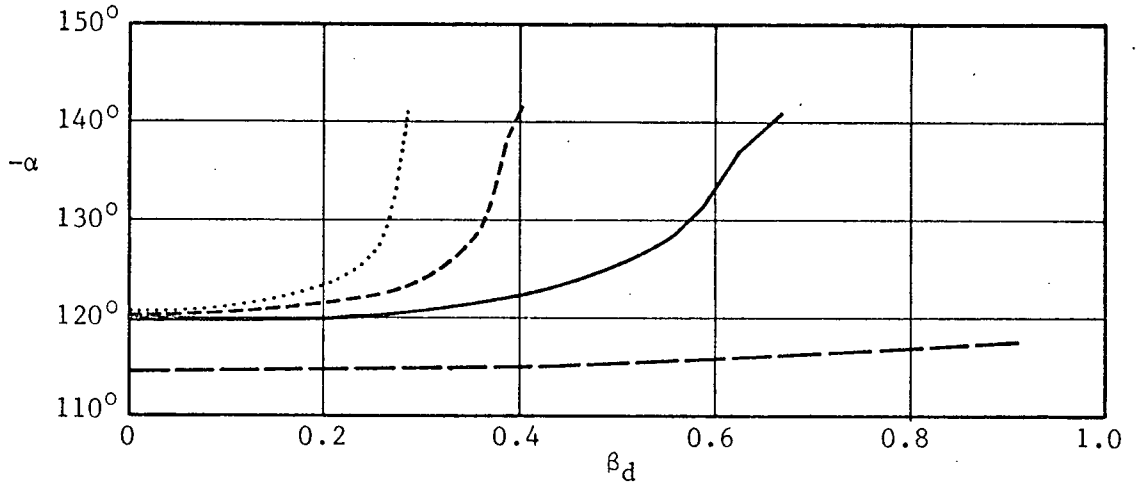
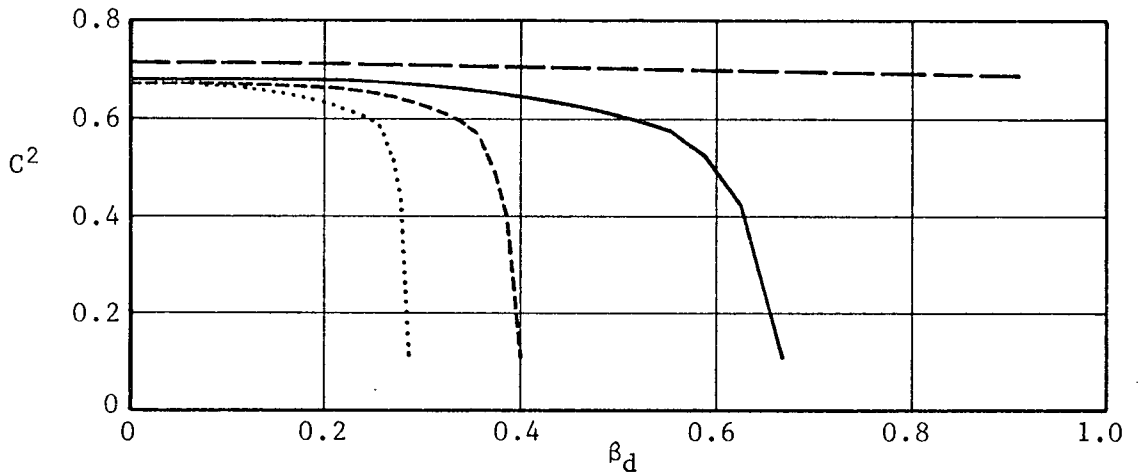
(a) $-\alpha$ versus β_d - Transmitted Field(b) C^2 versus β_d - Transmitted Field(c) $\langle I^2 \rangle$ versus β_d - Reflected Field

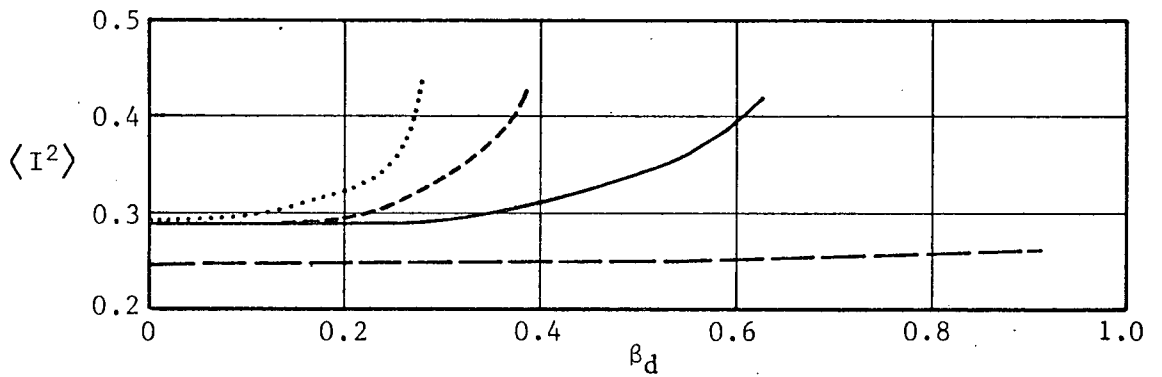
Figure C.1 Dependence of Average Field Functions on β_d for the Non-Uniform Distribution. $N = 10$, $w_\lambda = 0.1$, $\epsilon_r = 2.0$;
 — $d_\lambda = 2$ (discrete), - - $d_\lambda = 2$ (continuous),
 ○—○ $d_\lambda = 7$, - - - - $d_\lambda = 12$, $d_\lambda = 17$, — $d_\lambda = 97$



(a) $-\alpha$ versus β_d - Transmitted Field



(b) C^2 versus β_d - Transmitted Field



(c) $\langle I^2 \rangle$ versus β_d - Reflected Field

Figure C.2 Dependence of Average Field Functions on β_d for the Uniform Distribution. $N = 10$, $w_\lambda = 0.1$, $\epsilon_r = 2.0$;
 --- $d_\lambda = 2$, — $d_\lambda = 7$, - · - $d_\lambda = 12$, ····· $d_\lambda = 17$

for this distribution, only the first monotonically-varying portions of the curves are given. A comparison of figures C.1 and C.2 shows the single-scatterer-per-position requirement of the non-uniform distribution to be the predominant cause of deviation from the continuous distribution limit (i.e., $\beta_d = 0$) for low values of β_d and high ρ_λ , but the DPA to be increasingly more dominant for decreasing ρ_λ .

Since the physical differences between the one-dimensional planar-scatterer model and the three-dimensional spherical-scatterer model are considerable, the effect of the DPA in the latter can be expected to be somewhat different. Some comparison can be made, however, once the main scattering processes in each model are identified and written in the form of random phasor sums. The transmitted field, as discussed in section 2.8, can be written as

$$T_e j^\tau = A_0 e^{j\theta_0} + \sum_{s=1}^{N_I} A_s e^{j\theta_s} \quad (C.1)$$

where $A_0 e^{j\theta_0}$ is a constant phasor, the $A_s e^{j\theta_s}$ are random phasors representing the significant scattering contributions to the random component of the field, and N_I is the number of these contributions. The significant scattering processes present in the one-dimensional model have already been identified and the approximate transmitted field written in the form of (C.1) in section 2.8. For relatively low ρ in the three-dimensional model, it is well known that single scattering is the only significant process. In this case, $A_0 e^{j\theta_0} = 1$ and, for a field point on the beam axis (see figure C.3),

$$A_s = \frac{G(\alpha_s, \phi_s) |f(\gamma_s, \phi_s)| (d_t + d_r)}{G(0,0) t_s v_s} \quad (C.2)$$

$$\theta_s = -k(t_s + v_s - d_t - d_r) + \text{Arg}f(\gamma_s, \phi_s) \quad (C.3)$$

where $G(\alpha_s, \phi_s)$ = field pattern factor of transmitting antenna in the direction specified by α_s, ϕ_s

$G(0,0)$ = field pattern factor along the beam axis

$f(\gamma_s, \phi_s) = -g(\hat{v}_s, \hat{t}_s)/jk$ = scattering amplitude (unnormalized) of spherical scatterer in the direction specified by γ_s, ϕ_s

ϕ_s = polar coordinate in x,y-plane

$$t_s = \sqrt{(d_t + z_s)^2 + r_s^2}$$

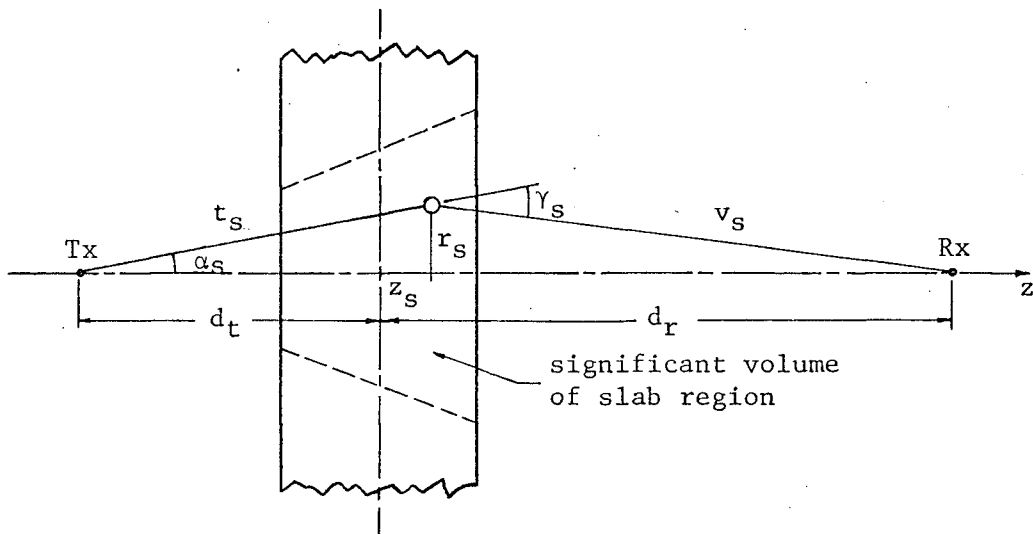
$$v_s = \sqrt{(d_r - z_s)^2 + r_s^2}$$


Figure C.3 Single-Scattering Geometry for the Three-Dimensional Model

The number of significant scattering contributions N_I is equal to the number of scatterers in the volume of illumination in which the A_s are significantly large. Although the A_s are functions of the scatterer amplitudes as well as the radiation pattern of the transmitting antenna, the limits of the significant volume may usually be assumed to lie between the limits of that illuminated by the half-power beam and that by the main lobe.

It seems reasonable that the validity of the DPA is related to the following interconnected factors:

- (i) the number of basic phase cycles over which the θ_s vary,
- (ii) the number of discrete values of the θ_s within a basic phase cycle

of variation,

(iii) the number of discrete values of the A_s over their range of variation, and

(iv) the average number of significant scattering contributions N_I to the random component of the field.

Since the A_s are constant in the one-dimensional model and random in the three-dimensional model, it is in the relative "discreteness" of the phases θ_s that comparisons between the two models can best be made.

In the one-dimensional model the range of θ_s variation is governed by d_λ and N (or ρ_λ). In particular, it has been shown in Chapter 5 that $\sigma_{\theta_s} \approx 4\pi d_\lambda / (N - 1)$ for uniformly-distributed scatterers. As seen from the results of figure C.2, the required number of discrete values of θ_s per basic cycle for a good approximation to a continuous distribution decreases for increasing σ_{θ_s} . With $\rho_\lambda = 5$ and $\sigma_{\theta_s} = 0.89\pi$, for example, a good approximation for the average field functions investigated is maintained for β_d as high as 0.6, or the number of discrete values of θ_s per 2π radians as low as four. For $\rho_\lambda = 0.103$ (i.e., $d_\lambda = 97$) and $\sigma_{\theta_s} = 43\pi$, a minimum of slightly greater than one discrete value of θ_s per basic phase cycle results in a good approximation and, except for a small interval of β_d values in the neighbourhood of resonance (for these parameters the first resonance occurs for $\beta_d \approx 0.05$), a discrete interval in θ_s even larger than 2π results in a reasonably good approximation (see figure C.1 for these results).

In the three-dimensional model the range of the θ_s variations is governed mainly by the average density of scatterers ρ , the distances of the source and field points from the medium, and the average locations of the scatterers within the significant volume. This may be shown as follows: The spherical scatterers are identified with average cylindrical-coordinate locations $(\langle r_s \rangle, \langle \phi_s \rangle, \langle z_s \rangle)$ in a manner analogous to that in which the planar

scatterers were considered in terms of their ordered-positions and essentially identified with their average positions $\langle z'_s \rangle$. For slowly-varying $\text{Argf}(\gamma_s, \phi_s)$, variation in θ_s is caused mainly by deviations in r_s and z_s from their means; to first-order terms¹⁴

$$\sigma_{\theta_s}^2 \approx \left[\frac{\partial \theta_s(\langle r_s \rangle, \langle z_s \rangle)}{\partial r_s} \right]^2 \sigma_{r_s}^2 + \left[\frac{\partial \theta_s(\langle r_s \rangle, \langle z_s \rangle)}{\partial z_s} \right]^2 \sigma_{z_s}^2 \quad (\text{C.4})$$

Physical reasoning or evaluation of both terms in (C.4) shows further that variation in θ_s is caused mainly by variation in r_s and hence that

$$\sigma_{\theta_s} \approx \left| \frac{\partial \theta_s(\langle r_s \rangle, \langle z_s \rangle)}{\partial r_s} \right| \sigma_{r_s} \quad (\text{C.5})$$

Thus, from equation (C.3),

$$\sigma_{\theta_s} \approx \frac{2\pi \langle r_s \rangle \sigma_{r_s}}{\lambda} \left[\frac{1}{\sqrt{(d_t + \langle z_s \rangle)^2 + \langle r_s \rangle^2}} + \frac{1}{\sqrt{(d_r - \langle z_s \rangle)^2 + r_s^2}} \right] \quad (\text{C.6})$$

For the uniform-randomness of the scatterers in the present model, the number of scatterers in a volume much smaller than that of the slab region is approximately Poisson distributed; or more specifically, the distribution of the increase in an arbitrarily-shaped volume V_s about an average location before a scatterer is reached is approximately exponential with $p(V_s) = \rho e^{-\rho V_s}$. In spherical polar coordinates $(r'_s, \theta'_s, \phi'_s)$ about the average locations, $V_s = 4\pi r_s'^3/3$ and

$$r_s^2 = \langle r_s \rangle^2 + r_s'^2 \sin^2 \theta'_s - 2 \langle r_s \rangle r'_s \sin \theta'_s \cos \phi'_s \quad (\text{C.7})$$

Thus,

$$\begin{aligned} \sigma_{r_s}^2 &= \langle r_s^2 \rangle - \langle r_s \rangle^2 \\ &= \rho \int_0^\infty \int_0^\pi \int_0^{2\pi} e^{-4\pi\rho r_s'^3/3} \left[r_s'^2 \sin^2 \theta'_s - 2 \langle r_s \rangle r'_s \sin \theta'_s \cos \phi'_s \right] r_s'^2 \sin \theta'_s \\ &\quad d\phi'_s d\theta'_s dr'_s \end{aligned}$$

$$\begin{aligned}\sigma_{r_s}^2 &= \frac{8\pi\rho}{3} \int_0^\infty r_s'^4 e^{-4\pi\rho r_s'^3/3} dr_s' \\ &= c^2 \rho^{-2/3}\end{aligned}\tag{C.8}$$

or

$$\sigma_{r_s} = c\rho^{-1/3}, \quad c \triangleq \frac{2}{3} \left(\frac{4\pi}{3} \right)^{-1/3} \sqrt{\Gamma(2/3)}\tag{C.9}$$

where Γ is the well-known Gamma function.

It is of interest to compare certain numerical results based on equations (C.6), (C.9), and the experimental parameters specified in Chapter 6 with those given for the one-dimensional model. The number m of equivalent discrete values of θ_s per basic phase cycle, where m_i is the number of discrete positions per inch, is given by

$$m = \frac{2\pi m_i \sigma_{r_s}}{\sigma_{\theta_s}}\tag{C.10}$$

For $\rho = 183$ scf and an average scatterer location on the x,y-plane (i.e., $\langle z_s \rangle = 0$) and the edge of the volume illuminated by the main lobe, $\sigma_{\theta_s} = 1.1\pi$ and $m = 3.6$; for $\rho = 366$ scf, $\sigma_{\theta_s} = 0.9\pi$ and $m = 3.6$ (independent of ρ). For $\rho = 183$ scf and an average location on the edge of the volume illuminated by the half-power beam, $\sigma_{\theta_s} = 0.47\pi$ and $m = 8.5$; for $\rho = 366$ scf, $\sigma_{\theta_s} = 0.38\pi$. For an average location at $\langle z_s \rangle = 0$ and $\langle r_s \rangle = \sigma_{r_s}$ with $\rho = 183$ scf, $\sigma_{\theta_s} = 0.27\pi$ and $m = 15$; with $\rho = 366$ scf, $\sigma_{\theta_s} = 0.18\pi$ and $m = 18$.

Although σ_{θ_s} in the three-dimensional model is a function of the average position of each scatterer, it is evident from the preceding results that the average σ_{θ_s} would be of the same order of magnitude as the value $\sigma_{\theta_s} = 0.89$ obtained for $\rho_\lambda = 5$ in the one-dimensional model. If it is assumed that the relationship between σ_{θ_s} and m for the DPA to be valid is the same as in the one-dimensional model, the difference in σ_{θ_s} for each scatterer does not matter since smaller σ_{θ_s} are accompanied by larger m . If it is further

assumed that actual values of σ_{θ_s} and m in the one-dimensional model can be used to predict the validity of the DPA in the three-dimensional model, the values of m for the three-dimensional σ_{θ_s} obtained appear to be approximately within the necessary limits. It is in fact possible that the numerical relationship between m and σ_{θ_s} for the validity of the DPA might need to be even less stringent than in the one-dimensional model, since the unequal truncation intervals in θ_s would seem to preclude the possibility of strong resonance effects as in the one-dimensional model.

The validity of the discrete non-uniform probability density which is made necessary in a DPA accounting for finite scatterer size is also of interest. As seen by the one-dimensional model results of figures C.1 and C.2 for $\rho_\lambda = 5$, the effect of the DPA is noticeable for lower values of β_d in the discrete non-uniform distribution than in the discrete uniform distribution. The explanation for this would seem to be that σ_{θ_s} remains relatively constant for increasing β_d in the uniform case whereas in the non-uniform case it does not, being given approximately by $\sigma_{\theta_s} \approx 4\pi(1-\beta_d)d_\lambda/(N-1) \approx 4\pi(1-\beta_d)/\rho_\lambda$ in analogy to equation (5.8) for the continuous non-uniform distribution. Thus, for a given β_d , σ_{θ_s} is smaller for the non-uniform distribution than for the uniform distribution while m is unchanged.

For the three-dimensional model it would seem plausible to account for the non-uniformity resulting from finite scatterer size in the same manner. While the replacement for $\sigma_{r_s} = c\rho^{-1/3}$ in equation (C.6) would be $\sigma_{r_s} = c[(1-\beta_o/\beta_m)/\rho]^{1/3}$ (where β_m is the maximum β_o physically possible) in the continuous case, it would be $\sigma_{r_s} = c[(1-\beta_d)/\rho]^{1/3}$ in the discrete case. If this one-third power (or any fractional power) correction in $1-\beta_d$ is actually valid, higher values of β_d in the three-dimensional model than in the one-dimensional model might be tolerated before breakdown of the DPA. Any estimation of the maximum tolerable β_d is complicated by the fact that the

validity of the single-scattering approximation is also dependent on β_d , however, and is thus impossible at present. The low values of $\beta_d = 0.013$ and $\beta_d = 0.026$ for the experimental distribution parameters of Chapter 6 would in any case seem easily tolerable since they change the numerical values already given for σ_{θ_s} very little.

Much further work including all four factors mentioned is necessary to establish definite criteria for the validity of the DPA in the three-dimensional model. Until such criteria are developed, however, one precaution can be taken to minimize the DPA error for higher density distributions than those used for the experimental results of Chapter 6. This is to use a discrete-position interval in the coordinate directions transverse to the beam smaller than the diameter of the scatterers, the one-scatterer-per-position requirement being modified accordingly. If no DPA were employed in these coordinate directions at all, a two-dimensional "rejection" technique similar to those used in Chapter 5 for the one-dimensional model could be employed. Although the necessity of support-medium layers in the present model limits the discrete-position interval parallel to the beam to be no smaller than the scatterer diameter, it is evident from the preceding discussion that the resulting error would be less important than that for the transverse coordinate directions as long as single scattering remains the only significant process. It is the presence of significant multiple-scattering effects and the necessity for a DPA in the coordinate direction parallel to the beam that must ultimately limit the range of average densities possible for study with the present model.

APPENDIX D DESIGN OF MICROWAVE ANECHOIC CHAMBER AND POSITIONING DEVICE

D.1 Design and Testing of Anechoic Chamber

A small microwave anechoic chamber has been designed and constructed for general use in scattering experiments of the type described in Chapter 6 and in antenna pattern measurements. The design is standard, a wedge-shaped back wall and longitudinally-baffled side walls being employed to achieve a central "quiet" volume region, and therefore only limited details are given.

A simplified plan-view diagram of the chamber is shown in figure D.1. Inside dimensions (not including absorbing material) are approximately 15'4" × 9'4" × 10' (height). The chamber shell is constructed of two-by-four framing and plywood sheeting in four foot sections bolted together which allows for easy extension in length. Power receptacles are located at suitable places both inside and outside, swivel-fixture lights are located in the four upper corners, and ventilation is provided by means of an exhaling fan and vents. All inside fixtures are located at least critical positions to minimize reflections.

The least critical surface areas are covered with Emerson & Cuming Eccosorb FR330 absorbing material. B. F. Goodrich VHP-4 absorbing material covers the critical back-wall area and a six foot wide area of the side walls. The minimum reflectivity levels for these absorbers at X-band are -20db and -45db respectively. The FR330 material limits the operating frequency range to frequencies above 2.3 GHz. The longitudinally-baffled side walls and wedge-shaped back wall produce a thirty-one inch diameter "quiet zone" (i.e., volume in which specularly-reflected contributions to the total field involve no fewer than two surface reflections) running the entire length of the chamber to within nineteen inches of the back-wall apex.

Detailed "one-way transmission" tests were performed on the chamber

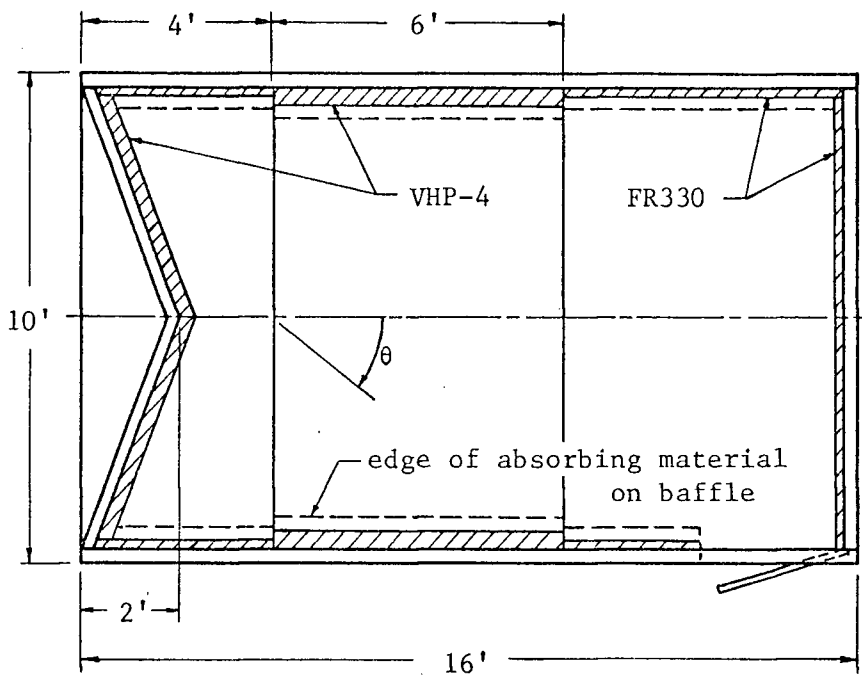


Figure D.1 Simplified Plan-View Diagram of the Anechoic Chamber

at 9.32 GHz and 35.0 GHz using the B. F. Goodrich "free-space VSWR" technique.^{60,61} With the remotely-controlled positioner described in the following section used as a mount for the receiving antenna (vertically polarized), traverses along two-foot horizontal and vertical radii from the room axis were made at a distance of twenty-five inches from the back-wall apex, with the aspect angle θ of the antenna (see figure D.1) set at 10° increments between 40° and 320° . The 9.32 GHz measurements were made with 16db Narda type 640 transmitter and receiver horns and the 35.0 GHz measurements with the horns used for the experiments described in Chapter 6. Calculations based on the standing-wave patterns obtained showed an average reflectivity level⁶² within a two-foot diameter section of the quiet zone of -53db at 9.32 GHz (averaged over all aspect angles and one foot horizontal and vertical radii) and better than -66db at 35.0 GHz. This level dropped to only -51db at 9.32 GHz along one-foot radii sections centered 1.5 feet from the chamber axis. Plots of the reflectivity level versus aspect angle showed the largest source of reflected power to be the back wall, as expected. For an aspect angle

of $\theta = 0^\circ$ (as used for the Chapter 6 experiments), no reflections from the side walls were evident and for other forward aspect angles the reflectivity level was considerably lower than the average.

D.2 Design of Remotely-Controlled Positioning Device

A remotely-controlled positioning device has been designed and constructed for general use as a scanning platform in the type of experiments described in Chapter 6 and as an antenna positioner for pattern measurements and tests on the anechoic chamber. This device is capable of a four-foot horizontal movement, a one-foot vertical movement, and a 390° azimuthal movement. The photograph shown in figure D.2 illustrates the main features of the mechanical design: The vertical-movement system is mounted on the azimuth rotator and both these systems are fixed to a platform which is propelled on wheels along two horizontal tracks. A screw coupled to a dc gear motor provides the horizontal drive and a screw coupled to a gear train and ac servo motor, the vertical drive. An ac servo motor and gear train also drives the azimuth rotator. The tubular center shaft allows either a scattering medium or an antenna to be easily mounted in place.

Accurate open-loop control of the three coordinate positions is achieved in the device by means of the speed-controllable motors and transmit-receive synchro systems. The control box, located outside the anechoic chamber, is shown in the center of the photograph on page 122. Position readout of the horizontal and vertical coordinates is derived by means of counters driven by single synchro receivers. Dual synchro transmitters and receivers in the azimuth system, with gear ratios of 1:1 and 36:1, provide both a course and fine indication of azimuth on two graduated circular dials. Position readout resolution is 0.00625 inches in the horizontal direction, 0.005 inches in the vertical direction, and 0.1° in azimuth; accuracy is only

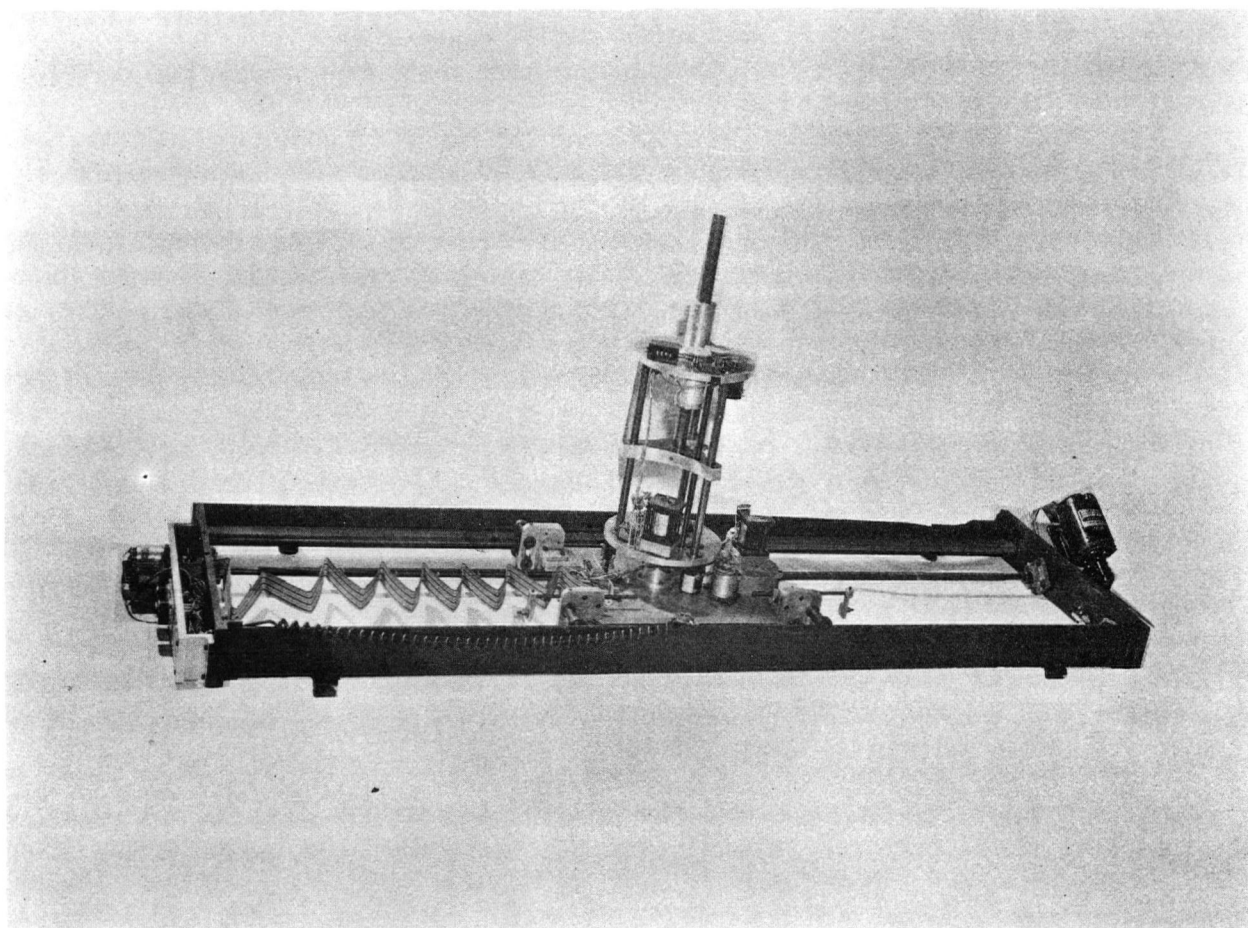


Figure D.2 View of the Positioning Device

slightly less.

Potentiometers coupled to all three coordinate systems in the positioner provide an electrical output of position for controlling an X-Y plotter used in the measurement of free-space standing-wave patterns and antenna patterns. A relay-battery circuit connected to the horizontal motor input provides a two-level control voltage for use in processing the data recorded during scanning of the physical model described in Chapter 6. Limit switches incorporated in all three motor-drive circuits remove power to the motors when the physical limits in the positioner are reached.

REFERENCES

1. Silver, S. "Delineation of Problems and Methodology in the Subject of Scattering by a Statistically Inhomogeneous Medium," in Electromagnetic Theory and Antennas, Part 2, E. C. Jordan (ed.). New York: Pergamon Press, 1963, pp. 661-663.
2. Keller, J. B. "A Survey of the Theory of Wave Propagation in Continuous Random Media," in Proceedings of the Symposium on Turbulence of Fluids and Plasmas, MRI Symposia Series, Vol. 18. Brooklyn: Polytechnic Press, 1969, pp. 131-142.
3. Beckmann, P. Probability in Communication Engineering. New York: Harcourt, Brace & World, Inc., 1967.
4. Twersky, V. "Signals, Scatterers, and Statistics," IEEE Trans. on Antennas and Propagation, AP-11 (1963), pp. 668-680.
5. Twersky, V. "Theory and Microwave Measurements of Higher Statistical Moments of Randomly Scattered Fields," in Electromagnetic Scattering, R. L. Rowell and R. S. Stein (eds.). New York: Gordon and Breach Science Publishers, 1967, pp. 579-695.
6. Keller, J. B. "Wave Propagation in Random Media," in Proceedings of the Symposium in Applied Mathematics on Hydrodynamic Instability, Vol. 13. Providence: American Mathematical Society, 1962, pp. 227-246.
7. Kay, I., and R. A. Silverman. "Multiple Scattering by a Random Stack of Dielectric Slabs," Nuovo Cimento, 9 (1958), pp. 626-645.
8. Twersky, V. "On Scattering of Waves by Random Distributions. I. Free-Space Scatterer Formalism," J. Math. Phys., 3 (1962), pp. 700-715.
9. Twersky, V. "Multiple Scattering by Arbitrary Configurations in Three Dimensions," J. Math. Phys., 3 (1962), pp. 83-91.
10. Twersky, V. "Multiple Scattering of Electromagnetic Waves by Arbitrary Configurations," J. Math. Phys., 8 (1967), pp. 589-610.
11. Twersky, V. "On Propagation in Random Media of Discrete Scatterers," in Proceedings of the Symposium in Applied Mathematics on Stochastic Processes in Mathematical Physics and Engineering, Vol. 16, R. Bellman (ed.). Providence: American Mathematical Society, 1964, pp. 84-116.
12. Collin, R. E. Field Theory of Guided Waves. New York: McGraw-Hill Book Company, 1960.
13. Marcus, P. M. The Interaction of Discontinuities on a Transmission Line. Massachusetts Institute of Technology, Cambridge, Mass., Radiation Laboratory Report 930, February 6, 1946.
14. Bennett, C. A., and N. L. Franklin. Statistical Analysis in Chemistry and the Chemical Industry. New York: John Wiley & Sons, Inc., 1954.

15. Burke, J. E., and V. Twersky. "On Scattering of Waves by Many Bodies," J. Res. Natl. Bur. Std., 68D (1964), pp. 500-510.
16. Twersky, V. "On Multiple Scattering of Waves," J. Res. Natl. Bur. Std., 64D (1960), pp. 715-730.
17. Foldy, L. L. "The Multiple Scattering of Waves," Phys. Rev., 67 (1945), pp. 107-119.
18. Lax, M. "Multiple Scattering of Waves," Rev. Mod. Phys., 83 (1951), pp. 287-310.
19. Lax, M. "Multiple Scattering of Waves. II. The Effective Field in Dense Systems," Phys. Rev., 85 (1952), pp. 621-629.
20. Waterman, P. C., and R. Truell. "Multiple Scattering of Waves," J. Math. Phys., 2 (1961), pp. 512-537.
21. Fikioris, J. G., and P. C. Waterman. "Multiple Scattering of Waves. II. 'Hole Corrections' in the Scalar Case," J. Math. Phys., 5 (1964), pp. 1413-1420.
22. Mathur, N. C., and K. C. Yeh. "Multiple Scattering of Waves by Random Scatterers of Finite Size," J. Math. Phys., 5 (1964), pp. 1619-1628.
23. Twersky, V. "On a General Class of Scattering Problems," J. Math. Phys., 3 (1962), pp. 716-723.
24. Twersky, V. "On Scattering of Waves by Random Distributions. II. Two-Space Scatterer Formalism," J. Math. Phys., 3 (1962), pp. 724-734.
25. Twersky, V. "Multiple Scattering of Waves in Dense Distributions of Large Tenuous Scatterers," in Electromagnetic Scattering, M. Kerker (ed.). New York: Pergamon Press, 1963, pp. 523-546.
26. Twersky, V. "Scattering by Random Media," in Electromagnetic Theory and Antennas, Part 2, E. C. Jordan (ed.). New York: Pergamon Press, 1963, pp. 701-715.
27. Twersky, V. "Correlated Signals from Uncorrelated Distributions of Scatterers," in Electromagnetic Wave Theory, J. Brown (ed.). New York: Pergamon Press, 1967, pp. 963-978.
28. Twersky, V. "Scattering by Discrete Random Media," in Proceedings of the Symposium on Turbulence of Fluids and Plasmas, MRI Symposia Series, Vol. 18. Brooklyn: Polytechnic Press, 1969, pp. 143-161.
29. Karlin, S. A First Course in Stochastic Processes. New York: Academic Press, 1966.
30. Beckmann, P., and A. Spizzichino. The Scattering of Electromagnetic Waves from Rough Surfaces. New York: Pergamon Press, 1963.
31. Beckmann, P. "Statistical Distribution of the Amplitude and Phase of a Multiply Scattered Field," J. Res. Natl. Bur. Std., 66D (1962), pp. 231-240.

32. Beckmann, P. "Rayleigh Distribution and its Generalizations," J. Res. Natl. Bur. Std., 68D (1964), pp. 927-932.
33. Bremmer, H. "On the Theory of Fading Properties of a Fluctuating Signal Imposed on a Constant Signal," National Bureau of Standards, Washington, D. C., NBS Circular 599, May 1959.
34. Hoyt, R. S. "Probability Functions of the Modulus and Angle of the Normal Complex Variate," Bell System Tech. J., 26 (1947), pp. 318-359.
35. Nakagami, M. "The m-Distribution - A General Formula of Intensity Distribution of Rapid Fading," in Statistical Methods in Radio Wave Propagation, W. C. Hoffman (ed.). New York: Pergamon Press, 1960, pp. 3-36.
36. Norton, K. A., et al. "The Probability Distribution of the Amplitude of a Constant Vector Plus a Rayleigh-Distributed Vector," Proc. IRE, 43 (1955), pp. 1354-1361.
37. Rice, S. O. "Mathematical Analysis of Random Noise," Bell System Tech. J., 23 (1944), pp. 282-332; 24 (1945), pp. 46-156.
38. Hammersley, J. M., and D. C. Handscomb. Monte Carlo Methods. London: Methuen & Co. Ltd., 1964.
39. Hochstim, A. R., and C. P. Martens. "Electromagnetic Scattering from Underdense Random Plasma Slabs," in Proceedings of the Symposium on Turbulence of Fluids and Plasmas, MRI Symposia Series, Vol. 18. Brooklyn: Polytechnic Press, 1969, pp. 187-215.
40. Hochstim, A. R., and C. P. Martens. Radar Scattering from Near-Overdense and Overdense Random, Plane Parallel Plasma Slabs. Institute for Defense Analyses, Science and Technology Division, Arlington, Va., Research Paper P-410, July 1968.
41. Chambers, R. P. "Random Number Generation on Digital Computers," IEEE Spectrum, 4 (February, 1967), pp. 48-56.
42. Hull, T. E., and A. R. Dobell. "Random Number Generators," SIAM Rev., 4 (1962), pp. 230-254.
43. Pike, M. C., and I. D. Hill. "Algorithm 266, Pseudo-Random Numbers," Communications of the ACM, 8 (1965), pp. 605-606.
44. Gebhardt, F. "Generating Pseudo-Random Numbers by Shuffling a Fibonacci Sequence," Math. Comput., 21 (1967), pp. 708-709.
45. MacLaren, M. D., and G. Marsaglia. "Uniform Random Number Generators," J. Assoc. Comput. Mach., 12 (1965), pp. 83-89.
46. Kendall, M. G., and A. Stuart. The Advanced Theory of Statistics, Vol. I. New York: Hafner Publishing Company, Inc., 1963.
47. Tocher, K. D. The Art of Simulation. London: The English Universities Press Ltd., 1963.

48. Twersky, V. "Scattering by Quasi-Periodic and Quasi-Random Distributions," IRE Trans. on Antennas and Propagation, AP-7, special supplement (1959), pp. S5307-S5319.
49. Beard, C. I., T. H. Kays, and V. Twersky. "Scattering by Random Distributions of Spheres Versus Concentration," IEEE Trans. on Antennas and Propagation, AP-15 (1967), pp. 99-118.
50. Beard, C. I., and V. Twersky. "Propagation Through Random Distributions of Spheres," IRE WESCON Convention Record, Part I (1958), pp. 87-100.
51. Beard, C. I. "Statistics of Phase Quadrature Components of Microwave Fields Transmitted Through a Random Medium," IRE Trans. on Antennas and Propagation, AP-10 (1962), pp. 721-731.
52. Beard, C. I., T. H. Kays, and V. Twersky. "Scattered Intensities for Random Distributions - Microwave Data and Optical Applications," Appl. Opt., 4 (1965), pp. 1299-1315.
53. Hawley, S. W., T. H. Kays, and V. Twersky. "Comparison of Distribution Functions from Scattering Data on Different Sets of Spheres," IEEE Trans. on Antennas and Propagation, AP-15 (1967), pp. 118-135.
54. Burke, J. E., et al. "Scattering by Two-Component Random Distributions of Spheres," Appl. Opt., 7 (1968), pp. 2392-2400.
55. Silver, S. Microwave Antenna Theory and Design. New York: McGraw-Hill Book Company, 1949.
56. de Balbine, G. "Note on Random Permutations," Math. Comput., 21 (1969), pp. 710-712.
57. Blackman, R. B., and J. W. Tukey. The Measurement of Power Spectra. New York: Dover Publications, Inc., 1958.
58. Korn, G. A. Random-Process Simulation and Measurements. New York: McGraw-Hill Book Company, 1966.
59. Berezin, I. S., and N. P. Zhidkov. Computing Methods, Vol. II. Massachusetts: Addison-Wesley Publishing Company, Inc., 1965.
60. Hiatt, R. E., E. F. Knott, and T. B. A. Senior. A Study of VHF Absorbers and Anechoic Rooms. The University of Michigan, Ann Arbor, Mich., Report 5391-1-F, February 1963.
61. Emerson, W. H., and F. P. Brownell. Measurement of the Horn Shaped Bunker-Ramo Chamber. The B. F. Goodrich Company, Shelton, Conn., Report MW-16, August 2, 1964.
62. Buckley, E. F. "Outline of Evaluation Procedures for Microwave Anechoic Chambers," Microwave Journal, 6 (August, 1963), pp. 69-75.